EXTRACELLULAR MATRIX BIOSCAFFOLDS FOR TREATMENT OF VOLUMETRIC MUSCLE LOSS

by

Jenna Lynn Dziki

Bachelor of Science in Bioengineering, University of Pittsburgh, 2014

Submitted to the Graduate Faculty of

Swanson School of Engineering in partial fulfillment

of the requirements for the degree of

Doctor of Philosophy

University of Pittsburgh

2017

UNIVERSITY OF PITTSBURGH

SWANSON SCHOOL OF ENGINEERING

This dissertation was presented

by

Jenna Lynn Dziki

It was defended on

April 27, 2017

and approved by

Bryan Brown, PhD, Professor, Department of Bioengineering

Lance Davidson, PhD, Professor, Department of Bioengineering

Donna Beer Stolz, PhD, Professor, Department of Cell Biology

Christopher Dearth, PhD, Professor, Physical Medicine & Rehabilitation, USUHS

Dissertation Director: Stephen F. Badylak, MD, PhD, Professor, Departments of Surgery and Bioengineering

EXTRACELLULAR MATRIX BIOSCAFFOLDS FOR TREATMENT OF VOLUMETRIC MUSCLE LOSS

Jenna Lynn Dziki, PhD

University of Pittsburgh, 2017

Overt loss of skeletal muscle tissue, or volumetric muscle loss (VML), overwhelms its inherent regenerative ability and is associated with robust scar tissue deposition and loss of function. VML is a significant problem in both military and civilian medicine. Current treatment options including muscle flaps, grafts, orthotics, and cell-centric strategies remain ineffective. Over the past decade, bioscaffolds composed of mammalian extracellular matrix (ECM) have been investigated as an acellular, inductive template to promote functional myogenesis for VML repair. ECM bioscaffolds obviate the need for exogenous stem cell delivery through the recruitment of endogenous stem / progenitor cells and promote a pro-remodeling microenvironment through modulation of the innate immune response. This immune-stimulatory approach, paired with endogenous stem / progenitor cell recruitment, represents a novel therapeutic strategy for treating VML. Mounting evidence suggests that site-appropriate mechanical loading can contribute to this pro-regenerative microenvironment. The objectives of the present thesis include determination of the spatial and temporal response of macrophages and progenitor cells within the ECM-treated VML injury site, investigation of the effects of ECM bioscaffolds upon macrophage phenotype and function, and determination of the effects of concomitant mechanical loading upon both macrophages and progenitor cells in the context of

ECM-mediated VML repair. Results show that ECM bioscaffolds can promote a shift in macrophage phenotype which is associated with downstream stem / progenitor cell recruitment. ECM bioscaffolds activate macrophages towards a pro-remodeling phenotype. Mechanical loading augments a pro-regenerative cross-talk between macrophages and myogenic progenitor cells following exposure to ECM degradation products. These preclinical investigations, among others, have driven the clinical translation of ECM bioscaffolds. Thirteen VML patients have been treated to date, with results that include strength and functional improvement and evidence of new muscle formation and innervation. This strategy which considers the responding innate immune response, stimulates endogenous progenitor cells, and includes early, site-appropriate mechanical loading, represents a promising and translatable approach to VML treatment.

TABLE OF CONTENTS

PREFACE ..... **XXI**

1.0 SKELETAL MUSCLE RESPONSE TO INJURY **1**

1.1 CLINICAL SIGNIFICANCE OF SKELETAL MUSCLE INJURY **1**

1.2 ACUTE SKELETAL MUSCLE REGENERATION **2**

1.2.1 Skeletal muscle response to acute injury **2**

1.2.2 The role of the innate immune system in acute skeletal muscle regeneration **3**

1.2.3 Macrophage-progenitor cell crosstalk **4**

1.3 TREATMENT STRATEGIES FOR VOLUMETRIC MUSCLE LOSS **4**

1.3.1 Current standard of care **4**

1.3.2 Cell-centric regenerative medicine approaches **5**

1.3.3 Physical rehabilitation / the benefits of mechanical loading **7**

1.4 FUTURE PERSPECTIVES **8**

1.5 CONCLUSIONS **9**

2.0 ECM BIOSCAFFOLDS AS IMMUNOMODULATORY MATERIALS **11**

2.1 ABSTRACT **11**

2.2 INTRODUCTION **12**

2.3 IMMUNOSUPPRESSION: THE IMPACT UPON ORGAN TRANSPLANTATION **14**

2.4 DEVELOPMENT OF "INERT" BIOMATERIALS **15**

2.5 BIOLOGIC SCAFFOLDS AS IMMUNE MODULATING BIOMATERIALS 17

2.6 DEVELOPMENT OF IMMUNORESPONSIVE MATERIALS 21

2.7 CONCLUSIONS 24

3.0 MECHANISMS BY WHICH ACELLULAR BIOLOGIC SCAFFOLDS PROMOTE FUNCTIONAL SKELETAL MUSCLE RESTORATION 25

3.1 ABSTRACT 25

3.2 INTRODUCTION 26

3.3 SKELETAL MUSCLE REGENERATION 30

3.3.1 Mediators of skeletal muscle regeneration 31

3.3.2 Biologic scaffolds composed of extracellular matrix (ECM) 32

3.3.3 Composition of ECM bioscaffolds 33

3.4 CONSTRUCTIVE REMODELING OUTCOMES 34

3.4.1 Degradation of extracellular matrix bioscaffolds and production of effector molecules 34

3.4.2 Recruitment of stem / progenitor cells by extracellular matrix bioscaffolds 35

3.4.3 Modulation of the host immune response 36

3.4.4 Preclinical evidence of ECM-mediated skeletal muscle remodeling 38

3.4.5 The role of mechanical loading / rehabilitation in ECM-induced skeletal muscle regeneration 40

3.4.6 ECM bioscaffolds can facilitate skeletal muscle restoration in the clinical setting 41

3.5 CONCLUSIONS AND FUTURE DIRECTIONS 43

4.0 OBJECTIVES 45

5.0 CENTRAL HYPOTHESIS AND SPECIFIC AIMS 46

6.0 IMMUNOMODULATION AND MOBILIZATION OF PROGENITOR CELLS BY EXTRACELLULAR MATRIX BIOSCAFFOLDS FOR VOLUMETRIC MUSCLE LOSS TREATMENT 49

6.1 ABSTRACT 49

6.2 INTRODUCTION 50

6.3 MATERIALS AND METHODS 52

6.3.1 Overview of experimental design 52

6.3.2 SIS-ECM bioscaffold preparation 53

6.3.3 Surgical procedure 53

6.3.4 Explant harvest 54

6.3.5 Immunolabeling 54

6.3.6 Image analysis 55

6.3.7 Statistical analysis 56

6.4 RESULTS 56

6.4.1 ECM bioscaffold treatment of VML results in cellular infiltration, neomatrix deposition, and skeletal muscle formation 56

6.4.2 Surgically placed SIS-ECM bioscaffolds are associated with a predominant constructive cellular infiltrate 60

6.4.3 ECM bioscaffolds promote PVSC mobilization 60

6.4.4 ECM bioscaffolds are associated with the presence of neurogenic precursor cells 63

6.4.5 Skeletal muscle presence following ECM treatment 63

6.4.6 The temporal host cellular response of ECM-treated versus untreated VML 67

6.5 DISCUSSION 69

6.6 CONCLUSIONS 72

6.7 ACKNOWLEDGEMENTS 73

7.0 SOLUBILIZED EXTRACELLULAR MATRIX BIOSCAFFOLDS DERIVED FROM DIVERSE SOURCE TISSUES DIFFERENTIALLY INFLUENCE MACROPHAGE PHENOTYPE 74

7.1 ABSTRACT 74

7.2 INTRODUCTION 75

7.3 MATERIALS AND METHODS 77

7.3.1 Overview of experimental design 77

7.3.2 Preparation of solubilized ECM bioscaffolds 78

7.3.3 SDS PAGE analysis 80

7.3.4 Macrophage isolation and polarization 80

7.3.5 Immunolabeling 81

7.3.6 Western blotting 82

7.3.7 Cell viability 82

7.3.8 Macrophage metabolism 83

7.3.9 Phagocytosis 84

7.3.10 Antimicrobial activity 84

7.3.11 Statistical analysis 85

7.4 RESULTS 85

7.4.1 ECM bioscaffolds derived from different source tissues have distinct compositions 85

7.4.2 ECM differentially affects macrophage surface marker expression 86

7.4.3 ECM differentially increases M1-like and M2-like macrophage protein expression 88

7.4.4 Exposure to ECM differentially affects macrophage viability 89

7.4.5 Exposure to ECM differentially affects macrophage metabolism 90

7.4.6 Phagocytic capability of macrophages does not significantly differ with phenotype 91

7.4.7 ECM treated macrophages exert antimicrobial effects 91

7.5 DISCUSSION 92

7.6 CONCLUSION 97

7.7 ACKNOWLEDGEMENTS 98

8.0 THE EFFECT OF MECHANICAL LOADING UPON EXTRACELLULAR MATRIX BIOSCAFFOLD-MEDIATED SKELETAL MUSCLE REMODELING .. 99

8.1 ABSTRACT 99

8.2 INTRODUCTION 100

8.3 MATERIALS AND METHODS 102

8.3.1 Overview of experimental design 102

8.3.2 Preparation of ECM bioscaffolds 102

8.3.3 Isolation and culture of murine bone marrow derived macrophages 103

8.3.4 Myoblast culture 103

8.3.5 ECM treatment and mechanical loading of myoblasts and macrophages 103

8.3.6 Immunolabeling analyses 104

8.3.7 Myoblast chemotaxis 105

8.3.8 Myoblast mitogenesis 106

8.3.9 Myoblast myogenesis 106

8.3.10 Surgical procedure and hind limb unloading 107

8.3.11 Tissue harvest and immunolabeling 108

8.3.12 Isometric torque measurement 108

8.3.13 Statistical analysis 109

8.4 RESULTS 110

8.4.1 Cyclic mechanical strain promotes a Fizz1+ macrophage phenotype 110

8.4.2 Cyclic mechanical strain promotes a pro-remodeling macrophage phenotype that induces myoblast chemotaxis 113

8.4.3 Cyclic mechanical strain promotes a pro-remodeling macrophage phenotype that reduces myoblast proliferation and promotes myoblast differentiation 115

8.4.4 Cyclic mechanical strain combined with SIS-ECM treatment promotes myoblast differentiation 116

8.4.5 Cyclic mechanical strain promotes myotube-mediated macrophage activation towards a pro-remodeling phenotype 118

8.4.6 Lack of mechanical stimulation alters the macrophage activation response in ECM-mediated skeletal muscle remodeling 118

8.4.7 Lack of mechanical stimulation hinders ECM bioscaffold-mediated constructive and functional remodeling in a mouse model of musculotendinuos injury 119

8.5 DISCUSSION 123

8.6 CONCLUSION 126

8.7 ACKNOWLEDGEMENTS 127

9.0 AN ACELLULAR BIOLOGIC SCAFFOLD TREATMENT FOR VOLUMETRIC MUSCLE LOSS: RESULTS OFA 13-PATIENT COHORT STUDY 128

9.1 ABSTRACT 128

9.2 INTRODUCTION 129

9.3 MATERIALS AND METHODS 131

9.3.1 Overview of study design 131

9.3.2 Subject selection and screening 134

9.3.3 Surgical procedure 135

9.3.4 Physical therapy 135

9.3.5 Isometric strength measurement 136

9.3.6 Range-of-motion and functional task analysis 137

9.3.7 Pre- and post-surgical imaging 137

9.3.8 Ultrasound-guided core biopsy of ECM 138

9.3.9 Electrodiagnostic studies 138

9.3.10 Histology and immunolabeling 139

9.4 RESULTS 140

9.4.1 Biologic scaffold implantation for the treatment of VML is associated with increased skeletal muscle force production 140

9.4.2 Biologic scaffolds for VML treatment are associated with improved range-of-motion and functional outcomes 140

9.4.3 ECM bioscaffold implantation is associated with PVSC mobilization, electromyographic evidence of innervation, the presence of neurogenic cells at the remodeling site, and muscle formation 145

9.4.4 ECM scaffolds degrade following implantation 147

9.4.5 ECM treatment increases bulk muscle content 149

9.4.6 ECM bioscaffold implantation improves electrophysiological function 152

9.5 DISCUSSION 161

9.6 ACKNOWLEDGEMENTS 166

10.0 SUMMARY OF MILESTONES AND FUTURE DIRECTIONS 168

APPENDIX A 172

BIBLIOGRAPHY 200

LIST OF TABLES

Table 1. Stem-cell based strategies for skeletal muscle repair 6

Table 2. Overview of the ECM mediated repair process 28

Table 3. Pre-clinical studies to determine the efficacy of ECM bioscaffolds as a skeletal muscle repair material 37

Table 4. Overview of decellularization protocols 79

Table 5. Patient information 133

Table 6. Force production 142

Table 7. Range of motion 143

Table 8. Nerve conduction study of eight of thirteen patients 151

Table 9. Needle electromyography 153

Table 10. Inclusion and exclusion criteria 155

Table 11. Functional task raw data 156

LIST OF FIGURES

Figure 1. Mechanisms of ECM-mediated skeletal muscle repair. Following implantation, ECM bioscaffolds degrade, releasing bioactive constituents that promote macrophage infiltration and activation as well as myogenic stem / progenitor cell recruitment, proliferation, and differentiation. In the presence of concomitant mechanical load, clinical results have shown that the resulting formation of skeletal muscle tissue is innervated and fully contractile. 27

Figure 2. Skeletal muscle formation following ECM bioscaffold implantation 56 days after injury. ECM bioscaffold implantation results in the formation of islands of skeletal muscle at the margin (denoted by dotted line) at the center (inset) of the defect surrounded by well-organized connective tissue as shown by desmin staining and Masson's trichrome (Scale bars = 50μm)... 39

Figure 3. CT images of human hamstring VML after ECM bioscaffold implantation. ECM bioscaffold implantation resulted in bulk muscle formation in the human hamstring after 8 months as shown by CT imaging (yellow arrow, bulk muscle tissue formation outlined in red). 43

Figure 4. Masson's trichrome staining of VML. (A) Masson's trichrome staining of untreated VML (100X magnification) shows deposition of collagenous tissue, consistent with a critical size defect with no resultant muscle formation..... 57

Figure 5 (continued on next page) 58

Figure 6. Perivascular stem cell migration. (A-D) CD146+ PVSCs are found in their normal anatomic location adjacent to vessels (CD31+) in both untreated and ECM treated defects. (A,B) Without ECM intervention, PVSCs remain vessel associated. (C,D) In contrast, ECM-treated defects are populated with PVSCs outside their normal anatomic location, a response that continues at 14 and 56 day time points. These PVSCs are shown to be localized at both the center and margin of the defect. (Scale bars = 50μm, error bars represent standard deviation *p <0.05, PVSC, perivascular stem cell). 62

Figure 7. β-III tubulin positive mononuclear cells are present within ECM treated VML defects. (A-D) Cross-sections of β-III tubulin+ nerve fibers are present at the margin of the defect in both treated and untreated VML at early time points. (C,D) β-III tubulin+ mononuclear cells are shown at the periphery and also at the center of the defect at 7, 14, and 56 days following ECM treatment, while these cells were absent in untreated defects. This finding may suggest that *de*

novo innervation following ECM treatment contributes to functional remodeling outcomes. (Scale bar = 50μm, error bars represent standard deviation, *p <0.05)..... 64

Figure 8. ECM treatment increases numbers of Nestin+ cells (A,B). Untreated VML defects were associated with diminished numbers of nestin+ nuclei when compared to (C,D) ECM treated VML. Nestin+ cells were localized at both the interface with native muscle and at the center of the defect following ECM treatment whereas untreated groups showed nestin+ cells mainly confined to the interface. Quantification shows that this result is consistent across all time points from 3 to 56 days post implantation. (Scale bars = 50μm, error bars represent standard deviation, *p <0.05). 65

Figure 9. Site appropriate skeletal muscle remodeling by ECM bioscaffolds (A,B) Few signs of MHC+ nuclei resulted after VML was left untreated. (C,D) ECM treatment resulted in increased numbers of MHC+ nuclei. Interestingly, these muscle fibers were also located in the center of the defect, suggesting *de novo* myogenesis. Temporal averages show increased numbers of MHC+ nuclei at 7, 14, and 56 day time points indicating ongoing remodeling. (Scale bars = 50μm, error bars represent standard deviation, *p <0.05). 66

Figure 10. Temporal host macrophage and progenitor cell response following VML. (A) ECM treatment corresponds with an early and robust transition to an M2 macrophage phenotype which coincides with increased PVSC mobilization and skeletal muscle formation when compared to the (B) predominant M1 macrophage response which occurs when VML is left untreated. Untreated groups were characterized by lower macrophage numbers overall and lower numbers of PVSCs, neurogenic cell types, and skeletal muscle. 68

Figure 11. SDS PAGE gel analysis of ECM degradation products. Degradation products of ECM bioscaffolds derived from different source tissues were separated using SDS PAGE gel electrophoresis and show distinct banding patterns. (SIS=small intestinal submucosa, UBM=urinary bladder matrix, mECM=skeletal muscle ECM, bECM= brain ECM, eECM = esophageal ECM, dECM= dermal ECM, LECM= liver ECM, coECM = colonic ECM)..... 86

Figure 12. Immunolabeling of ECM treated macrophages (A) Macrophages were fixed with 2% paraformaldehyde following 18 h of treatment with cytokines or ECM degradation products and immunolabeled for indicators of the M1 or M2 phenotypes (iNOS, Fizz1, respectively). F4/80 was used as a pan macrophage marker. (B) Results were quantified using CellProfiler Image Analysis software and show that SIS, bECM, eECM, and coECM promote a predominant M2-like macrophage phenotype, whereas dECM promotes a predominant M1-like macrophage phenotype. (MCSF = macrophage colony stimulating factor, SIS= small intestinal submucosa, UBM= urinary bladder matrix, mECM= skeletal muscle ECM, bECM= brain ECM, eECM= esophageal ECM, dECM= dermal ECM, LECM= liver ECM, coECM=colonic ECM) (* and # indicate $p < 0.05$ when compared to MCSF group for iNOS and Fizz1 quantification, respectively. n=8, error bars represent standard error of the mean. Light exposure times were standardized to a negative isotype control and kept constant across images). 87

Figure 13. Western blotting of ECM-treated macrophages. . (A) Macrophage lysates were collected and probed for the presence of iNOS and (C) CD206 as M1 and M2-like protein markers, respectively. (B) Treatment with SIS, UBM, bECM, and coECM promotes a significant

decrease in iNOS expression when compared to the vehicle (pepsin) control treatment. (D) Treatment with SIS, UBM, eECM, and coECM promotes a increase in CD206 expression, similarly to IL-4 treated macrophages when compared to the pesin treated macrophages. (MCSF= macrophage colony stimulating factor, SIS=small intestinal submucosa, UBM = urinary bladder matrix, mECM = skeletal muscle ECM, bECM = brain ECM, eECM = esophageal ECM, dECM = dermal ECM, LECM = liver ECM, coECM= colonic ECM). (* indicates $p < 0.05$ when compared to vehicle control. n=6. Error bars represent standard error of the mean)..... 88

Figure 14. Macrophage viability analysis. The viability of macrophages following treatment with cytokines or ECM degradation products was analyzed using trypan blue. Macrophage viability significantly decreases with eECM, LECM, and bECM treatment. (MCSF= macrophage colony stimulating factor, SIS=small intestinal submucosa, UBM = urinary bladder matrix, mECM = skeletal muscle ECM, bECM = brain ECM, eECM = esophageal ECM, dECM = dermal ECM, LECM = liver ECM, coECM= colonic ECM). (* indicates $p < 0.05$ when compared to MCSF group. n=3. Error bars represent standard deviation) 89

Figure 15. MTT metabolism of macrophages. MTT analysis shows treatment with mECM, dECM, cECM, or bECM reduces metabolic activity of macrophages when compared to the untreated control. UBM significantly increases MTT metabolism when compared to untreated macrophages, whereas mECM, bECM, dECM, and coECM result in a significant decrease. (MCSF= macrophage colony stimulating factor, SIS=small intestinal submucosa, UBM = urinary bladder matrix, mECM = skeletal muscle ECM, bECM = brain ECM, eECM = esophageal ECM, dECM = dermal ECM, LECM = liver ECM, coECM= colonic ECM). (* indicates $p < 0.05$ when compared to MCSF group. Error bars represent standard deviation).... 90

Figure 16. Phagocytic capacity of macrophages. Fluorophore-conjugated bioparticle uptake was used as a measure of phagocytic activity of macrophages. Treatment with cytokines or ECM degradation products did not significantly change phagocytosis. (MCSF= macrophage colony stimulating factor, SIS=small intestinal submucosa, UBM = urinary bladder matrix, mECM = skeletal muscle ECM, bECM = brain ECM, eECM = esophageal ECM, dECM = dermal ECM, LECM = liver ECM, coECM= colonic ECM). (* indicates $p < 0.05$ when compared to MCSF group. n=3. Error bars represent standard deviation) 91

Figure 17. Indirect antimicrobial activity of ECM degradation products. *S. aureus* growth was used to determine the antimicrobial effects of macrophages exposed to ECM degradation products. After 18 hours, secreted products from ECM-treated macrophages significantly inhibit *S. aureus* growth, similarly to cytokine-treated macrophages, when compared to untreated macrophages and the negative control (broth). (MCSF= macrophage colony stimulating factor, SIS=small intestinal submucosa, UBM = urinary bladder matrix, mECM = skeletal muscle ECM, bECM = brain ECM, eECM = esophageal ECM, dECM = dermal ECM, LECM = liver ECM, coECM= colonic ECM). (* indicates $p < 0.05$ when compared to MCSF group. n=4. Error bars represent standard error of the mean) 92

Figure 18. Overview of experimental design. The goal of the present study was to determine the ability of mechanical stimulation in the presence of ECM degradation products to promote skeletal muscle remodeling. The following questions were posed (A) How does mechanical

loading affect macrophage phenotype in the presence of an ECM bioscaffold and how is the macrophage secretome altered in the context of promoting myoblast chemotaxis, proliferation, and differentiation? (B) How does mechanical loading affect myoblast differentiation in the presence of an ECM bioscaffold and how does the myoblast/myotube secretome change in the context of promoting a change in activation in macrophages? (C) What is the effect of absence of mechanical loading upon the ECM-mediated skeletal muscle repair microenvironment?..... 111

Figure 19. Cyclic mechanical strain of bone marrow derived macrophages. Macrophages were subjected to 10% mechanical strain for 5 hours using the FlexCell system. 5 hours of mechanical strain resulted in an F4/80+/iNOS-/Fizz1+ macrophage phenotype, suggesting that mechanical strain alone can promote macrophage activation towards a pro-remodeling phenotype..... 112

Figure 20. The effect of ECM and mechanical stimulation upon the macrophage secretome. Macrophages were treated with activating cytokines IFNγ + LPS or IL-4 or 200 ug/ml of ECM degradation products for 18 hours. After 18 hours, cells were washed and media was replaced with serum-free, ECM-free media. Macrophages were strained for 5 hours and their conditioned mediat was collected for C2C12 experiments. (A,D) IL-4 and ECM treated macrophages promote increased C2C12 migration. Mechanically loaded macrophages significantly increase C2C12 migration compared the unloaded macrophages and the low serum negative control. (B,E) IFNγ+LPS treated macrophages promote increased C2C12 mitogenesis. Mechanically loaded macrophages significantly decreased C2C12 migotenesis compared to the unloaded and proliferation media positive control. (C,F) IL-4 stimulated and ECM stimulated macrophages significantly increase C2C12 myogenesis Mechanically loaded macrophages significantly increase C2C12 myogenesis compared to the unloaded and proliferation media negative control. (* indicates $p<0.05$. n=5. Error bars represent standard error of the mean) 114

Figure 21. Cyclic mechanical strain of C2C12 myoblasts. (A,C) Myoblasts were cultured and either kept in their proliferation media or (B,D) allowed to differentiate to form myotubes. (C,D) Cells were treated with solubilized ECM bioscaffolds for 18 hours or were left in media and were then mechanically strained for 5 hours or (A,B) were left unstrained. (F) SIS-ECM treatment increased expresson of desmin, with an additional increase after myoblasts were mechanically strained. (G) Mechanical strain increased myotbue formation shown by myosin heavy chain (MHC) expression. (*indicates $p < 0.05$, n=5, error bars represent standard error of the mean)..... 115

Figure 22. The effect of ECM and mechanical strain upon the myoblast secretome. C2C12 cells were cultured in proliferation media or allowed to form myotubes in differentiation media culture. Myoblasts or myotubes were treated with 200 ug/ml of ECM degradation products for 18 hours, after which the media was replaced with serum free, ECM free media and the cells were subjected to mechanical strain. Conditioned media was collected and added to bone marrow derived macrophages for 18 hours and the cells were fixed for immunolabeling.(B) The secretome of proliferating myoblasts promotes an iNOS-/Fizz1+ macrophge phenotype, (C) however, differentiated myotubes do not promote the same effect. Treating myotubes with ECM degradation products, however, alters their secretome allowing them to promote a Fizz1+ macrophage phenotype. E) This response is augmented when ECM-treated myotubes are subjected to mechaniacl strain. F) Percentage of iNOS and Fizz1 piositive macrophages were

quantified using CellProfiler (* indicaptes p <0.05, n=4, eror bars represent standard error of the mean)..... 117

Figure 23. Overview of animal model of VML and hind limb unloading. C57bl/6 mice were subjected to tail-suspension to achieve hind limb unloading for 2 weeks prior to surgery. Surgical excision of the distal gastrocnemius and proximal Achilles was replaced with either an SIS-ECM bioscaffold, an autologous graft, or left untreated. Animals were either allowed to walk normally or subjected to hind limb unloading and sacrificed according to the indicated timeline..... 120

Figure 24. Macrophage response to hind limb unloading following ECM-mediated VML remodeling. (A) Hind limb unloading results in increased infiltration of iNOS+ macrophages at 14 days following implantation and (B) decreased Fizz1+ macrophage infiltration in contrast to the (C,D) normal ambulation control. (E) Quantification of the Fizz1+:iNOS+ macrophage ratio across all animals showed a significant decrease following 14 days of hind limb unloading (** indiates p < 0.01, error bars represent standard error of the mean). 121

Figure 25. The effect of mechanical stimulation upon constructive remodeling following ECM implantation in a mouse model of VML. (A) Masson's trichrome staining shows site appropriate tissue deposition following ECM bioscafold implantation in mouse VML after 6 months in contrast to fatty tissue deposition and disorganized connective tissue formation in the autologous graft and untreated groups. Hind limb unloading for 6 months decreases the deposition of site appropriate tissue. (B) ECM treatment results in a significant improvement in gastrocnemius isometric torque production when compared to the untreated and autologous control groups. Hind limb unloading diminishes this increase in force production. (C) Hind limb unloading significantly decreases isometric torque production in the ECM treated animals and the healthy controls. (D) Peak isometric torque production is significantly decreased following hind limb unloading in the healthy control and ECM groups (HU= hind limb unloading, * indicaptes p < 0.05, n=4, error bars represent standard error of the mean)..... 122

Figure 26. Functional task performance. Functional measures as assessed by task / exercise completion from each patient. Data represent percent change from pre-surgical maximum. NT=not tested. 144

Figure 27. Site-appropriate tissue remodeling by ECM bioscaffolds (A-C) Masson's trichrome staining of human muscle biopsies shows islands of skeletal muscle present at 6-8 weeks, 10-12 weeks, and 24-28 weeks post surgery, respectively. (D-F) Human muscle biopsies are characterised by desmin expression at all time points, indicating new muscle formation within the site of implantation. (G-I) ECM bioscaffold implantation is associated with the presence of CD146+NG2+ perivascular stem cells. (J-L) PVSCs were shown to migrate away from their normal vessel associated anatomic location at all time points. Arrows indicate CD146+ PVSCs migrating away from vessels. (M,N) Migrating PVSCs and vasularity were quantified using CellProfiler Image Analysis software. (O) At 24-28 weeks post surgery, ECM bioscaffold implantation was associated with the presence of β-III tubulin+ cells, implicating innervated skeletal muscle (Scale bars = 50μm) 146

Figure 28. Ultrasound imaging shows that ECM bioscaffolds degrade upon implantation. (A) Grayscale ultrasound image 1 month after surgery in the posterior shoulder demonstrates a thin,

sheet-like hyperechoic structure, representing SIS-ECM (yellow arrows) overlying the posterior deltoid muscle. The posterior deltoid muscle is increased in echogenicity due to underlying fatty infiltration. (B) Ultrasound imaging 7 months after surgery shows that surgically-placed SIS-ECM is no longer identifiable superficial to the posterior deltoid. (C)Ultrasound image 1 month after surgery in the medial mid thigh demonstrates an ill-defined hypoechoic structure representing SIS-ECM (yellow arrows) adjacent to the sartorius muscle. (D) Ultrasound image 7 months after surgery shows that surgically-placed SIS-ECM is no longer identifiable and the sartorius muscle apears to have enlarged. (E) Ultrasound imaging 1 month after surgery in the posterior mid thigh demonstrates a shet-like echogenic structure representing dermal ECM (yellow arrows) with surrounding complex anechoic material (dashed-blue line) likely representing post-operative fluid collection. (F) Ultrasound imaging 7 months after surgery shows dermal ECM (yellow arrows) has decreased in echogenicity and now has a tubular or 'rolled-up' appearance as opposed to a sheet-like appearance. The previously identified post-operative fluid collection has essentially resolved..... 148

Figure 29. Representative CT imaging shows ECM bioscaffold implantation increases post-operative bulk muscle content. Overall, the area of the treated muscle was measured at three representative sites (proximal, middle, and distal) both prior to surgery and 7 months after surgery in multiple anatomic locations..... 150

Figure 30. Overview of study design. Patients underwent 6-8 weeks of pre-operative physical therapy followed up to 28 weeks of post-operative physical therapy. Tissue biopsies and functional assessments were evaluated 6-8, 10-12, and 24-28 weeks after ECM implantation. 159

Figure 31. Representative gross changes of quadriceps following ECM implantation. Gross appearance of injury site of patient 3 pre-operatively and 28 weeks post-ECM implantation... 159

Figure 32. ECM promotes muscle formation (A,C,E)) Before surgery, at this level of the proximal aspect in the posterior compartment, patient 13 shows complete absence or atrophy of hamstrings. ECM imlpantation is associated with an increase in post-operative bulk muscle with areas measuring 5.4, 6.9, and 7.3 cm^2 at the proximal, distal, and middle aspect of the posterior compartment, respectively (B,D,F)..... 160

Figure 33. Visual representation of study design..... 184

Figure 34. Gene expression of previously described “M1-like” and “M2-like” surface markers, cytokines, transcription factors, and metabolic markers. BMDM (left panel) and THP-1 (right panel) macrophages were treated with UBM-ECM, SIS-ECM, IFNγ + LPS, and IL-4 for 24 hours. Additionally, macrophages were pre-treated with IFNγ+LPS for 6 hours followed by 24 hours of UBM or SIS treatment (n=3). Samples were normalized to media treatment. Gene expression was evaluated using qPCR data and is demnostrated in heatmap form. Fold changes are presented using a color gradient bar 185

Figure 35. ECM degradation products promote an immunomodulatory "M2-like" phenotype (A) Human monocytes from the THP-1 cel line were cultured in media supplemented with PMA to derive macrophages. Macrophages were treated with 20 ng/ml IFNγ and 100 ngml LPS to derive "M1-like" macrophages, 20 ng/ml IL-4 to derive "M2-like" macrophages, 200 ug/ml SIS-ECM

degradation products, or 200 ug/ml pepsin control buffer. Additionaly, "M1-like" macrophages were exposed to either 200 ug/ml UBM-ECM or 200 ug/ml SIS-ECM degradation produts to simulate the physiologic scenario of an injury treated with an ECM scaffold. Macrophages were fixed and immunolabeled for the pan macrophage marker (Cd11b), and strong indicators of the M1-like (TNFα and iNOS) and M2-like (CD206 and TGM2) phenotype. ECM treated cells show increased expression of TGM2 and CD206, markers associated with the IL-4 pushed phenotype. (B) Immunolabeling results were corroborated using western-blot analysis of the TNFα, iNOS,CD206, and TGM2 markers (bottom panel). (C) Bone marrow was isolated from C57bl/6 mice and cultured in media supplemented with macrophage colony stimulating factor (MCSF) to derive macrophages. "M1-like" macrophages, "M2-like" macrophages, and ECM-activated macrophages were derived as described above. Additionally, "M1-like" macrophages were exposed to UBM-ECM or SIS-ECM degradation products as before. Macrophages were fixed and immunolabeled for the pan-macrophage marker (F4/80), and strong indicators of the M1-like (TNFα and iNOS) and M2-like (Fizz1 and arginase) phenotypes. ECM treated cells show increased expression of Fizz1 and arginase, associated with the IL-4 pushed phenotype, as well as TNFα, associated with the IFNγ/LPS pushed phenotype, suggesting that the ECM treated cells adopt a unique phenotype. (D) Immunolabeling resuls were further evaluated using western-blot analysis of the STAT1, arginase, Fizz1, iNOS, and TNFα markers (bottom panel). (Scale bars = 200 μm). 188

Figure 36. Functional assessment of ECM-treated macrophages. Phagocytosis activity in BMDM (A) and THP1 macrophages (B) was assessed using incubation with Vybrant FITC-labeled E.Coli particles then M.F.I analysis. Nitric oxide production from BMDM (C) and THP-1 macrophages (D) was assessed using the Greiss reagent system on macrophage supernatants following treatment 192

Figure 37. Principle component analysis (PCA) of delta Ct values scaled to unit variance. Biplot showign corrected principal component score values t(corr)[x] and loadings p(corr)[x] combined into one plot, where x is the component number. Genes that appear closer to the sample contributed to the distinction of that sample. The commonly cited genes associated with IFNγ+LPS and IL-4 activation that were chosen for further protein analyses for THP1 (A) and BMDM (B) derived macrophages and are highlighted..... 193

Figure 38. Densitometry was performed on western blots for all proteins that were probed. Color intensity of original blots was quantified using ImageJ for both the protein of interest and the respective loading control, β-actin. Intensity of the target protein band was normalized to its respective β-actin band 194

PREFACE

My doctoral studies in the Badylak laboratory have provided me a breadth of experiences and training that have been invaluable for my development as a scientist. The progress I've achieved has been a direct result of the exceptional mentors, collaborators, and friends that have guided me along the way.

Dr. Badylak has been an outstanding mentor, and I am forever grateful to be given the opportunity to work in his laboratory. His emphasis on translational research has given me a unique perspective, which has shaped my future career goals as an engineer and scientist. The training environment he has created has helped me accomplish and learn a great deal during my tenure in the lab, and I thank him for providing me with these opportunities and fostering a sense of collaboration, productivity, and hard work that drives me to emulate this in my future career.

My thesis committee members have been exceptional advisors and mentors throughout the graduate research process. I am grateful for their invaluable help and encouragement. Thank you, Dr. Bryan Brown, Dr. Lance Davidson, Dr. Donna Stolz, and Dr. Christopher Dearth.

The individuals I have worked alongside in the Badylak lab have made a huge impact, and none of my achievements would have been possible without them. Their intelligence, creativity, and expertise are immense and inspiring. Dr. Brian Sicari, who has been an extraordinary role model since my first day as an undergraduate in the lab to now, instilled in me both essential early science lessons and valuable life lessons. I attribute much of my success to

your incomparable mentorship and guidance and am forever grateful for everything you've done for me over the years.

Scott Johnson, Dr. Neill Turner, Li Zhang, and Janet Reing have been a constant source of knowledge, support, and patience, and their feedback has helped me solve more problems during my graduate tenure than I could count. I am grateful for their constant help. Dr. Luai Huleihel, Dr. Michelle Scarritt, Dr. Juan Diego Naranjo, Dr. George Hussey, Dr. Ale Costa, Dr. Pete Slivka, Dr. Lisa White, Dr. Beth Kollar, and Dr. Jeremy Kelly have been massively supportive as both mentors and friends, and I am so appreciative of their helpfulness and kindness. They inspire me to be a better scientist. My fellow graduate students over the years, Dr. Christopher Medberry, Dr. Matthew Wolf, Dr. Denver Faulk, Dr. Ricardo Londono, Dr. Christopher Carruthers, Dr. Timothy Keane, Lisa Carey, Catalina Pineda Molina, Lindsey Saldin, Mark Murdock, Yoojin Lee, Madeline Cramer, and Joseph Bartolacci were a better herd of friends than I could have asked for, and I would not have survived the most demoralizing moments nor enjoyed the happiest moments of graduate school quite as much without their friendship. They are enormously talented individuals and have helped me so much in lab and in life and will remain lifelong friends. DLAR staff members, Deanna Rhoads, Lori Walton, Jocelyn Runyon, Eve Simpson, Ally Lacovey, Rachel Thomas, and Emily Staysich have simplified my graduate student life and have been a constant source of guidance. Thank you.

My accomplishments in the lab were facilitated to a great degree by undergraduate students. I have had the opportunity to mentor several students who have made invaluable contributions to my work. Ross Giglio, Derek Wang, and Riddhi Gandhi are all high potential scientists who will enjoy fruitful careers. This work would not have been possible without you.

The Swanson School of Engineering (Bevier Fellowship), National Science Foundation (Graduate Research Fellowship), and McGowan Institute for Regenerative Medicine provided the funding necessary to complete this work, and I will always be thankful for this assistance.

This dissertation is dedicated to my parents Jeff and Cathy Dziki, my sister Katie Dziki, my grandparents Raymond Rusnic and Patricia Dziki, and my late grandparents Catherine Rusnic and Peter Dziki. Everything I achieve, or ever hope to accomplish, I owe to them. I am forever grateful for their love and encouragement and the values they have instilled in me. They consistently motivate me to pursue richness in perspective.

1.0 SKELETAL MUSCLE RESPONSE TO INJURY

1.1 CLINICAL SIGNIFICANCE OF SKELETAL MUSCLE INJURY

Volumetric muscle loss (VML) is a problem with significant clinical and economic consequences. VML is defined as the loss of at least 20% of a given muscle's mass resulting in functional impairment[1]. Such injuries can occur as the result of traumatic injury, excessive exercise, tumor ablation, or degenerative disease. It is estimated that 35-55% of all sports injuries and 53% of all battlefield extremity injuries involve damage to soft tissue and myofibers, resulting in approximately 4.5 million reconstructive surgical procedures annually, which contribute to billions of dollars in healthcare expenses[2]. Current treatment options include physical therapy or orthotics, which do not correct underlying strength deficits, and/or surgical tendon or muscle transfers, which are associated with issues including donor site morbidity, graft infection, and necrosis[3-5]. All of these treatment options fall short of restoring function which negatively impacts patient quality of life.

1.2 ACUTE SKELETAL MUSCLE REGENERATION

1.2.1 Skeletal muscle response to acute injury

Skeletal muscle tissue accounts for 40-45% of total body mass, and because of its relatively superficial location, it is subject to frequent injury. Efficient endogenous regeneration is critical to maintain normal muscle function. Fortunately, skeletal muscle is a tissue that possesses a robust capacity to regenerate following minor injury and is resilient to minor tears and strains, exercise-induced injuries, or minor experimentally induced injuries such as muscle freeze or crush[6-8]. This inherent regeneration is attributed to the activation of resident multipotent myogenic precursors known as satellite cells that reside in the interstitial space between the sarcolemma of myofibers and the basal lamina[9]. Satellite cells remain in a quiescent state, are activated in response to injury, and begin to proliferate to either replenish the satellite cell pool or to give rise to myogenic cells that differentiate to form myoblasts and eventually fuse to form myofibers that repair and replace the injured muscle tissue.

In cases of severe injury, however, skeletal muscle is unable to compensate with these endogenous mechanisms. Traditional signaling cascades needed for stem cell activation are overwhelmed and a pro-inflammatory microenvironment prevents myoblast formation and differentiation resulting in a fibrotic or adipogenic response and downstream functional deficits[10]. Loss of mechanical function in VML injuries is associated with physical deformities, significant loss of muscle volume, and a compromised quality of life[11,12].

1.2.2 The role of the innate immune system in acute skeletal muscle regeneration

The skeletal muscle injury microenvironment is complex, involving many cell types in addition to myogenic stem / progenitor cells that contribute to the injury response. In fact, upon injury, the majority of the first responding cells are macrophages, which have been shown to be positive regulators of skeletal muscle regeneration[13]. Specifically, previous work has shown that reducing macrophage numbers slows muscle regeneration following acute injury, and that distinct macrophage phenotypes are required for efficient muscle repair[14,15]. Macrophages are a heterogeneous cell population capable of activation along a spectrum of phenotypes dictated by cues from their local microenvironment[16]. Classically activated, M1-like, pro-inflammatory macrophages dominate the skeletal muscle injury scene as early as 1-2 days following injury and have been associated with early stages of muscle progenitor cell activation and proliferation. By 4 days after injury, proper muscle regeneration requires a phenotypic switch from this pro-inflammatory, M1-like macrophage, to a pro-remodeling, M2-like phenotype. M2-like macrophages have been associated with early stages of myogenic differentiation[13]. Without this phenotypic switch, regeneration is impaired and characterized by slowed growth of regenerative muscle fibers. Further, not only is the sequence of the phenotypic switch important, but the timing of the switch is also a critical factor in determining skeletal muscle remodeling outcomes following injury[15]. Macrophage-directed muscle regeneration is a complex and tightly controlled endogenous process that becomes perturbed in VML. Development of effective therapies for VML therefore lies in the understanding and manipulation of this complex microenvironment and the regulators of macrophage activation.

1.2.3 Macrophage-progenitor cell crosstalk

Macrophages influence stem / progenitor cell behavior in many tissue types, including skeletal muscle[17-25]. Interestingly, emerging evidence has shown that stem / progenitor cells can reciprocally regulate macrophage activation. Mesenchymal stem cells (MSCs) can promote expression of M2-like proteins including arginase-1 (Arg1). Additionally, co-culture of MSCs with bone-marrow-derived macrophages has been associated with a reduction in proinflammatory M1-like marker expression including inducible nitric oxide synthase (iNOS) and interleukin-6 (IL-6) and an increased expression of M2-like markers including interleukin-10 (IL-10), interleukin-4, (IL-4), and CD206[26]. Other work has shown that MSC-educated macrophages are a novel phenotype with distinct protein expression profiles when compared to activated M1-like and M2-like macrophage phenotypes[27]. It is plausible that the beneficial effects of MSC transplantation are partially attributed to their influence on macrophage phenotype. Targeting macrophage – stem / progenitor cell bidirectional crosstalk could be an important consideration for tissue remodeling therapies.

1.3 TREATMENT STRATEGIES FOR VOLUMETRIC MUSCLE LOSS

1.3.1 Current standard of care

Current, noninvasive treatment standards for patients suffering from volumetric muscle loss include maximization of the strength of the remaining muscle tissue with bracing / orthotics. Unfortunately, this approach cannot make up for the notable loss of strength which results from

VML. Muscle transposition (i.e. free flaps or grafts) or tendon transfer can replace muscle function, but have less-than-satisfactory success rates[1,3-5]. Such procedures typically involve significant donor-site morbidity and fail to provide efficient reconstruction or functional re-innervation of the lost muscle tissue. There is also a risk of graft infection which may lead to necrosis and the need for amputation. Overall, the current standard of care approaches for VML do not address persistent strength and functional deficits which ultimately contribute to disability, weakness, and poor quality of life for patients with VML.

1.3.2 Cell-centric regenerative medicine approaches

Tissue engineering and regenerative medicine-based strategies for the reconstruction of functional skeletal muscle tissue have included both cellular and acellular approaches. Cell-based strategies have attempted to augment skeletal muscle's natural regenerative response through the delivery of exogenous (typically autologous) stem / progenitor cells to the VML defect site[28,29]. Utilization of enriched muscle-derived stem cells, capable of long-term proliferation and myogenic potential, has been somewhat successful and increases the regenerative index when injected into sites of skeletal muscle injury in preclinical studies[30]. In addition to associated strict FDA regulatory restrictions, cell-based tissue engineering approaches are typically limited, however, by chronic pro-inflammatory activation of the host innate immune system and failure of the cells to incorporate within the host tissue[31-33]. The results of this approach have shown low cell viability[34], poor cell migration and engraftment[35], and the need for immunosuppressive therapy[36,37], as shown in Table 1.

Table 1. Stem-cell based strategies for skeletal muscle repair

Cell type	Description	Progress towards therapeutic potential	Challenges
Satellite cells [38,39]	• Adult stem cells • Express Pax7 transcription factor • Necessary for proliferation and maintenance of muscle stem cell pool	• Took nearly 50 years from first identification to a pure cell isolation. • Surface markers identified for satellite cell isolation are not necessarily reflected in human physiology. • There is a need for optimized isolation and more efficient expansion	• Very difficult to isolate and expand in culture to obtain enough cells for expansion • Limited engraftment efficiency
Muscle-derived stem cells [40,41]	• Adult stem cells • Identified in the interstitial space in mice • Non-adherent cell population	• Shown to improve muscle regeneration upon injection in preclinical murine models • Can be expanded in vitro up to 30 passages while retaining myogenic capacity	• Poor engraftment efficiency • No functional improvement
Perivascular stem cells [42,43]	• Adult stem cells • Found in muscle microvasculature typically vessel associated • CD146+/NG2+/ALP+ • Express satellite cell markers • Assume satellite cell position after injection	• Promising preclinical results have led to ongoing phase I/II clinical trial for pediatric muscular dystrophy • Grow extensively in culture • Better engraftment efficiency than satellite cells • Improve both morphology and function of muscle	• Variability in in-vitro scalability gives them a finite culture life-span
Embryonic stem cells [44-46]	• Pluripotent cells isolated from inner cell mass of blastocyst	• Generation of large quantities in vitro is possible • Engraftment ability has been demonstrated in murine models	• Difficult to recapitulate the skeletal muscle lineage in vitro • Potential immunologic mismatch • Ethical concerns
Induced pluripotent stem cells (iPS) [47]	• Genetically reprogrammed somatic cells inducing a pluripotent state	• Generation of Pax7+ iPS cells is possible • Generation of functional, human skeletal myogenic progenitors has been accomplished • Promote skeletal muscle regeneration and functional improvements	• Requirement for genetic correction • Risk of tumor generation

In fact, immunosuppressive therapy contributes to myoblast apoptosis[48]. Even if an ideal cell source and effective delivery method are identified, transplanted cells are often associated with less-than-optimal proliferative and differentiation potential within the host injury site[48]. Injected cells, lacking a scaffold material, are typically unable to redistribute throughout the injection site and do not migrate more than 200μm *in vivo*. Intravenous (IV) cell delivery frequently results in unintentional cell engraftment within tissues such as liver and spleen. Cells that are able to be adequately delivered to intended tissues are typically unable to engraft. In fact, it is widely accepted that myogenic stem / progenitor cell transplantation typically does not result in a significant engraftment of donor cells within the host tissue. Cell-centric strategies are also associated with a high economic burden due to the need for *ex vivo* cell expansion and manipulation. While some cell-based approaches have shown promise in preclinical studies, regulatory challenges and a lack of notable efficacy have prevented their widespread adoption for VML treatment.

1.3.3 Physical rehabilitation / the benefits of mechanical loading

There is mounting evidence to suggest that mechanical stimulation of the skeletal muscle microenvironment and its associated cells is an important determinant of remodeling outcomes after injury. Mechanical loading has been shown to be important in musculoskeletal strength maintenance, endurance, fatigue resistance, and development. Mechanical load has been shown to control skeleton and tendon development and is a key regulator of cartilage morphogenesis, joint formation, bone morphogenesis, and tendon homeostasis and repair[49]. More recently, the benefits of mechanical loading have been implicated in skeletal muscle's inherent regenerative capacity following acute injury. Specifically, mechanical loading has been associated with

activation of quiescent satellite cells, enhancement of muscle-derived stem cell proliferation and transplantation efficacy, improved alignment of regenerating myotubes, minimization of atrophy of surrounding myotubes, enhancement of immunomodulatory players, and modulation of niche elasticity, among other benefits[50]. The specific effects of mechanical loading at a cellular level in biomaterial-mediated skeletal muscle remodeling are unknown. Advances in the science of mechanotransduction, a process by which mechanical stimuli are translated into biologic responses, suggest that changes in both cellular and extracellular matrix mechanics may be contributing factors in the pathogenesis of certain muscle-related diseases. By applying mechanical stimuli in the form of targeted rehabilitation, there may be potential to augment the tissue remodeling response in severe, critical sized defects as is the case in VML.

1.4 FUTURE PERSPECTIVES

A multidisciplinary approach that considers the complex microenvironment of skeletal muscle injury is required for promoting effective functional and constructive remodeling, especially in the case of critically sized defects such as volumetric muscle loss. Favorable outcomes associated with the cell-based skeletal muscle tissue engineering approaches are most likely associated with a paracrine effect of the donor cells upon the host injured microenvironment rather than by direct myogenesis from the delivered cells[51-56]. Recent preclinical rodent studies have shown that skeletal muscle progenitor cells delivered in concert with an acellular biologic scaffold derived from mammalian extracellular matrix (ECM) have the potential to obviate the limitations associated with exogenous cell delivery[57,58]. Specifically, the studies combine

allogeneic muscle-derived cells (MDCs) and bladder acellular matrices (BAMs) which are then subjected to a period of *ex vivo* bioreactor mediated preconditioning prior to surgical placement. The most recent study showed that acellular BAMs were able to promote a 26% functional improvement while MDC seeded BAMs showed a 61% functional improvement in a rodent model of tibialis anterior (TA) VML[58]. These studies suggest that combination approaches may be able to augment a constructive remodeling outcome.

Additionally, positive outcomes associated with implantation of acellular biologic scaffolds for VML repair have been partially attributed to an aggressive, targeted physical therapy regimen which was implemented within 24-48 hours after ECM bioscaffold implantation. The application of a physiologic mechanical load during bioscaffold and tissue remodeling following injury promotes favorable preclinical and clinical outcomes including an increased cellular infiltrate, more rapid and extensive neovascularization, more organized and aligned connective tissue matrix, and a beneficial influence upon gene expression and cellular behavior[50,59-61]. While there is mounting evidence to suggest that mechanical stimulation of the extracellular matrix and its associated cells is an important determinant of remodeling outcomes, the specific effects of mechanical loading at a cellular level in extracellular matrix-mediated skeletal muscle remodeling is unknown and represents an important area of future investigation.

1.5 CONCLUSIONS

The ECM plays an important role in regulating the immune response to injury, especially in the context of acute skeletal muscle regeneration. The concept of dynamic reciprocity which describes the continuous cross talk between cells and matrix, and the influence of external

factors that affect the microenvironmental niche, is central to the understanding of the role of the ECM in musculoskeletal remodeling. While cell-centric regenerative medicine approaches have been extensively investigated, the use of an acellular approach that stimulates endogenous repair in the form of a biologic scaffold derived from extracellular matrix offers opportunities for circumventing the need for exogenous cell delivery. Tissue engineering/regenerative medicine efforts have shown promising early results in utilizing ECM bioscaffolds for VML remodeling. Furthermore, while mechanical loading has the potential to promote improved muscle remodeling outcomes, there remains a need to evaluate the mechanisms associated with the synergy between the immune response to bioscaffold implantation in concert with targeted rehabilitation to advance clinical practice and provide superior treatment options for skeletal muscle disease and injury.

2.0 ECM BIOSCAFFOLDS AS IMMUNOMODULATORY MATERIALS[1]

2.1 ABSTRACT

Suppression of the recipient immune response is a common component of tissue and organ transplantation strategies, and has also been used as a method of mitigating the inflammatory and scar tissue response to many biomaterials. It is now recognized, however, that long-term functional tissue replacement not only benefits from an intact host immune response, but depends on such a response. The present manuscript reviews the limitations associated with the traditionally held view of avoiding the immune response, the ability of acellular biologic scaffold materials to modulate the host immune response and promote a functional tissue replacement outcome, and current strategies within the fields of tissue engineering and biomaterials to develop immune-responsive and immunomodulatory biomaterials.

[1] Portions of this chapter were adapted from the following publication:
Dziki JL, Huleihel L, Scarritt M, Badylak SF. ECM bioscaffolds as immunomodulatory biomaterials. Tissue Engineering Special Edition. April 2017. DOI: 10.1089/ten.TEA.2016.0538

2.2 INTRODUCTION

The host response to whole organ transplant has been studied extensively and is well characterized. In contrast the host response to decellularized tissues and organs (i.e. bioscaffold materials composed of extracellular matrix (ECM)), or to synthetic biomaterials, has received much less attention and is relatively poorly understood. Tissue engineering (TE) strategies that include a biomaterial component but fail to consider the immune response are likely to yield sub-optimal outcomes. The immediate host response to any biomaterial involves blood/plasma protein adsorption on the material surface, and activation of the innate immune response including infiltration of neutrophils, macrophages, and the release of a diverse array of inflammatory cell-secreted signaling molecules[62,63]. Resolution of this pro-inflammatory microenvironment is necessary for a successful clinical outcome following the use of any biomaterial. Normal adult wound healing processes, tissue homeostasis, and normal fetal development easily navigate this transition, partly as a result of the endogenous signals embedded within the extracellular matrix (ECM) which regulate the immune response[64-67].

For example, when vascular endothelial cells are injured or denuded from their basement membrane, von Willebrand Factor (vWF) embedded within the ECM facilitates rapid tethering and adhesion of platelets[68]. In addition, interactions between sub-endothelial ECM proteins and platelet surface receptors such as immunoblugulin GPVI and integrins αIIbβ3 and α2β1 drive platelet activation and adhesion, respectively[69]. Separate from the effects of embedded signaling molecules, mechanotransduction, the mechanism by which cells translate mechanical stimulus

into biochemical responses, has been shown to influence cell fate. Within every tissue, variations in ECM composition, crosslinking, and 3-dimensional ultrastructure contribute to the biochemical and biophysical environment that regulates cell migration, proliferation, apoptosis, differentiation, and development[70,71].

Recently, mechanotransduction has been specifically implicated as a regulator of immune cell phenotype. McWhorter and colleagues demonstrated that cell shape, specifically degree of elongation can be influenced by micropatterning and subsequently modulate macrophage phenotype[72]. ECM remodeling in both post-injury healing environments and during homeostasis provides a mechanical feedback loop for the resident and/or infiltrating cells. As the ECM is degraded and replaced (i.e. remodeled), particularly during the resolution of inflammation, atypically expressed ECM molecules can modulate immune cell activation, differentiation, and persistence. These atypical ECM molecules, termed cryptic peptides, are bioactive peptides that are created or exposed by selective cleavage of ECM by proteases, particularly matrix metalloproteinases[66]. In a murine model of digit amputation, Agrawal and colleagues demonstrated that a C-terminal telopeptide of collagen IIIα present at the site of amputation recruited progenitor cells, increased calcium deposition, enchanced alkaline phosphatase activity, and amplified osteogenesis[73].In a mouse model of lung inflammation, MMP8 or MMP9 cleavage of type I collagen resulted in an acetylated Pro-Gly-Pro peptide that activated CXCR receptors and attracted neutrophils[74]. Recently, matrix-bound nano-vesicles (MBVs) have been identified as an integral and functional component of bioscaffolds composed of extracellular matrix[75]. These vesicles have the ability to act as vehicles to transfer RNA, proteins, and other signaling molecules between cells, and can regulate physiologic and/or pathologic processes. These MBVs have been shown to induce a phenotypic change in macrophage activation state in vitro; a

phenomenon now recognized as a mechanism by which ECM bioscaffolds mediate their functional remodeling outcomes in vivo.

Altogether, these examples point to an active role of the native ECM in tissue and organ development, homeostasis, inflammation, and healing. Analogous to these physiological roles for native tissue ECM, biologic scaffold materials composed of ECM activate many of these same endogenous signals[76-79]. Stated differently, biologic scaffolds composed of ECM serve as immunomodulatory biomaterials.

The present manuscript reviews the advantages and limitations of the use of synthetic biomaterials, especially in the context of tissue engineering applications, and suggests a rationale for the relative effectiveness of ECM-based scaffold materials. In addition, the critical role of the immune system in tissue engineering approaches is described and thus, the increasingly important contribution of immunomodulatory biomaterials.

2.3 IMMUNOSUPPRESSION: THE IMPACT UPON ORGAN TRANSPLANTATION

An understanding of the host response to biomaterials benefits from knowledge of the earliest attempts at tissue and organ replacement. The concept of replacing damaged or diseased tissues and organs has not been the exclusive pursuit of the tissue engineering community, but rather, has been a part of medical practice for millennia. One of the earliest documented cases of tissue and organ transplant, skin grating, occurred in approximately 3000 BC as revealed in Sanskrit texts of ancient India[80]. Documentation of tissue transplant and grafting that spans the 18th and 19th century includes the use of skin flaps to repair missing nose tissue after sword fights[80], teeth transplants, and the use of cadaveric tissues. It was not until the realization that

transplant failure was largely attributed to immunologic events[81] that the concept of immunosuppression was extensively investigated. The development of effective immunosuppression techniques allowed for organ transplantation to become commonplace. Immunosuppression progressed from a cell-centric approach that non-specifically targeted rapidly dividing cells by irradiation, to steroid therapy, to lymphocyte depletion, and eventually to inhibition of selected cytokines[82]. These immunosuppression strategies are associated with variable success rates, immune disorders, susceptibility to infections, and significant morbidity. Nonetheless, the discovery of major histocompatibility complexes (MHC) and the importance of human leukocyte antigen (HLA) matching led to improved success of immunosuppression compared to prior transplant methods, and has allowed for an exponential increase in the number of successfully transplanted organs and tissue grafts during the past 50 years.

2.4 DEVELOPMENT OF "INERT" BIOMATERIALS

As exhaustive studies were being conducted in the context of tissue and organ transplantation, the biomaterials community was identifying "inert" materials as desirable[83-85]. Biomaterials such as silicone that were isolated from the surrounding tissue by a defined fibrous capsule were grouped with materials identified as inert. In hindsight, the very formation of the capsule and the associated foreign body response was a manifestation of the host immune reaction toward the biomaterial. Attempts to mitigate fibrous tissue capsule thickness included steroid coatings or coating with cytotoxic agents[83,86]. Modifications of surface topology, functionalization with various ligands, and design changes that eventually included large (>75μm) pores were gradually added to biomaterials in attempts to control the local tissue response.

Arguably, there is no such thing as an "inert biomaterial." Upon implantation, such biomaterials, usually of synthetic composition, are subjected to a series of well-defined processes characterized as the foreign body reaction (FBR) that ultimately leads to fibrous encapsulation of the implant[87]. Implanted medical devices are often isolated from the body by a dense, collagenous capsule, which has long been an acceptable form of "biocompatibility" both by regulatory and historical standards. However, the inability to interface with normal host tissue as a result of intervening fibrous tissue eventually leads to diminished function for devices that require close contact with parenchymal cells or neurovascular structures. Metals and alloys have long been used for orthopedic implants and dental implants but are typically subject to corrosion, leaching, and adverse immune responses to wear debris. Silicone rubber and natural rubber have been used for breast implant and ocular lens applications, among others, but are associated with oil adhesions and other complications associated with the FBR including capsular contraction that may eventually necessitate explant[88-92]. Drug-eluting and other porous materials and sensor-based strategies to direct tissue repair are eventually ineffective if they fail to address the FBR, as the fibrous capsule that will inevitably surround the material will inhibit diffusion or controlled release of drug or sensor-related signals. It should be recognized that the inevitable inflammatory response that occurs to all biomaterials is virtually the same as the innate immune response, thus setting the stage for the concept of immunomodulatory biomaterials. The biologic processes of vascularization, cell response, fibrous tissue deposition, and the foreign body response have not changed; these events are now simply recognized as part of the host immune response. It is logical therefore, that modulation or redirection of the immune response rather than suppression of the immune response is important for long term biomaterial functionality.

2.5 BIOLOGIC SCAFFOLDS AS IMMUNE MODULATING BIOMATERIALS

Within the last decade, the essential and necessary role of an intact and fully functional immune system in normal development[93], regeneration[94], and tissue homeostasis[13,95-97], and in the constructive remodeling properties of ECM bioscaffolds[98-100] has been recognized. Biomaterials composed of extracellular matrix (ECM), typically derived from xenogeneic tissues have shown notable success in promoting constructive and functional tissue remodeling in multiple anatomic sites in both pre-clinical and clinical studies including hernia repair applications, esophageal mucosa replacement following cancer resection, volumetric muscle loss treatment, cardiac repair, and mitral valve replacement, among others[89,101-107]. It is important to note that ECM scaffolds prepared by methods that remove essentially all cellular remnants (i.e. xenogeneic antigens that would normally elicit a pro-inflammatory response), serve as an inductive niche to influence cell behavior and the downstream tissue remodeling response. Though xenogeneic in tissue origin, there has never been any clinical or histologic evidence of hyperacute or delayed rejection of efficiently decellularized ECM-derived bioscaffolds. Although, no immunosuppressive agents are used with these bioscaffold materials, this does not imply immune-privilege. In fact, there is a distinct immune response as described below.

Much is known about the mechanisms by which ECM bioscaffolds promote constructive tissue remodeling, including the fact that upon implantation, these bioscaffolds degrade, release chemoattractant[108-110], antimicrobial[111], and mitogenic peptides[109,110,112,113], growth factors[113,114], and extracellular vesicles[75] that contribute to endogenous stem cell recruitment among other bioactive effects. Perhaps most importantly, these scaffolds have been associated with a robust, but favorable host immune response that precedes constructive remodeling outcomes[76]. ECM bioscaffolds modulate the behavior of responding immune cells towards a regulatory, anti-

inflammatory phenotype. In 2001, a seminal study conducted by Allman et al showed that xenogeneic-derived ECM bioscaffolds promote a transition in the host innate immune response toward a Th2-restricted response. The study showed that there is indeed a robust host immune response to porcine-derived ECM bioscaffolds when implanted in a murine host, but the cytokine and antibody isotype profile is associated with production of anti-inflammatory cytokines including IL-4 and IL-10 and noncomplement fixing antibodies, indicators of biomaterial acceptance[115]. Stated differently, ECM bioscaffold materials are not inert, but rather, immunomodulatory.

The immunomodulatory effects of ECM bioscaffolds have since been extensively examined. The thoroughness of decellularization of the source tissue is a critical determinant of the ability of these materials to elicit an anti-inflammatory macrophage / T cell (M2-like/Th2-like) host response[116,117]. In addition, the use of chemical crosslinking[76,100], the anatomic origin of the source tissue from which ECM is derived[118], the source animal age[119], the terminal sterilization method utilized[120], and the supplementary use of NSAIDs[121], all can markedly affect the host response to ECM bioscaffolds. For example, compounds such as non-steroidal anti-inflammatory drugs (NSAID) that inhibit COX1/2 have been shown to reduce the constructive remodeling response driven by biologic scaffolds. Dearth et al. demonstrated that COX1/2 inhibition by aspirin led to less myogenesis and collagen deposition in an animal model of skeletal muscle injury[121]. In vitro, macrophages exposed to aspiring caused a reduction in ECM-driven prostaglandin secretion. Aspirin treatment also reduced the expression of CD206, a marker of M2-like macrophages. Thus, in clinical practice, the use of NSAIDs in conjunction with ECM scaffolds may dampen the healing process stimulated by the implant. In addition to the biomaterial properties, host-related factors can likewise contribute to the immune response to

biomaterials including age[122,123], nutritional status[124,125], anatomic site of implantation[62,126], and the presence of co-morbidities[127,128].

In 2009, Valentin et al showed that not only do ECM bioscaffolds elicit a favorable host innate immune response, specifically the macrophage response, but that this response is required for constructive ECM-mediated tissue remodeling[100]. Macrophages have recently been recognized as a critical determinant of regeneration in species such as the adult salamander [129]and in mammals during acute regenerative responses such as following skeletal muscle injury[13]. Brown et al further showed that the early phenotype profile of macrophages during the first weeks following ECM implantation can predict downstream remodeling outcomes[76]. It has since been shown that macrophages exposed to degradation products of ECM have a unique phenotype that is associated with suppression of inflammation and high antigen-presenting capabilities[130], even in the presence of a harsh pro-inflammatory microenvironment as in ulcerative colitis[131] or volumetric muscle loss[132]. Furthermore, the immunomodulatory properties of ECM bioscaffolds act not only by directly influencing macrophage phenotype[78,79], but also through paracrine effects, mediating macrophage cross-talk with endogenous stem / progenitor cells[78].

The immunomodulatory effects of ECM biomaterials include adaptive immune cells as well as cells of the innate immune system. Sadtler et al have expanded upon the early work of Allman by showing that, in a model of volumetric muscle loss, the remodeling response that follows implantation of an ECM bioscaffold critically relies upon T helper 2 pathways that guides macrophage polarization. It now appears likely that the cross talk between macrophages and T-regulatory cells initiated by ECM degradation products is a critical determinant of

downstream remodeling outcomes associated with not only the use of ECM bioscaffolds[130,133], but also during the native tissue response to disease and injury[134,135].

Sicari et al has shown that degradation products of extracellular matrix bioscaffolds can directly activate macrophages towards an iNOS-/Fizz1+ macrophage phenotype[79]. Further, Huleihel et al (in press) conducted an exhaustive analysis of macrophage phenotype following exposure to ECM degradation products showing that ECM is consistently associated with down-regulation of pro-inflammatory genes and proteins. As discussed above, the ability of ECM bioscaffolds to activate macrophages is well established. The specific macrophage surface receptors and associated intracellular pathways involved in bioscaffold-mediated immune activation have only been partially elucidated. Future work would benefit from identification of the specific components within ECM materials that contribute to macrophage activation including cryptic peptides, topical cues, and miRNA among other components.

Recent work has reinforced the need for caution in drawing broad conclusions regarding the immunomodulatory effects of biomaterials, specifically the effects attributed to macrophage phenotype[16]. Although it is clear that macrophage phenotype is a major determinant of the host response, use of a single cell marker or even several markers, may be inadequate to accurately characterize the functional and paracrine effects of these cells. Though desirable, it is often impractical to evaluate an exhaustive panel of markers to define macrophage phenotype. Recognizing this limitation, it is recommended that investigators select markers most relevant to the physiologic or pathologic condition being studied. When subsequently reporting the data, investigators should provide a justification for the selected markers.

A separate, but equally important consideration is the type of macrophage used for in vitro studies as this variable can markedly affect results and conclusions. A recent study

evaluated the use of primary mouse bone marrow derived macrophages (BMDM) versus a human monocyte cell line (ThP1) for in vitro activation studies. Drastically different gene expression profiles between BMDM and ThP1 after stimulation with LPS+IFNγ, IL-4, or ECM degradation products were reported. Phenotype nomenclature can also be misleading (i.e., M1 vs M2) can contribute to misinformation regarding cause-effect relationships between biomaterials and the host immune response. The terminology “M1” and “M2” has been widely used to describe pro-inflammatory and anti-inflammatory macrophage phenotypes, respectively. However, this dichotomy is an over-simplification that can contribute to misleading results. Macrophage phenotype exists as a spectrum from pro-inflammatory to anti-inflammatory cell types. A recent consensus report suggests nomenclature for macrophage phenotype that should minimize such problems[16]. In their review, Murray et al. recommended that key parameters be reported when describing in vitro experiments. These parameters should include cell source (mouse strain, tissue/organ, pathological condition, etc. as relevant), starting cell number, media and supplements utilized, tissue culture conditions, time in culture, source and concentration of cytokines, macrophage yield, activation conditions, and processing/analysis protocols. Reporting these parameters will then permit investigators to directly compare the results of different experiments. Moreover, Murray et al. propose that macrophages be described by the activator utilized, e.g. $M_{(IL4)}$ instead of M2.

2.6 DEVELOPMENT OF IMMUNORESPONSIVE MATERIALS

Many of the available immunosuppression strategies arose prior to an understanding of the normal immune response following tissue injury. The development of ECM-based biologic

scaffold materials, the relatively recent elucidation of macrophage plasticity and their derivatives, and a more in-depth understanding of the role of the immune response during development, normal wound healing, tissue homeostasis, and tissue/organ regeneration have sparked renewed interest in biomaterials as facilitators of functional tissue repair. For example, the use of ECM-coated synthetic polymers has been investigated as a method to promote a regulatory/anti-inflammatory host response as opposed to an otherwise pro-inflammatory response. Specifically, ECM hydrogel coatings have been shown to mitigate the chornic inflammatory response and associated downstream scar tissue formation after implantation of polyprolyene mesh, the most commonly used synthetic material used to manufacture surgical mesh devices[136]. Faulk et al. reported that the addition of an ECM hydrogel coating decreased the number of pro-inflammatory CD86+/CD68+ macrophages in the vicinity of the polypropylene fibers 2 weeks after implantation. Six months after implantation, the coated polypropylene was associated with less collagen deposition (i.e. fibrosis) than was associated with uncoated polypropylene. In similar work, the use of a porcine dermal ECM hydrogel to coat polypropylene mesh reduced macrophage accumulation and formation of foreign body giant cells[137]**.** At 35 days post-implantation, the ECM coating was fully degraded and replaced with a loose connective tissue.

The use of biomimetic ECM components has also been investigated to limit inflammatory responses to synthetic materials (i.e. immunomodulation. For example, in an in vitro model of sterile inflammation, addition of high sulfated hyaluronan reduced macrophage secretion of Proinflammatory cytokines, IL-1β, IL-6, IL-8, IL-12, and TNFα and induced secretion of the immunoregulatory cytokine IL-10 and the expression of CD163[138]. Direct coating of surgical meshes with pro-remodeling cytokines such as IL-4 has been associated with improved implant-

tissue integration[139]. Implantation of IL-4 coated mesh in mice was associated with an increased M2-like (regulatory/anti-inflammatory) macrophage to M1-like (pro-inflammatory) macrophage raito leading to reduction in the formation of a fibrotic capsule around the implant. In addition to bioactive coatings, hybrid hydrogels have been evaluated for modulating the immune response. PEG hydrogels containing a peptide mimic of the TNFα recognition loop on the TNF-receptor 1 were evaluated as a cell encapsulation material[140]. Because these hydrogels could sequester TNFα, encapsulated cells were protected from this pro-infalmmatory cytokine. Similarly, PEG hydorgels containing an inhibitory peptide for the IL-1 receptor was able to protect encapsulated islet cells[141].

Attempts to combine controlled-release technologies and biomaterials to alter the host immune microenvironment and promote better cell engraftment have also been investigated in preclinical animal studies with success[142,143]. Many of the successful cell-centric strategies for tissue engineered constructs have largely been due to the paracrine effects of such stem cells upon the responding immune cell infiltrate, particularly in the case of mesenchymal stem cell delivery (MSCs)[144,145]. MSC encapsulated in a poly(ethylene glycol) (PEG) hydrogel secreted PGE2, mediated immunoregulation of macrophages in vitro, and resolution of the foreign body response in vivo. Though the immune response to synthetic material is (or should be) a critical design consideration, the incorporation of a naturally occurring moiety places design constrains on polymer architecture, dynamics, and stabilization that can affect the long-term functionality of an implant[146]. It cannot be ruled out, however, that biomimetic strategies merely prolong the inevitable pro-inflammatory immune response (foreign body response) to a synthetic material. In short, immunomodulation is now recognized as an effective method for improving biomaterial performance.

2.7 CONCLUSIONS

Successful clinical translation of tissue engineering and biomaterial-based approaches for functional tissue replacement is critically dependent upon a compatible host response. Immunomodulatory strategies for limiting the foreign body reaction and resolving the inflammasome following material implantation / cell transplant are at the center of efforts to influence the host-biomaterial interface. The native extracellular matrix and ECM-based biomaterials possess signaling molecules that promote such events. Future studies will logically be aimed at investigation of specific components (both structural and soluble) within clinically used scaffold materials that activate the immune response. The reason(s) for mitigation of an adverse immune response to ECM bioscaffolds, even though they are largely xenogeneic in nature, represents an additional area of future investigation. In a broader context, it appears clear that a better understanding of the role of both the innate and adaptive immune systems in the host response to biomaterials, tissue remodeling, and regeneration will help shape the next generation of biomaterials and will be required to overcome current bottlenecks in the clinical translation pathway for tissue engineering and biomaterial-based technologies.

3.0 MECHANISMS BY WHICH ACELLULAR BIOLOGIC SCAFFOLDS PROMOTE FUNCTIONAL SKELETAL MUSCLE RESTORATION[2]

3.1 ABSTRACT

Acellular biologic scaffolds derived from extracellular matrix have been investigated in preclinical and clinical studies as a regenerative medicine approach for volumetric muscle loss treatment. The present chapter provides a review of previous studies supporting the use of extracellular matrix derived biologic scaffolds for the promotion of functional skeletal muscle tissue formation that is contractile and innervated. The chapter also identifies key mechanisms that have been associated with ECM-mediated skeletal muscle repair, and provides hypotheses as to why there have been variable outcomes, ranging from successful to unsatisfactory, associated with ECM bioscaffold implantation in the skeletal muscle injury microenvironment.

[2] Portions of this chapter were adapted from the following publication:
Badylak SF, **Dziki JL**, et al. Mechanisms by which acellular biologic scaffolds promote functional skeletal muscle restoration. *Biomaterials*. June 2016. DOI:10.1016/j.bioamterials.2016.06.047

3.2 INTRODUCTION

Select tissues in the adult mammal, including liver, epidermis, bone marrow, and the mucosal epithelium of the intestines[147-150] have robust regenerative capacity. Similarly, skeletal muscle has a remarkable ability to regenerate following injury: a process that partially recapitulates development. However, this regenerative response fails in skeletal muscle when a large volume of tissue is lost, a scenario referred to as volumetric muscle loss (VML)[1]. There are limited treatment options for VML including physical therapy debridement of scar tissue and/or muscle transposition, which are associated with morbidity and less-than-optimal outcomes[1,3-5,28]. Most attempts to induce or facilitate new functional skeletal muscle formation have been cell-centric[29,37,39,40,151] and have either been unsuccessful[36,152-156] or resulted in marginal improvement[34,157,158].

An acellular approach with bioscaffolds composed of extracellular matrix (ECM) has been used to promote functional tissue restoration in a variety of soft tissue locations, including skeletal muscle, a process identified as "constructive remodeling" (i.e., not regeneration)[159]. The physiologic events associated with ECM-induced constructive remodeling are remarkably similar to those which occur naturally in injured muscle that is capable of full recovery. Specifically, a robust cellular infiltrate is followed by a temporal sequence of myogenesis, remodeling, and maturation/functional repair[160]. These processes include the participation of muscle progenitor cells and macrophages, restoration of innervation and vascularization, and site-appropriate spatial reorganization of myocytes and stroma in response to mechanical loading (physical therapy) (Figure 1). For these reasons, ECM bioscaffolds have been investigated in both preclinical models of VML[161-164] and in patients with VML[107]. Outcomes have shown partial restoration of both structure and function. *In vitro* studies, preclinical and human clinical

studies, and the role of physical therapy, all of which support the translational aspects of these ECM-induced mechanisms will be described in the context of ECM bioscaffolds as an acellular therapeutic option for volumetric muscle loss.

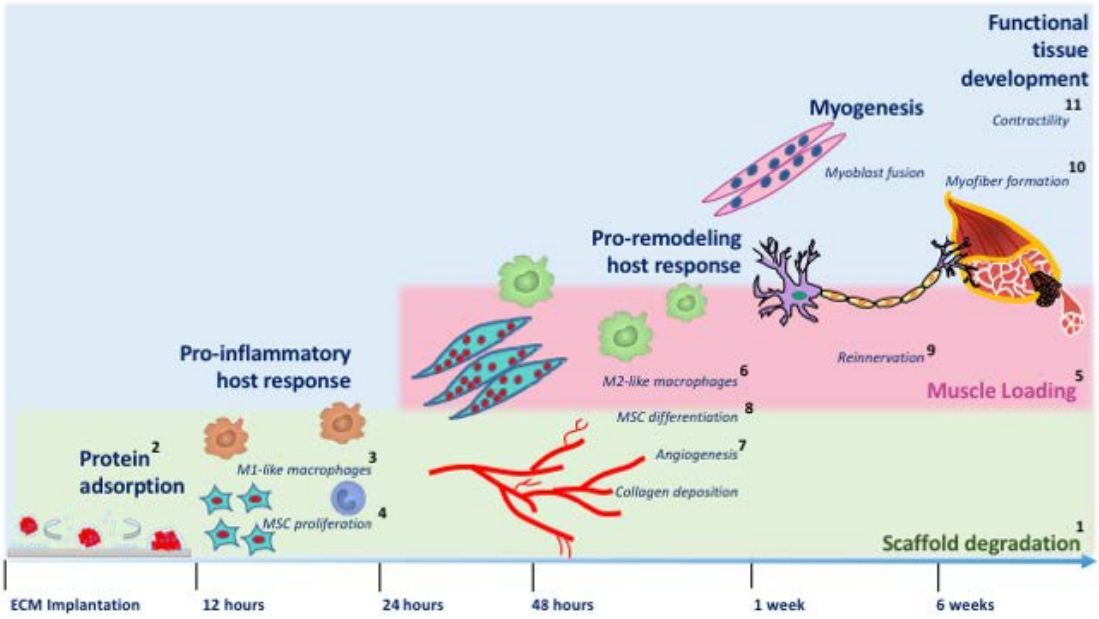

Figure 1. Mechanisms of ECM-mediated skeletal muscle repair. Following implantation, ECM bioscaffolds degrade, releasing bioactive constituents that promote macrophage infiltration and activation as well as myogenic stem / progenitor cell recruitment, proliferation, and differentiation. In the presence of concomitant mechanical load, clinical results have shown that the resulting formation of skeletal muscle tissue is innervated and fully contractile.

Table 2. Overview of the ECM mediated repair process

Skeletal muscle remodeling event	Report(s)	Summarized results
1. ECM bioscaffold degradation	Carey L et al. Biomaterials. 2014. Sep; 35(29):8297-304 Valentin et al. Tissue Eng Part A. 2009. Jul;15(7):1687-94 Gilbert et al. Biomaterials. 2007;28:147-50	Non-crosslinked ECM bioscaffolds degrade *in vivo* reaching 0% scaffold remaining by 24 weeks after implantation Macrophages are necessary for in vivo degradation of ECM bioscaffolds ECM bioscaffolds are populated and degraded by the host producing proteolytic enzymes that facilitate the degradation of the matrix and generating bioactive cryptic peptides.
2. Protein adsorption	Slack S et al. Ann N Y Acad Sci. 1987;516:223-43	Upon implantation, blood and plasma proteins adsorb to the biomaterial surface, a process determined by competitive protein exchange (the Vroman effect).
3.M1-like macrophage infiltration	Tidball JG et al. Am J Physiol Regul Integr Comp Physiol. 2010. May;298(5):R1173-87 Ruffell et al. PNAS. 2009;106:17475-80	M1-like macrophages are among the first responders to skeletal muscle injury, infiltrating within hours Inhibition of either M1 or M2 macrophages associated with lack of myogenic differentiation, chronic active inflammation, and necrosis.
4. Muscle stem cell proliferation	St Pierre B et al. J Appl Physiol. 1994. Jul;77(1):290-7 Crisan et al. J Cell Mol Med. 2012; 16:2851-60 Dellavalle et al. Nat Cell Biol. 2007;9:255-67	Macrophage subpopulations are associated with distinct phases of skeletal muscle regeneration. Perivascular stem cells are highly myogenic and participate in the adult mammalian response to skeletal muscle injury
5. Muscle loading	Kadi F et al. Histochem Cell Biol. 2000 Feb;113(2):99-103 Ambrosio F et al. Arch Phys Med Rehabil	Exercise and muscle loading can induce activation and proliferation of satellite cells Functional overloading enhances MSC contribution to muscle contraction.
6.M2-like macrophage infiltration	Deng B et al. J Immunol. 2012 Oct 1;189(7):3669-80 Sicari et al. Biomaterials. 2014. Oct;35(30):8605-12	A phenotypic switch from M1-like to M2-like macrophages are required for efficient muscle regeneration and normal muscle growth following injury ECM bioscaffolds promote an M2-like macrophage phenotype and these macrophages, in turn, promote skeletal muscle progenitor cell chemotaxis and myogenesis
7. Angiogenesis	Tidball JG et al. Development. 2014 Mar;141(6):1184-96 Li F et al. Endothelium. 2004 May-Aug;11(3-4):199-206	Immune cells play regulatory roles in muscle regeneration through permissive mechanisms that act to influence regeneration by modulating angiogenesis Bioactive peptides released as a result of ECM bioscaffold degradation recruit endothelial cells *in vivo*
8. Myoblast differentiation and fusion	Piccoli M et al. Biomaterials. 2016 Jan; 74:245-55 Sicari et al. Sci Transl Med. 2014 Apr30;(234)234ra58	ECM implantation in the diaphragm supported a regenerative environment and myogenesis ECM bioscaffold implantation results in de novo muscle formation in mice and humans with volumetric muscle loss

Table 2 (continued)

9. Reinnervation	Han N et al. Phys Ther. 2015 Nov 12	Clinical improvements in muscle strength and function following ECM implantation for VML treatment concomitant with the presence of electrical activity within the scaffold remodeling site
10.Myofiber formation	Sicari et al. Tissue Eng Part A. 2012 Oct;18(19-20);1941-8	Targeted placement of SIS-ECM scaffolds within mouse volumetric muscle loss resulted in the formation of site-appropriate skeletal muscle tissue
11. Contractile tissue development	Valentine et al. Biomaterials. 2010. Oct;31(29):7475-84 Turner et al. J Surg Res. 2012. Aug;176(2):490-502 Machingal et al. Tissue Eng Part A. 2011 Sep:17(17-18):2291-303 Mase et al. Orthopedics. 2010 Jul 13;33(7):511 Chen et al. JPRAS. 2013;66:1750-8 Aurora et al. Biomaterials. 2015 Oct:67-393-407	SIS-ECM implanted into the rat abdominal wall resulted in skeletal muscle formation with the same maximal contractile force as that of native tissue ECM bioscaffolds implanted in a gastrocnemius musculotendinous junction defect resulted in vascularized, innervated, contractile muscle tissue after 6 months. Latttissimus dorsi (LD) muscles in mice repaired with UBM roduced 50% of native muscle LD force at 2 months following implantation SIS ECM bioscaffold implantation in a 19 year old marine with ML resulted in marked gains In isokinetic performance, new tissue formation at the implant site, and no complications. Repair of VML with muscle ECM bioscaffolds in a rat resulted in significant improvements in LD muscle function. Repair of tibialis anterior VML by UBM ECM bioscaffolds reduced the functional deficit by 29% as determined by isometric torque measurement.

3.3 SKELETAL MUSCLE REGENERATION

A brief review of the natural response of skeletal muscle following recoverable injury[165,166] will facilitate an understanding and appreciation of ECM bioscaffold mediated muscle restoration. The inherent regenerative response of skeletal muscle involves three phases: the degeneration phase, the repair phase, and the remodeling phase[9,167,168]. The degeneration phase consists of myocyte and stromal (i.e. ECM) disruption and the influx of inflammatory cells[10,168]. The repair phase is characterized by the activation of quiescent myogenic stem cells that are stimulated to enter the cell cycle and migrate toward the site of injury[169,170]. These activated progenitor cells then receive signals to exit the cell cycle, differentiate, and fuse to form multinucleated myofibers[9,171]. During the remodeling phase the newly regenerated myofibers spatially organize, mature, and develop the ability to contract.

Skeletal muscle regeneration is contingent upon a population of cells defined anatomically as satellite cells. Satellite cells represent the putative skeletal muscle stem cell and, when quiescent, are located between the plasma and basal membrane of skeletal muscle myofibers[172,173]. Satellite cells divide asymmetrically and, following injury and in response to the associated microenvironmental cues, give rise to skeletal muscle myoblasts[9], which then proliferation, differentiate, and fuse to form multinucleated and functional contractile skeletal muscle myofibers[9,174]. Several primitive progenitor and/or stem cells, including perivascular stem cells, bone-marrow-derived cells, and other mesenchymal stromal cells, have also been shown to possess myogenic potential and/or occupy the satellite cell niche and give rise to skeletal muscle myoblasts[43,175].

3.3.1 Mediators of skeletal muscle regeneration

Regardless of the origin of myogenic progenitor cells, the microenvironmental cues that orchestrate their activity are provided, at least in part, by the host innate immune response, specifically macrophages[13,176,177]. Immediately following skeletal muscle injury, cytokines released by damaged myocytes and acute responder cells such as neutrophils activate the later-arriving host macrophages towards a pro-inflammatory (M1-like) phenotype. These pro-inflammatory macrophages exert paracrine effects which stimulate the proliferation and mobilization of resident satellite stem cells[13]. A shift in macrophage activation then occurs, and is characterized by a transition to a predominant anti-inflammatory, regulatory, and pro-remodeling (M2-like) phenotype[98]. In contrast to the pro-inflammatory phenotype, the paracrine effects of the remodeling macrophage promote cell-cycle exit and differentiation of the expanded myogenic satellite cells into functional contractile skeletal muscle[13]. Inhibition of either the pro-inflammatory or pro-remodeling phenotype is associated with lack of myogenic differentiation, chronic active inflammation, necrosis, and scar tissue formation[178]. Therefore, the secreted products of macrophages represent at least some of the mediators of skeletal muscle regeneration. However, questions remain regarding the biologic cues that promote the transition of pro-inflammatory macrophages to an anti-inflammatory, pro-remodeling phenotype, and the relationship of this phenotype transition to ECM bioscaffold-mediated muscle repair, especially in the context of VML. Studies have shown that ECM can directly influence macrophage phenotype[78], which in turn suggests that factors present within ECM bioscaffolds themselves have the ability to foster this phenotypic switch. It is likely, however, that a combination of direct and indirect (i.e. paracrine / cell-mediated) effects of ECM bioscaffolds contribute to macrophage modulation.

3.3.2 Biologic scaffolds composed of extracellular matrix (ECM)

Mammalian extracellular matrix (ECM) is composed of the secreted structural and functional molecules from resident cells of tissues or organs. The composition of native tissue ECM is dependent upon factors that affect the resident cell phenotype, such as microenvironmental mechanical forces, biochemical milieu, and innate and adaptive patterns of gene expression, among others. The ECM, in turn, influences the phenotype, chemotaxis, mitogenesis, and differentiation of resident cells, and facilitates cell-cell communication[73,108-110,113,179-184]. It is plausible, therefore, that ECM-derived signals are involved in phenomena such as macrophage phenotype transition during times of need; e.g., in response to muscle injury.

Native skeletal muscle ECM plays a critical role in the acute regeneration and normal developmental process. ECM molecules including collagens and proteoglycans have key roles in orchestrating skeletal muscle myoblast chemotaxis, proliferation, and fusion to form myotubes[185]. Following injury, degradation of the matrix releases growth factors and other biomolecules that trigger satellite cell activation and their associated contribution to the myoblast pool. These events in turn, facilitate myofiber differentiation and, ultimately, regeneration of functional skeletal muscle[9,186,187]. Furthermore, cell-matrix interactions are important in regulating satellite cell adhesion and translocation as well as promotion of re-innervation through activation of Schwann cells[188,189]. The appropriate regulation of ECM degradation and synthesis through synergy of matrix metalloproteinases (MMPs), tissue inhibitors of metalloproteinases (TIMPs), and myogenic cells results in the regenerative capacity for which skeletal muscle is known. State differently, ECM provides a crucial and complex microenvironmental niche to facilitate natural skeletal muscle regeneration.

3.3.3 Composition of ECM bioscaffolds

Biologic scaffold materials are prepared by removal of cells from source tissue such as dermis[190-192], small intestinal submucosa (SIS)[193-195], and urinary bladder matrix (UBM)[194,195]. ECM bioscaffolds, therefore are logically a rich source of effector molecules that influence cell behavior including the transition of macrophages to anti-inflammatory, regulatory phenotypes[76,78,98,116,196].

The molecular composition of ECM includes collagen, fibronectin, laminin, elastin, glycosaminoglycans (GAGs), growth factors, and cryptic peptides, among others[182,197]. Collagen is the most abundant molecule within mammalian ECM and comprises nearly 90% of its dry weight[198]. In addition to maintaining the structure of each tissue, GAGs, and low molecular weight cryptic oligopeptides released or exposed by the degradation of structural ECM such as collagen and fibronectin are known to possess significant biologic activity[73,108,180,199-201]. Type I collagen is the predominant isoform in skeletal muscle tissue[202]. Following injury, fibroblasts respond by producing type III collagen. Preclinical studies suggest that an increased collagen I: collagen III ratio may contribute to the return of strength in skeletal muscle tissue, and changes in collagen I and collagen III amounts have been evaluated in the initial phases of skeletal muscle injury repair. The balance of collagen isoforms may represent an important criterion for efficient skeletal muscle remodeling and a potential ECM-related therapeutic target[203].

Functional molecules within ECM include growth factors such as vascular endothelial growth factor (VEGF), fibroblast growth factor (FGF), stromal derived growth factor (SDF-1), epidermal growth factor (EGF), transforming growth factor beta (TGF-B), keratinocyte growth factor (KGF), hepatocyte growth factor (HGF), platelet derived growth factor (PDGF), and bone morphogenic protein (BMP), among others[114,204-207]. Stated differently, the ECM is a complex

mixture of structural and functional molecules that collectively represent the microenvironmental niche of its resident cells. However, it should be noted that variables such as source animal age[119], source tissue of ECM[208], extent of decellularization[117], use of chemical crosslinking agents[100], presence of residual detergents following decellularization[209], methods of terminal sterilization[120], and other processing parameters can influence the remodeling outcomes following ECM implantation.

3.4 CONSTRUCTIVE REMODELING OUTCOMES

When properly prepared and placed at sites of tissue injury in a variety of anatomic locations, ECM bioscaffolds have repeatedly shown constructive and functional remodeling in contrast to the default response to injury, which consists of inflammation and scar tissue formation[76,101,102,104,107,210,211]. Some of the cellular and subcellular events associated with ECM bioscaffold-mediated constructive remodeling are described below; the relevance and similarity of these events to naturally occurring skeletal muscle regeneration are noteworthy.

3.4.1 Degradation of extracellular matrix bioscaffolds and production of effector molecules

ECM bioscaffold degradation is mediated primarily by macrophages[100]. *In vivo* degradation occurs quickly and is important for several reasons. First, the mechanical properties of the bioscaffold show an initial decrease in strength, followed by a gradual increase as host tissue replaces the scaffold and responds to mechanical loading (i.e. physical therapy)[212]. This gradual

load transfer stimulates site-appropriate organization and orientation of new load bearing cells and connective tissue. ^{14}C labeling studies have shown 60% degradation of ECM bioscaffolds by 30 days post implantation and complete degradation after 90 days[213]. Dense ECM scaffolds such as those composed of human or porcine dermal ECM, degrade more slowly and can persist for 12-24 months[214]. Secondly, the temporary presence of the material avoids the foreign body reaction that occurs in response to non-degradable biomaterials. The third, and perhaps most important reason that degradation is desirable, is that the degradation products are bioactive[73,108,200,201]. Matricryptic peptides produced by cleavage of parent molecules such as collagen show antimicrobial activity[194,200], are chemotactic for stem / progenitor cells[108,180,181,199,201,215], and have marked influence on the host innate immune response[76,98-100,116,200]. Inhibition of degradation, as occurs with chemical crosslinking, prevents the participation of these bioactive molecules in the remodeling process[76].

3.4.2 Recruitment of stem / progenitor cells by extracellular matrix bioscaffolds

One of the hallmarks of ECM bioscaffold remodeling is a rapid and robust infiltration of host cells, which is mediated in a part by the ECM degradation products mentioned above. Constructive remodeling of an acellular scaffold obviously requires the involvement of a variety of site-appropriate cell types. For skeletal muscle applications, the new tissue would ideally have all the cell types of native muscle tissue including satellite cells, myocytes, endothelial cells, nerve cells, and fibroblasts, among others. Since an ECM bioscaffold is by definition acellular, all cells of the remodeling process must originate from the implanted host / patient.

ECM bioscaffolds and their degradation products have been associated with the *in vitro* and *in vivo* recruitment of endogenous stem / progenitor cells, including *in vitro* recruitment of

myogenic stem and progenitor cells[109], *in vivo* recruitment of Sox2+ cells[181]; *in vitro* and *in vivo* recruitment of skeletal muscle myoblasts[208], and *in vitro* and *in vivo* recruitment of multipotent perivascular stem cells (PVSCs)[175,180,216,217]. PVSCs are CD146+ , NG2+ cells found in the vascularized tissues of adult mammals and reside in a niche encircling microvessels and capillaries where they regulate vasoconstriction[175]. When mobilized from their typically quiescent niche, these cells are multipotent and give rise to cells with adipogenic, osteogenic, and chondrogenic cell lineages. PVSCs have been shown to be myogenic when transplanted into areas of injured muscle[175,218], while endogenous PVSCs have been shown to give rise to skeletal muscle myoblasts and participate in the adult mammalian regenerative response to skeletal muscle injury[42,43]. Therefore, an ECM bioscaffold with its recruited stem / progenitor cells would logically be well suited for VML injuries.

3.4.3 Modulation of the host immune response

In addition to the recruitment of endogenous stem / progenitor cells, ECM-mediated modulation of the innate immune response plays a pivotal role in the normal healing response of all tissues, including injured or missing skeletal muscle[100,219-222]. In fact, macrophage depletion or pharmacologic inhibition prevents both normal wound healing and degradation of ECM biologic scaffolds[100,223], thereby mitigating the formation and release of bioactive effector molecules (i.e. matricryptic peptides) that participate in normal wound healing and the constructive remodeling of ECM bioscaffolds. Recent studies have shown the robust ability of ECM degradation products to induce an anti-inflammatory, regulatory macrophage phenotype thus providing a logical and plausible explanation for ECM-mediated skeletal muscle reconstruction in the presence of such scaffolds[78]. In summary, although the mechanisms by which ECM scaffolds support functional

tissue reconstruction, including skeletal muscle restoration when used for VML, are only partially understood, there are well documented ECM-induced cellular events that clearly change the default host response to injury. These events include bioscaffold degradation and release of bioactive molecules that modulate macrophage phenotype and promote endogenous stem/progenitor cell recruitment, proliferation, and differentiation. The results of preclinical and clinical studies described below show the downstream morphologic and functional consequences of these ECM-mediated events (Figure 1, Table 3).

One of the primary factors responsible for the disappointing results of cell-based therapies is the rapid death of delivered cells, in part because of the unfavorable microenvironment into which they are typically placed[28,29,34,36,37,40,152,153,156,158]. Since the ECM in native tissue essentially represents the normal pericellular environment, it may be useful to think of an ECM bioscaffold as a compatible, temporary microenviornmental niche that can facilitate and/or promote endogenous remodeling.

Table 3. Pre-clinical studies to determine the efficacy of ECM bioscaffolds as a skeletal muscle repair material

Animal Species	**Mouse** **Rat** **Rabbit** **Canine**
Muscle Groups	Quadriceps Abdominal wall Gastrocnemius/Achilles tendon Diaphragm
Injury Sizes	(15-75% of tissue)
Source Tissues	Small intestinal submucosa (SIS) Urinary bladder matrix (UBM) Skeletal muscle ECM (mECM)

3.4.4 Preclinical evidence of ECM-mediated skeletal muscle remodeling

In 2010 Valentin et al showed that implantation of an acellular ECM bioscaffold in a rat abdominal wall partial thickness defect model could promote the formation of site-appropriate skeletal muscle with maximal contractile force similar to that of native muscle[164]. Turner et al. showed that 6 months following ECM implantation in a canine musculotendinous (gastrocnemius) defect, alpha-bungarotoxin positive motor end plates were present within islands of skeletal muscle tissue that replaced the scaffold material. The strength of the repaired muscle-tendon unit was approximately 40% of the strength of the contralateral gastrocnemius muscle[224]. In a separate study, islands of desmin positive skeletal muscle cells were present following ECM-bioscaffold implantation in a critically-sized quadriceps defect (i.e., VML) in the mouse[107,208]. A recent study showed that an ECM bioscaffold used for the repair of a diaphragmatic defect was replaced by islands of skeletal muscle, ultimately resulting in enhanced functional outcomes[225]. These preclinical studies by Valentine et al., Turner et al., Sicari et al., and Piccoli et al.[163,164,224,225] showed similar morphologic changes within the ECM scaffold material during the remodeling process; specifically, scaffold degradation by host cells, vascularization, and recruitment of stem / progenitor cells to the ECM remodeling site that were associated with variably sized islands of skeletal muscle. These islands of skeletal muscle were surrounded by well-organized collagenous connective tissue at later time points (Figure 2). Although the new muscle tissue following ECM bioscaffold implantation was associated with vascularization and re-innervation, it did not approach the volume or organization of the missing native muscle[61,163,224,225]. However, the new muscle tissue was associated with partially restored muscle function[164,224]. In the mouse model, a robust accumulation of CD146+ NG2+ perivascular stem cells was present within 14 days. The dense cell accumulation that occurs

within an ECM bioscaffold during the first several weeks following implantation is difficult to distinguish from an intense inflammatory response unless special effort is made to characterize the phenotype of the cells.

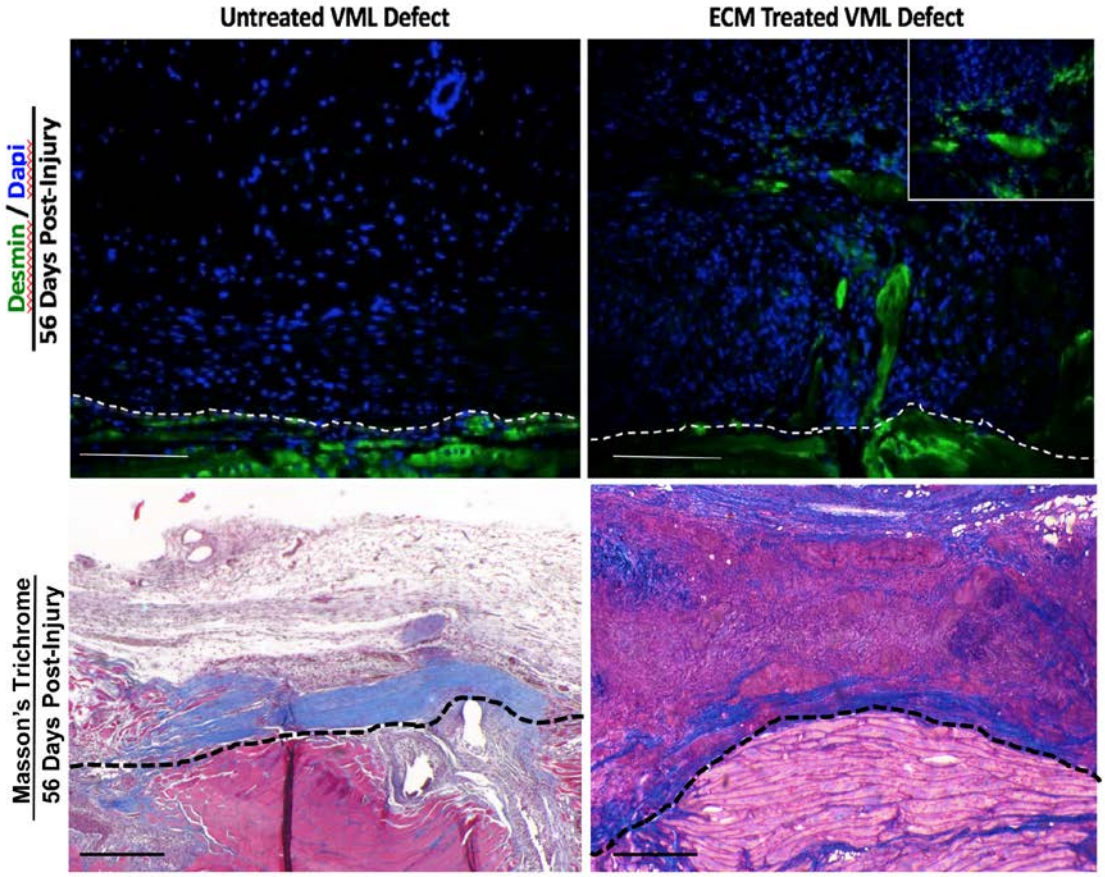

Figure 2. Skeletal muscle formation following ECM bioscaffold implantation 56 days after injury. ECM bioscaffold implantation results in the formation of islands of skeletal muscle at the margin (denoted by dotted line) at the center (inset) of the defect surrounded by well-organized connective tissue as shown by desmin staining and Masson's trichrome (Scale bars = 50μm).

3.4.5 The role of mechanical loading / rehabilitation in ECM-induced skeletal muscle regeneration

One of the necessary components of constructive, functional remodeling is the early onset of appropriate mechanical loading (i.e. physical therapy). Preclinical studies that have failed to delivery physical therapy within days of scaffold implantation, and in a consistent and progressive fashion, do not show the formation of site-appropriate skeletal muscle tissue and instead find the scaffold replaced by adipose tissue and fibrous tissue[61,226].

The microenvironmental niche is defined by all factors that influence the resident cells, including the mechanical / physical properties of the ECM, and the mechanical forces to which the cell / scaffold complex is subjected *in vivo*. There is robust evidence supporting biologic adaptations in response to both dynamic and static mechanical stimuli emanating from the cellular microenvironment[227-230]. This concept has served as a foundation for the application of clinical rehabilitation protocols for the treatment of diseased or injured tissues.

In the context of ECM-bioscaffold treatment for VML, the fate of recruited stem / progenitor cells is influenced by mechanical cues that contribute to the microenvironmental niche (i.e. physical therapy). The application of mechanical stimulation protocols in combination with cell therapy enhances stem cell transplantation efficacy and improves functional outcomes[227,231-233]. Specifically, muscle contractile activity and mechanical stimulation is an effective method for promoting tissue angiogenesis (reviewed in Ref.[50]), the release of myogenically favorable growth factors, and cellular alignment along the line of muscle axis[234], all variables that have been associated with favorable outcomes following ECM-bioscaffold implantation[2]. In fact, Grasman et al. suggest that, given the geometric architecture of myofibers, proper cellular alignment may be one of the most critical factors in muscle regeneration[2]. Taken

together, mechanical loading, delivered by exercise or neuromuscular electrical stimulation, is not only sufficient, but likely necessary for appropriate differentiation, alignment, and function of recruited stem/progenitor cells. Since the accumulation of these multipotential cells at the ECM-scaffold remodeling site occurs within a few days of scaffold implantation, application of a mechanical load (i.e. physical therapy) is required much earlier than typically provided in a clinical setting.

The application and enforcement of physical therapy in pre-clinical (i.e. animal) models is difficult at best. As an example, voluntary wheel running has been used in pre-clinical models of "rehabilitation" following the application of an ECM scaffold for the treatment of VML injuries[226]. However, without monitoring and diligent recording of running activity (which is voluntary), the influence of this critical variable cannot be determined and results are left in question.

3.4.6 ECM bioscaffolds can facilitate skeletal muscle restoration in the clinical setting

The constructive remodeling outcomes, including the temporospatial pattern of cell infiltration, scaffold degradation, formation of islands of new skeletal muscle, and the functional improvement shown in preclinical animal studies faithfully translated to humans when ECM-bioscaffolds were used to treat VML.

ECM bioscaffolds were implanted in 13 patients with VML who had all failed standard of care in a recent cohort study[107,235]. ECM intervention was associated with increased mobilization of perivascular stem cells (PVSCs), and the formation of randomly distributed and variably sized islands of desmin positive skeletal muscle. CT and MRI imaging corroborated immunolabeling findings in biopsy speicmens showing increased post-operative skeletal muscle

tissue mass (Figure 3). Patients showed an average improvement of 37.3 ± 12.4% in strength and 27.1 ± 10.5% in range of motion task performance, and 271.8 ± 62.6 % in functional task performance.

All subjects completed a rigorous pre-operative rehabilitation protocol that was customized to target the individual's specific functional deficits thus ensuring that any post-operative functional improvement could be attributed to ECM implantation and was not the result of an improved rehabilitation protocol or a loading induced hypertrophy of the existing muscle tissue.

It has been argued that irregularly sized and randomly distributed islands of skeletal muscle could not contribute to functional improvement following ECM bioscaffold implantation, and that any functional gains are a result of a fibrotic bridge that allows for force transduction across the defect site[161]. However, in patients treated for VML, the loss of tissue typically involves irregularly shaped deficits, multiple muscles within a compartment, and there may be a total loss of either a muscle origin or insertion. The ECM bioscaffold is placed in contact with adjacent native tissue to facilitate cell infiltration, remodeling, and integration. If merely a mechanical bridge were sufficient to restore strength and function, synthetic scaffold materials which elicit fibrosis and no new muscle tissue such as poly(glycolic acid) (PGA)[236], poly-e-caprolactone (PCL)[237], and polypropylene[164], would logically produce similar functional outcomes instead. The ECM is typically provided in a sheet configuration and serves both an initial mechanotransduction function for infiltrating cells and an inductive function for skeletal muscle remodeling as shown in Figure 1. Although ECM-induced functional remodeling has been disputed[226], these same manuscripts acknowledge the 25-52% improvement in function shown in preclinical studies[57,226].

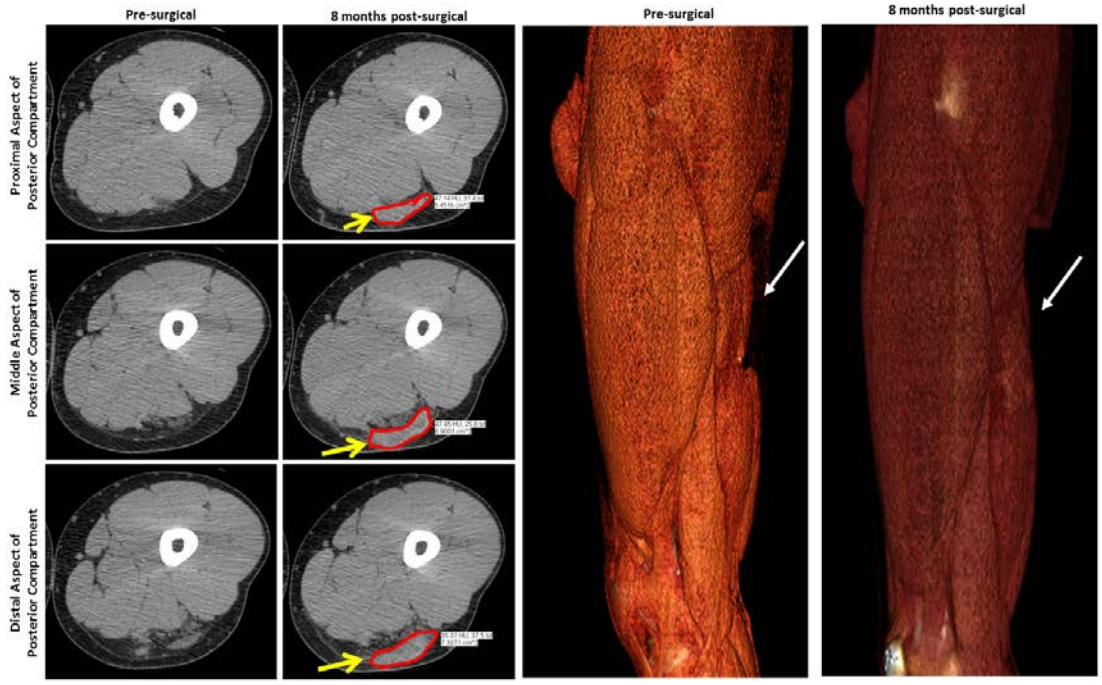

Figure 3. CT images of human hamstring VML after ECM bioscaffold implantation. ECM bioscaffold implantation resulted in bulk muscle formation in the human hamstring after 8 months as shown by CT imaging (yellow arrow, bulk muscle tissue formation outlined in red).

3.5 CONCLUSIONS AND FUTURE DIRECTIONS

It is evident that the effectiveness of ECM bioscaffolds for functional soft tissue reconstruction is dependent upon variables such as processing methods of bioscaffolds, patient age and

comorbidities, surgical technique, and the extent of surrounding viable muscle tissue, among other determinants. Further work is required to better define these factors. It should also be noted that the clinical study involved chronic VML injuries following repeated failure of all existing standard of care approaches. It is possible that there would be even greater success if an acellular bioscaffold approach was applied acutely after injury.

This opinion manuscript provides the scientific underpinnings that, at least partially, explain the rationale for ECM bioscaffolds as a treatment option for VML. This success has been substantial, with histologic electrophysiologic and clinical evidence for the creation of new, functional tissue. While acellular bioscaffolds are not the ultimate solution for treatment of VML, they do represent a notable improvement over existing treatment options. It is likely that a combination of cell-based, scaffold-based, and pharmacologically based approaches will be more effective than ECM bioscaffolds or physical rehabilitation alone. Such approaches have not been evaluated to date, and clearly warrant further study.

4.0 OBJECTIVES

Volumetric muscle loss as a result of trauma, tumor ablation, or degenerative disease remains a challenging clinical problem for which therapeutic options are limited. Current standards of care including muscle transposition or tendon transfer are associated with significant donor site morbidity and fail to restore strength or functional re-innervation of the host muscle tissue. Patients are therefore faced with a bleak prognosis: persistent strength and functional deficits that contribute to disability and a compromised quality of life. A regenerative medicine approach has shown promise for functional skeletal muscle reconstruction. Specifically, acellular bioscaffolds composed of extracellular matrix (ECM) have been shown to stimulate endogenous skeletal muscle repair via mechanisms that include modulation of the host innate immune response and recruitment of endogenous stem / progenitor cells. However, the specific role of these macrophages and progenitor cells, the influence of the ECM microenvironmental niche upon these cells, and the effect of concomitant physical rehabilitation (i.e. mechanical loading) are only partially understood. The proposed study will investigate the effect of ECM bioscaffolds upon macrophage phenotype and will evaluate potential bidirectional cross talk between skeletal muscle progenitor cells with and without mechanical loading and phenotypically activated (i.e. polarized) macrophages in the context of ECM-mediated skeletal muscle repair.

5.0 CENTRAL HYPOTHESIS AND SPECIFIC AIMS

***Central Hypothesis*:** ECM bioscaffolds can promote constructive remodeling of skeletal muscle via macrophage-mediated effects that are augmented by concomitant mechanical loading.

Specific Aim 1: To determine the spatiotemporal patterns of macrophage and progenitor cell infiltration following ECM treatment of murine volumetric muscle loss

Corollary Hypothesis: ECM implantation will promote an early and sustained M1-like to M2-like macrophage transition, increased progenitor cell recruitment, and increased myogenesis

Rationale: ECM has been shown to promote skeletal muscle remodeling in preclinical and clinical studies in which mobilization of perivascular stem cells (PVSCs) has been associated with the remodeling process. Furthermore, the prescence of macrophages and the transition from an M1-like to an M2-like phenotype is not just sufficient, but required for acute skeletal muscle repair. It is therefore expected that ECM implantation in a mouse model of VML will result in an appropriately timed transition to an M2-like macrophage phenotype, increased PVSC mobilization, and myogenesis.

Specific Aim 2: To characterize the effects of ECM derived from small intestinal submucosa (SIS-ECM) upon macrophage phenotype as defined by surface marker expression, protein expression, phagocytic capacity, and antimicrobial effects.

Subaim 2.1: To compare SIS-ECM treated macrophages to macrophages treated with ECM derived from urinary bladder (UBM), skeletal muscle (mECM), brain (bECM), esophagus (eECM), colon (coECM), dermis (dECM), and liver (LECM)

Corollary Hypothesis: SIS-ECM will promte an alternative macrophage phenotype characterized by M2-like surface markers, protein expression, increased phagocytic capacity, and antimicrobial effects. Not all ECM types will promote the same effect upon macrophage phenotype.

Rationale: Previous work has shown the effect of ECM in promoting a shift from a predominant M1-like to M2-like macrophage population and associated downstream constructive remodeling outcome. Since the ECM from ach tissue and organ differs in composition, at least to a small extent, it is hypothesized that ECM can directly affect macrophage phenotype, but that not all types (i.e. tissue sources of ECM) will affect phenotype identically.

Specific Aim 3: To determine the effects of hind limb unloading upon ECM-mediated skeletal muscle remodeling in a mouse gastrocnemius/Achilles injury model

Subaim 3.1 To determine the effects of mechanical loading upon macrophage-skeletal muscle progenitor cell crosstalk

Corollary Hypothesis: Mechanical loading results in improved ECM-mediated skeletal muscle remodeling when compared to unloading

Rationale: Concomitant physical rehabilitation during the ECM remodeling period is associated with favorable preclinical and clinical outcomes including an increased cellular infiltrate, more rapid and extensive neovascularization, and more organized connective tissue matrix. The cellular mediators of the improved outcome with mechanical loading are unknown.

Since macrophages play a critical role in tissue remodeling following injury, it is possible that absence of mechanical loading will result in a reduced macrophage infiltrate, a lower M2-like/M1-like ratio, and decreased myogenesis and force production.

6.0 IMMUNOMODULATION AND MOBILIZATION OF PROGENITOR CELLS BY EXTRACELLULAR MATRIX BIOSCAFFOLDS FOR VOLUMETRIC MUSCLE LOSS TREATMENT[3]

6.1 ABSTRACT

Acellular bioscaffolds composed of extracellular matrix (ECM) have been effectively used to promote functional tissue remodeling in both preclinical and clinical studies of volumetric muscle loss, but the mechanisms that contribute to such outcomes are not fully understood. Thirty-two C57bl/6 mice were divided into eight groups of four animals each. A critical-sized defect was created in the quadriceps muscle and was repaired with a small intestinal submucosa ECM bioscaffold or left untreated. Animals were sacrificed at 3, 7, 14, or 56 days after surgery. The spatiotemporal cellular response in both treated and untreated groups was characterized by immunolabeling methods. Early time points showed a robust M2-like macrophage phenotype following ECM treatment in contrast to the predominant M1-like macrophage phenotype present in the untreated group. ECM implantation promoted perivascular stem cell mobilization, increased presence of neurogenic progenitor cells, and was associated with myotube formation. These cell types were present not only at the periphery of the defect near uninjured muscle, but

[3] Portions of this chapter have been adapted from the following publication:
Dziki JL, Sicari BM, Wolf MT, Cramer MC, Badylak SF. Immunomodulation and mobilization of progenitor cells by extracellular matrix bioscaffolds for volumetric muscle loss treatment. *Tissue Engineering Part A.* November 2016. DOI:10.1089/ten.tea.2016.0340

also in the center of the ECM-filled defect. ECM bioscaffolds modify the default response to skeletal muscle injury and provide a microenvironment conducive to a constructive healing response.

6.2 INTRODUCTION

The well-recognized ability of adult skeletal muscle tissue to regenerate following acute injury is contingent upon activated resident myogenic progenitor or "satellite" cells. Activated satellite cells give rise to proliferative committed skeletal muscle myoblasts, which subsequently undergo regulated stages of expansion and differentiation[42,43,172,175,238,239]. Other multipotent myogenic stem / progenitor cells including multipotent perivascular stem cells (PVSCs) and mesenchymal stem cells participate in myogenesis via direct and indirect mechanisms. The progression of myogenic progenitor cells through stages of proliferation and differentiation is dependent upon the host inflammatory response, including the number, phenotype, and temporal pattern of infiltrating macrophages and T-helper lymphocytes[10,13,133,240-242]. A transition in the activation/polarization state of macrophages and lymphocytes at the injury site from a predominant classically activated and Proinflammatory M1/Th1 phenotype, to a predominant alternatively activated and constructive M2/Th2 phentoype not only facilitates, but also is required for downstream functional remodeling by regulating the stages of myogenic progenitor cell activity following muscle injury[13,15,133,241]. Specifically, paracrine factors secreted by M1 macrophages prompt local progenitor cells to enter the cell cycle and proliferate, thus facilitating an expansion of readily available cells with myogenic potential present at the site of injury. In contrast, paracrine factors produced by M2 macrophages induce the expanded progenitor cell

population to exit the cell cycle, which promotes the differentiation of these cells into functional skeletal muscle cells[15,178,243,244]. The source and temporal pattern of molecular signals that initiate and sustain the M1 to M2 transition *in vivo* remain unknown.

Sever skeletal muscle injury resulting from trauma, tumor ablation, or degenerative disease may cause a massive or overt loss of skeletal muscle tissue known as volumetric muscle loss (VML). VML injuries overwhelm the inherent regenerative ability of skeletal muscle tissue and are associated with robust scar tissue deposition, loss of function, and serious morbidity[1,163]. Current therapeutic options for VML include scar tissue debridement, muscle transposition, and/or the use of cell-centric regenerative medicine strategies. Cell-based approaches remain generally ineffective as they typically fail to thrive in the unfavorable tissue injury microenvironment[31-33,245]. An approach that facilitates the necessary macrophage phenotype transition and simultaneously provides a supportive microenvironmental niche for progenitor cell proliferation and differentiation would be desirable[107,163].

The surgical placement of acellular extracellular matrix (ECM) bioscaffolds has been shown to promote a microenvironment that supports constructive and functional tissue remodeling in both preclinical models and human patients with VML[107,133,163,179,246,247]. Other studies with ECM bioscaffolds in the context of skeletal muscle injury have not shown similar results, but differences in study design, including postoperative rehabilitation protocols, may have contributed to the disparate results[61,226]. *In vitro* and *in vivo* studies have shown that degradation products from ECM bioscaffolds promote a pro-healing, M2-like macrophage phenotype and are chemotactic for stem/progenitor cells[78,199,248,249]. Paracrine factors from these ECM-treated macrophages, in turn, promote chemotaxis and myogenesis of skeletal muscle progenitor cells[78]. However, the spatial and temporal pattern of such events *in vivo* remains only

partially understood in the context of VML. Likewise, although the presence of neurogenic cells at early time points following ECM bioscaffold treatment for various soft tissue applications has been associated with favorable outcomes, the presence of these cells in skeletal muscle applications has not been investigated[108,179,250]. The objective of this study was to quantitatively analyze the spatiotemporal pattern of myogenic and neurogenic progenitor cells and the pattern of macrophage activation following ECM bioscaffold treatment in a mouse model of VML.

6.3 MATERIALS AND METHODS

6.3.1 Overview of experimental design

Thirty-two C57bl/6 mice were randomly divided equally into four treated or four untreated groups. Surgically created volumetric muscle loss was treated with an ECM bioscaffold or left untreated[163]. Animals were sacrificed at 3, 7, 14, and 56 days post implant (4 animals per group per time point). Explants were fixed in 10% neutral buffered formalin (NBF) and immunolabeled for M1 and M2 macrophage phenotype markers iNOS and Fizz1[251,252], strong indicators of the pro-inflammatory vs pro-remodeling macrophage phenotype, respectively. F4/80 was used as a pan-macrophage marker. Perivascular stem cells (CD146+), differentiated myotubes (myosin heavy chain, MHC+), and cells with markers of neurogenesis (β-III tubulin and nestin+) were also identified by immunolabeling. Positively labeled cells were quantified and results compared between groups. All animal studies were approved by the Institutional Animal Care and Use Committee at the University of Pittsburgh. Animal care complied with the National Institutes of Health Guidelines for the Care and Use of Laboratory Animals.

6.3.2 SIS-ECM bioscaffold preparation

The jejunum was harvested from market weight (approximately 240 lbs) pigs and was decellularized via mechanical and chemical methods as previously described to prepare small intestinal submucosa (SIS) ECM[253-255]**.** Decellularized material was lyophilized and milled to form a comminuted form of SIS-ECM with dimensions of approximately 850 and 250 μm^2 which were combined at a ratio of 2:1, respectively and lyophilized to form a 25 x 12.5 x 3 mm powder pillow construct. The pillow was subdivided into smaller pillows with 4 x 4 x 3 mm dimensions at approximately 27.6 $\pm$ 4.5 mg.

6.3.3 Surgical procedure

A 3 x 4 mm defect was made in the mouse quadriceps as previously described[163]**.** Briefly, female C57bl/6 mice (Jackson Laboratories, Bar Harbor, ME) were anesthetized with 1.5-2.5% isoflurane in oxygen and positioned in dorsal recumbency. A 1.5 cm incision was made unilaterally and longitudinally in the epidermis, dermis, and fascia to expose the underlying quadriceps muscle. A 4 x 4 x 3 mm thickness segment was resected from the tensor fasciae latae and the underlying rectus femoris. Marker sutures (7-0 prolene, Ethicon Inc.) were placed to identify the injury site at the time of tissue harvest. Defects were treated with size-matched SIS-ECM powder pillows. Lyophilized single SIS-sheets were positioned over the pillow implant and sutured to native muscle to secure the implant within the defect. The pillow was hydrated using normal saline before dermal closure with 7-0 prolene. All animals survived the surgical procedure and study period without complications.

6.3.4 Explant harvest

Animals were sacrificed at 3, 7, 14, and 56 days via CO_2 inhalation and cervical dislocation. The defect site and adjacent native quadriceps muscle was harvested and fixed in 10% neutral buffered formalin (NBF). Tissue was then embedded in paraffin and cut into 5 um-thick sagittal sections and mounted onto glass slides for Masson's Trichrome staining or for immunolabeling.

6.3.5 Immunolabeling

Tissue sections were deparaffinized with xylene and rehydrated with a graded ethanol series followed by enzymatic antigen retrieval with 0.1% (v/v) trypsin/0.1% (w/v) calcium chloride digestion at 37° C followed by heat-mediated antigen retrieval with citrate buffer (10 mM, pH 6) for 20 minutes at 95-100° C. Tissue sections were exposed to blocking buffer (0.1% Triton X-100, 0.1% Tween-20, 2% bovine serum albumin, 4% goat serum) to reduce nonspecific antibody binding for 1 hour at room temperature. Tissue sections were then incubated in the following primary antibodies diluted in blocking buffer at 4° C for 18 h: (1) rat monoclonal F4/80 (abcam, Cambridge, MA), (2) rabbit polyclonal iNOS (abcam) at 1:200, (3) rabbit polyclonal Fizz1 (Peprotech, Rocky Hill, NJ) at 1:200, (4) mouse monoclonal CD146 (abcam) at 1:350, (5) rabbit polyclonal CD31 (abcam) at 1:200, (6) mouse monoclonal sarcomeric myosin (MF-20, Developmental Studies Hybridoma Bank, University of Iowa) at 1:200, (7) mouse monoclonal beta-3-tubulin (TU-20, Pierce, Rockford, IL) at 1:100, or (8) monoclonal anti-Nestin (EMD Millipore, Darmstadt, Germany) at 1:200. Following primary antibody incubation, tissue was washed with PBS and incubated in secondary antibody at 1:200 dilution: (1) AlexaFluor 488 anti-rat (Invitrogen), (2) AlexaFluor 594 anti-rabbit (Invitrogen), (3) AlexaFluor 488 anti-rabbit

(Invitrogen), or (4) AlexaFluor 594 anti-mouse (Invitrogen) for 1 hour at room temperature. Tissue sections were then washed with PBS and incubated for 5 minutes at room temperature with 4',6-diamidino-2-phenylindole (DAPI) nuclear stain. Following PBS washing, mounting media was applied to each tissue section and slides were cover slipped.

6.3.6 Image analysis

Tissue sections were imaged using a Nikon E600 microscope with a Nuance multispectral imaging system (CRI Inc.) with appropriate fluorescent filter sets. Six images were taken from each biopsy using exposure times that were normalized using isotype and positive controls. These exposure times were maintained for all images taken with the same immunolabel marker and positive controls. Nuance unmixing software was used to remove auto-fluorescence using a high-throughput tunable filter distinctly matched to the bandwidths of the markers. Three 20X fields of view were taken at the interface with native underlying muscle marked by sutures, and three 20X fields of view were taken within the center of the defect, defined as 50% of the distance between the proximal and distal edge of the defect, 50% of the distance between the medial and lateral edges of the defect, and 50% of the distance between the base of the defect and surface of the ECM bioscaffold as measured by Nuance software. CellProfiler image analysis software was used to count positively-labeled cells per field of view.

6.3.7 Statistical analysis

A one-way ANOVA was used for all comparisons between groups with an LSD post-hoc analysis. All statistical analysis used SPSS Statistical Analysis Software (SPSS, IBM, Chicago, IL, USA).

6.4 RESULTS

6.4.1 ECM bioscaffold treatment of VML results in cellular infiltration, neomatrix deposition, and skeletal muscle formation

Masson's trichrome staining shows a change in default mammalian wound healing response following ECM bioscaffold treatment of VML when compared to the untreated group. ECM treatment is characterized by increased cellular infiltration and neomatrix deposition compared to the untreated control (Figure 4).

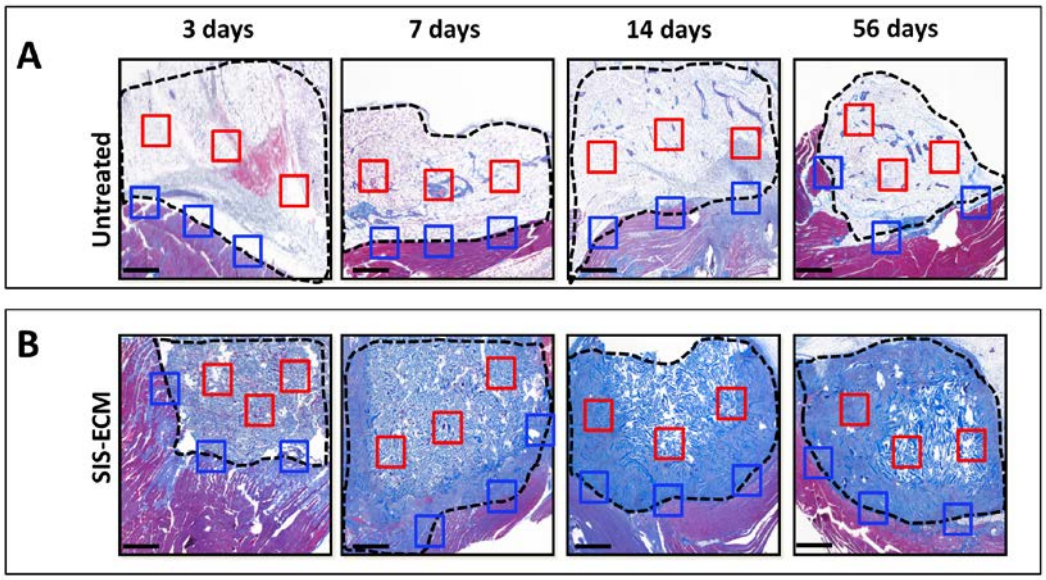

Figure 4. Masson's trichrome staining of VML. (A) Masson's trichrome staining of untreated VML (100X magnification) shows deposition of collagenous tissue, consistent with a critical size defect with no resultant muscle formation.

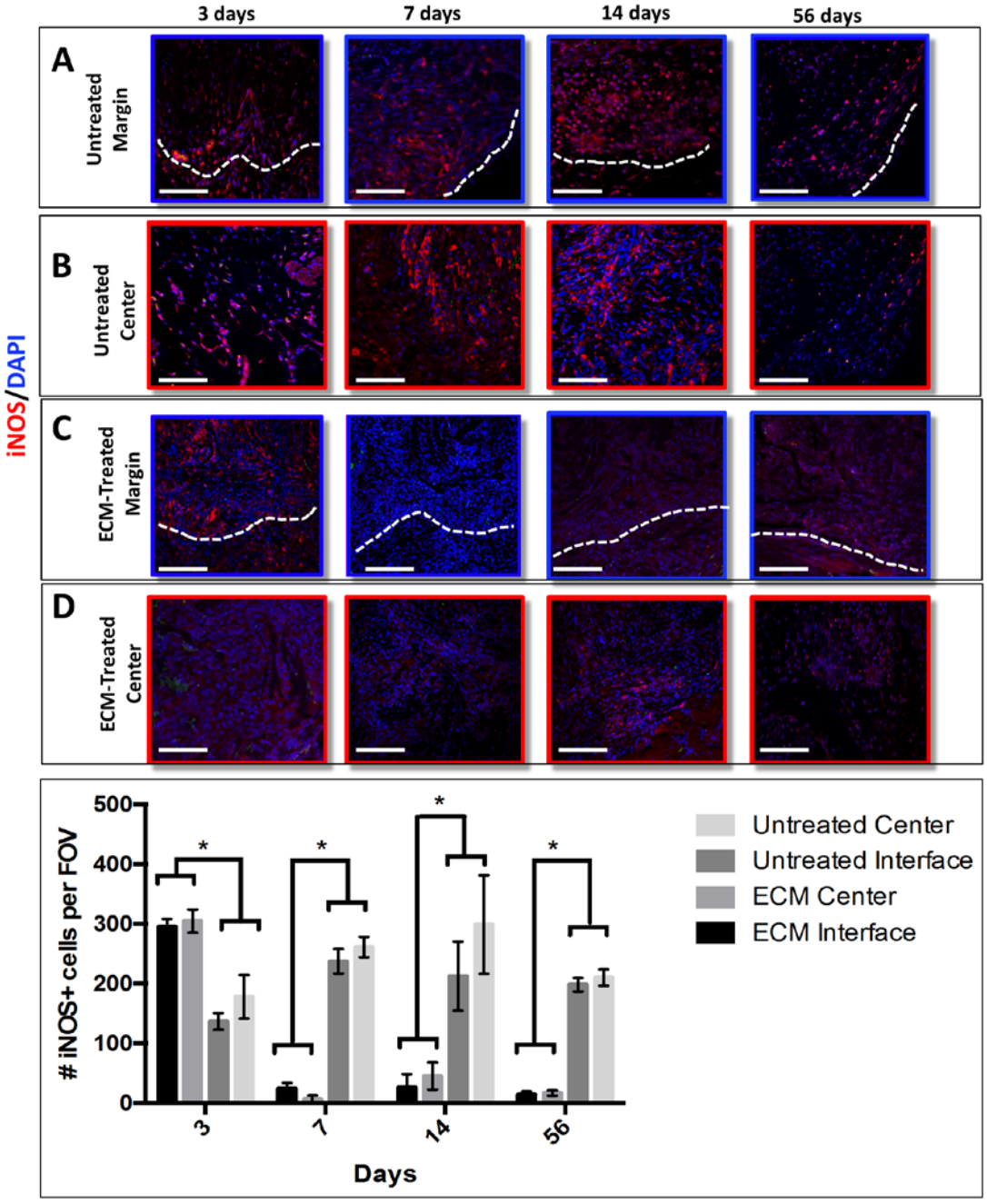

Figure 5 (continued on next page)

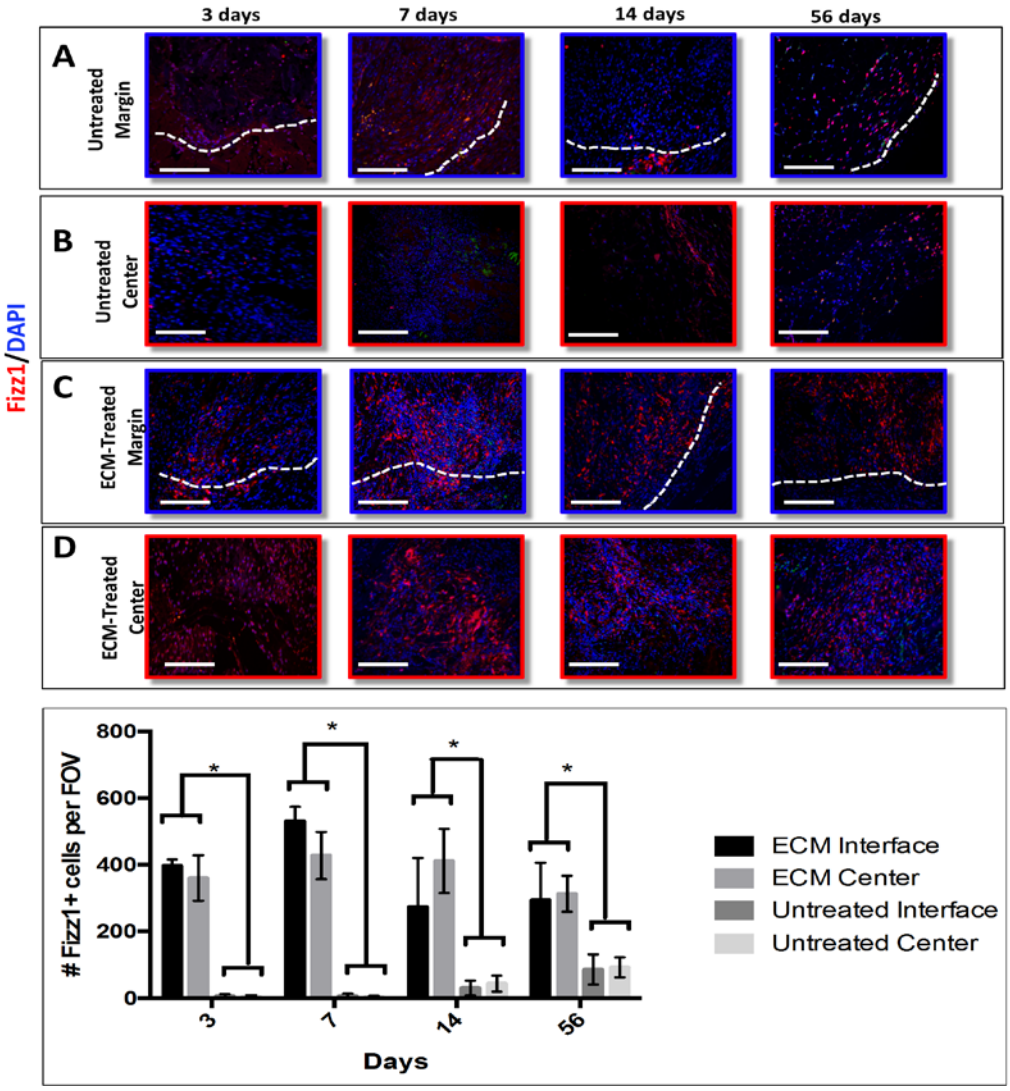

Figure 5. Macrophage polarization (A, B, E, F) When compared to the untreated control which is characterized by a predominant iNOS+ M1-like macrophage population at all time points **(C,D,G,H)**, ECM treatment alters the default response to critical size injury of skeletal muscle from one of a predominant pro-inflammatory, M1-like macrophage activation to the constructive M2-like macrophage phenotype. Spatial quantification shows few differences between the margin and center of the defect within groups, but highlights the contrasting iNOS+ versus Fizz1+ macrophage phenotypes when left untreated or treated with ECM, respectively. Temporal quantification shows that a high number of Fizz1+ cells are present at all time points following ECM treatment, with the highest number occurring at 7 days following injury. Untreated defects are associated with a lower number of infiltrating macrophages with those present being predominantly iNOS+ (Scale bars = 50μm, error bars represent standard deviation, *p<0.05).

6.4.2 Surgically placed SIS-ECM bioscaffolds are associated with a predominant constructive cellular infiltrate

The ECM-treated group shows an early transition from a predominant iNOS+ macrophage activation profile to the Fizz1+ macrophage phenotype. Specifically, after 3 days, both treated and untreated groups show a high percentage of iNOS+ macrophages, characterized by F4/80 and iNOS expression, within the defect site (Figure 5A,C). However, ECM treated injury sites show a large population of Fizz1+ macrophages, characterized by F4/80 and Fizz1 expression, as early as 3 days after implantation (Figure 5C,D). By 7 and 14 days, the total number of macrophages present in ECM injury sites is increased and shows a predominant Fizz1+ macrophage phenotype with low numbers of iNOS+ macrophages (Figure 5). This response is present at both the interface with underlying native muscle and throughout the expanse of the defect site (Figure 5). In contrast, untreated VML sites show a predominant iNOS+ population at all time-points.

6.4.3 ECM bioscaffolds promote PVSC mobilization

Perivascular stem cells are multipotent progenitor cells that are typically found encircling microvessels and capillaries; however, they have the potential to mobilize away from their normal perivascular niche and contribute to remodeling of acute skeletal muscle injury and contribute to the satellite cell pool[43]. In the present study, untreated VML sites show CD146+ perivascular stem cells present at all time-points localized around CD31+ microvessels **(**Figure 6A). These PVSCs are identified mostly along the margin of the defect site near the native underlying muscle. These cells are absent in the granulation tissue and scar tissue within the

center of the untreated defects. In contrast, ECM treatment shows a significant increase in the number of migratory PVSCs, at both the margin and center of the defect (Figure 6B)**.** The number of PVSCs dissociated from the normal perivascular location peaks at 7 days, which coincides with an increase in Fizz1+ macrophages and is sustained through 56 days after implantation (Figure 6D**).**

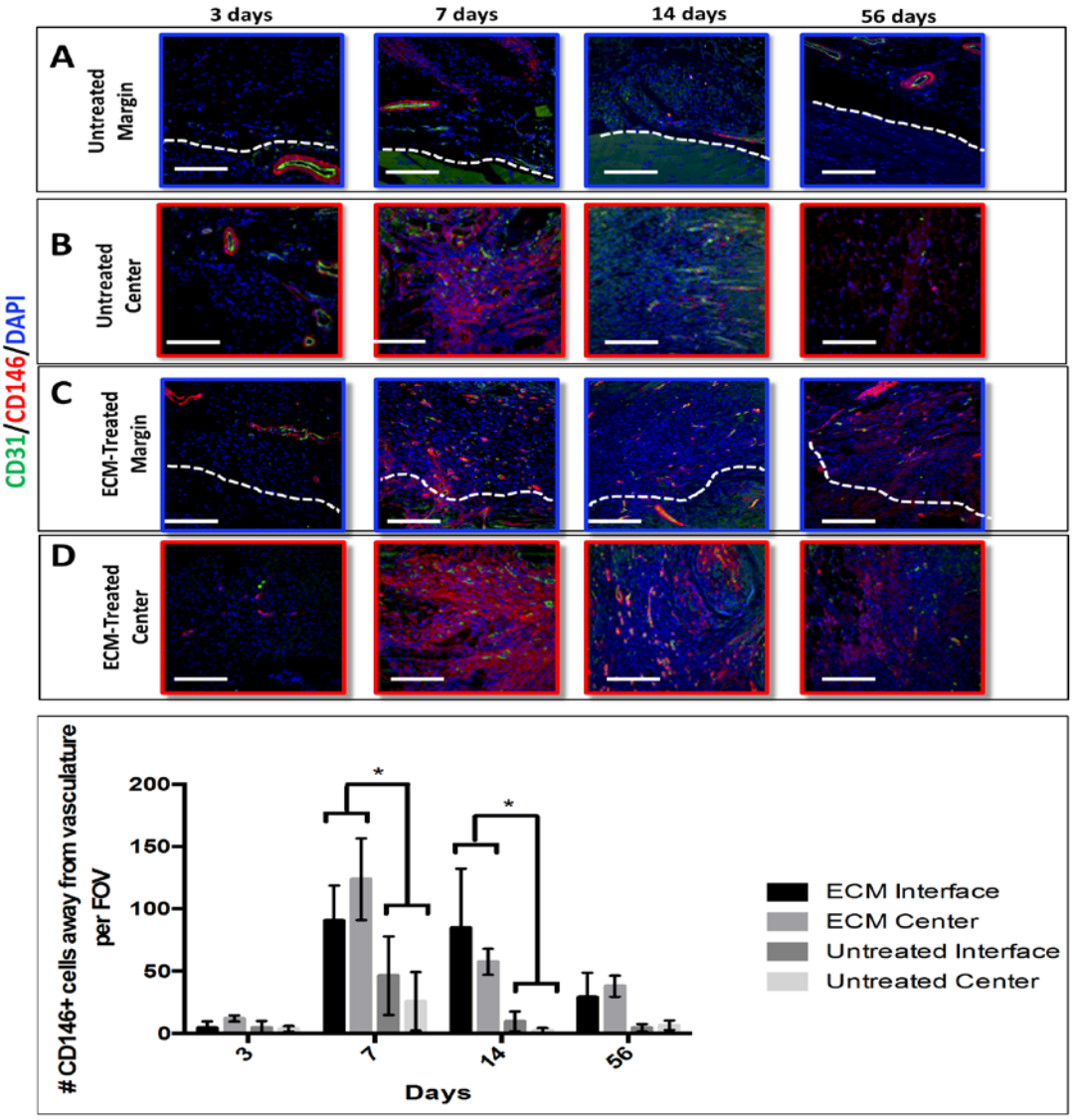

Figure 6. Perivascular stem cell migration. (A-D) CD146+ PVSCs are found in their normal anatomic location adjacent to vessels (CD31+) in both untreated and ECM treated defects. **(A,B)** Without ECM intervention, PVSCs remain vessel associated. **(C,D)** In contrast, ECM-treated defects are populated with PVSCs outside their normal anatomic location, a response that continues at 14 and 56 day time points. These PVSCs are shown to be localized at both the center and margin of the defect. (Scale bars = 50μm, error bars represent standard deviation *p <0.05, PVSC, perivascular stem cell).

6.4.4 ECM bioscaffolds are associated with the presence of neurogenic precursor cells

ECM-treated VML defects show an increase in β-III-tubulin positive cells both along the periphery and within the center of the implantation site (Figure 7B**),** in contrast with minimal presence of such cells in untreated defects (Figure 7A). Nestin+ cells are also present in increased numbers following ECM treatment when compared to the untreated control at early time points of 3, 7, and 14 days (Figure 8B,C). The number of nestin expressing cells diminishes by 56 days however, while β-III-tubulin expressing cells persisted through 56 days after ECM treatment.

6.4.5 Skeletal muscle presence following ECM treatment

Occasional cells showing myotube formation were present in untreated VML sites near the edge of the defect as determined by myosin heavy chain immunolabeling (Figure 9A). In contrast, ECM treatment shows skeletal muscle myotube formation at both the interface with native underlying muscle and within the center of the defect (Figure 9B). Quantification by CellProfiler shows increased MHC+ nuclei in the ECM treated defects when compared to untreated defects and persistence of MHC+ nuclei until the 56-day time point, suggesting ongoing remodeling (Figure 9C, D).

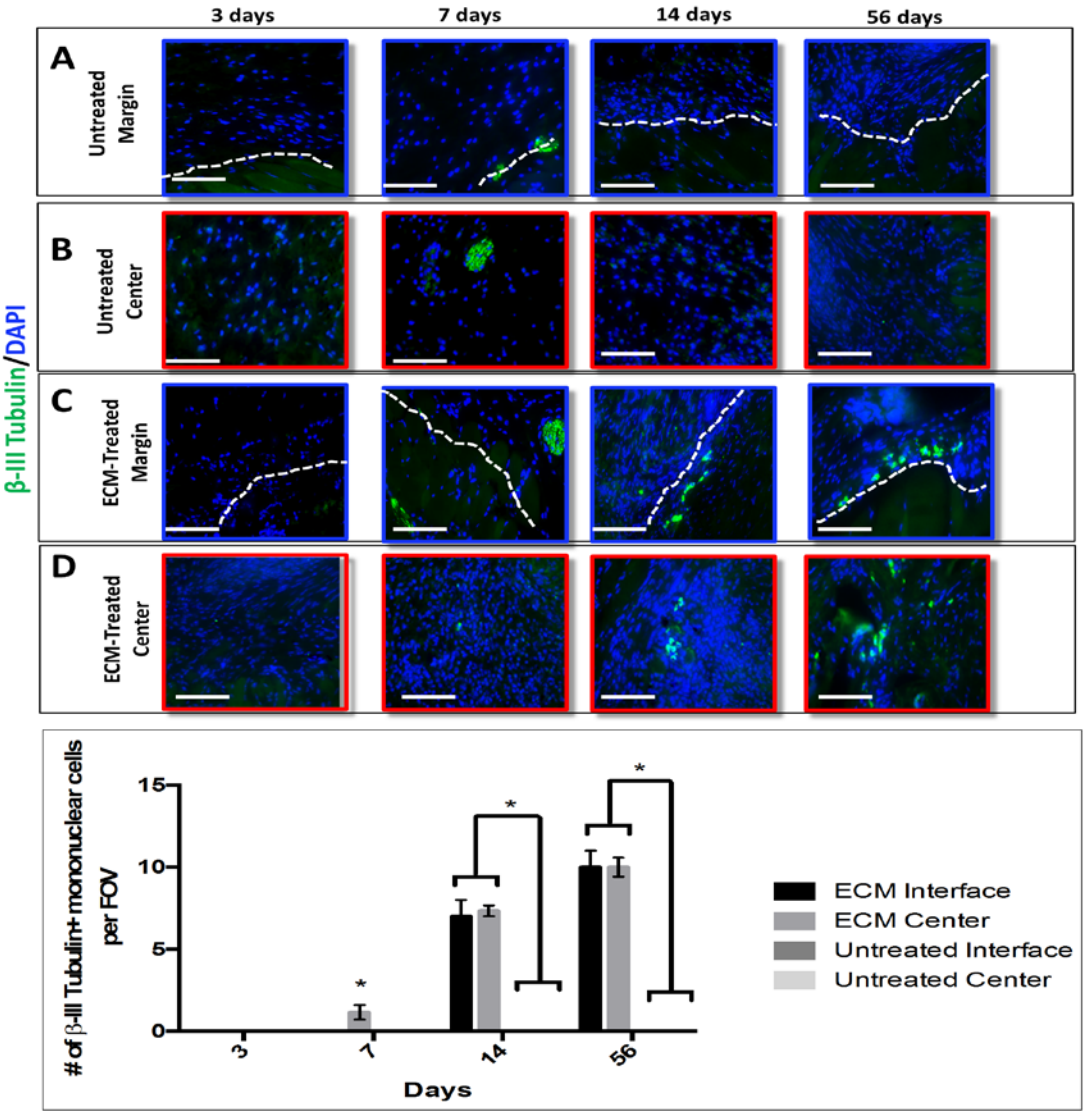

Figure 7. β-III tubulin positive mononuclear cells are present within ECM treated VML defects. (A-D) Cross-sections of β-III tubulin+ nerve fibers are present at the margin of the defect in both treated and untreated VML at early time points. **(C,D)** β-III tubulin+ mononuclear cells are shown at the periphery and also at the center of the defect at 7, 14, and 56 days following ECM treatment, while these cells were absent in untreated defects. This finding may suggest that *de novo* innervation following ECM treatment contributes to functional remodeling outcomes. (Scale bar = 50μm, error bars represent standard deviation, *p <0.05).

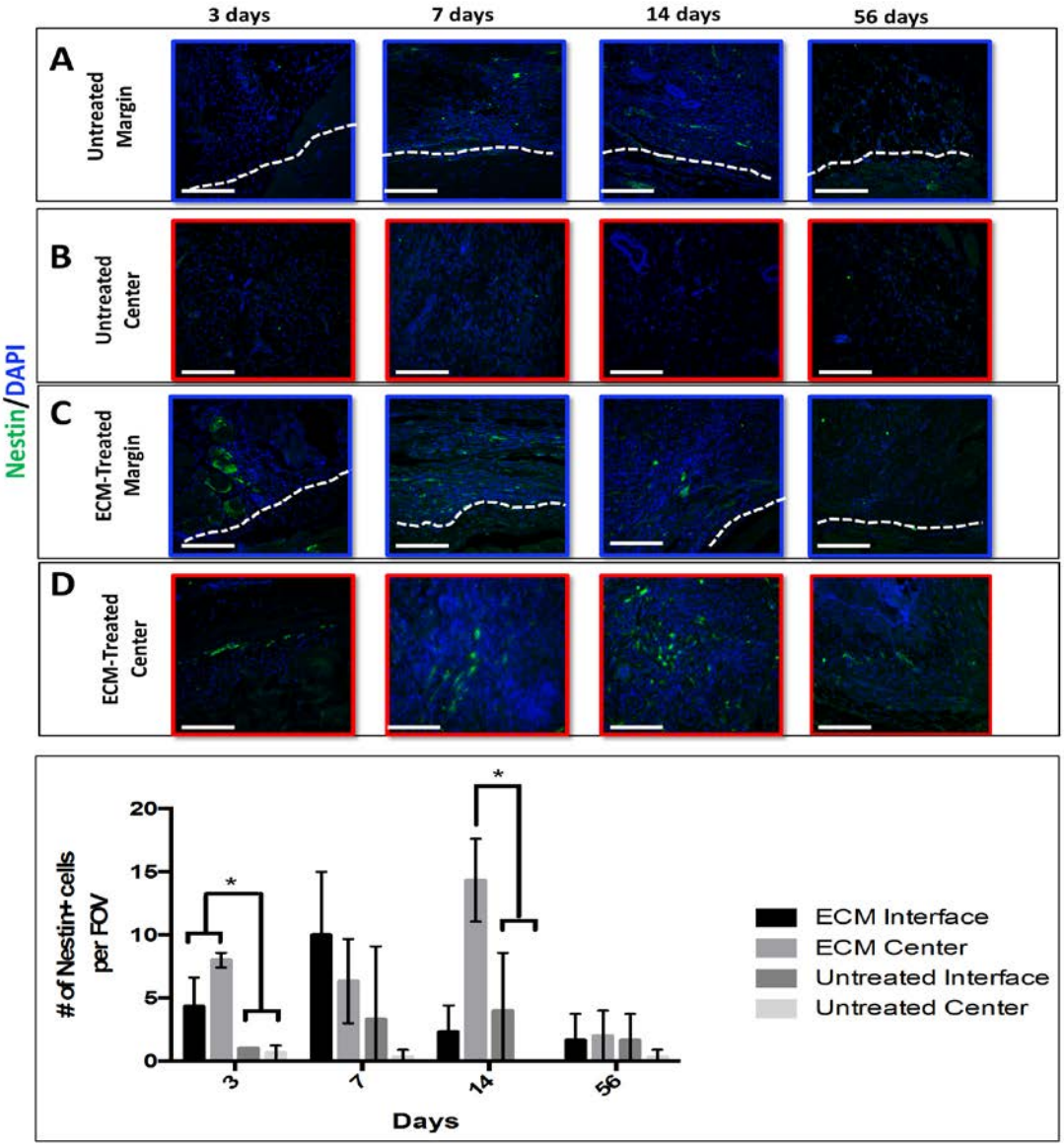

Figure 8. ECM treatment increases numbers of Nestin+ cells (A,B). Untreated VML defects were associated with diminished numbers of nestin+ nuclei when compared to **(C,D)** ECM treated VML. Nestin+ cells were localized at both the interface with native muscle and at the center of the defect following ECM treatment whereas untreated groups showed nestin+ cells mainly confined to the interface. Quantification shows that this result is consistent across all time points from 3 to 56 days post implantation. (Scale bars = 50μm, error bars represent standard deviation, *p <0.05).

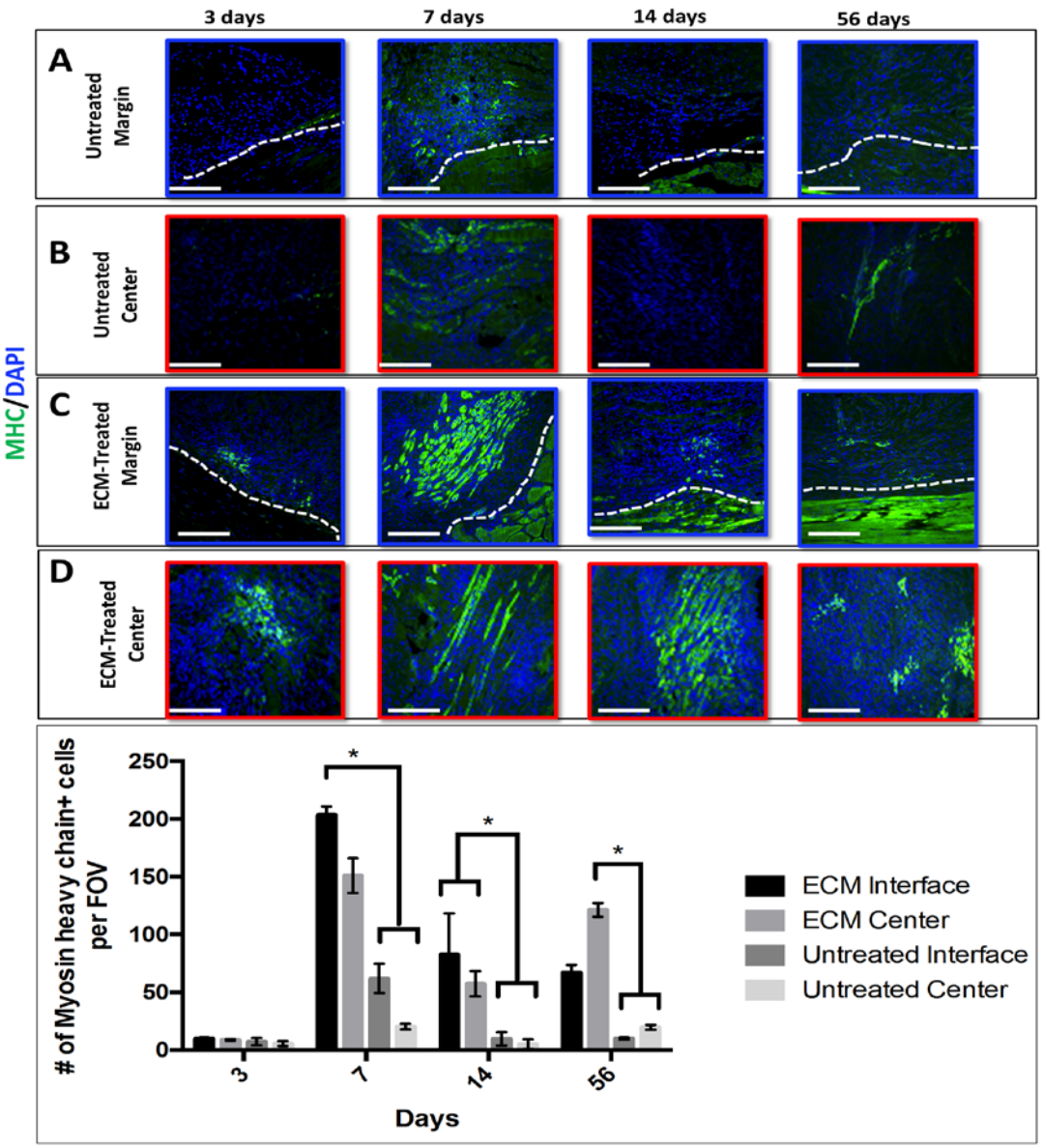

Figure 9. Site appropriate skeletal muscle remodeling by ECM bioscaffolds (A,B) Few signs of MHC+ nuclei resulted after VML was left untreated. **(C,D)** ECM treatment resulted in increased numbers of MHC+ nuclei. Interestingly, these muscle fibers were also located in the center of the defect, suggesting *de novo* myogenesis**.** Temporal averages show increased numbers of MHC+ nuclei at 7, 14, and 56 day time points indicating ongoing remodeling. (Scale bars = 50μm, error bars represent standard deviation, *p <0.05).

6.4.6 The temporal host cellular response of ECM-treated versus untreated VML

Global averages of immunolabeled cells at both the margin and center of treated and untreated defects show that ECM treatment corresponds with an early and robust transition to a Fizz1+ macrophage phenotype which coincides with increased PVSC mobilization and skeletal muscle formation when compared to the predominant iNOS+ macrophage response and diminished progenitor cell populations which occurred when VML was left untreated (Figure 10).

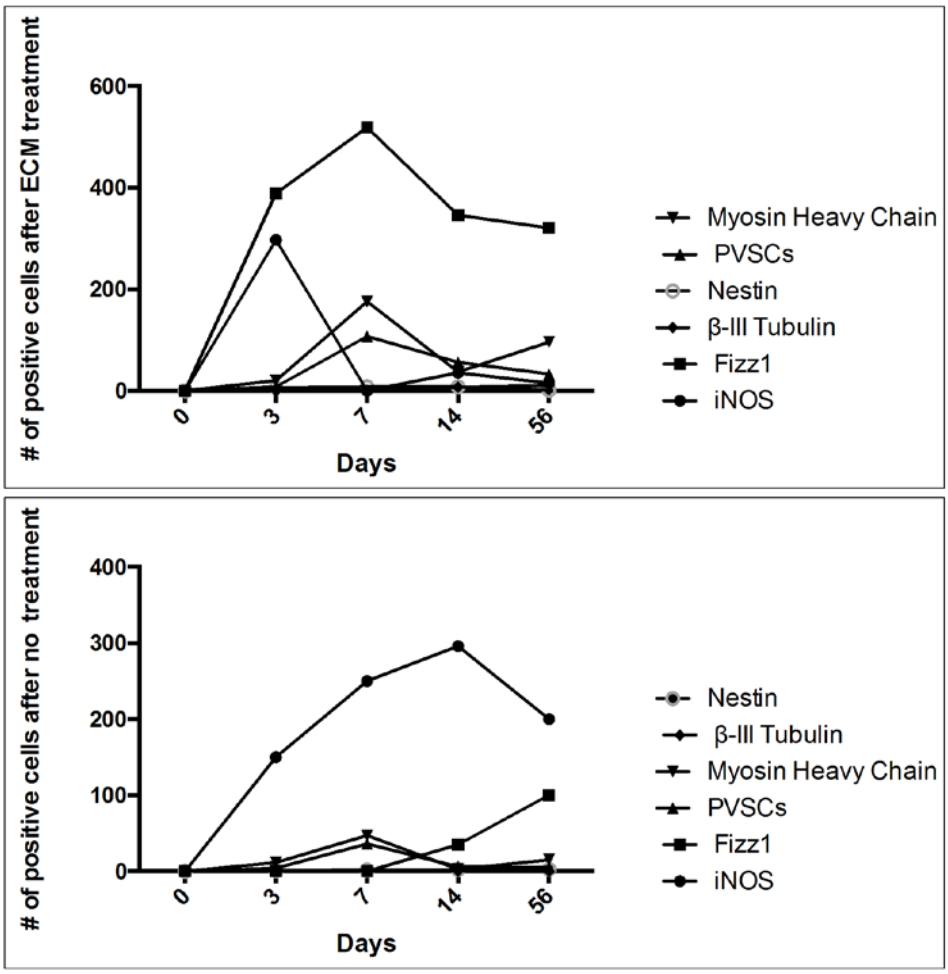

Figure 10. Temporal host macrophage and progenitor cell response following VML. (A) ECM treatment corresponds with an early and robust transition to an M2 macrophage phenotype which coincides with increased PVSC mobilization and skeletal muscle formation when compared to the **(B)** predominant M1 macrophage response which occurs when VML is left untreated. Untreated groups were characterized by lower macrophage numbers overall and lower numbers of PVSCs, neurogenic cell types, and skeletal muscle.

6.5 DISCUSSION

This study advances the findings of previous *in vitro* and *in vivo* studies that ECM treatment facilitates a robust and rapid transition to an M2 macrophage phenotype and an attenuated M1 macrophage phenotype. This phenomenon has not been previously shown to be a part of the response to VML when treated with ECM bioscaffolds. Such a mechanism likely contributes to downstream functional skeletal muscle remodeling, as it has been shown that failure of the phenotypic switch of macrophages results in impaired muscle regeneration[13]. Recent *in vitro* work has shown that macrophages activated by exposure to ECM degradation products are able to induce myogenic progenitor cell chemotaxis and differentiation[78]. Although the ability of macrophages to exert paracrine effects upon resident stem/progenitor cells *in vivo* has previously been shown, and the resulting feedback from macrophage-progenitor cell crosstalk may contribute to a sustained M2 macrophage response and differentiation of such stem cells[27], the source of signals that promote these events has not been identified. Results of this study suggest that ECM-derived signals may contribute to such events.

One progenitor cell population known to contribute to skeletal muscle remodeling and myogenesis is the PVSC. PVSCs, typically found encircling microvessels and capillaries, are multipotent stem cells that have myogenic potential. ECM implantation in this study was characterized by a robust accumulation of CD146+ PVSCs away from their normal vessel-associated location, implicating their participating in remodeling. Importantly, these cells were evident both at the interface of the ECM bioscaffold with native uninjured muscle and at the

center of the ECM bioscaffold. In contrast, untreated defects showed very few PVSCs migrating away from vessels, the majority of which remained encircling CD31+ vasculature. ECM alone has been shown to be conducive to PVSC growth *in vitro*[175,256,257], and these cells have also been shown to be responsive to ECM-polarized macrophages with enhanced chemotactic and myogenic potential[43,256]. PVSCs have been implicated as key contributors to constructive and functional remodeling following VML[107]. Whether such cells are instructed by ECM itself or through permissive ECM-macrophage signaling, or both, warrants further investigation.

Innervation is an essential component of tissue development and also a requirement of functional muscle recovery. Innervation is obviously required for voluntary contractility and motor coordination. VML often results in denervation atrophy of the associated muscle, which leads to functional impairment[258-260]. Previous work has shown the functional innervation via needle electromyography in remodeled ECM when used for VML treatment[107], though the mechanisms responsible for this response have not been investigated. This study corroborates and extends these findings, and shows an early presence and a persistence of β-III-tubulin-positive cells as a part of ECM-mediated remodeling in the skeletal muscle location. A population of β-III tubulin positive mononuclear cells was present in both the center of the ECM-treated defect and at the interface with native muscle. ECM treatment was also characterized by an increase in nestin positive cells at both the interface and center of the defect. The currently accepted innervation paradigm of skeletal muscle following minor muscle injury involves outgrowth of neurons from existing tissue. Whether or not the population of mononuclear β-III tubulin positive cells or nestin positive cells within the center of the defect contributes to *de novo* innervation in this model of VML warrants further investigation. Nestin positive cells have been shown to retain differentiation potential to become motor neurons[261]. It should be noted,

however, that developing myofibers have also been shown to transiently express nestin during development of myotendinous and neuromuscular junctions[262,263].

Analysis of the spatial and temporal distribution pattern of specialized progenitor cell types following ECM treatment, while not conclusive, contributes to an understanding of the pattern of ECM-mediated skeletal muscle remodeling. Temporally, macrophages dominate the cellular infiltrate at 3-, 7-, and 14-day time points in both ECM treated and untreated defects though their phenotype was clearly different between groups. In the ECM-treated groups, there was little difference in the number of PVSCs and myoblasts present at the interface versus the center of the defect, which was notably different from the pattern of PVSC presence in the untreated groups at any time point. Whether or not the response seen in the ECM-treated site is the same or similar to *classical* muscle fiber regeneration has not been determined. Regardless, the ability of ECM to promote site-appropriate tissue formation (i.e. the formation of myoblasts throughout the defect site) is promising, and is reflected in the functional and electromyographical improvements observed in clinical ECM-mediated remodeling[107,246,264].

There are several limitations to this study. Although macrophages are known to be a plastic cell population capable of phenotypic heterogeneity, the analysis described herein utilizes only two markers to characterize the extremes of the macrophage phenotypic spectrum (iNOS and Fizz1). Utilization of multiple markers and functional assays could allow for a more comprehensive analysis of macrophage phenotype. Additionally, while cells expressing neuron-associated markers were evident by immunolabeling techniques, functional improvement was not determined at each time point. It would be interesting to assess functional innervation at the studied time points to determine whether there is a correlation between function and histologic presence of neurogenic cell types in the VML remodeling site. Finally, while islands of skeletal

muscle were evident in later time points, scaffold degradation was not complete at 56 days. This study utilized a powder pillow construct to entirely fill the VML defect. Clinical studies, in contrast, have utilized a sheet form of ECM bioscaffolds. It is likely that the higher surface area of the powder pillow construct resulted in a slower degradation rate in this model, compared to the relatively rapid degradation rate seen in the clinical use for VML[102,104,246]. A longer duration study will help to determine whether ECM-associated myogenesis seen in this study can contribute to formation of functional contractile skeletal muscle tissue deposition.

6.6 CONCLUSIONS

This study shows that when implanted in a mouse model of VML, ECM bioscaffolds change the default response to injury and facilitate a constructive remodeling outcome. This response is characterized by a rapid and predominant M2 macrophage activation profile, increased mobilization of endogenous PVSCs, the presence of cells showing neural differentiation markers, and the presence of skeletal muscle myoblast differentiation and site-appropriate tissue deposition. The ability of an ECM bioscaffold to influence the local skeletal muscle injury microenvironment allows for synergy and cross-talk among key immune regulators and skeletal muscle progenitor cells, the spatiotemporal distribution of which is associated with *de novo* skeletal muscle formation and site-appropriate remodeling.

6.7 ACKNOWLEDGEMENTS

The authors would like to thank Lori Walton and the McGowan Histology Center for histologic section preparation. J.D. was partially supported by the National Science Foundation Graduate Research Fellowship.

7.0 SOLUBILIZED EXTRACELLULAR MATRIX BIOSCAFFOLDS DERIVED FROM DIVERSE SOURCE TISSUES DIFFERENTIALLY INFLUENCE MACROPHAGE PHENOTYPE[4]

7.1 ABSTRACT

The host response to biomaterials is a critical determinant of their success or failure in tissue-repair applications. Macrophages are among the first responders in the host response to biomaterials and have been shown to be predictors of downstream tissue remodeling events. Biomaterials composed of mammalian extracellular matrix (ECM) in particular have been shown to promote distinctive and constructive remodeling outcomes when compared to their synthetic counterparts, a property that has been largely attributed to their ability to modulate the host macrophage response. ECM bioscaffolds are prepared by decellularizing source tissues such as dermis and small intestinal submucosa. The differential ability of such scaffolds to influence macrophage behavior has not been determined. The present study determines the effects of ECM bioscaffolds derived from eight different source tissues upon macrophage surface marker expression, protein content, phagocytic capability, metabolism, and antimicrobial activity. The results show that macrophages exposed to small intestinal submucosa (SIS), urinary bladder

[4] Portions of this chapter were adapted from the following publication:
Dziki JL, Wang DS, Pineda C, Sicari BM, Rausch T, Badylak SF. Solubilized extracellular matrix bioscaffolds derived from diverse source tissues differentially influence macrophage phenotype. *Journal for Biomedical Materials Research Part A.* July 2016. DOI:10.1002/jbm.b.35894

matrix (UBM), brain ECM (bECM), esophageal ECM (eECM), and colonic ECM (coECM) expresses a predominant M2-like macrophage phenotype, which is pro-remodeling and anti-inflammatory (iNOS-/Fizz1+/CD206+). In contrast, macrophage exposure to dermal ECM resulted in a predominant M1-like pro-inflammatory phenotype (iNOS+/Fizz1-/CD206-), whereas liver ECM (LECM) and skeletal muscle ECM (mECM), did not significantly change the expression of these markers. All solubilized ECM bioscaffold treatments resulted in an increased macrophage antimicrobial activity, but no differences were evident in macrophage phacoytic capabilities and macrophage metabolism was decreased following exposure to UBM, bECM, mECM, coECM, and dECM. The present work could have imporatn implications when considering the macrophage response following ECM implantation for site-appropriate tissue remodeling.

7.2 INTRODUCTION

The use of biomaterials for the repair or reconstruction of damaged or diseased tissues is commonplace across a wide range of clinical applications. The success (i.e., safety and efficacy) or failure of these biomaterials is dependent, in large part, upon the host tissue response following implantation. The host innate immune response, especially the macrophage response, is a critical determinant of downstream tissue remodeling outcomes. Macrophages represent a cell population with heterogenous phenotypes that are involved in a variety of biologic processes including tissue homeostasis, inflammation, disease progression, and functional tissue reconstruction. Macrophages are among the first responders to pathogens, tissue injury, and also, implanted biomaterials[76,100,265,266]. Macrophage phenotypes have been classified along a

spectrum ranging from M1 or pro-inflammatory cells to M2 or pro-healing and regulatory cells. These various phenotypes can be distinguished by cell surface markers, associated cytokines and effector molecules, and functional activity including nitric oxide (NO) production or orthinine synthesis, respectively[267,268], among others.

Biomaterials have been manufactured from both synthetic and biologic substrates and each has their associated advantages and disadvantages[62]. Of relevance to the present study, biologic scaffolds composed of mammalian extracellular matrix (ECM) are associated with a constructive remodeling outcome following injury, as opposed to fibrosis or the classic foreign body reaction, and have been used in many clinical applications including dermal[269-271], cardiac[272], musculoskeletal[107,273-275], and gastrointestinal repair[102]. The host macrophage phenotypic response was shown to be a determining factor in ECM bioscaffold-mediated remodeling outcomes[78]. In turn, scaffold preparation and processing methods were shown to have a profound influence upon macrophage phenotype in a study utilizing small intestinal submucosa (SIS) ECM as a body wall repair device[98]. Subsequent studies have confirmed and expanded the importance of macrophage phenotype in biomaterial-mediated tissue remodeling[196,276-280]. Specifically, it has been shown that the process of ECM-mediated tissue remodeling relies upon the infiltration and activation of host macrophages toward an immunomodulatory, M2-like phenotype[76,100] and that a higher M2/M1 ratio at early time points is indicative of a favorable, constructive remodeling outcome at later time points. Although it has been shown that pepsin-solubilized SIS-ECM bioscaffolds activate macrophages toward an M2-like phenotype, with increased Fizz1 and CD206 expression[78], the mechanisms by which ECM bioscaffolds directly affect macrophage phenotype remain poorly understood.

ECM bioscaffolds have been prepared from many source tissues including small intestine[212], urinary bladder[194], brain[184,281], esophagus[257], liver[282], skeletal muscle[208], and dermis[192], among others, but the differential effects of these bioscaffolds upon macrophage phenotype have not been characterized. The objective of the present study is to characterize the phenotype of macrophages exposed to a variety of ECM scaffold materials, each of which is derived from a different source tissue. Phenotypic analysis includes surface marker profile, protein expression, viability, metabolic activity, phagocytic capacity, and antimicrobial activity. The findings of this study may influence the choice of ECM bioscaffolds for clinical use.

7.3 MATERIALS AND METHODS

7.3.1 Overview of experimental design

ECM bioscaffolds were prepared from porcine tissues utilizing established protocols in accordance with previously established decellularization guidelines[283]. Murine bone-marrow derived macrophages were treated with pepsin-solubilized ECM bioscaffolds, and then harvested to analyze surface marker expression via immunolabeling, protein expression via western blotting, cell integrity by trypan blue exclusion, MTT metabolism, phagocytic capability, and antimicrobial activity.

7.3.2 Preparation of solubilized ECM bioscaffolds

Biologic scaffolds composed of porcine small-intestinal submucosa (SIS), urinary bladder matrix (UBM), skeletal muscle ECM (mECM), brain ECM (bECM), esophageal ECM (eECM), dermal ECM (dECM) liver ECM (LECM), and colon ECM (coECM), were prepared following previously established decellularization protocols (Table 4). All scaffold materials met stringent requirements for sufficient decellularization; specifically, no visible intact nuclei by DAPI and hematoxylin and eosin (H&E) staining, remnant DNA concentration less than 50 ng/mg total scaffold dry weight, and DNA fragment length less than 200 base pairs. Scaffolds were lyophilized and milled to form a particulate powder. The powder was then solubilized with pepsin as previously described for the preparation of an ECM hydrogel to yield a 10 mg/ml solution of solubilized ECM. The solubilized ECM was then neutralized by addition of one-tenth digest volume of 0.1 N NaOH and one-ninth digest volume of 10X PBS to bring pH to 7.4, phosphate buffer to 0.01 M, and sodium chloride concentration to 0.15M.

Table 4. Overview of decellularization protocols

ECM Bioscaffold	Decellularization Method	Reference
Small intestinal submucosa (SIS)	Mechanical removal of muscular layers followed by 0.1% peracetic acid and water washes	Badylak SF. Tissue Eng. 1993..
Urinary bladder matrix (UBM)	Mechanical removal of surrounding muscular layers followed by 0.1% peracetic acid and water washes.	Freytes DO et al. J Biomed Mater Res B Appl Biomater. 2006.
Skeletal muscle ECM (mECM)	Mechanical removal of fat and connective tissue, washes with 2:1 (v/v) chloroform:methanol, graded ethanol series, 0.02% trypsin/0.05% EDTA, 2% deoxycholate, 1% Triton X-100, 0.1% peracetic acid, and water	Wolf et al. Biomaterials. 2012.
Brain ECM (bECM)	Mechanical removal of dura matter, water wash, washes with 0.02% trypsin/0.05% EDTA, 3.0% Triton X-100, 1.0 M sucrose, 4.0% deoxycholate, and 0.1% peracetic acid	Crapo et al. Biomaterials. 2012.
Esophageal ECM (eECM)	Mechanical removal of mucsularis layer,, washes with 1% trypsin/0.05% EDTA, 1.0 M sucrose, 3% Triton X-100, 10% deoxycholate, 0..1% peracetic acid, 4% ethanol, 100 U/ml DNAse, water, and PBS	Keane et al. Biomaterials. 2013.
Dermal ECM (dECM)	Mechanical removal of fat, connective tissue, and epidermis, washes with 0.25% trypsin, 70% ethanol, 3% H_2O_2 1% Triton X-100, 0.26% EDTA/0.69% Tris, water, 0.1% peracitic acid/0.4% ethanol, and PBS	Reing et al. Biomaterials. 2013.
Liver ECM (LECM)	Mechanical slicing / massage to aid cell lysis followed by washes with 0.02% trypsin/0.05% EDTA, 3% Triton X-100, 4% deoxycholate, and water	Sellaro et al. Tissue Eng. 2007.
Colonic ECM (coECM)	Mechanical isolation of submucosa, washes with 2:1 (v/v) chloroform:methanol, graded ethanol series, 0.02% Trypsin/0.05% EDTA, 4% deoxycholate, 0.1% peracetic acid/4% ethanol, and water	Keane et al. J Biomed Mater Res B Appl Biomater. 2015.

7.3.3 SDS PAGE analysis

Protein composition of each of the solubilized ECM from the various tissues was compared qualitatively using SDS PAGE and a See Blue Pre-stained Molecular Weight Marker (Invitrogen). Five (5) ug of each ECM was added to a 4-20% polyacrylamide gel and run at 120V for two hours. The gels were stored in fixing buffer overnight and then stained with a Pierce Silver Stain for Mass Spectrometry Kit (Life Technologies) following the manufacturer's instructions.

7.3.4 Macrophage isolation and polarization

Mouse bone marrow was harvested as previously described[78,284]. Briefly, female 6 to 8 week old C57bl/6 mice (Jackson Laboratories, Bar Harbor, ME) were euthanized via CO_2 inhalation and cervical dislocation. Aseptically, the skin from the proximal hind limb to the foot was removed, the tarsus and stifle disarticulated, and the tibia isolated. The coxafemoral joint was disarticulated for isolation of the femur. After removal of excess tissue, bones were kept on ice and rinsed in a sterile dish containing macrophage complete medium consisting of DMEM (Gibco, Grand Island, NY), 10% fetal bovine serum (FBS) (Invitrogen, Carlsbad, CA), 10% L929 supernatant, 50 uM beta-mercaptoethanol (Gibco), 100 U/ml penicillin, 100 ug/ml streptomycin, 10 mM non-essential amino acids (Gibco) and 10 mM hepes buffer**.** The ends of the bones were transected and the marrow cavity was flushed with complete medium to collect bone marrow. Cells were washed, plated at 2 x 10^6 cells/ml, and allowed to differentiate into macrophages for 7 days at 37°C, 5% CO_2 with complete medium changes every 48 hours as

previously described[285]. After 7 days, resulting naïve macrophages were treated with basal medium consisting of 10% FBS, 100 ug/ml streptomyocin, 100 U/ml penicillin in DMEM and one of the following conditions as previously described: (1) 20 ng/ml IFNγ and 100 ng/ml of LPS to promote an M1-like phenotype, (2) 20 ng/ml IL-4 to promote an M2-like phenotype, (3) 200 ug/ml of pepsin control buffer, or (4) 200 ug/ml of ECM for 18 hours at 37°C, 5% CO_2.

7.3.5 Immunolabeling

After 18 hours, macrophages were washed and fixed with 2% paraformaldehyde. Following PBS washes, cells were incubated in blocking solution consisting of 0.1% Triton-X 100, 0.1% Tween 20, 4% normal goat serum, and 2% bovine serum albumin (BSA) for 1 hour at room temperature to prevent non-specific antibody binding. The following primary antibodies were diluted in blocking solution: (1) monoclonal anti-F4/80 (Abcam, Cambridge, MA) at 1:200 dilution for a pan-macrophage marker, (2) polyclonal anti-iNOS (Abcam, Cambridge, MA) at 1:100 dilution for an M2 marker, and (3) polyclonal anti-Fizz1 (Peprotech, Rocky Hill, NJ) for an M2 marker[287-289]. Cells were incubated in primary antibodies for 16 h at 4°C. After PBS washes, cells were incubated in fluorophore-conjugated secondary antibodies (Alexa Fluor donkey anti-rat 488 or donkey anti-rabbit 488, Invitrogen) for 1 hour at room temperature. After PBS washes, nuclei were counterstained with 4’6’diamidino-2-phenylindole (DAPI) prior to imaging three 200X fields containing on average 900 cells each, using a live-cell microscopes. Light exposure times were standardized to a negative isotype control and kept constant across images. Images were quantified utilizing CellProfiler Image Analysis software to obtain positive F4/80, iNOS, and Fizz1 percentages.

7.3.6 Western blotting

After treatment with cytokines or ECM, macrophages were lysed for western blot analysis. Cell lysates were diluted 1:1 in 2x Laemmili sample buffer with 5% beta-mercaptoethanol. Twenty (20) ug of protein was loaded per well in 4-20% Bio-Rad Mini-PROTEAN TGX Stain-Free polyacrylamide gels. Gels were run at 100 V for 15 minutes and then 150 V in 1X running buffer (30.3 g Tris, 144 g glycine, 10 mL 10% SDS solution in water). Separated proteins were transferred to Immobilon-P polyvinylidene difluoride (PVDF) membranes for 3 hours at 150 mA in transfer buffer (10% 10X running buffer, 20% methanol, 70% water). The membranes were then incubated in blocking buffer (5% BSA and 0.1% Tween-20 in TBS) for one hour to prevent non-specific antibody biding. Membranes were incubated in primary antibodies for 16 hours at 4°C at a 1:500 dilution for M1-like iNOS (abcam, Cambridge, MA) and M2-like CD206 (abcam) in 0.5% BSA and 0.1% Tween-20 in TBS**.** Membranes were washed 0.1% Tween-20 in TBS and incubated with horseradish peroxidase secondary antibodies applied at 1:5000 in 0.5% BSA and 0.1% Tween-20 in TBS. Five (5) mL Bio-Rad Western ECL solution (Bio-Rad, Hercules, MA) was applied to each membrane for five minutes before imaging. Densitometry was calculated with ImageJ software.

7.3.7 Cell viability

Macrophage viability following treatment with ECM was evaluated using the trypan blue exclusion assay[290]. Exposed macrophages were washed with PBS and harvested with Accutase® (Stem Cell Technologies, Vancouver, CA) solution for 10 minutes, followed by inactivation with medium containing 10% FBS. Trypan blue solution (0.4% w/v) was mixed in a proportion 1:1

with the cell suspension. The number of viable cells (trypan blue excluded) and non-viable cells (trypan blue included) were determined using a hemocytometer. The percentage of cells showing trypan blue exclusion was determined dividing the amount of trypan blue excluding cells by the total number of cells.

7.3.8 Macrophage metabolism

Metabolism of exposed macrophages to the tissue-specific ECM was measured using the MTT assay (Vibrant®MTT Cell Proliferation Assay Kit, V-13154, Molecular Probes, Eugene, OR) following the manufacturer instructions with slight modifications. Briefly, $1*10^5$ bone marrow derived cells were plated and differentiated into macrophages as previously described. Macrophages were treated with 200 ug/ml of ECM or cytokine controls for 18 hours at 37°C, 5% CO_2. After treatment, macrophages were washed with PBS and incubated with 1.2 mM MTT (3-(4,5-dimethythiazol-2-yl)-2,5-diphenyltetrazolium bromide) solution for 2 hours. The straight-line equation from the standard curve was used to interpolate the concentration of cells reducing the MTT after the exposure to the ECM digests. As $1*10^5$ cells were initially seeded, the value is presented as the percentage of reducing cells relative to the initial value ($1*10^5$ cells).

The formazan produced by reduction of the MTT was diluted with 50 ul of dimethyl sulfoxide (DMSO) and its concentration determined by optical density at 540 nm. The metabolic activity of macrophages was calculated from a standard curve. Results were presented relative to untreated (MCSF only) macrophages.

7.3.9 Phagocytosis

The ability of macrophages to phagocytose fluorescent latex microspheres was evaluated as previously described with some modifications. After treatment of $1*10^6$ bone marrow-derived macrophages with 200 ug/ml of ECM or cytokine controls for 18 hours, macrophages were rinsed with PBS and incubated with $4.55*10^7$ particles/ml of Fluoresbrite YG Microspheres 1.00 um (Polysciences, Warrington, PA) in complete medium for 15 minutes at 37°C, 5% CO_2. After incubation with microparticles, macrophages were washed with PBS and harvested with Accutase® solution. Cells were centrifuged and rinsed with PBS followed by a counterstain with viability dye eFluor 780 (eBioscience, San Diego, CA) at a dilution of 1:1000. A non-phagocytic cell line, C2C12 mouse myoblasts, was used as a negative control. The percentage of phagocytic macrophages was determined by flow cytometry.

7.3.10 Antimicrobial activity

ECM bioscaffolds from each tissue-type were exposed to proliferating *Staphylococcus aureus (S. aureus*) bacteria for evaluation of antimicrobial activity as previously described[200]. Briefly, an isolated colony of *Staphylococcus aureus* (American Type Culture Collection 29213, clinical isolate) grown on tryptic soy agar was used to inoculate 10 m of tryptic soy broth. The bacteria were expanded in suspension overnight on a rotary shaker at 37ºC. The bacteria were then diluted to 5 x 10^5 CFU/ml, and 150 ml of bacterial suspension were added to each well of a 96-well microplate; ECM was added at a concentration of 200 ug/ml to the bacterial suspension. Secreted products of ECM-treated macrophages were derived using the following method: macrophages were treated for 18 hours with solubilized ECM or cytokine controls as described.

After 18 hours, cells were washed with PBS and medium was replaced with serum free, antibiotic free, ECM-free medium for 5 hours, after which time the medium was collected and was diluted at a 1:1 ratio with broth. Samples tested included solubilized ECM from each tissue type, a negative control of medium alone, and pepsin as a carrier control. Each sample was tested in triplicate. The bacterial growth in each well was monitored over the course of 24 h using absorbance readings at 570 nm with a BioRad 680 microplate reader.

7.3.11 Statistical analysis

A one-way ANOVA was used for all comparisons between groups with an LSD post hoc analysis. All statistical analysis used SPSS Statistical Analysis Software (SPSS, IBM, Chicago, IL, USA). Error bars represent standard deviation.

7.4 RESULTS

7.4.1 ECM bioscaffolds derived from different source tissues have distinct compositions

SDS PAGE gel analysis of solubilized ECM bioscaffolds show distinct banding patterns following silver stain, indicating that ECM bioscaffolds derived from different source tissues have distinct compositions (Figure 11).

7.4.2 ECM differentially affects macrophage surface marker expression

Immunolabeling for indicators of the M1 or M2 phenotype using iNOS and Fizz1, respectively shows that ECM bioscaffolds derived from different source tissues promote different expression patterns (Figure 12A). Specifically, SIS-ECM, UBM, bECM, eECM, and coECM promote a predominant Fizz1+ (M2-like) macrophage phenotype with minimal iNOS expression (Figure 12B). Conversely, dECM shows a predominant iNOS+ (M1-like) phenotype (Figure 12B). mECM and LECM do not show significant increases in iNOS or Fizz1 expression when compared with untreated controls (Figure 12B).

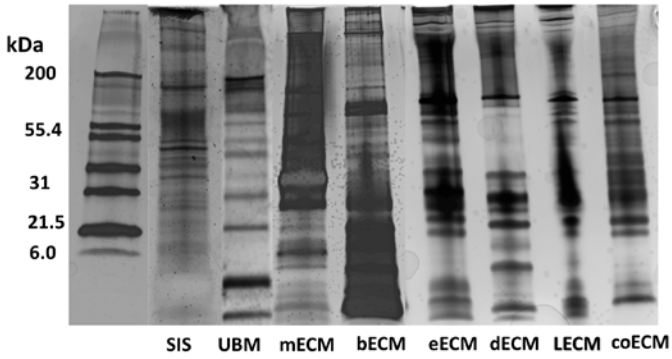

Figure 11. SDS PAGE gel analysis of ECM degradation products. Degradation products of ECM bioscaffolds derived from different source tissues were separated using SDS PAGE gel electrophoresis and show distinct banding patterns. (SIS=small intestinal submucosa, UBM=urinary bladder matrix, mECM=skeletal muscle ECM, bECM= brain ECM, eECM = esophageal ECM, dECM= dermal ECM, LECM= liver ECM, coECM = colonic ECM).

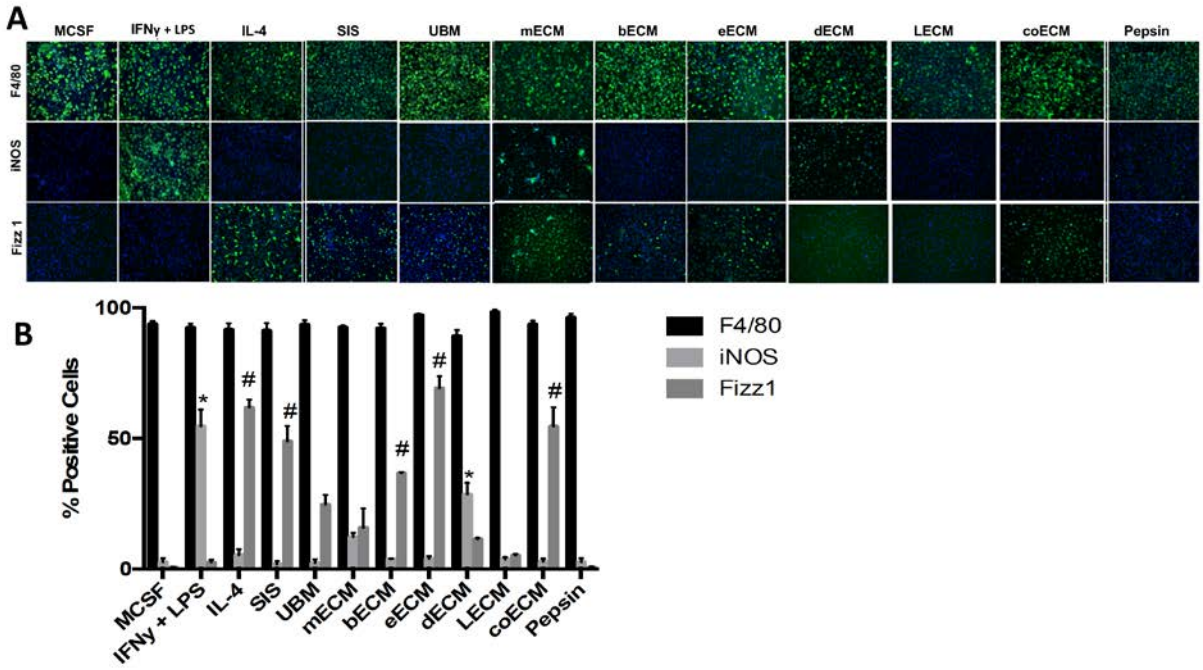

Figure 12. Immunolabeling of ECM treated macrophages (A) Macrophages were fixed with 2% paraformaldehyde following 18 h of treatment with cytokines or ECM degradation products and immunolabeled for indicators of the M1 or M2 phenotypes (iNOS, Fizz1, respectively). F4/80 was used as a pan macrophage marker. **(B)** Results were quantified using CellProfiler Image Analysis software and show that SIS, bECM, eECM, and coECM promote a predominant M2-like macrophage phenotype, whereas dECM promotes a predominant M1-like macrophage phenotype. (MCSF = macrophage colony stimulating factor, SIS= small intestinal submucosa, UBM= urinary bladder matrix, mECM= skeletal muscle ECM, bECM= brain ECM, eECM= esophageal ECM, dECM= dermal ECM, LECM= liver ECM, coECM=colonic ECM) (* and # indicate $p < 0.05$ when compared to MCSF group for iNOS and Fizz1 quantification, respectively. n=8, error bars represent standard error of the mean. Light exposure times were standardized to a negative isotype control and kept constant across images).

7.4.3 ECM differentially increases M1-like and M2-like macrophage protein expression

Western blotting shows that SIS, UBM, eECM, and coECM treated macrophages significantly increased CD206 expression similarly to the IL-4 treated control (Figure 13B). IFNy/LPS treatment as well as mECM, bECM, dECM, and LECM are characterized by decreased CD206 expression (Figure 13). SIS, bECM, and eECM are characterized by a significant decrease of macrophage iNOS expression when compared to the IFNy/LPS treated control; where as UBM, mECM, dECM, LECM, and coECM do not decrease macrophage iNOS expression (Figure 13D).

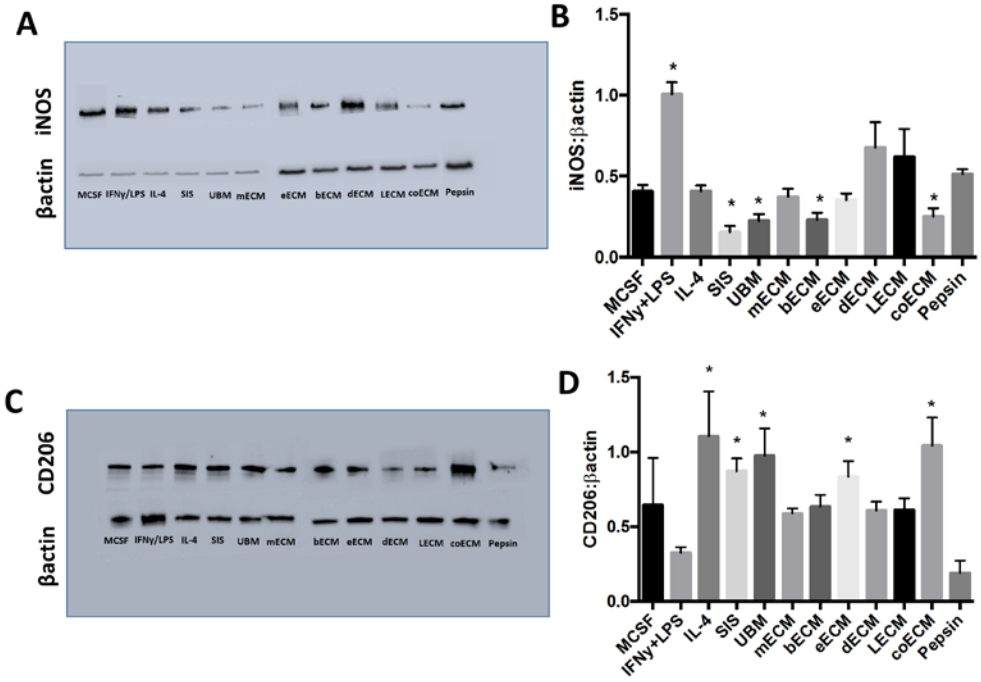

Figure 13. Western blotting of ECM-treated macrophages. . (A) Macrophage lysates were collected and probed for the presence of iNOS and **(C)** CD206 as M1 and M2-like protein markers, respectively. **(B)** Treatment with SIS, UBM, bECM, and coECM promotes a significant decrease in iNOS expression when compared to the vehicle (pepsin) control treatment. **(D)** Treatment with SIS, UBM, eECM, and coECM promotes a increase in CD206 expression, similarly to IL-4 treated macrophages when compared to the pesin treated macrophages. (MCSF= macrophage colony stimulating factor, SIS=small intestinal submucosa, UBM = urinary bladder matrix, mECM = skeletal muscle ECM, bECM = brain ECM, eECM = esophageal ECM, dECM = dermal ECM, LECM = liver ECM, coECM= colonic ECM). (* indicates $p < 0.05$ when compared to vehicle control. n=6. Error bars represent standard error of the mean)

7.4.4 Exposure to ECM differentially affects macrophage viability

ECM bioscaffolds differentially affect macrophage viability. At the evaluated concentration, none of the tissue-type ECMs cause a decrease in cell viability of more than 20%. Macrophages exposed to eECM (84.14%), LECM (83.34%), and bECM (83.28%) showed the lowest cell viability with significant differences when compared with non-activated M0 macrophages (93.74%) (Figure 14).

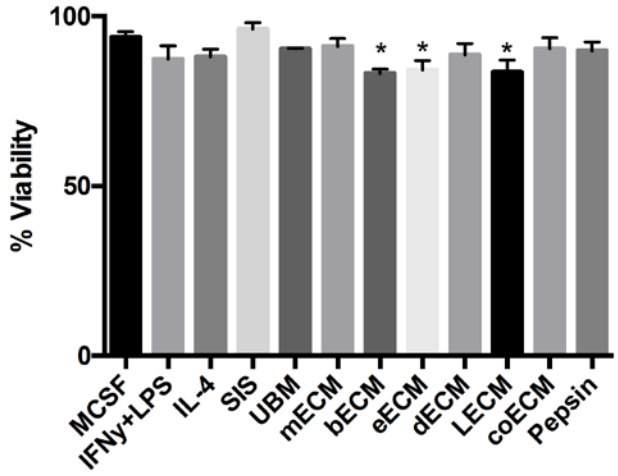

Figure 14. Macrophage viability analysis. The viability of macrophages following treatment with cytokines or ECM degradation products was analyzed using trypan blue. Macrophage viability significantly decreases with eECM, LECM, and bECM treatment. (MCSF= macrophage colony stimulating factor, SIS=small intestinal submucosa, UBM = urinary bladder matrix, mECM = skeletal muscle ECM, bECM = brain ECM, eECM = esophageal ECM, dECM = dermal ECM, LECM = liver ECM, coECM= colonic ECM). (* indicates $p < 0.05$ when compared to MCSF group. n=3. Error bars represent standard deviation)

7.4.5 Exposure to ECM differentially affects macrophage metabolism

Exposure of macrophages to tissue-specific ECM differentially modified the macrophage metabolic activity. SIS-ECM, eECM, and LECM maintain cell metabolism activity when compared to untreated macrophages and cytokine-treated macrophages. In contrast, mECM, dECM, coECM, and bECM decrease macrophage MTT metabolism by more than 50%. UBM treatment also resulted in a significant decrease in MTT metabolic activity when compared to the untreated control (Figure 15).

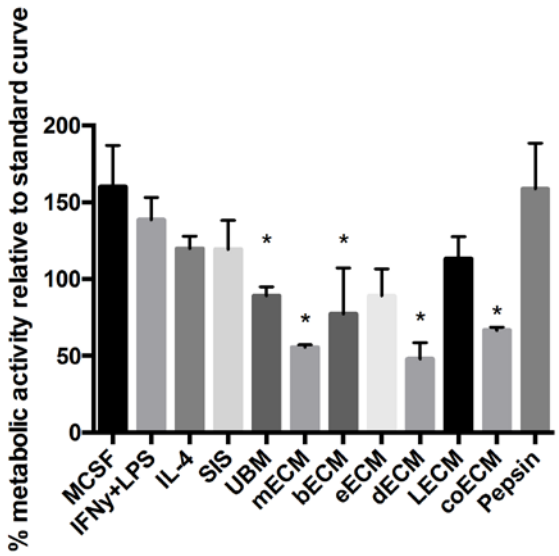

Figure 15. MTT metabolism of macrophages. MTT analysis shows treatment with mECM, dECM, cECM, or bECM reduces metabolic activity of macrophages when compared to the untreated control. UBM significantly increases MTT metabolism when compared to untreated macrophages, whereas mECM, bECM, dECM, and coECM result in a significant decrease. (MCSF= macrophage colony stimulating factor, SIS=small intestinal submucosa, UBM = urinary bladder matrix, mECM = skeletal muscle ECM, bECM = brain ECM, eECM = esophageal ECM, dECM = dermal ECM, LECM = liver ECM, coECM= colonic ECM). (* indicates $p < 0.05$ when compared to MCSF group. Error bars represent standard deviation)

7.4.6 Phagocytic capability of macrophages does not significantly differ with phenotype

Phagocytic capability of macrophages was unaffected by treatment with ECM and/or cytokine controls (Figure 16).

7.4.7 ECM treated macrophages exert antimicrobial effects

Secreted products from cytokine-treated and ECM-treated macrophages show an increased antimicrobial affect when compared to pepsin-treated and untreated controls. ECM activates macrophages similarly to cytokine-treated macrophages with respect to antimicrobial activity (Figure 17).

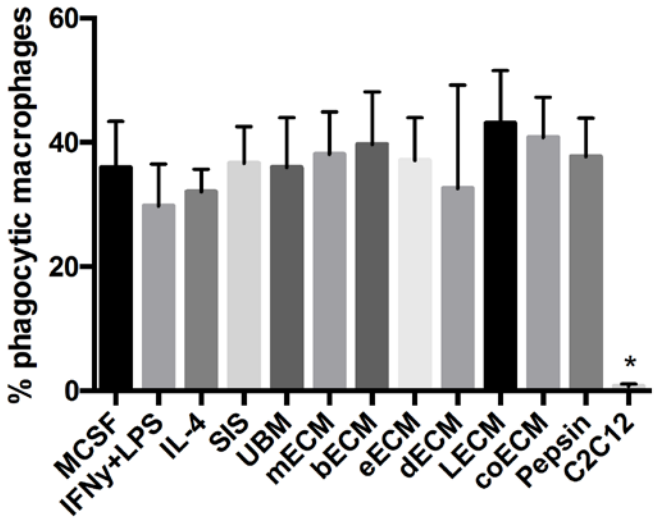

Figure 16. Phagocytic capacity of macrophages. Fluorophore-conjugated bioparticle uptake was used as a measure of phagocytic activity of macrophages. Treatment with cytokines or ECM degradation products did not significantly change phagocytosis. (MCSF= macrophage colony stimulating factor, SIS=small intestinal submucosa, UBM = urinary bladder matrix, mECM = skeletal muscle ECM, bECM = brain ECM, eECM = esophageal ECM, dECM = dermal ECM, LECM = liver ECM, coECM= colonic ECM). (* indicates $p < 0.05$ when compared to MCSF group. n=3. Error bars represent standard deviation)

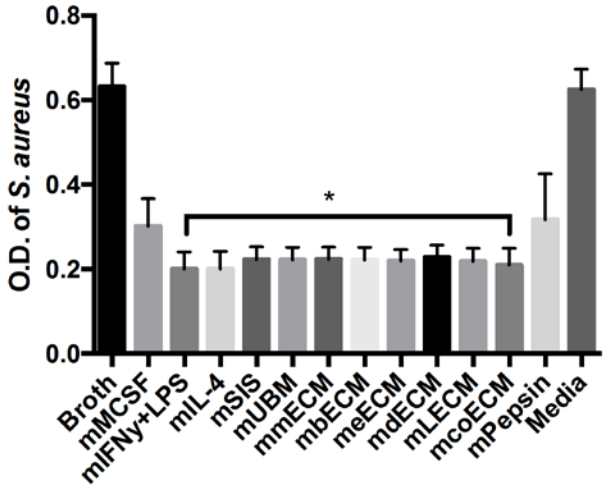

Figure 17. Indirect antimicrobial activity of ECM degradation products. *S. aureus* growth was used to determine the antimicrobial effects of macrophages exposed to ECM degradation products. After 18 hours, secreted products from ECM-treated macrophages significantly inhibit *S. aureus* growth, similarly to cytokine-treated macrophages, when compared to untreated macrophages and the negative control (broth). (MCSF= macrophage colony stimulating factor, SIS=small intestinal submucosa, UBM = urinary bladder matrix, mECM = skeletal muscle ECM, bECM = brain ECM, eECM = esophageal ECM, dECM = dermal ECM, LECM = liver ECM, coECM= colonic ECM). (* indicates $p < 0.05$ when compared to MCSF group. n=4. Error bars represent standard error of the mean)

7.5 DISCUSSION

Biologic scaffold materials composed of mammalian extracellular matrix (ECM) have been associated with favorable preclinical and clinical remodeling outcomes when used as a therapeutic approach following tissue damage or disease[102,107,163,291,292]. Xenogeneic ECM bioscaffolds that are thoroughly decellularized and relatively free of cell remnants are typically associated with robust biologic activity including the ability to recruit endogenous stem/progenitor cells and modulate the host innate immune response to injury[117]. It has previously been established that ECM is able to promote a shift from the default wound healing response to injury (i.e., fibrous scar tissue formation) toward constructive (i.e., functional and

site-appropriate) tissue remodeling[246]. Though the mechanisms responsible for this response are only partially understood, one important and necessary event is an early transition in responding macrophage phenotype; specifically, from an M1-like, pro-inflammatory phenotype to an M2-like, regulatory and pro-remodeling phenotype following scaffold implantation and subsequent degradation within host tissue[76,100,196].

The extent of ECM mediated constructive remodeling can differ depending upon a number of variables involved in ECM bioscaffold preparation including source animal age[119], use of chemical crosslinking agents[100], storage conditions[293], extent of decellularization[117], terminal sterilization methods[294] and the tissue from which the ECM was derived[295,296], among others. ECM bioscaffolds have been shown to direct endogenous cell behavior and influence the local tissue microenvironment. The availability of these bioactive molecules to surrounding host tissue / cells is dependent upon the degradation of ECM bioscaffolds following implantation, subsequently releasing and/or exposing matricryptic peptide sites that have been shown to be chemotactic and mitogenic[108,109] for progenitor cells and able to induce their differentiation[78]. It is logical to assume that ECM derived from homologous source tissue (i.e. from the same tissue that is to be replaced) would contain the inherent structural and biochemical milieu required for tissue-specific differentiation and would represent the optimal environment for such a tissue's associated cells. Some studies have shown that homologous ECM is preferable and maintains tissue specific cell phenotypes[295-300]. However, other studies show that heterologous ECM is adequate in promoting site-appropriate tissue deposition[102,208]. Whether there are differences in the ability of ECM bioscaffolds derived from different source tissues to directly influence macrophage phenotype has not been previously evaluated. The present study shows that the source tissue from which an ECM bioscaffold is derived can indeed be a determining factor with

respect to the macrophage response. While most ECM bioscaffolds promote an M2-like phenotype *in vitro*, surface marker expression shows some exceptions including skeletal muscle ECM (mECM), dermal ECM (dECM), and liver ECM (LECM) treated macrophages which show lower M2-like Fizz1 and CD206 expression with higher levels of M1-like iNOS expression.

It is plausible that these differences in phenotype could be a result of the preparation methods, specifically the method of decellularization utilized for different tissue types. In the present study, all ECMs were decellularized in accordance with previously established protocols designed to meet recognized minimum criteria for decellularization (i.e., no visible intact nuclei by hematoxylin and eosin staining, remnant DNA concentration less than 50 ng/mg dry weight, and DNA fragment length less than 200 base pairs) [283 283 283]. For example, SIS-ECM and UBM are prepared with relatively mild decellularization methods whereas skeletal muscle ECM or esophageal ECM are exposed to a series of enzymatic, detergent, and chemical treatments. Variations of decellularization protocols likely contribute to the distinct protein profile for each tissue ECM as shown in the SDS PAGE gel analysis. A proteomic analysis has been conducted using solubilized urinary bladder matrix with hundreds of proteins identified within the solubilized scaffold[301]. However, it should be noted that proteomic analysis is a function of the particular solubilization process, which in itself generates even more proteins. The present study shows that while there are differences in protein content between each ECM bioscaffold type, it would be difficult to determine which of these differences contribute to any differences in bioactivity, let alone macrophage phenotype specifically due to the sheer number and overlap of proteins within the different scaffolds. Previous studies have shown that the macrophage response differs when exposed to fractions of structural and soluble components of the ECM[249]. It is likely that decellularization protocols also impact the relative constituents of solubilized

ECM utilized in the present study. However, whether a specific peptide or combinations of peptides is responsible for a phenotypic change in macrophages is unknown and warrants future study. The presence of residual detergent could also be a contributing factor in the differences in macrophage responses to different ECM bioscaffolds. Variation in detergents used for tissue decellularization has been shown to have an impact upon the basement membrane complex of urinary bladder matrix, specifically the extent of collagen denaturation, glycosaminoglycan (GAG) concentration, and cellular infiltration, growth, and differentiation[209]. It is likely that residual detergent remains within the pepsin-solubilized scaffolds used in the present study, and could have an impact upon the macrophage response. However, the objective of the present work was to compare the effects of ECM bioscaffolds and not decellualrization methods, though the question of the impact of specific detergents upon the macrophage response warrants investigation.

A plausible rationale for selecting ECM bioscaffolds derived from one tissue source over another for a given application could include the ability to influence macrophage phenotype. Interestingly, gastrointestinal-derived ECM analyzed in the present study (SIS-ECM, eECM, coECM) promotes a heightened M2-like protein expression profile and diminished M1-like protein expression profile. Moreover, it has been shown that resident macrophages within the gastrointestinal tract retain a more immunotolerant (i.e. more M2-like) phenotype. Perhaps macrophage phenotype is partially determined by the native ECM within the gastrointestinal tract.

In general, the present study shows that regardless of the source tissue from which it is derived, ECM stimulated macrophages show a distinct phenotype when compared to the canonically activated IFNγ/LPS and IL-4 treated macrophages. In general, ECM induces a shift

toward an M2-like phenotype. No significant differences were seen in macrophage phagocytosis. Metabolic activity of ECM treated macrophages, in the case of treatment with mECM, dECM, coECM, or bECM, is lowered. The results herein suggest that this decreased metabolic activity is not generated by loss of cell viability (i.e. apoptosis and necrosis), as corroborated by trypan blue exclusion assay results, but by changes in redox states. In this sense, it has been previously shown that cellular metabolism is differentially regulated in macrophage activation to meet the energetic needs of each phenotype in the local microenvironment[302,303], with M1-like macrophages requiring greater amounts of NADH (increased redox potential) than its counterpart M2-like phenotype[304,305]. Since MTT assay, widely used to determine cell viability, incorporates the reduction of MTT to formazan in a NADH-dependent mechanism mainly outside the mitochondria[304], this technique could be used as an indirect first approximation to determine the metabolic changes in macrophages. However, additional studies are required to identify the mechanisms involved in the metabolic activation of the macrophages exposed to tissue-specific ECM.

ECM treated macrophages show similar antimicrobial activity to both IFNγ/LPS and IL-4 treated macrophages. When compared to untreated or pepsin-treated macrophages, cytokine or ECM activated macrophages promoted a more potent antimicrobial effect, though no significant differences were found when comparing the effects from macrophages treated with different ECM bioscaffolds. These results show that ECM can indirectly contribute to antimicrobial activity through macrophage activation. Such results also highlight the heterogeneity of macrophages and emphasize the need to evaluate these cells using multiple metrics for comprehensive characterization.

The present study has several limitations. Although macrophages are a key player in tissue-mediated remodeling across species, only mouse bone marrow derived macrophages were utilized for phenotypic characterization following ECM exposure. Whether these same trends will be corroborated utilizing human macrophages should be investigated. Additionally, the present study did not investigate the specific effects of individual decellularization methods upon an ECM's ability to influence macrophage phenotype. It is likely that a different decellularization protocol, one that does not sufficiently lower DNA content as those used in the present study or otherwise modifies the molecular profile of the ECM, would influence macrophage phenotype.

7.6 CONCLUSION

The results herein show that ECM is able to induce changes in macrophage phenotype and function. Overall, ECM promotes a macrophage phenotype that is distinct from that of cytokine-activated macrophages. The direct effects of ECM bioscaffolds upon macrophage phenotype could have implications for the use of site-specific ECM in therapeutic applications. The findings reported show the heterogeneity of macrophages and the differences in bioactive molecules generated from ECM derived from diverse source tissues.

7.7 ACKNOWLEDGEMENTS

The authors gratefully acknowledge Lynda Guzik for her assistance with flow cytometry analysis. Jenna Dziki was partially supported by the National Science Foundation Graduate Student Research Fellowship.

8.0 THE EFFECT OF MECHANICAL LOADING UPON EXTRACELLULAR MATRIX BIOSCAFFOLD-MEDIATED SKELETAL MUSCLE REMODELING[5]

8.1 ABSTRACT

Mounting evidence suggests that site-appropriate loading of implanted extracellular matrix (ECM) bioscaffolds and the surrounding microenvironment is an important tissue remodeling determinant, though the role at the cellular level in ECM-mediated skeletal muscle remodeling remains unknown. The present study evaluates cross-talk between progenitor cells and macrophages during mechanical loading in ECM-mediated skeletal muscle repair. Myoblasts were exposed to solubilized ECM bioscaffolds and were mechanically loaded at 10% strain, 1 Hz for 5 hours. Conditioned media was collected and applied to bone-marrow-derived macrophages followed by immunolabeling for pro-inflammatory M1-like and pro-remodeling M2-like markers. Macrophages were subjected to the same loading protocol and their secreted products were collected for myoblast migration, proliferation, and differentiation analysis. A mouse hind limb unloading, volumetric muscle loss (VML) model was used to evaluate the effect of loading upon the skeletal muscle microenvironment after ECM implantation. Animals

[5] Portions of this chapter were adapted from the following publication: **Dziki JL**, Giglio RM, Sicari BM, Wang DS, Gandhi R, Londono R, Dearth CL, Badylak SF. The effect of mechanical loading upon extracellular matrix bioscaffold-mediated skeletal muscle remodeling. *Tissue Eng Part A.* March 2017. DOI: 10.1089/ten.tea.2017.0011

were sacrificed at 14 or 180 days. Isometric torque production was tested and tissue sections were immunolabeled for macrophage phenotype and muscle fiber content. Results show that loading augments the ability of myoblasts to promote an M2-like macrophage phenotype following exposure to ECM bioscaffolds. Mechanically loaded macrophages promote myoblast chemotaxis and differentiation. Lack of weight-bearing impaired muscle remodeling as indicated by Masson's trichrome stain. Isometric torque was significantly increased following ECM implantation when compared to controls, a response not present in the hind limb unloaded group. The present work provides important mechanistic insight of the effects of rehabilitation upon ECM-mediated remodeling and could have broader implications in clinical practice, advocating multidisciplinary approaches to regenerative medicine, emphasizing rehabilitation.

8.2 INTRODUCTION

Severe skeletal muscle injury, such as volumetric muscle loss (VML), as a result of trauma, tumor ablation, or prolonged denervation is a challenging problem in civilian and military medicine with significant clinical and economic consequences[1,2,306]. Treatment strategies include muscle grafts, orthotic devices, and/or physical rehabilitation and typically leave patients with a bleak prognosis of persistent strength and functional deficits[3-5]. To address this unmet clinical need, extensive efforts within the field of tissue engineering / regenerative medicine have attempted to develop alternative approaches to VML therapy which can facilitate the restoration of functional skeletal muscle.

The use of acellular biologic scaffolds composed of mammalian extracellular matrix (ECM) as an inductive myogenic template has been investigated for more than two decades in

multiple animal models, a variety of tissues and types of injury, and with diverse bioscaffold source tissues. Outcomes have ranged from successful to unsatisfactory[61,161-164,224-226,307,308]. The findings from these preclinical studies served as the basis for the clinical use of ECM bioscaffolds for VML treatment in a pilot, 13 patient cohort study, with promising results including partial restoration of muscle strength, function, and range of motion[107,246,247]. Although the preliminary clinical outcome of ECM bioscaffold-based treatment for VML is encouraging, it is likely that the use of ECM bioscaffolds alone will not yield complete restoration of skeletal muscle function.

Evidence suggests that mechanical loading is not only beneficial but necessary for musculoskeletal development, strength and endurance gains, fatigue resistance, and even acute regeneration[309-313]. However, the role of mechanical loading in the context of ECM bioscaffold-mediated repair following volumetric muscle loss is not fully understood. The innate immune response is a required component of the response to injury and also plays a regulatory role in tissue development and homeostasis. Moreover, macrophage presence and phenotype have been shown to be a critical regulator of acute skeletal muscle regeneration and predictive of downstream ECM-mediated tissue repair. Since mechanical loading has been shown to have myogenic benefits, it is plausible that incorporation of early post-injury mechanical loading may foster a pro-regenerative cross-talk between macrophages and myogenic progenitor cells following ECM implantation for VML repair. The objective of the present study was to investigate the role of mechanical stimulation upon the macrophage and myoblast response in ECM bioscaffold-mediated VML repair, in well accepted in vitro and in vivo models.

8.3 MATERIALS AND METHODS

8.3.1 Overview of experimental design

The role of mechanical stimulation upon cell processes known to be important in ECM bioscaffold-mediated skeletal muscle remodeling was evaluated in a two-part study (Figure 18**)**. In vitro characterization of the macrophage and myoblast response to concurrent exposure to ECM degradation products and mechanical stimulation was conducted (FlexCell International, Burlington, NC). Conditioned media (containing secreted factors) from myoblasts and macrophages following exposure to ECM degradation products and/or mechanical strain were collected. The corresponding cell type was then exposed to these conditioned media to evaluate the effect on well-established functional outcome metrics (Figure 18A,B). In a parallel study, the effect of mechanical stimulation on ECM bioscaffold mediated skeletal muscle reconstruction was evaluated using tail-suspension induced hind limb unloading in an established in vivo model of volumetric muscle loss (Figure 18C).

8.3.2 Preparation of ECM bioscaffolds

Small intestinal submucosa extracellular matrix (SIS-ECM) was prepared as previously described[118,132,253]. Briefly, porcine small intestine was obtained (Animal Biotech Industries, Danboro, PA) and the stratum compactum, muscularis mucosa, and tunica submucosa were isolated from the jejunum of animals weighing approximately 240-260 lbs. Peracetic acid, deionized H_2O, and phosphate buffer saline washes were used to decellularize the tissue. SIS-ECM sheets were lyophilized to form sheets or milled to form a powder. The powder was then

solubilized with 1.0% pepsin as previously described for the preparation of an ECM hydrogel to yield a 10 mg/ml solution of ECM degradation products[194].

8.3.3 Isolation and culture of murine bone marrow derived macrophages

Murine bone marrow derived macrophages were isolated and cultured as previously described[78]. Briefly, bone marrow was isolated from the femurs and tibias of female C57BL/6 mice and was subsequently cultured in complete growth media including macrophage colony-stimulating factor (M-CSF) for 7 days with complete media changes every 48 hours until mature bone marrow derived macrophages were obtained, as confirmed by F4/80 immunolabeling. Macrophages were cultured on Uniflex culture plates (FlexCell International) for mechanical loading.

8.3.4 Myoblast culture

C2C12 myoblasts (ATCC) were cultured in accordance with ATCC guidelines. The cells were grown in Dulbecco's Modified Eagles Medium (DMEM)/High Glucose (4500 mg/L), 10% fetal bovine serum, and 1% penicillin-streptomycin. Cells were grown at 37°C, 5% CO_2 and were assayed at approximately 80% confluence.

8.3.5 ECM treatment and mechanical loading of myoblasts and macrophages

Macrophages and myoblasts were treated with solubilized small intestinal submucosa (SIS-ECM) at 200 ug/mL in media containing 10% fetal bovine serum and 1% penicillin/streptomycin

in DMEM/High Glucose for 18 hours or treated with canonical activation controls of IFNγ and LPS to derive a pro-inflammatory macrophage phenotype, or IL-4 to derive a pro-remodeling phenotype. Cells designated for mechanical loading were plated on 35mm collagen I-coated 6-well Uniflex culture plates (FlexCell International) and were subjected to 10% uniaxial strain at a cyclic rate of 1 Hz using the F-4000 FlexCell machine after being cultured to approximately 70% confluence. Cells were kept in normal growth media with or without SIS-ECM to analyze the effect of mechanical loading upon cell phenotype, or were mechanically loaded in serum-free, ECM-free media for secreted product collection for cross-talk analyses.

8.3.6 Immunolabeling analyses

Macrophages and myoblasts were fixed following mechanical strain with 2% paraformaldehyde for 20 minutes and then washed with phosphate buffered saline (PBS). Cells were then immunolabeled for macrophage activation markers iNOS and Fizz1 or myogenic markers MyoD, desmin, and sarcomeric myosin. Prior to immunolabeling, cells were incubated for 1 hour in blocking solution consisting of 0.1% Triton-X 100, 0.1% Tween-20, 2% bovine serum albumin, and 4% normal goat serum. Cells were then incubated with the following primary antibodies diluted in blocking solution for 16 hours at 4˚C (1) monoclonal anti-F4/80 (abcam, Cambridge, MA) as a pan macrophage marker at 1:200, (2)polyclonal anti-iNOS (abcam) as an $M_{pro\text{-}inflammatory}$ macrophage marker at 1:100, (3) polyclonal anti-Fizz1 (Peprotech, Rocky Hil, NJ) as an $M_{pro\text{-}remodeling}$ macrophage marker at 1:200, (4) monoclonal anti-MyoD (ThermoFisher, Pittsburgh, PA) at 1:500 as an early myogenic marker, (5) monoclonal anti-desmin (abcam), and (6) anti-sarcomeric myosin heavy chain (Developmental Studies Hybridoma Bank, University of Iowa) at 1:500. Cells were then washed with PBS and incubated in Alexa Fluor 488 goat anti-rat,

goat anti-rabbit, or goat anti-mouse diluted to 1:200 in blocking solution for 1 hour at room temperature and nuclei were counterstained with DAPI.

8.3.7 Myoblast chemotaxis

The effect of macrophage conditioned media upon C2C12 skeletal muscle myoblast chemotaxis was examined using a modified Boyden Chamber cell migration assay as previously described[314314314]. C2C12 myoblasts were cultured in starvation media (DMEM, 0.5% FBS, 1% penn/strep) for 18 hours prior to use. Cells were then trypsinized, re-suspended in growth-factor-free DMEM, and transferred to a 15 ml conical tube for 1 hour incubation at 37 ˚C, 5% CO_2. Polycarbonate chemotaxis membranes with 8μm pores were coated with 0.05 mg/ml collagen type I. Macrophage conditioned media ($M_{IFNy+LPS}$, M_{IL-4}, M_{ECM}, and their mechanically loaded counterparts) or positive (DMEM with 20% FBS) or negative (growth factor-free DMEM) controls were added to the lower wells of Neuro Probe 48-well micro chemotaxis chamber. Collagen-coated membranes were placed over the chemoattractants and 2 x 10^5 cells were added to each of the upper wells of the chamber. Cells were allowed to migrate across the chamber for 3 hours at 37 ˚C, 5% CO_2. Following the migration period, non-migrating cells were scraped from the upper side of the membrane using a rubber scraper. Migrated cells that attached to the bottom of the membrane were fixed with 95% methanol and stained with DAPI prior to imaging. Membranes were imaged using a Zeiss Axiovert microscope and the number of migrated cells was quantified using a CellProfiler pipeline.

8.3.8 Myoblast mitogenesis

C2C12 myoblasts were seeded in normal growth media at 1 x 10^3 cells per well in a 96 well plate. Media was switched to starvation media (DMEM, 0.5% FBS, 1% pennicllin strep) for 18 hours. Following the starvation period, cells were treated with one of the macrophage secreted product samples or positive (DMEM with 20% FBS) or negative (growth factor-free DMEM) control media for 18 hours. Treatments were supplemented with 10 µM 5-bromo-2'deoxyuridine (BrdU) for the final 4 hours. Cells were fixed with 95% methanol for 10 minutes and washed with PBS. Cells were then treated with 2 N HCl for 30 min at 37 ˚C. Following HCl treatment, cells were blocked using the previously described blocking solution for 1 h at room temperature. Following the blocking period, cells were incubated in G3G4 (Anti-BrdU) antibody (Developmental Studies Hybridoma Bank, University of Iowa) at a dilution of 1:1000 for 16 hours at 4 ˚C. After primary antibody incubation, cells were washed 3 times with PBS and incubated in Alexa Fluor donkey anti-mouse 488 secondary at a dilution of 1:300 for 1 hour at room temperature before being subjected to DAPI nuclear stain. BrdU incorporation was imaged using a Zeiss Axiovert microscope and quantified using an ImageJ macro.

8.3.9 Myoblast myogenesis

High serum media (10% FBS) and low serum media (1% FBS, 1% horse serum) were used as negative and positive controls for C2C12 myotube formation as described previously[315]. These media will be referred to as proliferation and differentiation media, respectively. Myogenic differentiation potential following exposure to macrophage secreted products was determined by examining myotube formation. C2C12 myoblasts were cultured in proliferation media until they

reached approximately 70% confluence. Media was then changed to treatment media consisting of a 1:1 solution of macrophage supernatants and 20% FBS DMEM to yield a final serum concentration of 10% FBS, or controls of proliferation or differentiation media. Following 4-5 days or when differentiation media controls showed myotube formation, cells were fixed for immunolabeling with 2% paraformaldehyde. Fixed cells were blocked according to the previously described protocol for 1 hour at room temperature and incubated with anti-sarcomeric myosin heavy chain as described previously. Images of five 20X fields were taken for each well using a Zeiss Axiovert microscope.

8.3.10 Surgical procedure and hind limb unloading

All animal studies were conducted in accordance with the University of Pittsburgh Institutional Animal Care and Use Committee (IACUC) guidelines. Seventy-two C57bl/6 mice (Jackson Laboratories, Bar Harbor ME) were randomly divided into six equal groups. All mice were subjected to tail-suspension to achieve hind limb unloading with full access to the cage floor for two weeks to acclimate prior to the surgical procedure. A mouse model of volumetric muscle loss was used to evaluate the in vivo remodeling response to SIS-ECM in the presence or absence of mechanical load. A 5 mm segment including the distal third of the gastrocnemius and proximal half of the Achilles tendon was surgically excised, or left uninjured as a healthy control. In the VML groups, the segmental defect was repaired with an SIS-ECM sheet, autologous test sample, or was allowed to heal normally without intervention (i.e. no treatment). The device or autologous graft was placed over the proximal and distal stumps and fixed in place with interrupted 7-0 prolene sutures. The skin closure was subcuticular with absorbable sutures. Animals were then allocated into the tail suspended hind limb unloaded group or the normal

ambulation group. Animals were checked twice daily to assure slippage from the tail-suspension apparatus had not occurred, and were sacrificed at 14 or 180 days post-surgery.

8.3.11 Tissue harvest and immunolabeling

Animals were sacrificed at their predetermined time point and the gastrocnemius and Achilles tendon unit was excised from the surrounding tissue, fixed in neutral buffered formalin, and paraffin embedded. Sections were deparrafinized and rehydrated using a graded ethanol series and subjected to heat-mediated antigen retrieval with citrate buffer (pH=8). Following antigen retrieval tissue sections were incubated in blocking solution consisting of 0.1% Triton X-100, 0.1% Tween-20, 2% bovine serum albumin, and 4% goat serum to prevent non-specific antibody binding. After the blocking step, tissue sections were incubated with the following primary antibodies diluted in blocking solution for 16 h at 4°C (1) anti-iNOS (abcam) and (2) anti-Fizz1 (Peprotech). After incubation in primary antibody, tissue sections were washed with phosphate buffered saline (PBS) and incubated for 1 hour at room temperature with fluorescent secondary antibody diluted in blocking solution: (1) Alexa Fluor 488 goat anti rabbit at 1:200. Sections were washed again and counterstained with 4',6-diamidino-2-phenylindole, dihydrochloride (DAPI) and cover-slipped for imaging using a Nuance multispectral microscope with appropriate fluorescent filter sets.

8.3.12 Isometric torque measurement

Functional analysis was performed by measuring isometric torque production of the gastrocnemius 180 days post-surgery using a protocol previously described[316]. This method

allows for determination of the contractile properties of the isolated gastrocnemius, while maintaining normal muscle orientation, innervation, and vascular supply. Animals were anesthetized while the hind limb was stabilized by platform supports with the foot in the flexed position. Needle electrodes were inserted into the belly of the muscle injury site approximately 2-3 µm beneath the skin. Muscles were stimulated at nine different frequencies (1 Hz to 200 Hz) with a two-minute rest period between each frequency. Twitch contraction and tetanic contraction were analyzed using a Dynamic Muscle Analysis program (Aurora Scientific Inc., Canada) and data was normalized to the animals' weight.

8.3.13 Statistical analysis

All statistical analysis was conducted using SPSS Statistical Analysis Software (IBM, Chicago, IL). Data was normally distributed and tested for homogeneity of variance. Data was compared between groups using a one-way independent ANOVA and Tukey's post hoc analysis with an alpha value of 0.05. Error bars represent standard deviation. A two-way ANOVA and LSD post-hoc analysis was used to compare isometric torque between treatment groups at each frequency with an alpha value of 0.05. Error bars represent standard deviation.

8.4 RESULTS

8.4.1 Cyclic mechanical strain promotes a Fizz1+ macrophage phenotype

After 18 hours, degradation products derived from SIS-ECM promote a predominant iNOS-/Fizz1+ macrophage phenotype. When exposed to mechanical load, naïve macrophages begin to express the M2-like marker Fizz1 similarly to IL-4 and ECM-treated resting macrophages (Figure 19).

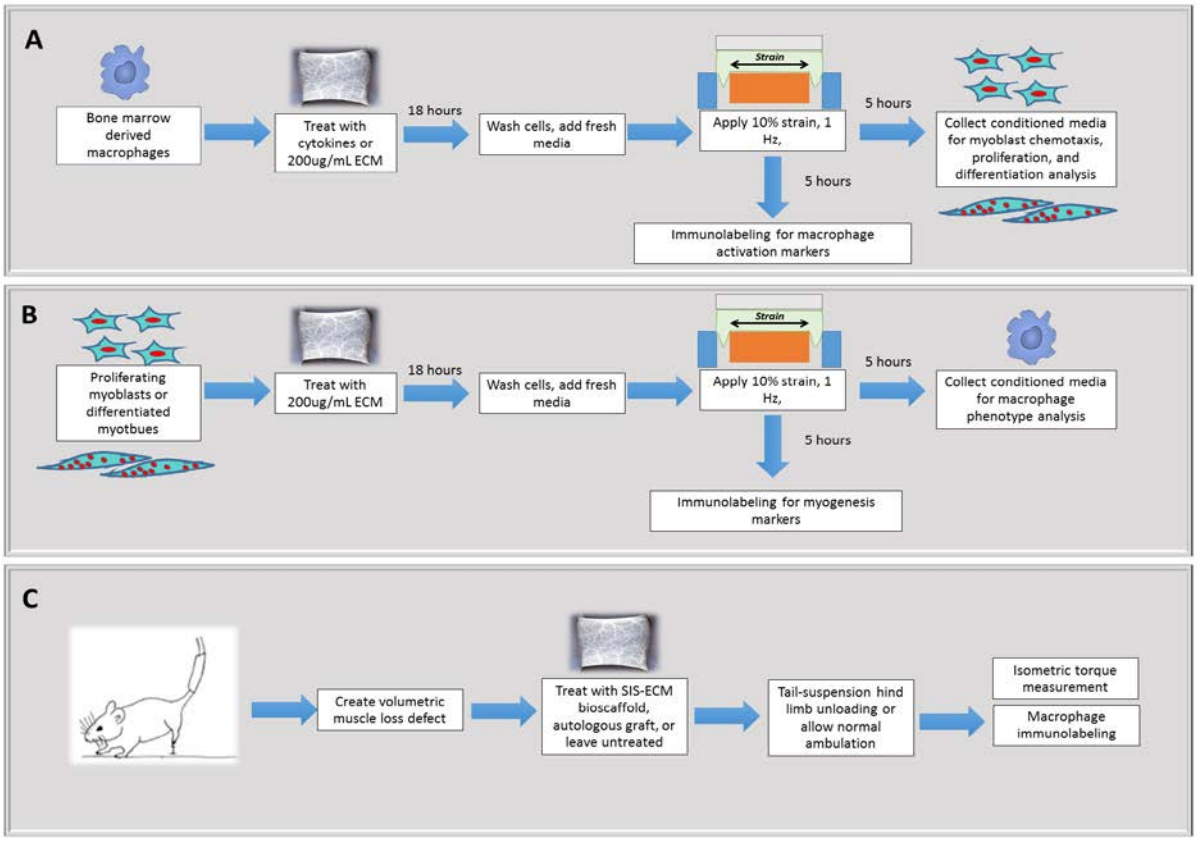

Figure 18. Overview of experimental design. The goal of the present study was to determine the ability of mechanical stimulation in the presence of ECM degradation products to promote skeletal muscle remodeling. The following questions were posed **(A)** How does mechanical loading affect macrophage phenotype in the presence of an ECM bioscaffold and how is the macrophage secretome altered in the context of promoting myoblast chemotaxis, proliferation, and differentiation? **(B)** How does mechanical loading affect myoblast differentiation in the presence of an ECM bioscaffold and how does the myoblast/myotube secretome change in the context of promoting a change in activation in macrophages? **(C)** What is the effect of absence of mechanical loading upon the ECM-mediated skeletal muscle repair microenvironment?

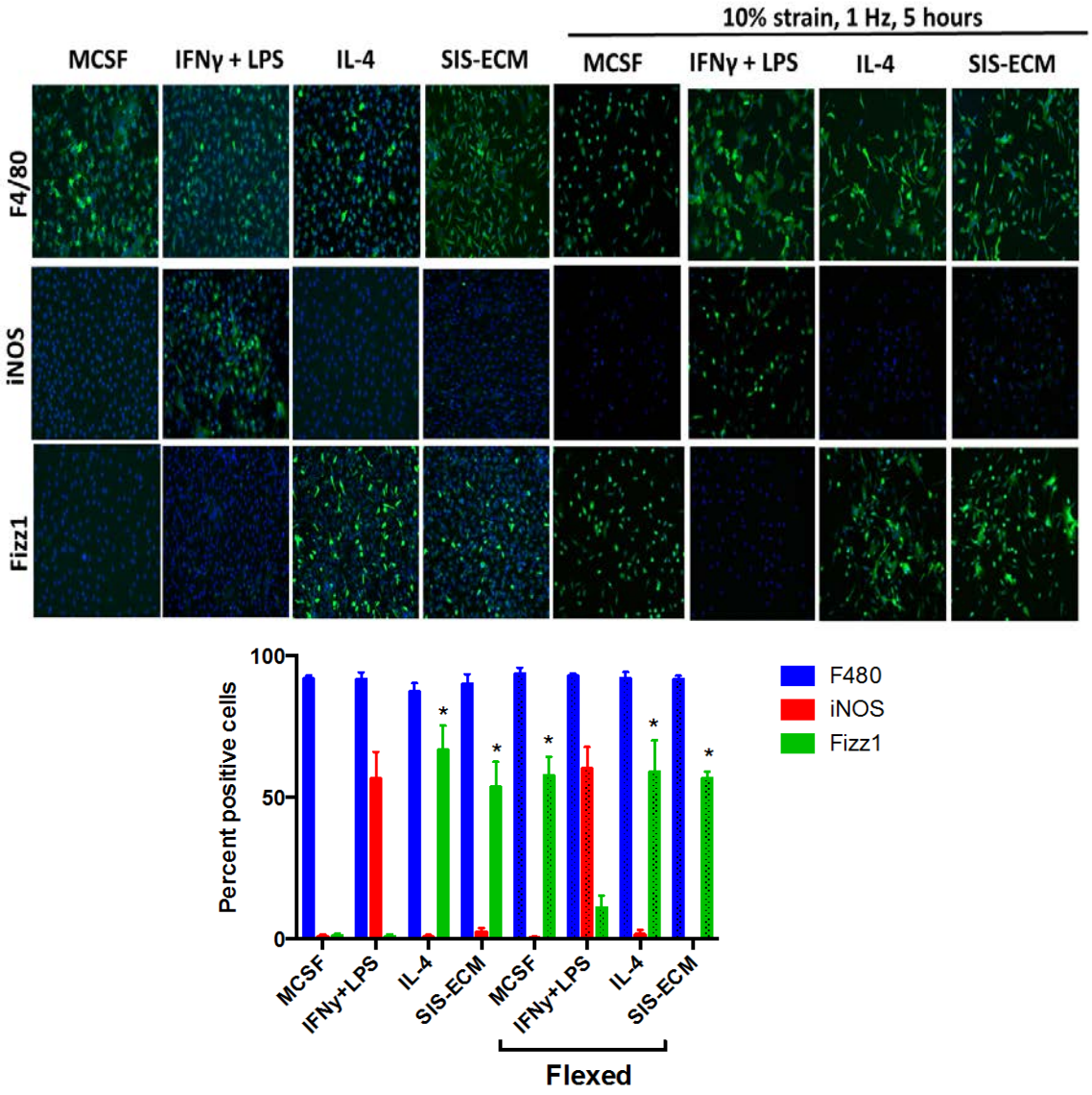

Figure 19. Cyclic mechanical strain of bone marrow derived macrophages. Macrophages were subjected to 10% mechanical strain for 5 hours using the FlexCell system. 5 hours of mechanical strain resulted in an F4/80+/iNOS-/Fizz1+ macrophage phenotype, suggesting that mechanical strain alone can promote macrophage activation towards a pro-remodeling phenotype.

8.4.2 Cyclic mechanical strain promotes a pro-remodeling macrophage phenotype that induces myoblast chemotaxis

As previously shown, naive macrophages treated with SIS-ECM behave similarly to macrophages treated with IL-4. Specifically, both promote a significant increase in myoblast chemotaxis and myotube formation (Figure 20A,D,C,F). In contrast, macrophages treated with IFNy+LPS increase myoblast mitogenesis. Interestingly, when mechanically strained, all macrophage types (IFNy+LPS treated, IL-4 treated, or SIS-ECM treated) promote a significant increase in myoblast chemotaxis when compared to their resting, unstrained counterparts (Figure 20D).

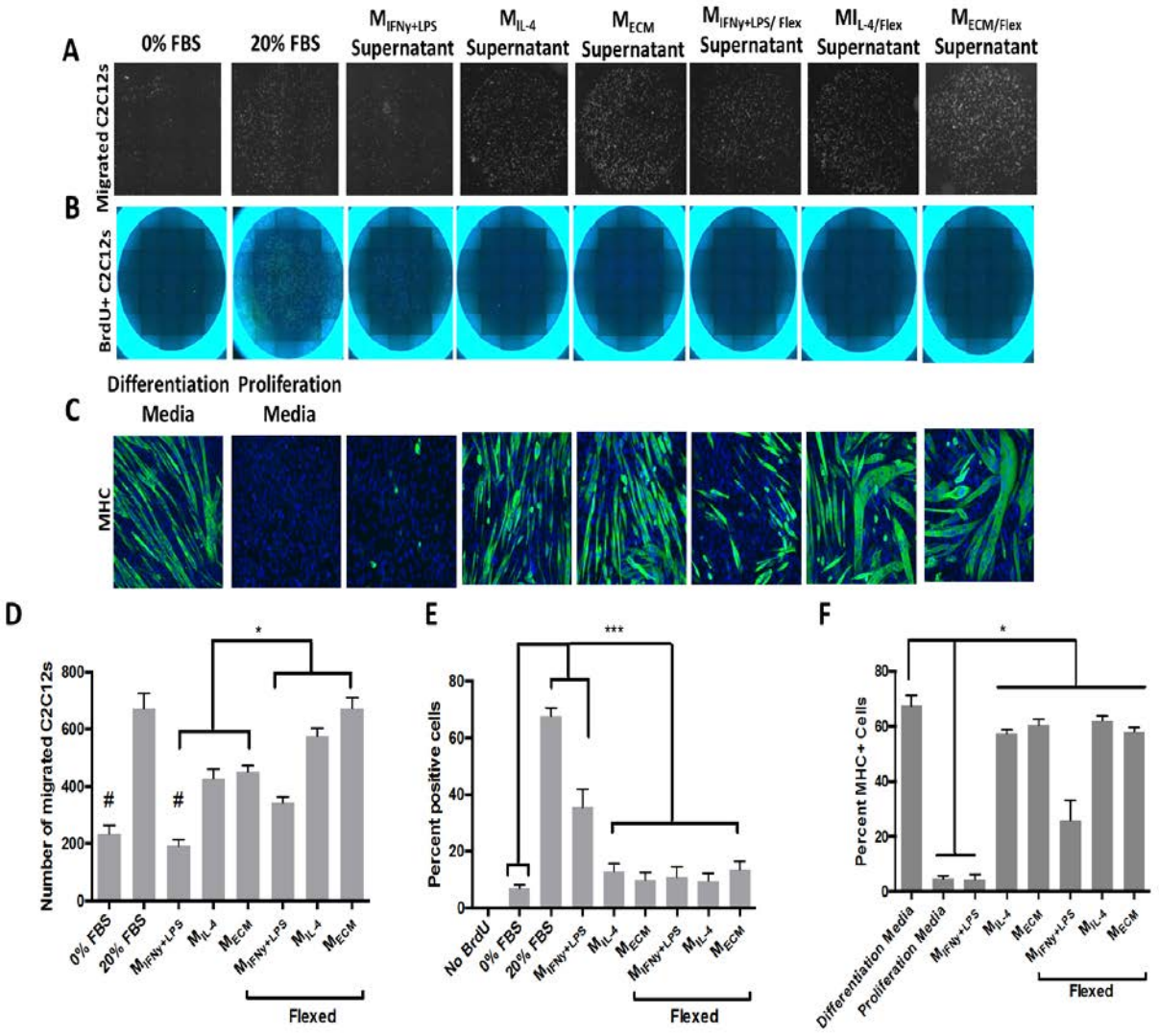

Figure 20. The effect of ECM and mechanical stimulation upon the macrophage secretome. Macrophages were treated with activating cytokines IFNγ + LPS or IL-4 or 200 ug/ml of ECM degradation products for 18 hours. After 18 hours, cells were washed and media was replaced with serum-free, ECM-free media. Macrophages were strained for 5 hours and their conditioned mediat was collected for C2C12 experiments. (**A,D**) IL-4 and ECM treated macrophages promote increased C2C12 migration. Mechanically loaded macrophages significantly increase C2C12 migration compared the unloaded macrophages and the low serum negative control. (**B,E**) IFNγ+LPS treated macrophages promote increased C2C12 mitogenesis. Mechanically loaded macrophages significantly decreased C2C12 migotenesis compared to the unloaded and proliferation media positive control. (**C,F**) IL-4 stimulated and ECM stimulated macrophages significantly increase C2C12 myogenesis Mechanically loaded macrophages significantly increase C2C12 myogenesis compared to the unloaded and proliferation media negative control. (* indicates $p<0.05$. n=5. Error bars represent standard error of the mean)

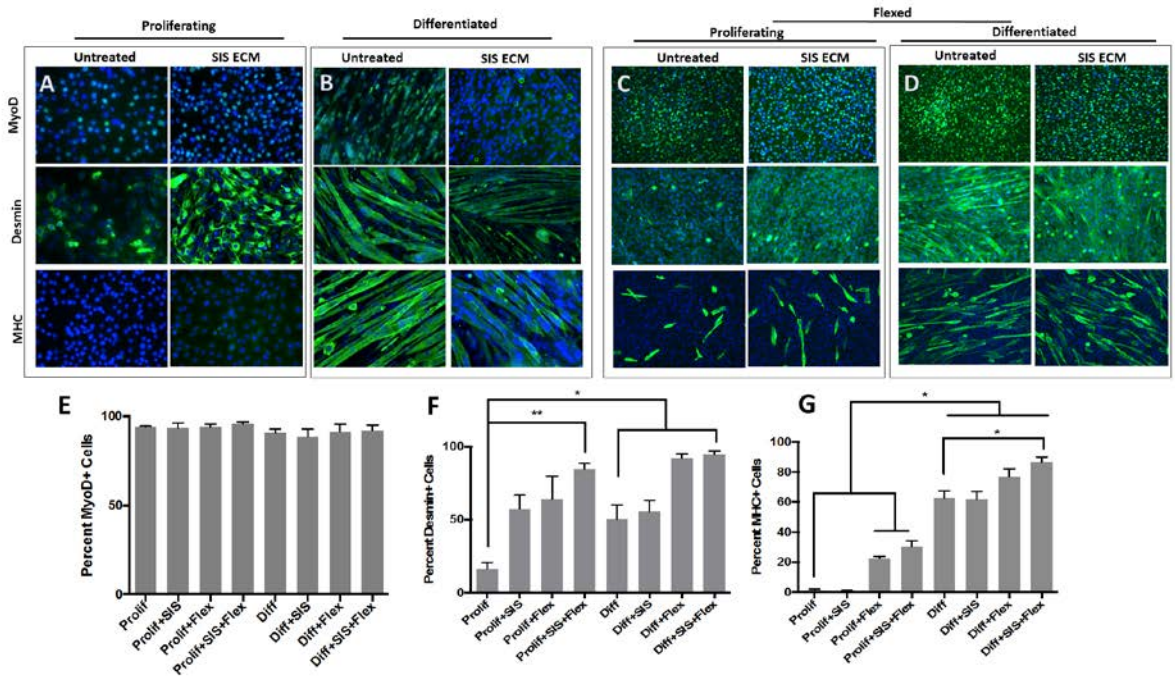

Figure 21. Cyclic mechanical strain of C2C12 myoblasts. (A,C) Myoblasts were cultured and either kept in their proliferation media or (B,D) allowed to differentiate to form myotubes. **(C,D)** Cells were treated with solubilized ECM bioscaffolds for 18 hours or were left in media and were then mechanically strained for 5 hours or **(A,B)** were left unstrained**. (F)** SIS-ECM treatment increased expresson of desmin, with an additional increase after myoblasts were mechanically strained. **(G)** Mechanical strain increased myotbue formation shown by myosin heavy chain (MHC) expression. (*indicates $p < 0.05$, n=5, error bars represent standard error of the mean)

8.4.3 Cyclic mechanical strain promotes a pro-remodeling macrophage phenotype that reduces myoblast proliferation and promotes myoblast differentiation

IFNγ+LPS stimulated macrophages promote a significant increase in the number of BrdU positive, proliferating, myoblasts (Figure 20B,E**).** However, if IFNγ+LPS stimulated

macrophages are first subjected to mechanical strain, this response is significantly diminished and is similar to IL-4 or SIS-ECM treated macrophages (Figure 20B,E). Mechanical strain applied to IFNγ+LPS stimulated macrophages also increased the ability of their collective secretome to promote C2C12 myotube formation **(**Figure 20C,F).

8.4.4 Cyclic mechanical strain combined with SIS-ECM treatment promotes myoblast differentiation

Treatment of proliferating myoblasts with SIS-ECM coupled with mechanical strain resulted in a significant increase in desmin expression (Figure 21F). Consistent with previous findings, the application of mechanical strain alone resulted in sarcomeric myosin heavy chain positive myotube formation in the proliferating group, suggesting the ability of mechanical strain to promote myoblast differentiation as shown in Figure 21G[317]. This response was augmented by the addition of SIS-ECM treatment. Further, when subjected to both SIS-ECM treatment and mechanical strain, the number of differentiated myotubes expressing the terminal differentiation marker, sarcomeric myosin heavy chain, significantly increased compared to the resting, untreated myotubes (Figure 21F).

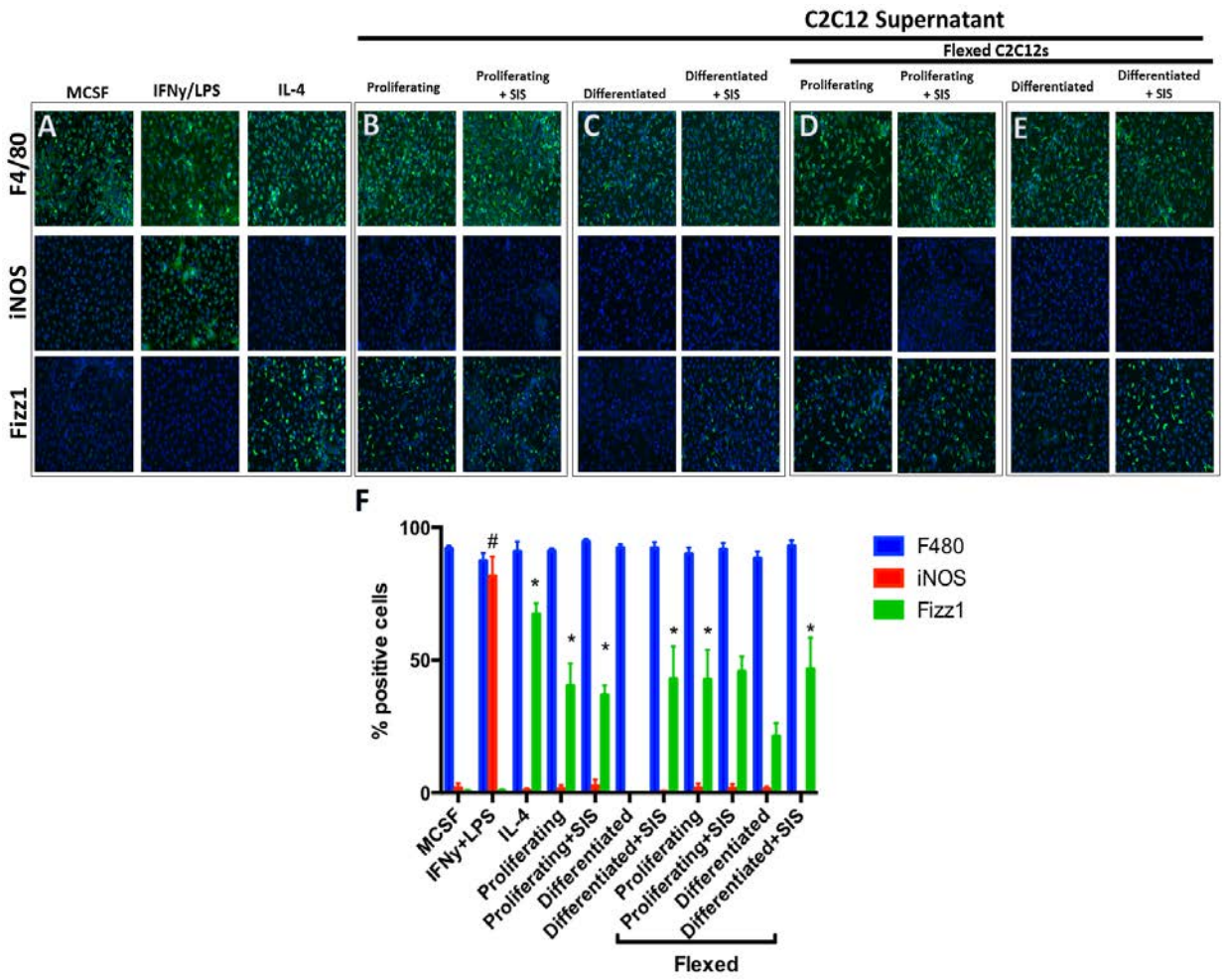

Figure 22. The effect of ECM and mechanical strain upon the myoblast secretome. C2C12 cells were cultured in proliferation media or allowed to form myotubes in differentiation media culture. Myoblasts or myotubes were treated with 200 ug/ml of ECM degradation products for 18 hours, after which the media was replaced with serum free, ECM free media and the cells were subjected to mechanical strain. Conditioned media was collected and added to bone marrow derived macrophages for 18 hours and the cells were fixed for immunolabeling.**(B)** The secretome of proliferating myoblasts promotes an iNOS-/Fizz1+ macrophge phenotype, **(C)** however, differentiated myotubes do not promote the same effect. Treating myotubes with ECM degradation products, however, alters their secretome allowing them to promote a Fizz1+ macrophage phenotype**. E)** This response is augmented when ECM-treated myotubes are subjected to mechaniacl strain. **F)** Percentage of iNOS and Fizz1 piositive macrophages were quantified using CellProfiler (* indicaptes $p < 0.05$, n=4, eror bars represent standard error of the mean)

8.4.5 Cyclic mechanical strain promotes myotube-mediated macrophage activation towards a pro-remodeling phenotype

It is well established that the secretome of stem cells can promote a pro-remodeling macrophage phenotype[144]. The secretome of proliferating C2C12 myoblasts (i.e. those upstream of the terminal differentiation pathway) can shift macrophages towards an iNOS-/Fizz1+ phenotype regardless of whether the myoblasts are treated with SIS-ECM or mechanically strained (Figure 22). However, when allowed to exit the cell cycle and fuse to form myotubes following serum withdrawal, the secretome of C2C12 myotubes does not alter macrophage phenotype towards an iNOS-/Fizz1+ phenotype. In contrast, when first treated with SIS-ECM the C2C12 myotube secretome is altered and promotes the iNOS-/Fizz1+ macrophage phenotype (Figure 22). A similar response is seen when myotubes are mechanically strained. Exposure to both SIS-ECM and mechanical strain augments this response; specifically, there is significant increase in the number of Fizz1+ macrophages after exposure to this secretome (Figure 22F).

8.4.6 Lack of mechanical stimulation alters the macrophage activation response in ECM-mediated skeletal muscle remodeling

After 14 days, hind limb unloading results in a significant decrease in the Fizz1+:iNOS+ macrophage infiltrate within the defect site (Figure 24).

8.4.7 Lack of mechanical stimulation hinders ECM bioscaffold-mediated constructive and functional remodeling in a mouse model of musculotendinuos injury

SIS-ECM treatment promotes site-appropriate tissue deposition following VML (i.e. gastrocnemius-Achilles muscuoltendinous unit) injury in the mouse hind limb (Figure 25) whereas fatty tissue deposition and disorganized connective tissue occurs in the autologous graft or untreated controls (Figure 25). When prevented from weight-bearing on their hind limbs, the SIS-ECM treatment results in more fatty tissue deposition and less muscle formation within the defect site (Figure 25). Isometric torque production in the SIS-ECM treated group is significantly increased compared to the autologous graft treated and untreated control groups following after 6 months when animals were allowed to weight-bear normally (Figure 25). This functional gain is significantly diminished in the absence of mechanical loading upon the hind limbs (Figure 25). Peak isometric torque is reduced in both the SIS-ECM treated groups and the healthy control animals in the absence of hind limb weight bearing (Figure 25). In general, there is a positive correlation between histologically evident new skeletal muscle tissue formation and a regain of isometric torque following injury.

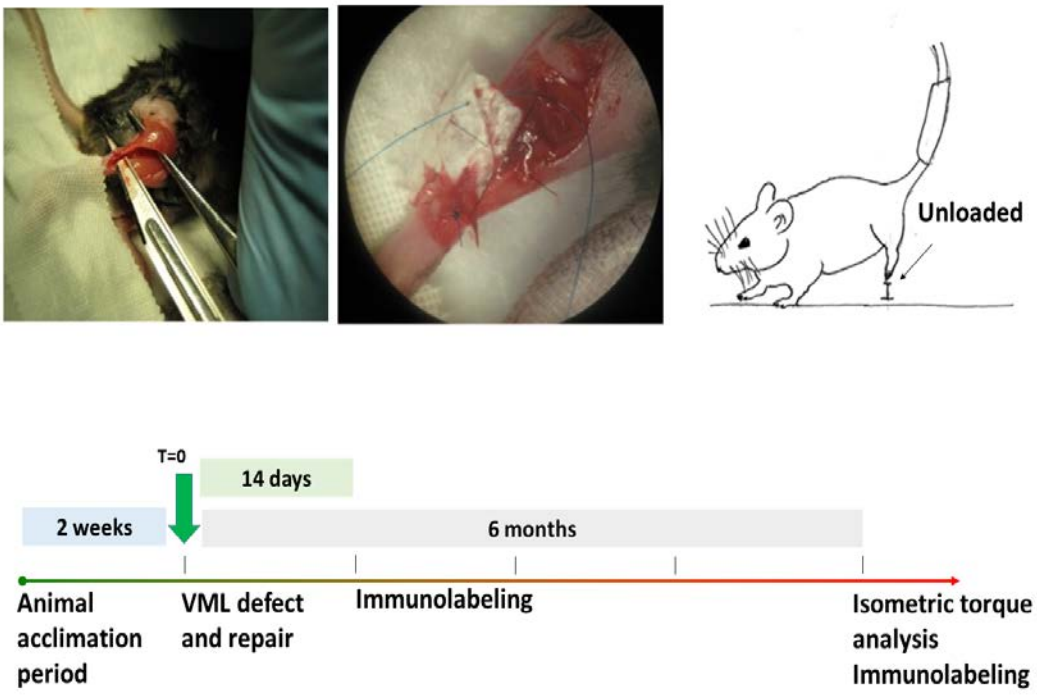

Figure 23. Overview of animal model of VML and hind limb unloading. C57bl/6 mice were subjected to tail-suspension to achieve hind limb unloading for 2 weeks prior to surgery. Surgical excision of the distal gastrocnemius and proximal Achilles was replaced with either an SIS-ECM bioscaffold, an autologous graft, or left untreated. Animals were either allowed to walk normally or subjected to hind limb unloading and sacrificed according to the indicated timeline.

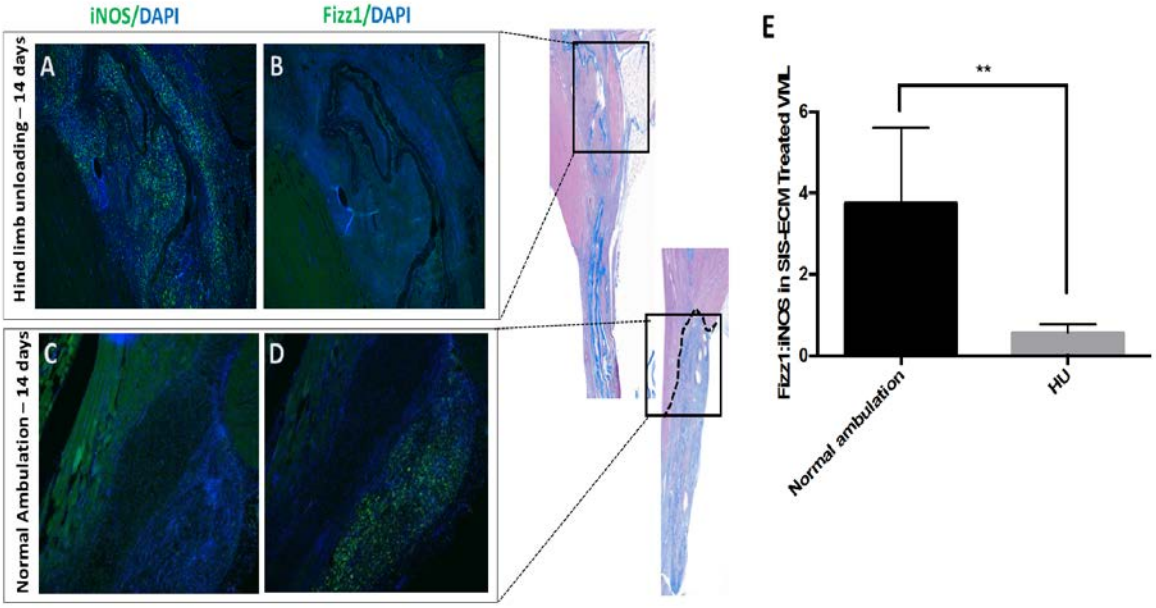

Figure 24. Macrophage response to hind limb unloading following ECM-mediated VML remodeling. **(A)** Hind limb unloading results in increased infiltration of iNOS+ macrophages at 14 days following implantation and **(B)** decreased Fizz1+ macrophage infiltration in contrast to the **(C,D)** normal ambulation control. **(E)** Quantification of the Fizz1+:iNOS+ macrophage ratio across all animals showed a significant decrease following 14 days of hind limb unloading (** indiates $p < 0.01$, error bars represent standard error of the mean).

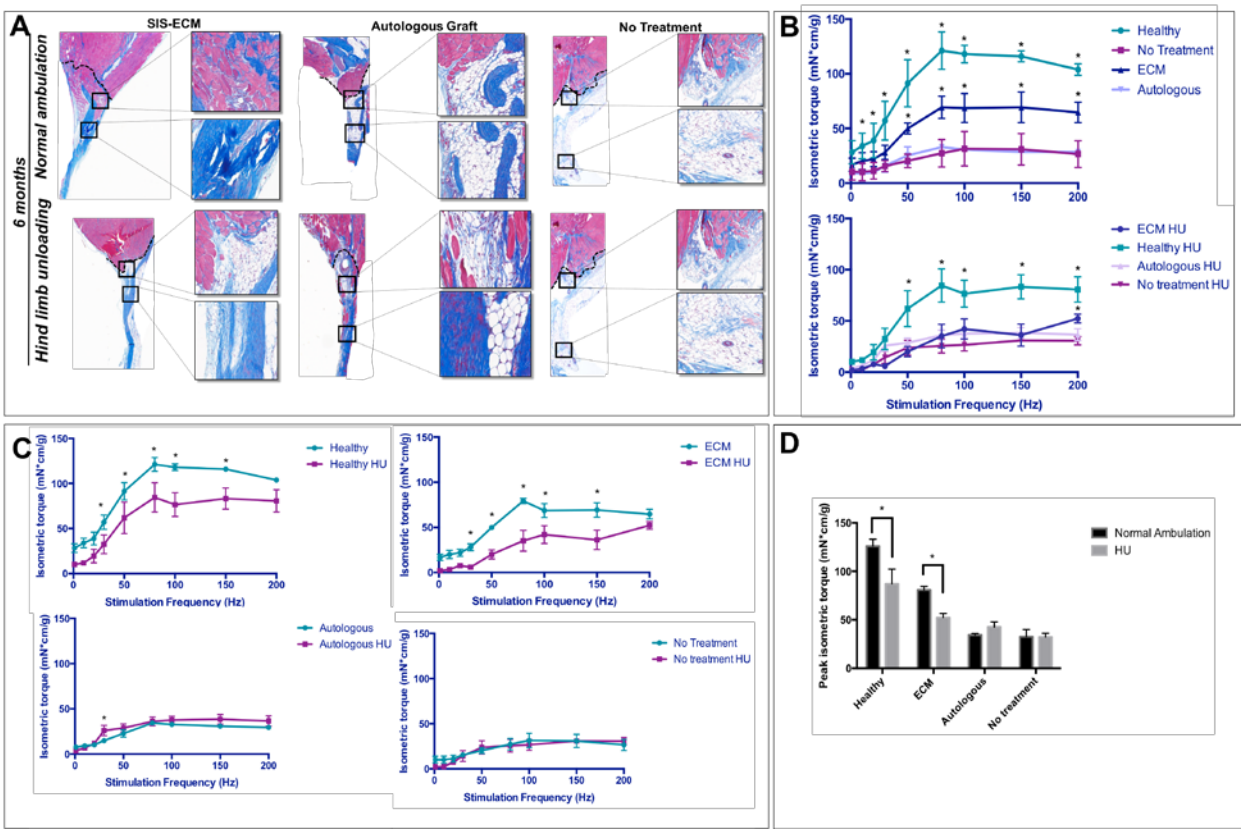

Figure 25. The effect of mechanical stimulation upon constructive remodeling following ECM implantation in a mouse model of VML. (A) Masson's trichrome staining shows site appropriate tissue deposition following ECM bioscafold implantation in mouse VML after 6 months in contrast to fatty tissue deposition and disorganized connective tissue formation in the autologous graft and untreated groups. Hind limb unloading for 6 months decreases the deposition of site appropriate tissue**. (B)** ECM treatment results in a significant improvement in gastrocnemius isometric torque production when compared to the untreated and autologous control groups. Hind limb unloading diminishes this increase in force production. **(C)** Hind limb unloading significantly decreases isometric torque production in the ECM treated animals and the healthy controls. **(D)** Peak isometric torque production is significantly decreased following hind limb unloading in the healthy control and ECM groups (HU= hind limb unloading, * indicaptes $p < 0.05$, n=4, error bars represent standard error of the mean).

8.5 DISCUSSION

The results of the present study show that mechanical stimulation fosters a pro-remodeling macrophage and myoblast cross talk with both direct and indirect promotion of an M2-like macrophage phenotype and increased myoblast chemotaxis and differentiation after exposure to the macrophage secretome. Lack of mechanical stimulation mitigates ECM-mediated skeletal muscle remodeling and reduces restoration of function. This less robust functional response was associated with a reduced M2:M1 macrophage ratio at early time points, which has previously been shown to be a critical regulator of downstream skeletal muscle remodeling[76].

The mechanisms by which ECM bioscaffolds promote restoration of innervated, vascularized, skeletal muscle tissue with associated increased strength and improvement in functional performance in VML patients have not been totally elucidated, but it is well-established that ECM bioscaffolds modify the default wound healing response by promoting an early transition in macrophage phenotype and mobilization of progenitor cells[132,246]. The successful clinical use of ECM bioscaffolds for VML has been coupled with aggressive, early (i.e. immediate) physical rehabilitation. This regimen of post-operative physical therapy has been considered an important contributor to downstream functional remodeling when ECM bioscaffolds are used[107,246,318]. The present study supports this concept and provides evidence of the complex signaling and, to at least some extent, dependency between mechanical loading, the innate immune system, and stem/progenitor cell development and differentiation. The incorporation of structured mechanical loading (i.e physical therapy), supported by data such as

that provided in the present study, could narrow the gap between some of the disparate outcomes seen with studies of ECM-mediated skeletal muscle remodeling[226,319,320].

While the benefits of muscle loading and exercise have long been recognized, the impact upon the innate immune response and the benefits of early mechanical loading (i.e. within 24-48 hours after injury and ECM placement) in the presence of a biomaterial intervention have not been appreciated. Macrophages are key regulators of many complex physiologic processes not only in wound healing but also in tissue homeostasis and development, and these cells appear to have particular importance in regulating skeletal muscle regeneration. The importance of macrophages has also been investigated in the broader context of ECM bioscaffold-mediated tissue repair[76,78,79,98-100,116,118,196,321]. The results of the present study confirm earlier findings that ECM-based signaling molecules influence macrophage behavior both directly[78,79,118] and through myogenic progenitor signaling mechanisms[78]. These findings also show that mechanical stimulation can accentuate this response. While sensitivity of myoblasts to cyclic loading has been extensively studied, the early macrophage response to mechanical cues has not been generally appreciated. Previous work has shown that cell elasticity and cyclic strain can regulate macrophage phenotype and can drive biomaterial design[322,323]. Though in-vitro cyclic loading of macrophages was shown to push macrophages towards a pro-remodeling phenotype, the present study also shows a similar in vivo macrophage response. These findings show that macrophage behavior can be influenced by not only changing surface topography of a bioscaffold substrate, but also by providing external cues in the form of mechanical loading following severe skeletal muscle injury. Seminal studies investigating the response of macrophages to substrates of varying elasticities and rigidities have shown that changes in the cytokine secretion profile and gene / surface marker expression patterns of macrophages occurs through mechanotransduction

pathways including actin-polymerization, activation of stretch-sensitive ion channels, and/or activation or denaturation of G-proteins[311,323,324]. Through these and other mechanisms, a link between mechanics and biologic processes can be established, allowing for another controllable factor to drive the design of biomaterials, and the proscription of rational physical therapy / rehabilitation regimens to facilitate functional skeletal muscle restoration.

Though attempts to directly relate *in vitro* strain regimens to the complexities of the *in vivo* response to injury are generally over-reaching, studies have shown that altering strain regimens can promote both beneficial and detrimental cell responses[322,325,326]. The present study did not investigate a range of straining protocols, but it is noteworthy that mechanical loading in general, and in combination with cues from ECM bioscaffold degradation products, can foster a constructive cross-talk between myoblasts and macrophages. The results of this cross-talk include immunomodulation, myoblast chemotaxis and differentiation, site-appropriate tissue deposition, and increased isometric torque production. Future work would logically be aimed at investigating strain-related changes to macrophages, skeletal muscle progenitor cells, myofiber alignment, angiogenesis, and innervation among other important components of functional skeletal muscle regeneration. Such strain related variables would include a range of strain magnitude, duration, and rate in both *in vitro* constructs and in rehabilitation medicine.

There are several limitations to the present study. Macrophage phenotype cannot be characterized by analysis of a single marker as this inevitably ignores other important aspects such as the metabolic state, gene expression pattern, the secretome, and functional capacity[16,327]. This limitation being recognized, iNOS and Fizz1 are frequently utilized as pro-inflammatory and immunomodulatory macrophage markers, respectively, and they have been shown to be regulated by mechanical loading and play important roles in ECM remodeling following acute

skeletal muscle injury[23,328,329]. Changes in arginine metabolism by iNOS have been widely investigated in skeletal muscle and can affect muscle health[23,328], and therefore iNOS and Fizz1 were chosen as macrophage markers in the present study.

Another limitation of the present study is the use of only one cell type for analysis of the skeletal muscle response to injury. Skeletal muscle regeneration in vivo involves the coordination of many cell types, not only myoblasts but also satellite cells[330], perivascular stem cells[43,331], and other myogenic progenitor cells. The effect of mechanical stimulation has been investigated particularly in satellite cell involvement[312,332,333] but likely will affect most if not all of the cell types involved in skeletal muscle regeneration. Finally, though the hind limb unloading model sufficiently reduced weight bearing in the remodeling gastrocnemius/Achilles, it did not allow for complete immobilization. It is noteworthy, though, that the lack of weight-bearing alone was clearly detrimental to the remodeling process after ECM intervention. Future work should evaluate the effects of complete immobilization, and conversely – overloading of the gastrocnemius upon remodeling outcomes to better understand the mechanisms through which mechanical stimulation contributes to skeletal muscle repair.

8.6 CONCLUSION

The results of the present work substantiate the relevance and importance of incorporation of mechanical cues in conjunction with acellular biologic scaffold therapies to support skeletal muscle remodeling following volumetric muscle loss. Appropriate mechanical loading may narrow the gap between ECM bioscaffold-mediated constructive remodeling and complete

skeletal muscle regeneration and has important implications when utilizing biologic scaffold therapies for volumetric muscle loss in clinical practice.

8.7 ACKNOWLEDGEMENTS

The authors gratefully acknowledge the work of Lori Walton for histology and Xi Yin and Bing Wang for force production analysis. Jenna Dziki was supported by the National Science Foundation Graduate Research Fellowship.

9.0 AN ACELLULAR BIOLOGIC SCAFFOLD TREATMENT FOR VOLUMETRIC MUSCLE LOSS: RESULTS OFA 13-PATIENT COHORT STUDY[6]

9.1 ABSTRACT

Volumetric muscle loss (VML) is a severe and debilitating clinical problem. Current standard of care includes physical therapy or orthotics, which do not correct underlying strength deficits, and surgical tendon transfers or muscle transfers, which involve donor site morbidity and fall short of restoring function. The results of a 13-patient cohort study are described herein and involve a regenerative medicine approach for VML treatment. Acellular bioscaffolds composed of mammalian extracellular matrix (ECM) were implanted and combined with aggressive and early physical therapy following treatment. Immunolabeling of ultrasound-guided biopsies, and magnetic resonance imaging and computed tomography imaging were performed to analyze the presence of stem/progenitor cells and formation of new skeletal muscle. Force production, range-of-motion, and functional task performance were analyzed by physical therapists. Electrodiagnostic evaluation was used to analyze presence of innervated skeletal muscle. This study is registered with ClinicalTrials.gov, numbers NCT01292876. *In vivo* remodeling of ECM

[6] Portions of this chapter were adapted from the following publication:
Dziki JL, Badylak SF, Yabroudi M, Sicari BM, Ambroiso F, Stearns K, Turner NJ, Wyse A, Boninger ML, Brown E, Rubin JP. An acellular biologic scaffold treatment for volumetric muscle loss: results of a 13-patient cohort study. *Nature Regenerative Medicine.* July 2016. DOI: 10.1038/npjregenmed.2016.8

bioscaffolds was associated with mobilization of perivascular stem cells, formation of new, vascularized, innervated islands of skeletal muscle within the implantation site; increased force production; and improved functional task performance when compared with pre-operative performance. Compared with pre-operative performance, by 6 months after ECM implantation, patients showed an average improvement of 37.3% ($p < 0.05$) in strength and 27.1% improvement in range-of-motion tasks ($p < 0.05$). Implantation of acellular bioscaffolds derived from ECM can improve strength and function, and promotes site-appropriate remodeling of VML defects. These findings provide early evidence of bioscaffolding as a viable treatment of VML.

9.2 INTRODUCTION

Volumetric muscle loss (VML) as a result of tumor ablation, trauma, or disease remains a challenging clinical problem for which therapeutic options are limited. Current noninvasive treatment for VML includes maximizing strength of remaining muscle and bracing. Unfortunately, this approach cannot make up for the lost strength associated with VML. Muscle transposition or tendon transfer can replace muscle function, but have less than satisfactory success rates[1,3-5]. Such procedures typically involve significant donor site morbidity and fail to provide efficient reconstruction or functional re-innervation of the lost muscle tissue. These approaches often result in persistent strength and functional deficits, which contribute to disability, weakness, and compromised quality of life for patients with VML.

Skeletal muscle retains a limited capacity to regenerate following a severe acute injury. The regenerative process is dependent on resident progenitor cell populations, including satellite

cells and myoblasts, which have the potential to proliferate and differentiate into functional myofibers. Cell-based regenerative medicine strategies have attempted to augment this regenerative process through the delivery of exogenous (typically autologous) stem / progenitor cells to the VML defect site. Utilization of enriched muscle-derived stem cells, capable of long-term proliferation and myogenic potential, has been somewhat successful and has been shown to increase the regenerative index when injected into sites of skeletal muscle injury[28,29,40]. Such approaches are limited, however, by issues of low cell viability[37], poor cell migration and engraftment, and the need for immunosuppressive therapy, among others[34,35]. In fact, immunosuppressive therapy can further contribute to myoblast apoptosis[36]. Even if an ideal cell source and an effective delivery method are utilized, transplanted cells are often associated with less-than-optimal proliferative and differentiation potential within the host injury site[48]. Cell-centric strategies are also associated with high cost due to the need for *ex vivo* cell expansion and manipulation. While some cell-based approaches have shown promise in preclinical studies, regulatory challenges, and a lack of notable efficacy have prevented their widespread adoption of treatment for VML[151].

We recently described an acellular bioscaffold approach for treatment of VML in five patients that showed encouraging results[107]. This approach involved the use of extracellular matrix (ECM) derived from decellularized porcine urinary bladder to promote scaffold-associated skeletal muscle tissue formation and partial restoration of function. ECM bioscaffold implantation was also associated with the recruitment of endogenous perivascular stem cells (PVSCs). While ECM bioscaffolds have been used in reconstructive surgery, they are typically employed only as a barrier or reinforcing layer of soft tissue. In our prior report[107], we provided evidence for functional remodeling of the ECM scaffold with formation of new muscle tissue.

An aggressive early post-operative rehabilitation protocol was a component of this strategy to place dynamic strain on the ECM and contribute to site-appropriate differentiation of the recruited stem / progenitor cells. The mechanism(s) of action responsible for ECM bioscaffold mediated VML repair are partially understood and include host cell-mediated scaffold degradation and recruitment of endogenous progenitor cells[100,107,163,224]. The recruitment of neurogenic cells and modulation of the innate immune response are also considered as common features associated with ECM-mediated constructive remodeling in preclinical studies[108,179,180,334]. Overall, ECM bioscaffolds have been shown to stimulate endogenous repair[334].

The present manuscript describes the results from the first 13 patients treated using the acellular bioscaffold approach, including results from the first 5 patients previously reported[107]. The results reported herein advance the previously reported findings in several respects: first, it expands the number of patients and anatomic sites of VML subjected to treatment; second, it includes the use of three different source tissues of ECM bioscaffolds; third, it includes the investigation of neurogenic cells as a component of the functional remodeling process; and finally, it includes electrodiagnostic evaluation of the remodeled muscle tissue.

9.3 MATERIALS AND METHODS

9.3.1 Overview of study design

A cohort study examining functional and histomorphologic outcomes following VML repair with acellular biologic scaffolds was conducted with informed consent and approvals from the

Institutional Review Board of the University of Pittsburgh and the US Department of Defense Human Research Protection Office (Clinicaltrials.gov, identifier NCT01292876). Subjects were screened for established exclusion criteria. A total of 13 subjects were enrolled and subjected to a custom designed physical therapy regiment both before and following implantation of one of three different xenogenic scaffold materials, all of which were composed of porcine ECM (Table 5). Patients were enrolled in pre-operative physical therapy and required to reach a functional plateau before the surgical procedure so that post-operative improvements in function could not be attributed to therapy alone. Force production, functional task improvement, EMG analysis, CT or MRI imaging, and histology were used to evaluate return of strength, function, and bioscaffold remodeling characteristics at 6-8 weeks, 10-12 weeks, and 24-28 weeks post implantation.

Table 5. Patient information

Subject	Age	Sex	Injury Site (Side)	Cause of Injury	Months Between Injury and Surgery	Number of Previous Surgeries	Tissue Deficit (estimate)	Device Used
1	34	M	Anterior Tibial Compartment (Left)	Exercise induced	13	5	58%	Acell, Matristem®
2	37	M	Anterior Tibial Compartment (Left)	Skiing accident	32	4	67%	Acell, Matristem®
3	28	M	Quadriceps (Left)	IED blast	18	14	68%	Acell, Matristem®
4	27	M	Quadriceps (Right)	IED blast	89	50	83%	Acell, Matristem®
5	32	M	Anterior/Lateral Tibial Compartment (Left)	Skiing accident	85	8	90%	Acell, Matristem®
6	31	M	Brachialis (Left)	Wakeboarding accident	25	0	90%	Acell, Matristem®
7	31	M	Biceps (Right)	IED Blast	86	8	33%	Cook, BioDesign®
8	66	F	Quadriceps (Left)	MVA	85	1	50.2%	Cook BioDesign®
9	35	M	Quadriceps (Right)	MVA	120	6	80%	Cook Biodesign®
10	44	F	Rectus Femoris (Right)	Tendon Rupture	7	2	48-56%	Bard, XenMatrix™
11	31	M	Biceps/Deltoid (Left)	MVA	72	4	50%	Cook BioDesign®
12	39	M	Sartorius (Left)	Electrocution	12	11	25%	Cook BioDesign®
13	30	M	Hamstring (Left)	Sports Injury	72	0	27%*	Bard, XenMatrix™
Average	35.8				55.07	10.0	66.2%	
SEM	10.2				10.5	4.0	6.3	

9.3.2 Subject selection and screening

Participants ranging from 18 to 70 years of age with a minimum 20% structural volume deficit as determined by MRI or CT, and/or 25% functional deficit of the muscle group mass when compared with the contralateral limb were eligible for inclusion in the study. All study subjects acquired VML at least 6 months prior to study inclusion. Exclusion criteria included poor nutrition, chronic disease, active infection, neoplasia, denervation or other medical comorbidities with the potential to impair wound healing.

Prior to inclusion in the trial, all subjects were screened by a licensed physical therapist to establish strength and functional deficits related to the anatomic location of interest, with respect to the contralateral limb. A detailed subject history was taken and the subject's goals for participation in the study were recorded. Active and passive range-of-motion measurements were obtained at the joints both proximal and distal to the affected area using a goniometer. Isometric strength of the affected muscles was quantified using a hand-held dynamometer. Specific functional outcome variables were selected and evaluated for each subjected based on their functional deficits and the objective measurements of strength and joint range-of-motion. Patient-reported outcomes, including the Disabilities of the Arm Shoulder and Hand (DASH) scale and Lower Extremity Functional Scale (LEFS) were administered, as appropriate. Subjects were also asked to provide a self-report of functional status at each of the tested time points. Outcome variables were established *a priori* for each subject through ha study team consensus based on findings from the clinical examination specific to each subject and their observe strength and functional deficits. When possible, outcome variables were selected that were previously established as valid, reliable, and aligned with the subject's goals for the trial. Video

recordings were performed during evaluations when possible so as to ensure consistency in the testing positions across time points.

9.3.3 Surgical procedure

All procedures were performed in a tertiary care medical center under general anesthesia and tourniquet control of the extremity used. The injured muscle compartment was accessed, scar tissue was debrided, and selective tenolysis performed. One of the following three ECM bioscaffolds was implanted at the site of missing muscle: MatriStem (ACell, Columbia, MD, USA); BioDesign (Cook Medical, Bloomington IN, USA), or XenMatrix (C.R. Bard, Warwick RI, USA) which were derived from porcine urinary bladder (UBM), small intestinal submucosa (SIS), or dermis, respectively. All three scaffold materials were decellularized to meet established minimum criteria for DNA removal. MatriStem was used in the first six subjects, and the remaining seven subjects received either BioDesign or XenMatrix, randomly assigned. The ECM bioscaffold was cut to defect size-matched appropriate length width and implanted within the injury site with contact to adjacent native healthy tissue, and secured under tension with monofilament absorbable sutures. Care was taken to prevent folding or wrinkling and to ensure adequate soft tissue coverage. All empty space was closed before closure of the surgical site to ensure maximum scaffold-host tissue interaction, and a closed suction drain was placed.

9.3.4 Physical therapy

Subjects were required to participate in rigorous pre-operative physical therapy for 4-16 weeks prior to surgery. The goal of the pre-operative physical therapy program was to maximize

performance with respect to the strength and functional outcome deficits identified during the screening examination. Due to the unique clinical presentation of each subject, physical therapy programs were customized for each subject to address the specific strength and functional deficits identified during the screening visit. Subjects were evaluated weekly on their progress by the treating physical therapist. Subjects were cleared to proceed to surgery after they reached a plateau in performance on their involved side, defined as functional gains of < 2-3% over the course of any 2-week period, as determined by the treating physical therapist. The treating physical therapist was not a member of the investigative team. Outcome variables were tested by the same evaluating physical therapist who was a member of the investigative team at each time point.

Post-surgical physical therapy was initiated between 24 and 48 hours following surgery. No limitations were placed on the exercises or functional movements within the limits of tolerable pain. As early as the first post-operative day, targeted exercises were performed with the goal of stimulating muscle contraction and load bearing across the scaffold implantation site. Pain level, range-of-motion, strength, and functional capacity were evaluated at each visit, and exercises were continued as tolerated. The post-operative physical therapy phase lasted 24 weeks.

9.3.5 Isometric strength measurement

Isometric strength testing of the affected limb was measured 1-2 days prior to ECM implantation, and again at 6-8 weeks, 10-12 weeks, and 24-28 weeks post-operatively. All tasks were performed on both the affected and contralateral limb. Each task was repeated three times, and the average of the three trials was calculated as representative of performance on the task.

9.3.6 Range-of-motion and functional task analysis

Range-of-motion and functional task analysis was conducted pre-operatively and at 6-8 weeks, 10-12 weeks, and 24-28 weeks post-operatively. All tasks were performed on both the affected and contralateral limb. Each task was repeated three times, and the average of three trials was calculated as representative of performance on the task.

9.3.7 Pre- and post-surgical imaging

Initial pre-operative CT imaging was performed on a 64-slice CT scanner (LightSpeed VCT, GE Healthcare, Chicago, IL, USA) at a slice thickness of 1.25 and 2.5 mm and a pitch of 1.375 in both bone and soft tissue algorithms. MRI protocols included a variety of sequences in sagittal, coronal, and axial planes using T1-weighted spin echo, T2-weighted fast spin echo with or without fat suppression, and STIR sequences. The KVp and mA were optimized with respect to the subject habitus and site imaged. Coronal and sagittal reformations were obtained. Three-dimensional volumetric reformatted imaging was also performed using Vitrea (Vital Images, Minnetonka, MN, USA) with surface rendering, as well as emphasis on the underlying musculature and osseous structures. Pre-operative imaging was reviewed by a musculoskeletal trained radiologist (4 years' experience). Initial CT imaging was assessed primarily for the presence of volumetric loss of bulk and/or fatty infiltration in the affected musculature. The overall percentage loss of muscle volume and severity of fatty infiltration was graded, where appropriate. Imaging was also evaluated for concomitant soft tissue (e.g. tendinous) and osseous injury. Post-operative imaging was performed at a ~ 7-month interval with similar imaging parameters. Post-operative imaging included characterization of the location and appearance of

the surrounding musculature. Overall percentage change in affected muscle volume was measured.

9.3.8 Ultrasound-guided core biopsy of ECM

Ultrasound-guided biopsy of the surgically-placed ECM was performed ~ 6 weeks and 26 weeks post-operatively. Pre-procedural grayscale and color/Power Doppler ultrasound of the operative site was performed to identify and characterize the surgically-placed ECM. After an appropriate needle trajectory was selected, the area was prepped and draped in sterile fashion. Local anesthesia with skin infiltration and deeper injection was achieved with 1% lidocaine. Under ultrasound guidance, biopsy samples of the ECM bioscaffold and surrounding soft tissue were obtained using an 18-gauge spring-loaded biopsy needle (Temno, CareFusion, McGaw Park, IL, USA). A total of eight core samples were obtained at two separate biopsy sites. Biopsies spanned the proximal to distal length and medial to lateral width of the implantation site. Specimens were snap-frozen in liquid nitrogen and stored at -80°C.

9.3.9 Electrodiagnostic studies

As previously reported, nerve conduction and electromyography studies were performed for 8 of the 13 subjects using a Synergy EMG machine (Cardinal Health, Dublin, OH, USA). The specific nerve conduction studies completed and the specific muscles tested with needle examination were determined by location of the VML. Needle EMG analysis used concentric needle electrodes placed in the standard muscle belly and was performed at the proximal and distal site of the injured muscle if the standard muscle belly showed no evidence of electrical activity. Improvement in nerve conduction was defined as $\geq$ 20% increase in motor nerve conduction amplitude. For EMG studies, improvement was defined as

either evidence of increased firing in volitional recruitment of muscles or a decrease in abnormal spontaneous activity compared with pre-operative results. Differences in amplitudes of CMAP were compared between pre-and post-ECM bioscaffold implant.

9.3.10 Histology and immunolabeling

Frozen tissue sections were fixed in an ice cold 50:50 solution of methanol/acetone for 5 min and washed in phosphate-buffered saline (PBS). Tissue sections were incubated in blocking buffer to prevent non-specific antibody binding composed of 1% (w/v) bovine serum albumin (BSA), 2% (v/v) normal horse serum, 0.05% (v/v) Tween-20, 0.05% (v/v) Triton X-100 in PBS for 1 h at room temperature. Tissue sections were then incubated with primary antibodies diluted in blocking buffer as follows: mouse monoclonal CD146 (Abcam, Cambridge, MA, USA) at 1:350 and rabbit polyclonal Neurogenin-2 (NG2, Millipore, Billerica, MA, USA) at 1:200 as perivascular stem cell markers, monoclonal anti-desmin (Abcam) at 1:200 for a muscle cell marker, and β-III tubulin at 1:200 for a neurogenic marker. After 16 h of incubation at 4°C, tissue sections were washed with PBS and incubated with fluorphore-conjugated secondary antibodies (Alexa Fluor donkey anti-mouse 488 or 594 or donkey anti-rabbit 488, Invitrogen, Carlsbad, CA, USA) for 1 h at room temperature. After secondary incubation, nuclei were counterstained with 4’6-diamidino-2-phenylindole (DAPI) and slides were coated with anti-fade mounting media (Dako, Carpinteria, CA, USA). Tissue sections were imaged using a Zeiss Axio-observer Z1 microscope using a x20, 0.4 numerical aperture objective with a 1.6x optovar magnification changer (Carl Zeiss, Oberkochen, Germany). Three fields of view were taken from each biopsy sample.

9.4 RESULTS

9.4.1 Biologic scaffold implantation for the treatment of VML is associated with increased skeletal muscle force production

Thirteen subjects with VML were enrolled in this cohort study and the average tissue deficit for all patients was 66.2%, when compared with the contralateral limb (Table 5). All subjects met established inclusion criteria (Table 10) and had received standard of care options, including surgical intervention and/or physical therapy. Strength testing showed that 7 of 13 patients had improvement from their pre-surgical maximum strength as early as 6-8 weeks after surgery, by an average of 15.2% $\pm$ 12.6 with a maximum of 127.9% and a minimum of -33.3% (Table 6). By 10-12 weeks, patients showed an average change of 21.1% $\pm$ 12.2 with a maximum of 149.2% and a minimum of -33.0%. At 24-28 weeks, patients showed an average force production changed of 37.3% $\pm$ 12.4 with a significant improvement when compared with pre-operative measurements ($P < 0.05$), with a maximum of 136.1% and a minimum of -17.88%.

9.4.2 Biologic scaffolds for VML treatment are associated with improved range-of-motion and functional outcomes

Tasks to assess range-of-motion were performed and data is reported for all patients who showed range-of-motion deficits pre-operatively. At 6-8 weeks post-surgery, all tested subjects showed improvement in at least one range-of-motion task with an average change of 16.7% $\pm$ 4.9. At 10-12 weeks, average range-of-motion change compared with pre-operative measures was

significantly increased ($P<0.05$) at 24.0% $\pm$ 6.8. By 24-28 weeks after surgery, this improvement increased to 27.1% $\pm$ 10.5 ($p<0.05$) (Table 7).

At 6-8 weeks post-surgery, 10 out of 13 patients showed $\geq$ 20% improvement in performance of at least one functional task when compared with pre-surgical performance (range 20-1980%). By 10-12 weeks, 12 of 13 patients showed a $\geq$ 20% improvement (range 20-2460%), and by 24-28 weeks 9 of 13 patients showed a $\geq$ 20% improvement (range 25-1820%). Patient 3 showed particularly notable improvement in the single-leg hop test improving by 1980%, 2460%, and 1820% at 6-8, 10-12, and 24-28 weeks after surgery, respectively (Table 11). Patient 5 showed a dramatic increase in single-leg jump landing distance, improving by 400%, 783.3%, and 1050% at 6-8, 10-12, and 24-28 weeks after surgery, respectively (Table 11). Likewise, patient 8 showed improvements in the single-leg step down task of 200%, 900%, and 1600% (Figure 26). Twelve of thirteen patients showed improvement in at least 1 functional task by 24-28 weeks after surgery.

Table 6. Force production

Subject	Injury Site (Side)	Activity	Baseline force measurement (lb)	6-8 weeks post surgical (%)	10-12 weeks post surgical (%)	24-28 weeks post surgical (%)
1	Anterior Tibial Compartment (Left)	Dorsiflexion		0.0	0.0	0.0
2	Anterior Tibial Compartment (Left)	Dorsiflexion	0.0	0.0	0.0	0.0
3	Quadriceps (Left)	Knee extension	6.0	*-10.0*	**18.3**	**20.0**
4	Quadriceps (Right)	Knee extension	6.1	**127.9**	**149.2**	**136.1**
5	Anterior/Lateral Tibial Compartment (Left)	Dorsiflexion	3.6	*-33.3*	**16.7**	**33.3**
6	Brachialis (Left)	Biceps Flexion	35.8	NT	*-19.5*	*-17.9*
7	Biceps (Right)	Wrist supination Biceps flexion	42.0 38.1	**66.7** **12.3**	**102.4** **7.6**	**126.2** **16.8**
8	Quadriceps (Left)	Knee extension	10.3	**15.0**	**12.0**	**64.1**
9	Quadriceps (Right)	Knee extension	33.3	**19.0**	**27.0**	**61.9**
10	Rectus Femoris (Right)	Knee extension	6.6	**11.0**	**30.0**	**86.4**
11	Biceps/Deltoid (Left)	Shoulder abduction Shoulder flexion Shoulder extension Elbow flexion Elbow extension	69.2 46.6 51.3 66.9 49.0	-4.6 **41.9** **13.3** 0.0 *-8.2*	*-4.1* **42.5** **22.6** *-0.3* **31.0**	**20.1** **104.1** **46.8** *-4.0* **1.6**
12	Sartorius (Left)	Hip flexion Knee extension	68.1 92	NT	*-15.6* *-28.0*	*-3.5* *-1.1*
13	Hamstring (Left)	Knee flexion Knee extension	53.5 99.2	**11.8** *-33.0*	**11.0** *-33.0*	*-3.4* **0.5**
			Average	**15.2**	**21.1**	**37.3**[#]
			SEM	**12.6**	**12.2**	**12.4**

Table 7. Range of motion

Subject	Injury Site (Side)	Activity	Baseline force measurement (deg)	6-8 weeks post surgical (%)	10-12 weeks post surgical (%)	24-28 weeks post surgical (%)
1	Anterior Tibial Compartment (Left)			0.0	0.0	0.0
2	Anterior Tibial Compartment (Left)	Active dorsiflexion Passive dorsiflexion	0 8	0.0 **50.0**	0.0 **88.0**	0.0 **88.0**
3	Quadriceps (Left)	Active knee extension	22	**18.2**	**18.2**	**18.2**
4	Quadriceps (Right)	Active knee extension	40	**25.0**	**38.0**	**NT**
5	Anterior/Lateral Tibial Compartment (Left)	Active dorsiflexion Passive dorsiflexion	0 10	0.0 **20.0**	0.0 **20.0**	0.0 **NT**
6	Brachialis (Left)	External rotation (elbow 90°) Internal rotation (elbow 90°)	31 29	NT NT	**32.9** **33.5**	**13.6** **43.5**
8	Quadriceps (Left)	Active knee extension	45	**11.1**	*-11.1*	**0.0**
11	Biceps/Deltoid (Left)	Shoulder external rotation Shoulder internal rotation Shoulder flexion Shoulder extension	35.2 46.2 46.6 51.3	*-11.7* **33.6** **41.2** **13.3**	**8.5** **42.4** **42.5** **22.6**	*-30.4* **41.6** **104.1** **46.8**
			Average	**16.7**	**24.0**[#]	**27.1**[#]
			SEM	4.9	6.8	10.5

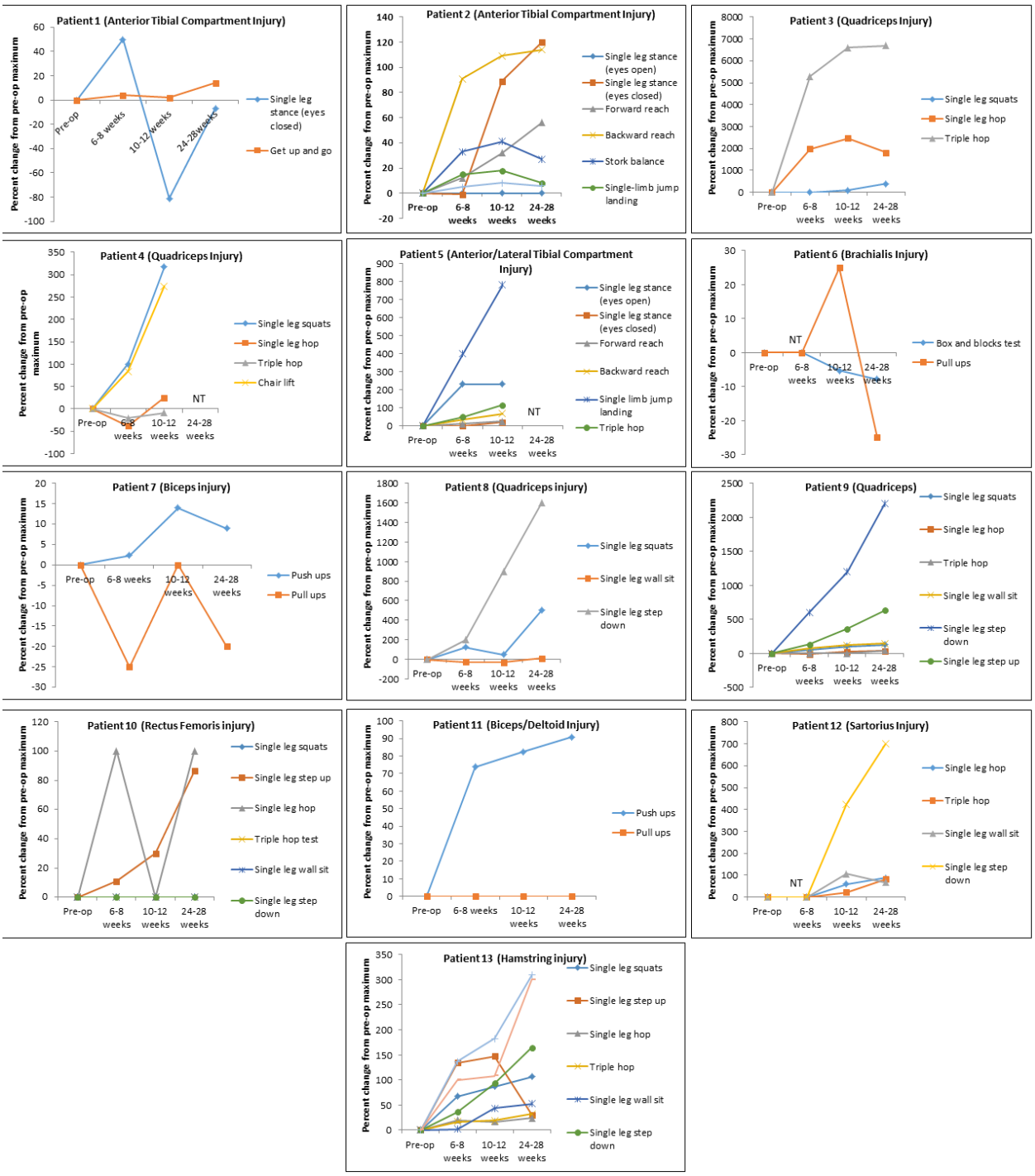

Figure 26. Functional task performance. Functional measures as assessed by task / exercise completion from each patient. Data represent percent change from pre-surgical maximum. NT=not tested.

9.4.3 ECM bioscaffold implantation is associated with PVSC mobilization, electromyographic evidence of innervation, the presence of neurogenic cells at the remodeling site, and muscle formation

Tissue biopsies of the remodeling implantation site were obtained at 6-8 weeks, 10-12 weeks, and 24-28 weeks post-surgery, and showed a robust mononuclear cellular infiltration into the bioscaffold site along with evidence of muscle formation into the bioscaffold site along with evidence of muscle formation as early as 6-8 weeks post-surgery (Figure 27A), which was increased at each subsequent biopsy time point. Immunolabeling studies showed CD146+NG2+ PVSCs localized around vWF+ vessels at all time points (Figure 27G-I). PVSCs were also found removed from their normal anatomic location, suggesting their potential contribution to skeletal muscle formation (Figure 27J-L). Desmin+ cells with central nuclei were present as early as 6-8 weeks post-surgery (Figure 27D) with striated desin+ muscle fibers present in all biopsy samples at both 10-12 and 24-28 weeks after surgery (Figure 27E-F). These desmin+ muscle fibers were present at locations both near the interface with native uninjured muscle and within the center of the scaffold site with no evidence for continuity with adjacent native healthy muscle. Biopsies also showed an increase in the presence of β-III tubulin+ nerve bundles by 6 months after implantation throughout the scaffold implant site (Figure 27O) CellProfiler (Broad Institute, Cambridge, MA, USA) quantification showed no significant differences in the number of migrating PVSCs or vessels between time points (Figure 27M-N).

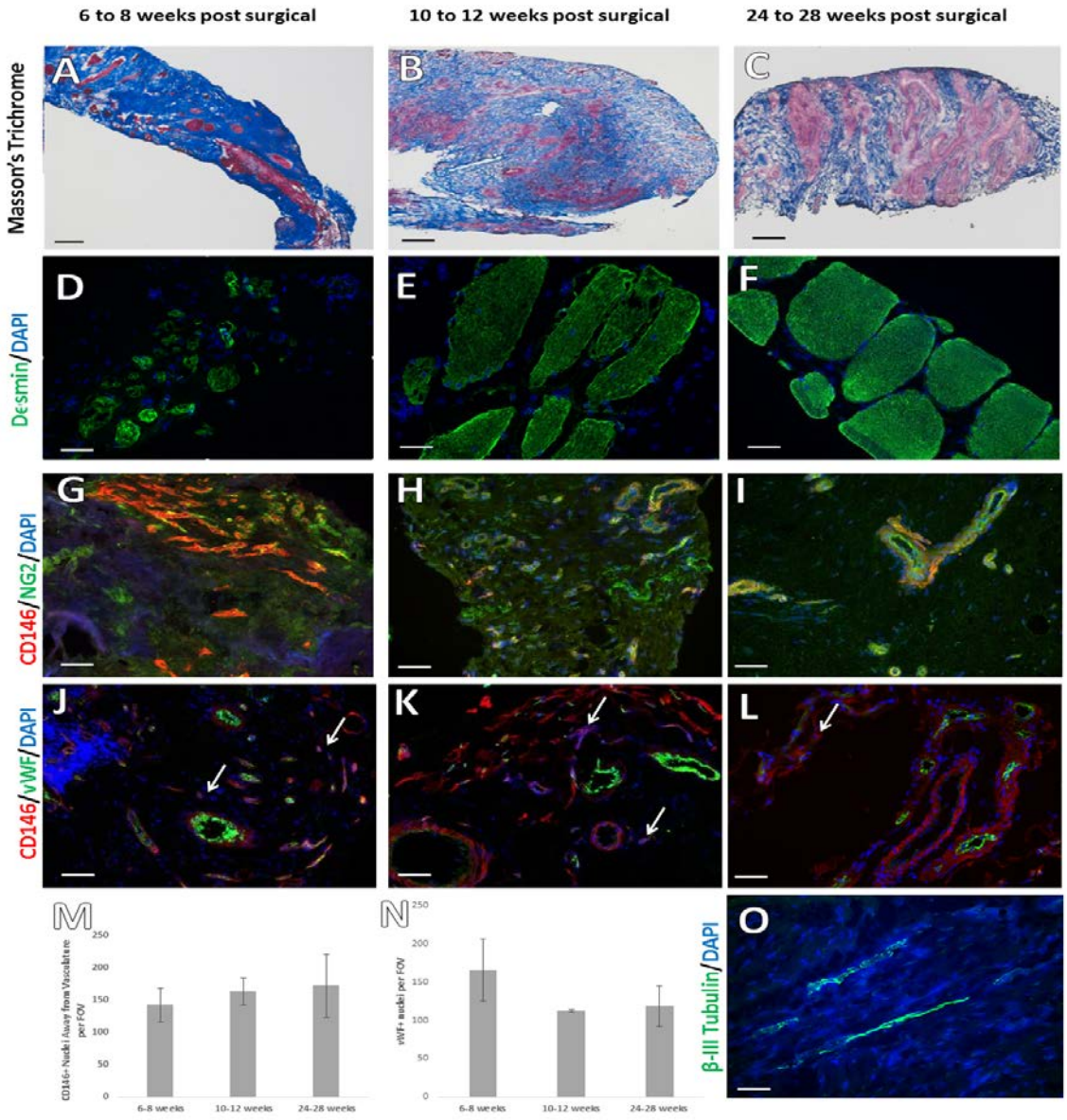

Figure 27. Site-appropriate tissue remodeling by ECM bioscaffolds (A-C) Masson's trichrome staining of human muscle biopsies shows islands of skeletal muscle present at 6-8 weeks, 10-12 weeks, and 24-28 weeks post surgery, respectively. **(D-F)** Human muscle biopsies are characterised by desmin expression at all time points, indicating new muscle formation within the site of implantation. **(G-I)** ECM bioscaffold implantation is associated with the presence of CD146+NG2+ perivascular stem cells. **(J-L)** PVSCs were shown to migrate away from their normal vessel associated anatomic location at all time points. Arrows indicate CD146+ PVSCs migrating away from vessels. **(M,N)** Migrating PVSCs and vasularity were quantified using CellProfiler Image Analysis software. **(O)** At 24-28 weeks post surgery, ECM bioscaffold implantation was associated with the presence of β-III tubulin+ cells, implicating innervated skeletal muscle (Scale bars = 50µm)

9.4.4 ECM scaffolds degrade following implantation

Representative ultrasound imaging at 1 month after surgery showed a sheet-like hyperechoic structure consistent with the ECM scaffold overlying and adjacent to the native uninjured muscle (Figure 28A). By 7 months, BioDesign (SIS-ECM) and Matristem (UBM-ECM) ECM scaffold materials were no longer identifiable (Figure 28B,D) whereas XenMatrix (dermis-ECM) ECM scaffold was still identifiable (Figure 28F). In addition, increased muscle tissue, identified by an imaging signal consistent with muscle, was present at the site of ECM scaffold placement (Figure 28).

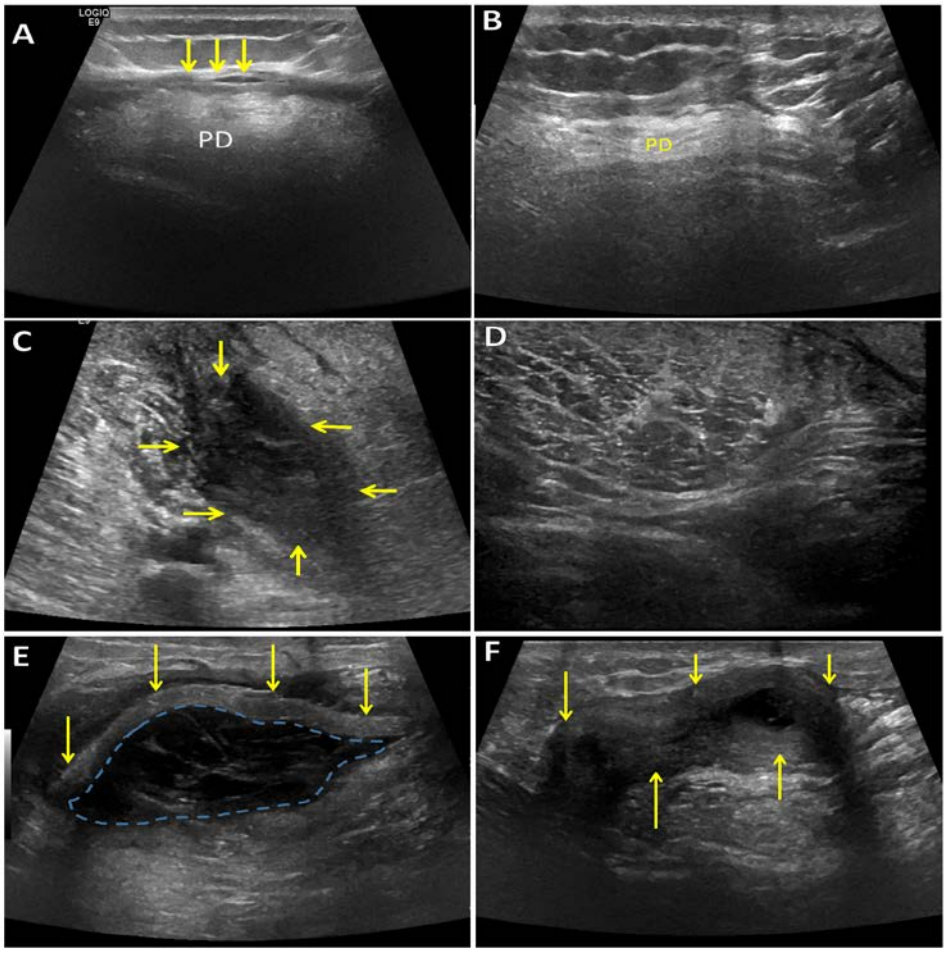

Figure 28. Ultrasound imaging shows that ECM bioscaffolds degrade upon implantation. (A) Grayscale ultrasound image 1 month after surgery in the posterior shoulder demonstrates a thin, sheet-like hyperechoic structure, representing SIS-ECM (yellow arrows) overlying the posterior deltoid muscle. The posterior deltoid muscle is increased in echogenicity due to underlying fatty infiltration. **(B)** Ultrasound imaging 7 months after surgery shows that surgically-placed SIS-ECM is no longer identifiable superficial to the posterior deltoid. **(C)**Ultrasound image 1 month after surgery in the medial mid thigh demonstrates an ill-defined hypoechoic structure representing SIS-ECM (yellow arrows) adjacent to the sartorius muscle. **(D)** Ultrasound image 7 months after surgery shows that surgically-placed SIS-ECM is no longer identifiable and the sartorius muscle apears to have enlarged. **(E)** Ultrasound imaging 1 month after surgery in the posterior mid thigh demonstrates a shet-like echogenic structure representing dermal ECM (yellow arrows) with surrounding complex anechoic material (dashed-blue line) likely representing post-operative fluid collection. **(F)** Ultrasound imaging 7 months after surgery shows dermal ECM (yellow arrows) has decreased in echogenicity and now has a tubular or 'rolled-up' appearance as opposed to a sheet-like appearance. The previously identified post-operative fluid collection has essentially resolved

9.4.5 ECM treatment increases bulk muscle content

Before surgery, the average percent of muscle loss ranged from 25-90% of contralateral limb tissue (Table 5). By 8 months, computed tomography (CT) or magnetic resonance imaging (MRI) showed an increase in dense tissue consistent with that of skeletal muscle within the implantation site. Post-operative muscle bulk was calculated by selecting a region-of-interest in CT or MRI images. Bulk muscle increased in all patients post-operatively with an average increase of 27.2% (Figure 29). Interestingly, patient 13 showed complete atrophy and absence of hamstrings due to rupture pre-operatively. Following ECM treatment, the implant site was replaced with tissue characterized by an imaging signal consistent with muscle at measurements of 5.45 cm^2, 6.90 cm^2, and 7.39 cm^2, at the proximal, middle, and distal aspect of the defect in the posterior compartment, respectively (Figure 29).

Subject	Location	Pre-surgical	8 Months Post Surgical	Increase in post operative bulk muscle
10	Proximal Quadriceps	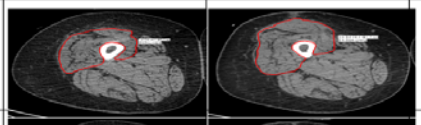		38.2 %
	Middle Quadriceps	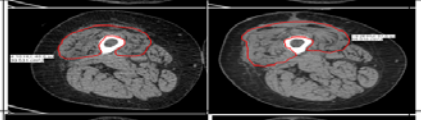		39.2%
	Distal Quadriceps	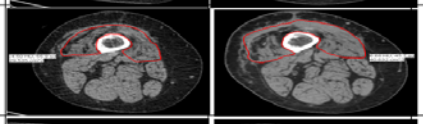		37.5%
11	Proximal Posterior Deltoid	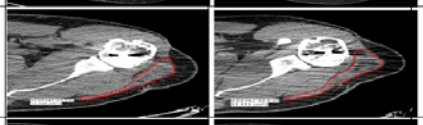		42.8%
	Middle Posterior Deltoid	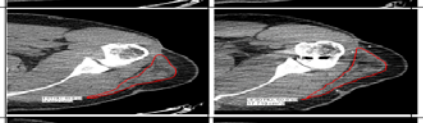		19.1%
	Distal Posterior Deltoid	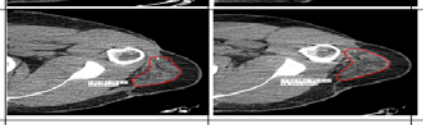		26.1%
12	Proximal Sartorius	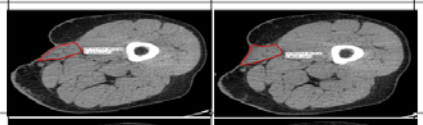		22.8%
	Mid Sartorius	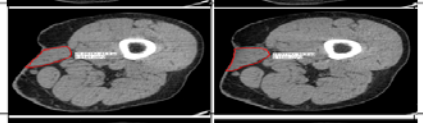		13.7%
	Distal Sartorius	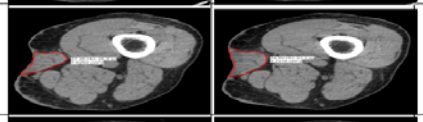		37.5%
13	Proximal Hamstring Musculature	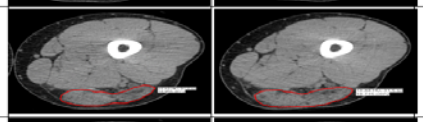		25.1%
	Middle Hamstring Musculature	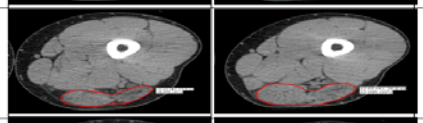		13.4%
	Distal Hamstring Musculature	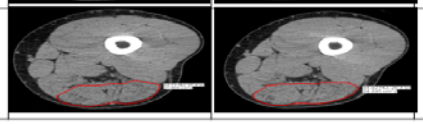		11.1%

Figure 29. Representative CT imaging shows ECM bioscaffold implantation increases post-operative bulk muscle content. Overall, the area of the treated muscle was measured at three representative sites (proximal, middle, and distal) both prior to surgery and 7 months after surgery in multiple anatomic locations

Table 8. Nerve conduction study of eight of thirteen patients

		Latency/Amplitude (ms/mV)		
Subject	**Evaluation site**	**Contralateral**	**Pre-op**	**Post-op**
1	Peroneal motor	2.5/3.7	2.6/3.7	2.5/2.5
2	Peroneal motor	2.7/6.8	2.8/2.5	2.5/**2.5**
3	Femoral motor	3.0/9.7	2.7/3.9	3.6/**4.8**
4	Femoral motor	NT/NT	3.1/10.9	3.6/4.8
5	Peroneal motor	3.7/10.0	2.3/1.7	2.1/1.5
7	Musculocutaneous Motor	2.1/8.4	2.6/5.6	3.4/**6.9**
8	Femoral motor	2.5/7.2	1.2/3.8	2.9/**5.0**
9	Femoral motor	NT/NT	2.6/9.7	4.6/5.4

9.4.6 ECM bioscaffold implantation improves electrophysiological function

Electrodiagnostics studies were conducted on 8 of the 13 patients. At baseline, seven of the eight tested subjects presented with patterns of mononeuropathies, with three subjects with anterior compartment injures in the lower leg presenting with deep peroneal mononeuropathy and three of the four subjects quadriceps injury presenting with femoral mononeuropathy and one individual presented no abnormal finding. The abnormalities were limited to the injury site and did not extend distally along the nerve. Two tested subjects showed severe atrophy with undetectable compound motor action potentials (CMAPs). Post-operatively, four subjects increased CMAP amplitude: one in the tibialis anterior, two in the vastus medialis, and one in the biceps brachii (Table 8). The remaining subjects showed no appreciable change in nerve conduction. Electromyography (EMG) analysis showed disappearance in abnormal spontaneous activity and improved recruitment patterning following ECM bioscaffold implantation (Table 9).

Table 9. Needle electromyography

Subject	Evaluation site		Pre-op	Post-op
1	Tibialis anterior	ASA	-	-
		Recruitment	No unit	No unit
2	Tibialis anterior	ASA	-	-
		Recruitment	No unit	No unit
3	Vastus medialis	ASA	++++	+++
		Recruitment	No unit	No unit
	Vastus intermedius	ASA	++++	+++
		Recruitment	MD	GD
	Vastus lateralis	ASA	+++	+++
		Recruitment	GD	No unit
4	Vastus medialis	ASA	+++	+++
		Recruitment	No unit	No unit
	Vastus intermedius	ASA	++	-
		Recruitment	No unit	No unit
	Vastus lateralis	ASA	-	+
		Recruitment	Normal	Normal
5	Tibialis anterior	ASA	++	-
		Recruitment	GD	SD
	Extensor digitorum longus	ASA	++	-

Table 9 (continued)

		Recruitment	**Single unit**	**SD**
7	**Biceps (proximal)**	**ASA**	**-**	**-**
		Recruitment	**Normal**	**Normal**
	Biceps (distal)	**ASA**	**NT**	**++**
		Recruitment	**NT**	**poly**
8	**Vastus medialis**	**ASA**	**+**	**-**
		Recruitment	**Normal**	**Normal**
	Vastus intermedius	**ASA**	**-**	**-**
		Recruitment	**Normal**	**Normal**
	Vastus lateralis	**ASA**	**-**	**-**
		Recruitment	**Normal**	**Normal**
9	**Vastus medialis**	**ASA**	**-**	**-**
		Recruitment	**Normal**	**Normal**
	Vastus lateralis	**ASA**	**-**	**-**
		Recruitment	**Normal**	**Normal**
	Rectus femoris	**ASA**	**-**	**-**
		Recruitment	**Normal**	**Normal**

Table 10. Inclusion and exclusion criteria

Exclusion criteria	Inclusion criteria
Inability to provide informed consent	18 to 70 years of age
Poor nutrition (demonstrated by abnormal lab range for serum albumin)	Civilian and current or former military personnel are eligible
Cancer diagnosis within the last 12 months	Minimum structural deficit of 20% of muscle group mass
Complete muscle/tendon gaps greater than 5 cm	Minimum functional deficit of 25% when compared to contralateral limb
Infection	Injury may encompass a single muscle belly or compartment
Known coagulopathy	Injury suffered within the last 18 months; subjects may be enrolled with injury outside this range if PI determines there is viable muscle in the injured compartment by clinical exam and imaging analysis
Diagnosis of schizophrenia or bipolar disorder	Eligible for study procedures 3 months post injury
Chronic disease (i.e. congestive heart failure, liver disease, renal disease, diabetes)	Willing and able to comply with follow up examinations radiographic studies, physical therapy, muscle biopsy, and laboratory tests
Active and unstable disease state or infection per doctor's evaluation	
Pregnancy	
Hypersensitivity to bovine serum or porcine products	

Table 11. Functional task raw data

Subject	Activity	Baseline measurement (pre-op)	6-8 weeks post surgical (%)	10-12 weeks post surgical (%)	24-28 weeks post surgical (%)
1	Single leg stance (eyes closed)	13.3 s	50.0	-81.2	-7.0
	Get up and go	5.0 s	4.0	2.0	14.0
2	Single leg stance (eyes open)	>15 s	0.0	0.0	0.0
	Single leg stance (eyes closed)	> 30 s	-1.0	89.0	120.0
	Forward reach (in)	8.33 in	12.0	32.0	56.0
	Backward reach (in)	4.67 in	91.0	109.0	114.0
	Stork balance test (s)	30 s	33.0	41.0	27.0
	Single limb jump landing (in)	66.4 in	15.0	18.0	8.0
	Triple hop test (in)	220 in	5.0	8.0	6.0
3	Single leg squats (reps)	unable	unable	4.0 (compared to contralateral)	13.3 (compared to contralateral)
	Single hop (in)	1.25 in	1980.0	2460	1820
	Triple hop (in)	unable	24.2 (compared to contralateral)	29.3 (compared to contralateral)	29.5 (compared to contralateral)
	LEFS	45/80	22.2	22.20	35.56
4	Single leg squats (reps)	6 reps	NT	100	317
	Single hop for distance (in)	16 in	NT	-38	25
	Triple hop (in)	52 in	NT	-21	-9
	LEFS	61	NT	6.56	3
	Chair lift test (reps)	38 reps	NT	84	274
5	Single leg stance (eyes open)	27.1 s	NT	232	232
	Single leg stance (eyes closed)	10.0 s	NT	0	20
	Forward reach (in)	12.5 in	NT	12	24
	Backward reach (in)	6 in	NT	33	67
	Stork balance test (s)	Unable	NT	Unable	Unable
		3 in	NT NT	400	783

Table 11 (continued)

	Single limb jump landing (in)	45.5 in	NT	49	115
	Triple hop (in)	44		9	2
	LEFS				
6	Box and blocks test (s)	76 s	NT	-5.3	-7.9
	Pull ups (reps)	4 reps	NT	25.0	-25.0
7	Push ups (reps)	43 reps	2.3	14.0	9.0
	Pull ups (reps)	5 reps	-25	0	-20.0
	Elbow flexion endurance (s)	43 s	120.93	116.28	272.09
8	Single leg squats (reps)	4 reps	125.0	50.0	500.0
	Single leg hop for distance (in)	Unable	unable	unable	unable
	Triple hop (in)	Unable	unable	unable	unable
	Single leg wall sit (s)	30 s	-26.7	-30.0	10.0
	Single leg step down (reps)	1 rep	200.0	900.0	1600
9	Single leg squats (reps)	11 reps	45.0	100.0	127.3
	Single leg hop (in)	15 in	-13.0	20.0	33.0
	Triple hop test (in)	42 in	unable	unable	42.9
	Single leg wall sit (s)	23 s	78.3	117.0	143.0
	Single leg step down (reps)	1 rep	600.0	1200.0	2200.0
	Single leg step up (reps)	10 reps	130.0	360.0	630.0

Table 11 (continued)

10	Single leg squats (reps)	0 reps	0	0	0
		0 reps	100	0	100
	Single leg step up (reps)	0 in	0	0	0
	Single leg hop (in)	0 in	0	0	0
	Triple hop test (in)	0 s	0	0	1900
	Single leg wall sit (s)	0 reps	0	0	0
	Single leg step down (reps)				
11	Push ups (reps)	23 reps	-11.7	8.6	-30.4
	Pull ups (reps)	2 reps	0	0	0
12	Single leg hop (in)	14.5 in	NT	59.0	88.3
	Triple hop test (in)	67 in	NT	22.0	82.1
	Single leg wall sit (s)	18 s	NT	106.0	67.0
	Single leg step down (reps)	4 reps	NT	425.0	700.0
13	Single leg squats (reps)	15 reps	67.0	87.0	106.7
		77 reps	134.0	147.0	30.0
	Single leg step up (reps)	39.5 in	20.0	16.0	24.0
	Single leg hop (in)	141 in	16.0	19.0	32.0
	Triple hop test (in)	69 s	1.5	43.0	52.0
	Single leg wall sit (s)	14 reps	36.0	93.0	164.0
	Single leg step down (reps)	11 reps	136.4	182.0	309.0
		25 s	100.0	108.0	300.0
	Single leg bridge (reps)				
	Single leg bridge (s)				

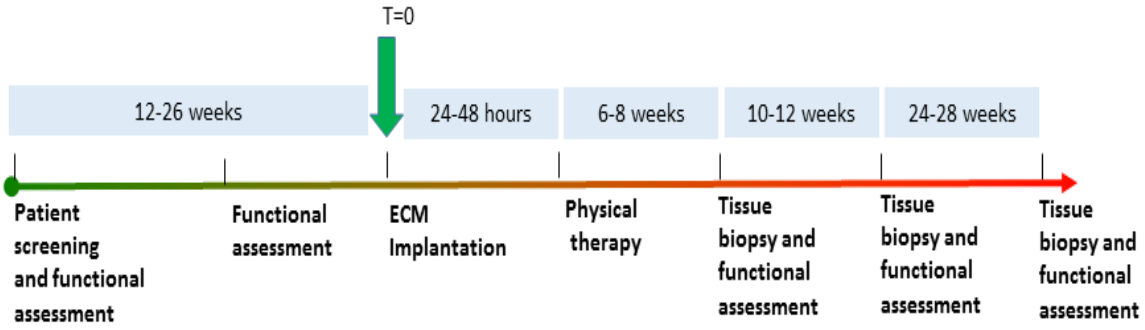

Figure 30. Overview of study design. Patients underwent 6-8 weeks of pre-operative physical therapy followed up to 28 weeks of post-operative physical therapy. Tissue biopsies and functional assessments were evaluated 6-8, 10-12, and 24-28 weeks after ECM implantation.

Figure 31. Representative gross changes of quadriceps following ECM implantation. Gross appearance of injury site of patient 3 pre-operatively and 28 weeks post-ECM implantation

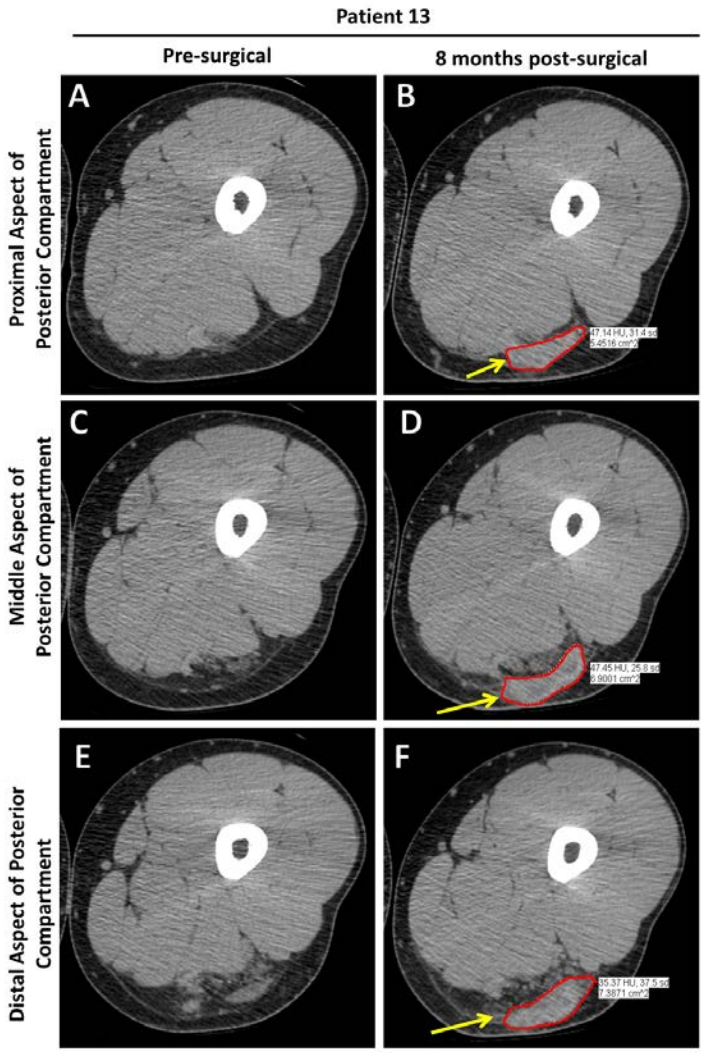

Figure 32. ECM promotes muscle formation (A,C,E)) Before surgery, at this level of the proximal aspect in the posterior compartment, patient 13 shows complete absence or atrophy of hamstrings. ECM imlpantation is associated with an increase in post-operative bulk muscle with areas measuring 5.4, 6.9, and 7.3 cm^2 at the proximal, distal, and middle aspect of the posterior compartment, respectively **(B,D,F).**

9.5 DISCUSSION

The present study provides a comprehensive analysis of the structural remodeling, strength, and functional outcomes after VML defects were treated with extracellular matrix (ECM) bioscaffolds in thirteen human subjects. The study corroborates and extends the findings of previous work by not only increasing the number of patients, but also utilizing three different forms of ECM bioscaffolds, identifying neurogenic cell types in the remodeling site, and documenting electrophysiologic evidence of innervation and its association with functional remodeling outcomes.

Acellular bioscaffolds for VML treatment represent an “off-the-shelf” approach to muscle repair. As opposed to cell-based strategies, a bioscaffold approach obviates the requirements of cell isolation, manipulation, expansion, storage, and delivery strategies. In the present study, ECM bioscaffolds derived from three different xenogeneic (porcine) source tissues – small intestinal submucosa (SIS), urinary bladder matrix (UBM), and dermal ECM were utilized. The first five patients were treated with UBM as previously reported, and the subsequent eight patients were treated with a randomly assigned scaffold derived from UBM, SIS or dermal ECM. To conclusively discriminate between the abilities of each scaffold type to promote muscle remodeling would require a much larger study. Although our study was not powered to detect variation based on ECM, no differences in outcomes were seen based upon bioscaffold used. These findings suggest that though the mechanical and physical properties vary between the three scaffold types, the signaling mechanisms associated with each type of scaffold seem to be similar and a spectrum of commercially available products can be used for this

therapeutic approach. A comparative analysis of the differences between ECM source tissues and their effects upon skeletal muscle reconstruction could only be reliably performed in a very large sample due to the variety of anatomic sites at which they need to be placed. Each of the bioscaffolds used differ in their preparation methods including method of decellularization and terminal sterilization. Such differences will logically confer differences in their mechanical and biochemical properties. Further investigation could provide insight into the preparation parameters that are associated with positive tissue remodeling outcomes and could implicate the specific bioscaffold constituents and/or properties that contribute to ECM-mediated skeletal muscle remodeling.

While the exact mechanism(s) by which ECM bioscaffolds promote constructive tissue remodeling are only partially understood, previous work has shown that their degradation upon implantation generates low molecular weight matricryptic oligopeptides with the ability to recruit and influence endogenous progenitor cells[78,109]. It has been shown that perivascular stem cells (PVSCs) play a role in ECM-mediated skeletal muscle repair[107]. The present study shows CD146+NG2+ PVSCs are not only localized around their typical microvascular niche, but, following ECM implantation, mobilize away from this traditional anatomic site. All muscle biopsies showed this phenomenon as well as evidence for neovascularization and the presence of site-appropriate desmin+ striated muscle as early as six weeks after bioscaffold implantation. The ability of ECM bioscaffolds to influence the local skeletal muscle injury microenvironment may allow for synergy and cross-talk between PVSCs, myoblasts, neuronal progenitors, and other responding cell types which contribute to skeletal muscle formation at the implant site. The presence of PVSCs and myoblasts within this site strongly suggests their participation in the remodeling process. Whether or not the behavior of PVSCs and myoblasts is mediated directly

by signaling from the ECM or via paracrine mechanisms is unknown; however, it is plausible and logical that other stem and progenitor cell populations also play a role in this constructive and functional remodeling process. Many progenitor cell populations have been shown to contribute to myogenesis following injury. PVSCs are among the most primitive source of stem cells that have been shown to give rise to myogeneic cells. In fact, such cells have been shown to give rise to satellite cells, the putative skeletal muscle precursor.

Desmin+ skeletal muscle fibers were found not only at the interface of the bioscaffold with native, adjacent, uninjured muscle, but also within the center of the scaffold implantation site. The spatial distribution of skeletal muscle fibers clearly separated from the interface with adjacent uninjured native muscle suggests *de novo* skeletal muscle generation rather than simple integration of native muscle with the scaffold-filled defect site. *In vitro* studies have shown the ability of ECM signaling molecules to promote mitogenesis and myogenesis of skeletal muscle progenitor cells[78]. The presence of β-III tubulin+ cells in association with these new islands of skeletal muscle, combined with positive EMG recordings, further supports the conclusion that functional islands of new skeletal muscle have been formed.

The degradation rate of biologic scaffolds has been investigated and studies have shown that this degradation is rapid – with the ECM being completely replaced by host tissue by 90 days. There is evidence of islands of new skeletal muscle formation present throughout the collagenous tissue. However, we cannot determine with certainty whether this collagen is from the implanted ECM bioscaffold or is newly deposited host tissue ECM within the implant site. However, the accurate real time imaging enabled precise retrieval of tissue from the zone of regeneration. Moreover, the histologic findings are consistent with new muscle formation, and not mature native muscle or scar tissue.

CT or MRI imaging corroborated the histologic findings showing an increase in post-operative soft tissue formation consistent with bulk skeletal muscle tissue in all thirteen patients. Whether or not this increase was due to an increase in the size or the number of muscle fibers requires further investigation. However, the needle EMG findings of decreased ASA and improved recruitment would seem to indicate new muscle fiber formation.

The histomorphologic and imaging studies were accompanied by clear and clinically relevant functional improvement. Two of the thirteen patients showed an unappreciable change in force production compared to pre-operative outcomes, but eleven of thirteen patients increased their pre-operative force production measured via dynamometer by 20% to 140% at six months after surgery. Twelve out of thirteen patients showed improvement in functional task performance. It is important to note that all patients had previously undergone standard of care treatments, and custom designed, aggressive physical therapy regimens prior to ECM implantation and showed a plateau in force production or functional task performance. The improvements in performance following ECM bioscaffold implantation are thus likely due to ECM intervention. The importance of a rigorous physical therapy program following ECM implantation and its association with successful outcomes should not be underestimated. The application of a physiologic mechanical load (i.e., concomitant physical rehabilitation) during the entirety of the remodeling period following ECM implantation has been shown to promote favorable outcomes[60,61,258,322]. It has been suggested that ECM bioscaffolds contribute to force improvement by simple force transduction based upon results of a rodent model in which post-operative physical therapy could not be controlled[226]. While the scar release of the procedure and the mechanical transduction effect of the ECM layer may both be contributing factors to the improved function, the histologic imaging and electrophysiologic evidence of vascularized,

innervated skeletal muscle within the defect site in the present cohort of human patients suggests a positive and contributing role for new skeletal muscle in the functional outcomes. Taken together, the data from this study shows that ECM implants for soft tissue reconstruction, while long regarded as a passive reinforcing layer, can undergo important functional remodeling during the healing process.

Electrodiagnostic studies conducted on eight of the thirteen patients showed concomitant nerve and muscle remodeling following ECM treatment. Specifically, seven subjects presented with a pre-operative electrodiagnosis of incomplete mononeuropathy in the area of the VML defect. After treatment with ECM, five of the eight patients showed improvements in nerve conduction or needle electromyography parameters including compound motor action potential (CMAP). These results indicate electrically active, functionally innervated muscle. Electrical activity present within the ECM implant site is consistent with a concomitant strength improvement. Histologic outcomes further corroborate these results showing presence of β-III tubulin+ cells within the remodeling site by six months after surgery.

The present study has several limitations. It was not possible to include an untreated control to determine the effects of scar tissue debridement and tenolysis alone. However, twelve of thirteen patients had been subjected to extensive standard of care therapy (i.e. average of ten previous surgeries across all patients) and failed to improve. Placebo effects (i.e. patients having more confidence after treatment which could translate to improved functional outcomes) were uncontrolled. Although histologic outcomes show the presence of perivascular stem cells and desmin+ muscle fibers within the ECM implantation site, and these findings were associated with improved functional and strength outcomes, the present study does not provide conclusive evidence that there is a causal relationship between the presence of these cells and the

downstream functional improvements. The diverse nature of anatomic implant sites and physical therapy activities performed by the subjects made determination of an “average” functional improvement following bioscaffold implantation impossible. No two patients had the same injury or comorbidities, and thus each had a personalized physical therapy regimen composed of specific exercises depending on the site of injury and other comorbidities.

The results of this thirteen patient cohort study show that an acellular biologic scaffold approach can facilitate constructive and functional tissue remodeling following volumetric muscle loss. The mechanisms by which such materials mediate remodeling effects appear to include recruitment of myogenic progenitor cells, improved innervation, and functional skeletal muscle formation. The findings reported herein support the use of ECM bioscaffolds as a viable treatment option for VML treatment.

9.6 ACKNOWLEDGEMENTS

The US Department of Defense’s Limb Salvage and Regenerative Medicine Initiative and the Muscle Tendon Tissue Unit Repair and Reinforcement Reconstructive Surgery research study is collaboratively managed by the Office of the Secretary of Defense. The Initiative is focused on rapidly and safely transitioning advanced medical technology in commercially viable capabilities to provide our wounded warriors the safest and most advanced care possible today. We would like to gratefully acknowledge the work of Ally Lacovey, Debra Smith, Douglas Weber, Tyler Simpson, Lee Fisher, and Spencer Brown, as well as the surgical expertise of Ernest Manders, Jeffery Gusenoff, and Oguz Acarturk. This study is supported by research grants to S.B., J.P.R., by the U.S. Department of the Interior, the National Buisness Center, Acquisition Services

Directorate, Sierra Vista Branch (award no. D11AC00006). A. Russell was instrumental in the acquisition of this funding. J.D. was supported by the National Science Foundation Graduate Student Research Fellowship.

10.0 SUMMARY OF MILESTONES AND FUTURE DIRECTIONS

The central hypothesis addressed in this thesis is that ECM bioscaffolds support constructive remodeling of skeletal muscle tissue by modulation of the microenvironment; specifically, macrophages and stem / progenitor cells, and that this response is augmented by concomitant mechanical loading. The following milestones were achieved:

Milestone 1: The spatiotemporal cell response to ECM treatment of volumetric muscle loss was determined.

Summary Milestone 1: Acute skeletal muscle regeneration relies upon the responding host innate immune response, specifically the transition in macrophage phenotype from pro-inflammatory to pro-remodeling macrophages to drive myogenesis. This transition, however, is absent in cases of a critically-sized injury like volumetric muscle loss. Utilizing an acellular biologic scaffold approach, ECM treatment of VML promotes a phenotypic switch in macrophages, and this switch is subsequently followed by an increase in myogenic and neurogenic progenitor cells, contributing to constructive remodeling outcomes. Spatiotemporal quantification shows that these cells appear at both the margin of the defect near native uninjured muscle, but also at the center of the remodeling site.

Future Directions Milestone 1: Future experiments should focus on determining if there is a cause-effect relationship between the macrophage transition and the stem / progenitor cell

response in ECM-mediated VML remodeling. By preventing a macrophage transition, does constructive tissue remodeling still occur with ECM treatment? Additionally, while it was shown that some cells express neural progenitor markers by immunolabeling, temporal functional innervation should be tested to determine whether there is a correlation between function and the histologic presence of neurogenic cell types in the VML remodeling site.

Milestone 2: The effect of ECM derived from diverse source tissues on the phenotype of macrophages was characterized.

Summary Milestone 2: ECM-mediated constructive tissue remodeling has been associated with a modulation of macrophage phenotype at early time points. Macrophage activation has been established as a critical determinant of acute skeletal muscle regeneration, and is likely a key player in promoting remodeling in the case of volumetric muscle defects. Chapter 7 shows that ECM (1) directly affects macrophage phenotype, (2) the macrophage response to ECM is unique depending upon the source tissue from which the ECM is derived, (3) in general, ECM treatment prompts a pro-remodeling, M2-like macrophage phenotype and suppression of pro-inflammatory markers as evidenced through gene expression (Appendix), surface marker and protein expression (Chapter 7), and functional activity. However, an "M_{ECM}" macrophage is distinct from macrophages activated with canonical stimuli such as IFNγ and LPS and IL-4.

Future Directions Milestone 2: Future experiments should focus on determining what component(s) of ECM elicit the macrophage response to determine the cause of the differential responses to diverse source tissues. In addition, while the present thesis shows that the ECM materials promote a shift in innate immune cell phenotype, future experiments should aim to

determine the effect of these materials on the adaptive immune response that also contributes to remodeling outcomes. An *in vivo* comparison of the macrophage response of ECM derived from diverse source tissues would provide valuable information regarding the impact of the macrophage response on constructive remodeling outcomes.

Milestone 3: The impact of mechanical load on macrophage-progenitor cell crosstalk and ECM-mediated skeletal muscle remodeling as determined and the clinical efficacy of ECM bioscaffolds for VML treatment was evaluated.

Summary Milestone 3: Mechanical loading has been associated with proper musculoskeletal strength and endurance maintenance, fatigue resistance, development, and acute regeneration. Chapter 8 shows that mechanical loading (1) activates macrophages towards a pro-remodeling phenotype, (2) alters the secretome of macrophages to promote increased myoblast chemotaxis and differentiation, (3) promotes myogenesis, and (4) alters the secretome of myotubes to promote a pro-remodeling macrophage phenotype. The effect of mechanical loading augments the response of macrophages and myogenic progenitor cells to ECM bioscaffolds. The lack of concomitant mechanical load during ECM-mediated skeletal muscle remodeling impacts the local responding macrophage phenotypic ratio (decreases the M2-like to M1-like ratio), and hinders site-appropriate tissue deposition and negatively impacts strength restoration. Clinically, the use of ECM bioscaffolds can promote strength, range-of-motion, and functional improvements in a diverse set of patients who had exhausted all previous standard-of-care therapies for VML as shown in Chapter 9. Early targeted physical rehabilitation seems to be a key determinant of this outcome. Patients were also shown to have an electromyographic and histologic improvement in nerve conduction, muscle formation, and mobilization of progenitor cells, respectively. Together these results could create a paradigm shift in the approach to VML

treatment away from the less-than-satisfactory methods currently used and towards incorporation of targeted, early physical therapy to stimulate the responding macrophages / progenitor cells and promote ECM-mediated constructive remodeling. Clinical translation of ECM bioscaffolds for VML repair is an efficient method to promote partial strength and functional gains and improve patient quality of life after suffering from volumetric muscle loss.

Future Directions Milestone 3: Future experiments should focus on a multi-center clinical trial to shift the standard-of-care for VML patients. Determining the mechanisms by which mechanical load stimulates a pro-regenerative microenvironment could guide clinical practice and physical therapy regimens for VML patients and other myogenic injuries / diseases. Further study is also necessary to determine whether the time between injury and treatment can improve outcomes, and if different forms of ECM (i.e. ECM hydrogels) can be used acutely to treat injured tissue noninvasively. Synergy between biomaterials, stem cell biology, pharmacology, and physical rehabilitation should be the focus for development of optimal therapies for VML.

APPENDIX A

MACROPHAGE PHENOTYPE IN RESPONSE TO ECM BIOSCAFFOLDS[7]

A.1 ABSTRACT

Macrophage presence and phenotype are critical determinants of the healing response following injury. Downregulation of the pro-inflammatory macrophage phenotype has been associated with the therapeutic use of bioscaffolds composed of extracellular matrix (ECM), but phenotypic characterization of macrophages has typically been limited to a small number of non-specific cell surface markers or expressed proteins. The present study determined the response of both primary murine bone marrow derived macrophages (BMDM) and a transformed human mononuclear cell line (THP-1) to degradation products of two different, commonly used ECM

[7] Portions of this chapter were adapted from the following publication:
Huleihel L**, Dziki JL**, Bartolacci J, Rausch T, Scarritt M, Cramer M, Vorobyov T, LoPresti S, Swinehart I, White L, Brown B, Badylak SF. Macrophage phenotype in response to ECM bioscaffolds. *Seminars in Immunology.* April 2017.

bioscaffolds; urinary bladder matrix (UBM-ECM) and small intestinal submucosa (SIS-ECM). Quantified cell responses included gene expression, protein expression, commonly used cell surface markers, and functional assays. Results showed that the phenotype elicited by ECM exposure (M_{ECM}) is distinct from both the classically activated IFNγ+LPS phenotype and the alternatively activated IL-4 phenotype. Furthermore, the BMDM and THP-1 macrophages responded differently to identical stimuli, and UBM-ECM and SIS-ECM bioscaffolds induced similar, yet distinct phenotypic profiles. The results of this study not only characterized an M_{ECM} phenotype that has anti-inflammatory traits, but also showed the risks and challenges of making conclusions about the role of macrophage mediated events without consideration of the source of macrophages and the limitations of individual cell markers.

A.2 INTRODUCTION

Biologic scaffold materials composed of extracellular matrix (ECM) have been used in both preclinical and clinical studies to facilitate the functional reconstruction of soft tissues including the esophagus[102], skeletal muscle[107], and myocardium[272], among others[335-337]. Results of such studies have varied from excellent to unacceptable[338338], and the reasons for disparate results have been attributed to variables such as the methods used to decellularize source tissues[116,117], the use of chemical crosslinking agents that inhibit scaffold degradation[100], and other factors[339,340]. Arguably the most important mechanism by which ECM bioscaffolds influence tissue remodeling and functional outcome is the modulation of macrophage phenotype[99]. In fact, the ratio of M2-like/M_{IL-4} (regulatory/anti-inflammatory) to M1-

like/$M_{IFN\gamma+LPS}$ (pro-inflammatory) macrophages has been shown to be a predictor of favorable outcomes in multiple studies[76,341-343].

Macrophages have long been recognized as phagocytes with pro-inflammatory and cytotoxic functions. However, it is now understood that these cells also play essential roles in the resolution of inflammation[344,345], normal tissue development[346], and in blastemal-based epimorphic regeneration in species such as the axolotyl[129]. These "non-classical" macrophage activities are increasingly tied to shifts in the balance of M1:M2 macrophages participating in the host inflammatory reaction. While the description of macrophages as having an M1 or M2 phenotype is operationally simple and facilitates discussion, supra-physiologic amounts of signaling molecules such as cytokines, toll-like receptor agonists, and growth factors have been used *in-vitro* to induce these extremes of pro-inflammatory or anti-inflammatory phenotype[327,347,348]. However, such conditions do not mimic the *in-vivo* complexity of macrophage activation. In fact, virtually any stimulus will likely elicit a macrophage phenotype that exists somewhere between the extremes.

Given the diversity and broad scope of endogenous signaling molecules resident within extracellular matrix (e.g., growth factors, cytokines, cryptic peptides and miRNA), and the widespread clinical use of ECM bioscaffolds in tissue reconstruction, the "M_{ecm}" phenotype is characterized in the present study. In contrast to commonly used methods of identifying macrophage phenotype by one or two markers, within the biomaterials and regenerative medicine literature as a whole, the present study includes transcription factor analysis, gene expression, protein expression, cell surface markers and functional assays to comprehensively characterize cell phenotype. ECM bioscaffolds derived from two separate tissue sources (porcine small intestine and urinary bladder) are used to activate two commonly used macrophage

populations: primary mouse bone marrow derived macrophages and THP-1 cells (a human mononuclear cell line). Both naive macrophages and macrophages that have been activated with IFNγ+LPS are examined to determine whether ECM signaling molecules can contribute to phenotype switching.

A.3 MATERIALS AND METHODS

A.3.1 Overview of study design

The present study determined macrophage phenotype following exposure to degradation products derived from ECM bioscaffolds. Two macrophage populations commonly used in in-vitro studies examined: human THP-1 monocytes [American Type Culture Collection (ATCC)] and murine bone marrow derived macrophages. A comprehensive characterization of macrophage cell surface markers, gene expression, protein content, phagocytic capacity, and nitric oxide production was conducted. Based on previous studies, over 30 different surface markers, transcription factors, cytokines and metabolic markers were selected to evaluate the ECM-induced macrophage phenotype, termed M_{ECM}. Additionally, the production of proteins selected based upon PCA analysis was determined by western blotting and immunolabeling. Lastly, macrophage phagocytic activity and nitric oxide production post-treatment was determined. The methods used to assess the changes in macrophage phenotype are described below.

A.3.2 Preparation of ECM bioscaffolds

Porcine urinary bladders from market weight (approximately 110 kg) animals were acquired from Tissue Source, LLC. (Lafayette, Indiana, USA). Urinary bladder matrix (UBM-ECM) was prepared by decellularization using mechanical and chemical methods as previously reported[247]. Briefly, the tunica serosa, tunica muscularis externa, tunica submucosa, and tunica muscularis mucosa were mechanically removed. The luminal urothelial cells of the tunica mucosa were

dissociated by washing with sterile water. The remaining tissue consisting of basement membrane and subjacent tunica propria of the tunica mucosa was decellularized by agitation in 0.1% peracetic acid with 4% ethanol for 2 hours at 300 rpm. The tissue was then extensively rinsed with phosphate-buffered saline (PBS) and sterile water. The UBM-ECM was then lyophilized and milled into particulate form using a Wiley Mill with a #60 mesh screen.

Preparation of SIS-ECM has been previously described[253]. Briefly, jejunum was harvested from market weight pigs and split longitudinally. The superficial layers of the tunica mucosa were mechanically removed. Likewise, the tunica serosa and tunica muscularis externa, tunica submucosa, and tunica muscularis mucosa were mechanically removed, leaving the tunica submucosa and basilar portions of the tunica mucosa. Decellularization and disinfection of the tissue occurred by agitation in 0.1% peracetic acid with 4% ethanol for 2 hours at 300 rpm. The tissue was then extensively rinsed with phosphate-buffered saline (PBS) and sterile water. The SIS-ECM was then lyophilized and milled into particulate form using a Wiley Mill with a #60 mesh screen.

A.3.3 Derivation of ECM degradation products

UBM-ECM and SIS-ECM were enzymatically degraded as previously described with pepsin from porcine stomach mucosa (MP Biomedicals) by mixing lyophilized, powdered UBM-ECM (10 mg/mL) and pepsin (1 mg/mL) in 0.01 M HCl (pH 2.0). This solution was stirred at room temperature for 48 hours. After stirring, the UBM slurry was neutralized to a pH of 7.4 in 1× PBS (137 mM NaCl, 2.7 mM KCl, 12 mM Phosphate, Fisher Scientific, Waltham, MA) to inactivate the pepsin.

A.3.4 Macrophage culture

THP-1 human monocytes (TIB-202™) were obtained from the American Tissue Culture Collection (ATCC, Manassas, VA) and maintained in RPMI, 10% FBS, 1% penicillin/streptomycin, and 50 uM of 2-Mercaptoethanol in a humidified atmosphere at 37 °C with 5% CO2. Two million THP-1 cells were plated with 320 nM phorbol 12-myristate 13-acetate (PMA) to induce differentiation into macrophages. After 24 hours adherent macrophages were washed in PBS and placed in fresh media, followed by 72 hours incubation in fresh media to acquiesce. This protocol has been shown to result in a phenotype that is nearly indistinguishable from human peripheral blood macrophages[79].

Murine bone marrow derived macrophages (BMDM) were isolated as previously described. Briefly, the tibia and femur were isolated from adult, female 6–8-week old C57bl/6 mice obtained from Jackson Laboratories (Bar Harbor, ME). Bones were kept on ice and rinsed in a sterile dish containing macrophage complete medium consisting of DMEM (Gibco, Grand Island, NY), 10% fetal bovine serum (FBS) (Invitrogen, Carlsbad, CA), 10% L929 supernatant, 0.1% beta-mercaptoethanol (Gibco), 100 U/ml penicillin, 100 ug/ml streptomyocin, 10 mM non-essential amino acids (Gibco), and 10 mM hepes buffer. In a sterile environment, the ends of each bone were transected and the marrow cavity flushed with complete medium using a 30-gauge needle. Harvested cells were washed and plated at 10^6 cell/ml, and allowed to differentiate into macrophages for 7 days at 37 °C, 5% CO2 with complete media changes every 48 h resulting in naïve macrophages.

A.3.5 Macrophage activation

Macrophages were activated for 24 hours with one of the following: (1) 20 ng/ml IFNγ and 100 ng/ml LPS to promote an $M_{IFNy+LPS}$ phenotype, (2) 20 ng/ml IL-4 to promote an M_{IL-4} phenotype, or (3) 250 ug/ml of UBM-ECM, or SIS-ECM to promote an M_{ECM} phenotype. An equivalent concentration of pepsin was used as control buffer. In a separate group, macrophages were just activated with IFNy+LPS for 6 hours, as described above, and then exposed to UBM-ECM or SIS-ECM for 24 hours. After the incubation period at 37 °C, cells were washed with sterile PBS and fixed with 2% paraformaldehyde for immunolabeling or harvested with TRIZOL/RIPA buffer for RNA/Protein assessment, respectively. Cells were also assessed for phagocytosis and nitric oxide production.

A.3.6 RNA isolation and cDNA synthesis

Cellular RNA was isolated using the miRNeasy Mini kit (Qiagen, Valencia, CA) according to the manufacturer's instructions. Reverse transcriptase from RNA to cDNA was performed via high capacity RT kit (ABI, Foster City, CA) according to the manufacturer's instructions.

A.3.7 Quantitative polymerase chain reaction (PCR)

Sybr Green gene expression assays (ABI, Foster City, CA) were used to determine the relative expression levels of THP-1: iNOS, TNF□, STAT1, STAT2, STAT5, IRF3, IRF4, IRF5, IL1RN, CD206, TGM2, STAT3, STAT6, KLF4, KLF6, PPARy BFKBF3, GLUT1, HIF1a, PGK1, LDHA, HK3, PDK4, RPIA, PPARy, G6PC3 and PCK2. For BMDM gene expression levels: inos, tnf, stat1, stat2, stat5, irf3, irf4, irf5, il1rn, cd206, tgm2, stat3, stat6, klf4, klf6, fizz-1, arg1, bfkbf3, glut1, hif1a, hk3, pgk1, pdk4, rpia, ldha, pck1, pck2, g6pc3 and ppary . Results were analyzed by the ΔΔCt method using β-glucuronidase (β -GUS) control for human, and Glyceraldehyde 3-phosphate dehydrogenase (GAPDH) for mouse, to normalize the results. Fold change was calculated taking untreated as the baseline. Results are displayed in a heat map format created by Java Treeview.

A.3.8 Macrophage immunolabeling

To determine macrophage surface marker expression profiles, activated cells were fixed with 2% paraformaldehyde (PFA) for 45 minutes. Primary antibodies used for immunofluorescent labeling on BMDM were: (1) monoclonal anti-F4/80 (Abcam, Cambridge, MA) at 1:200 dilution for a pan-macrophage marker, (2,3) polyclonal anti-iNOS (Abcam, Cambridge, MA) at 1:100 dilution and anti-TNF□ (Abcam, Cambridge, MA) at 1:1000 for an M1-like marker, and (4,5) polyclonal anti-Fizz1 (Peprotech, Rocky Hill, NJ) and anti-arg1 (Abcam, Cambridge, MA) at 1:100 dilution for M2-like markers. Primary antibodies used on THP-1 were: (1) monoclonal anti-CD11b (Abcam, Cambridge, MA) at 1:200 dilution for a pan-macrophage marker, (2,3)

polyclonal anti-iNOS (Abcam, Cambridge, MA) at 1:100 and anti-TNF□ (Abcam, Cambridge, MA) at 1:1000 for an M1-like marker, and (4,5) polyclonal anti-TGM2 (Abcam, Cambridge, MA) and anti-CD206 (Abcam, Cambridge, MA) at 1:1000 dilution for M2 markers. Cells were incubated in blocking solution consisting of PBS, 0.1% Triton-X, 0.1% Tween-20, 4% goat serum, and 2% bovine serum albumin to prevent non-specific binding for 1 h at room temperature. Blocking solution was removed and cells were incubated in primary antibodies for 16 h at 4 °C. After washing in PBS, cells were incubated in fluorophore-conjugated secondary antibodies (Alexa Fluor donkey anti-rat 488 or donkey anti-rabbit 488, Invitrogen, Carlsbad, CA) for 1 h at room temperature. After washing again with PBS, nuclei were counterstained with 4′6-diamidino-2-phenylindole (DAPI) prior to imaging. Images of three 20× fields were taken for each well using a live-cell microscope. Light exposure times for ECM-activated macrophages were standardized based upon cytokine-activated macrophages (positive control). Exposure time was kept constant for each marker.

A.3.9 Western blot

Western blots were performed on treated macrophage cell lysates. Cell lysates were boiled at 95 °C for 5 min and electrophoresed on 4-20% gradient acrylamide gels. Specifically, 10 ug of protein was loaded into each well. Separated proteins were transferred to Polyvinylidene difluoride (PVDF) membranes (Bio-rad) using a wet transfer set up. Following transfer, membranes were then blocked for 45 min with Pierce protein-free blocking buffer (Pierce Chemical, Rockford, IL) and incubated overnight with the following primary antibodies: iNOS, TNF-□, STAT1, IRF3 CD206, TGM2, and KLF4, for THPI and iNOS, TNF-□, STAT1, Arg1,

Fizz-1 and KLF4 for BMDM. Membranes were washed three times for 15 min in 1X PBS, before and after they were incubated with appropriate secondary antibody. The washed membranes were exposed to chemiluminescent substrate (Bio-Rad) and then visualized using chemidoc touch instrument (Bio-Rad). Image Densitometry was evaluated using the shareware ImageJ (http://rsbweb.nih.gov/ij/index.html).

A.3.10 Nitric oxide quantification

Bone marrow macrophages and THP-1 cells were cultured and treated as previously described above. Following treatment, the supernatant from the wells was transferred to another plate and frozen at -80°C. The supernatant was thawed then 50 μL was added to another plate. 50 μL of standards consisting of sodium nitrite from 100 μM to 1.56 μM in a 1:2 serial dilution were added to the plate. The wells were treated with 50 μL of 1% sulfanilamide in 5% phosphoric acid for 10 minutes. Then 50 μL of 0.1% N-1-napthylethylenediamine [NED] dihydrochloride in water was added for an additional 10 minutes. The wells were then read at 540 nm and compared to the standard curve. Readings were normalized to the amount of DAPI-stained cells in each well as quantified by Cell Profiler.

A.3.11 Phagocytosis assay

Following activation, cells were incubated with Vybrant Phagocytosis Kit FITC-labeled E. Coli beads for 2 hours. Wells were then washed once with 1XPBS and fixed with 2% paraformaldehyde for 30 minutes. Wells were washed 3 times with 1X PBS then stained with DAPI for 10 minutes and washed again three times with 1X PBS. Wells were imaged using an

automated Live Cell Scope and quantified for mean intensity of the cells using Cell Profiler software. Mean intensity averages were calculated as percent changes from M0 naïve macrophage controls.

A.4 RESULTS

The terminology used to describe various states of macrophage activation (often referred to as "polarization") has contributed to potentially misleading conclusions regarding the role of macrophages in various physiologic and pathologic processes. For example, macrophages have been identified as M1 (pro-inflammatory) or M2 (anti-inflammatory), or given labels such as "regulatory" based upon selected surface markers or associated effector molecules. Recommendations for standard nomenclature based upon definition of the activator were published in 2014[16,24716], and this terminology will be used herein whenever possible (e.g., $M_{IFNy+LPS}$ and M_{IL-4}). Macrophages stimulated with solubilized extracellular matrix (ECM) will be designated as M_{ECM} ($M_{UBM-ECM}$ and $M_{SIS-ECM}$).

A.4.1 Overview of study design Human THP-1 monocytes and mouse bone marrow (BMDM) were differentiated into macrophages to generate an M∅ phenotype. M∅ macrophages were then treated for 24h with IFNγ+LPS to establish an $M_{IFNγ+LPS}$ phenotype, IL-4 to establish an M_{IL-4} phenotype, or either UBM-ECM or SIS-ECM to establish an MECM ($M_{UBM-ECM}$ / $M_{SIS-ECM}$) phenotype. In a separate experiment, M∅ macrophages were challenged with IFNγ+LPS

for 6 hours followed by a 24 hour treatment with UBM or SIS. Downstream analyses included: 1) Gene expression of 30 commonly investigated macrophage activation markers, surface markers, cytokines, transcription factors and metabolic markers; 2) Protein expression of the most highly regulated markers; and 3) macrophage function as assessed by phagocytosis and nitric oxide production (Figure 33).

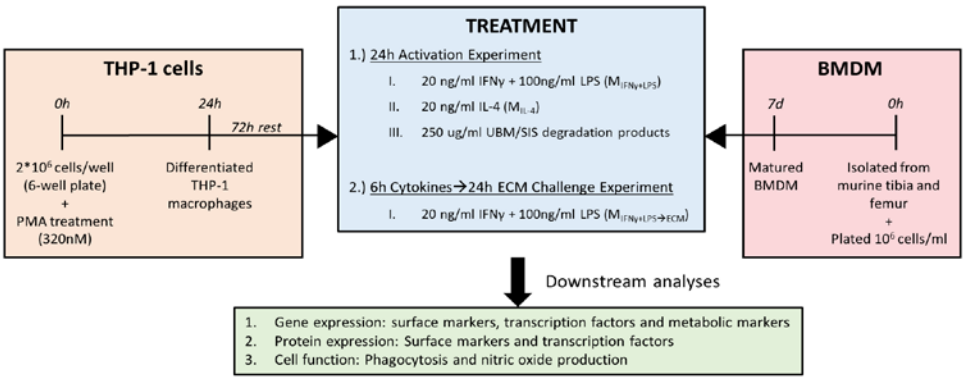

Figure 33. Visual representation of study design

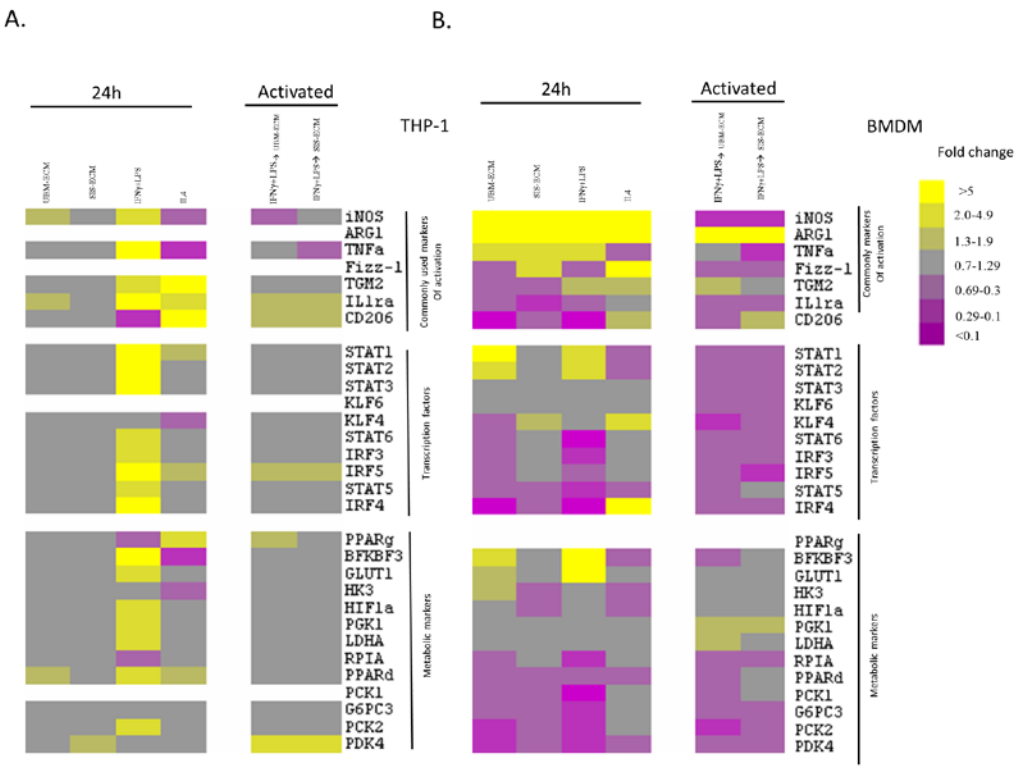

Figure 34. Gene expression of previously described "M1-like" and "M2-like" surface markers, cytokines, transcription factors, and metabolic markers. BMDM (left panel) and THP-1 (right panel) macrophages were treated with UBM-ECM, SIS-ECM, IFNγ + LPS, and IL-4 for 24 hours. Additionally, macrophages were pre-treated with IFNγ+LPS for 6 hours followed by 24 hours of UBM or SIS treatment (n=3). Samples were normalized to media treatment. Gene expression was evaluated using qPCR data and is demnostrated in heatmap form. Fold changes are presented using a color gradient bar

A.4.2. M_{ECM} has a distinct gene expression profile

Thirty commonly used macrophage markers of activation, including surface markers, cytokines, transcription factors, and metabolic markers were analyzed by qPCR to better understand the gene expression signature of treated macrophages. Gene expression data are displayed as a heatmap in Figure 34. Clear differences between the gene expression signature of THP-1 macrophages and BMDMs were shown. Exposure of THP-1 macrophages to IFNγ+LPS resulted in an increase in almost the entire gene panel, while changes following exposure to IL-4 were relatively mild. In contrast, exposure to either UBM-ECM or SIS-ECM degradation products resulted in only minor changes in gene expression (Figure 34A).

Exposure of BMDMs to IFNγ+LPS treatment and IL-4 treatment both led to substantial changes in gene expression with contrasting profiles. The phenotype generated by exposure to UBM-ECM differed from the phenotype generated by exposure to SIS-ECM but there were areas of overlap. Notably, IFNγ+LPS and UBM-ECM treated BMDMs have a similar gene expression profile (Figure 34B).

When THP-1 macrophages were challenged with IFNγ+LPS for 6 hours followed by exposure to UBM-ECM or SIS-ECM for an additional 24 hours, no major changes in gene expression were observed (Figure 34A). However, there was a significant change in the gene expression signature in BMDMs (Figure 34B). In addition to the different response between the two macrophage populations, there were also clear differences between UBM-ECM and SIS-ECM treatment groups post-cytokine treatment. Both UBM-ECM and SIS-ECM treatment groups showed a decrease in the transcription factor gene expression cluster, particularly when

pre-treated with IFNγ+LPS. Gene expression was normalized to untreated macrophages (M∅). IFNγ+LPS activated macrophages were normalized to IFNγ+LPS followed by media treatment.

Principal component analysis (PCA) was conducted to identify the dominant members of the transcriptional signature associated with the test groups for further downstream protein expression. BMDMs and THP-1 macrophages treated for 24 hours with cytokines or ECM degradation products were scored and visually clustered by PCA. For THP-1 macrophages, CD206, KLF4 and TGM2 were found to be the genes most associated with IL-4 activation, and TNFα, STAT1 and IRF3 were associated with IFNγ+LPS activation (Figure 37A). The BMDMs showed Fizz-1, KLF-4 and Arg1 as the most differentially expressed genes associated with IL-4 activation, and TNFα, STAT1 and iNOS were the most highly regulated genes with IFNγ+LPS activation (Figure 37B). Genes that are commonly cited in the literature as macrophage activation markers, and the genes identified in PCA data output, were chosen for further downstream protein analyses.

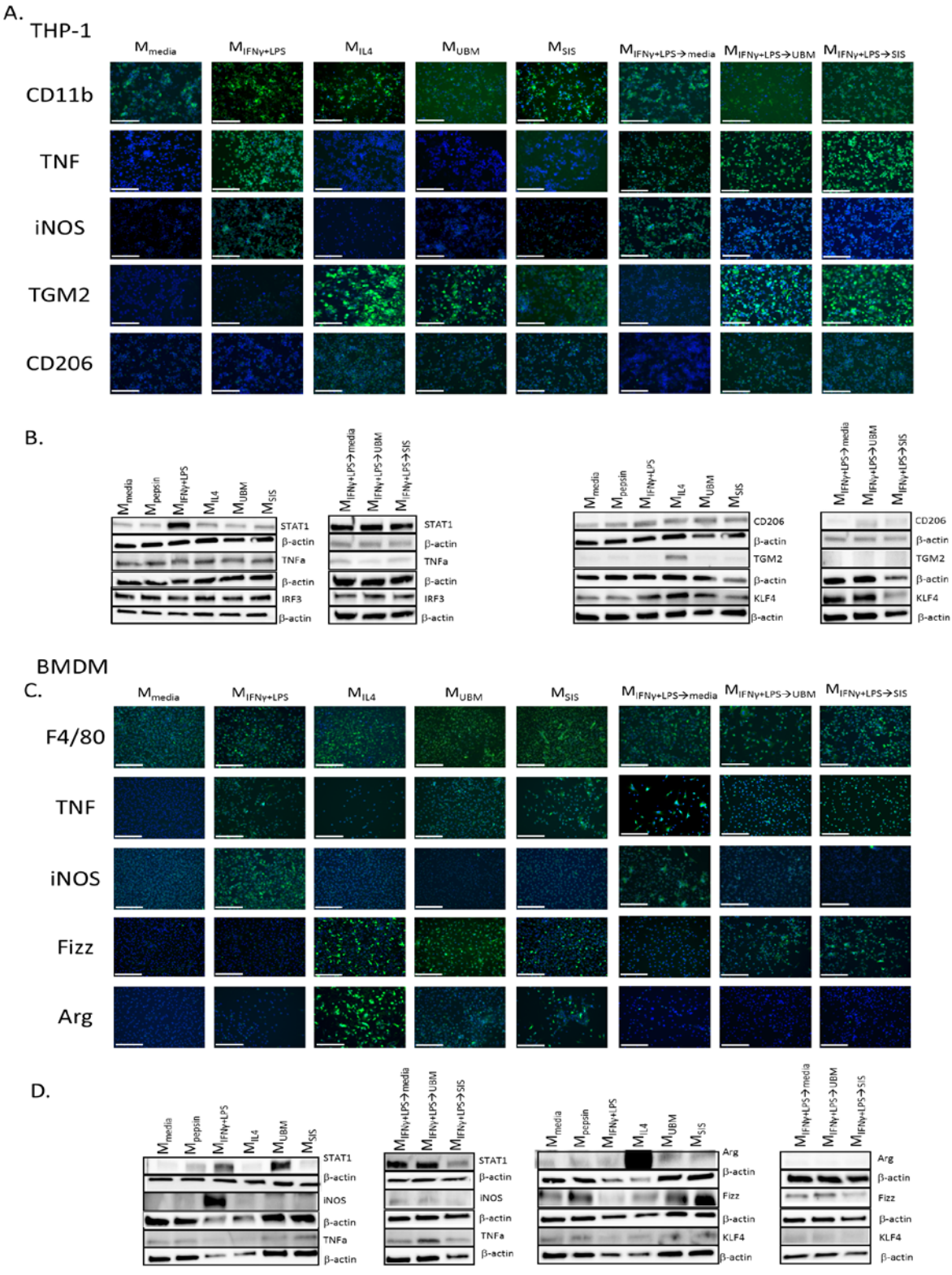

Figure 35. ECM degradation products promote an immunomodulatory "M2-like" phenotype (A) Human monocytes from the THP-1 cel line were cultured in media supplemented with PMA to derive macrophages. Macrophages were treated with 20 ng/ml IFNγ and 100 ngml LPS to derive "M1-like" macrophages, 20 ng/ml IL-4 to derive "M2-like" macrophages, 200 ug/ml SIS-ECM degradation products, or 200 ug/ml pepsin control buffer.

Additionaly, "M1-like" macrophages were exposed to either 200 ug/ml UBM-ECM or 200 ug/ml SIS-ECM degradation produts to simulate the physiologic scenario of an injury treated with an ECM scaffold. Macrophages were fixed and immunolabeled for the pan macrophage marker (Cd11b), and strong indicators of the M1-like (TNFα and iNOS) and M2-like (CD206 and TGM2) phenotype. ECM treated cells show increased expression of TGM2 and CD206, markers associated with the IL-4 pushed phenotype. **(B**) Immunolabeling results were corroborated using western-blot analysis of the TNFα, iNOS,CD206, and TGM2 markers (bottom panel). **(C)** Bone marrow was isolated from C57bl/6 mice and cultured in media supplemented with macrophage colony stimulating factor (MCSF) to derive macrophages. "M1-like" macrophages, "M2-like" macrophages, and ECM-activated macrophages were derived as described above. Additionally, "M1-like" macrophages were exposed to UBM-ECM or SIS-ECM degradation products as before. Macrophages were fixed and immunolabeled for the pan-macrophage marker (F4/80), and strong indicators of the M1-like (TNFα and iNOS) and M2-like (Fizz1 and arginase) phenotypes. ECM treated cells show increased expression of Fizz1 and arginase, associated with the IL-4 pushed phenotype, as well as TNFα, associated with the IFNγ/LPS pushed phenotype, suggesting that the ECM treated cells adopt a unique phenotype. **(D)** Immunolabeling resuls were further evaluated using western-blot analysis of the STAT1, arginase, Fizz1, iNOS, and TNFα markers (bottom panel). (Scale bars = 200 μm).

A.4.3 ECM degradation products and IL-4 promote similar protein expression profile

Protein expression was evaluated by western blot analysis and immunofluorescent labeling. THP-1 macrophages activated for 24 hours with UBM-ECM or SIS-ECM induced TGM2 and CD206 ($M_{IL\text{-}4}$ associated markers). However, no changes were noted in the $M_{IFN\gamma+LPS}$ associated marker TNFα and only a mild change in iNOS expression with SIS-ECM activation. CD11b was used as a pan macrophage control marker for THP-1 macrophages (Figure 35) Macrophages activated with IFNγ+LPS followed by exposure to ECM degradation products showed a similar trend to the 24 hours treatment groups. When THP-1 macrophages were exposed to either UBM-ECM or SIS-ECM following activation with IFNγ+LPS, both ECMs induced TGM2 and CD206 positive cells. UBM-ECM and SIS-ECM both caused a reduction in iNOS expression by THP-1 macrophages that had been activated with IFNγ+LPS. However, both UBM-ECM and SIS-ECM induced TNFα positive cells when macrophages were activated with IFNγ+LPS (Figure 35A).

BMDMs show Fizz-1 and Arg1 ($M_{IL\text{-}4}$ associated markers in mice) expression after activation with UBM-ECM and SIS-ECM for 24 hours. In addition, BMDMs were positive for the $M_{IFN\gamma+LPS}$ associated marker TNFα after exposure to ECM degradation products, but were not

positive for iNOS. F4/80 was used as a pan macrophage control marker for BMDMs (Figure 35C). Similarly, macrophages activated with IFNγ+LPS followed by treatment with ECM degradation products showed enhanced Fizz-1 expression, but not enhanced Arg1 expression. Interestingly, both UBM-ECM and SIS-ECM inhibited iNOS expression and enhanced TNFα expression after pre-activation with IFNγ+LPS.

Western blot analysis was used to determine relative protein expression of the specified genes that showed the greatest change in activity in response to specific treatments. For the $M_{IFN\gamma+LPS}$ associated markers, the THP-1 macrophages activated for 24 hours with UBM-ECM or SIS-ECM showed that the amount of STAT1 was comparable to that of M∅ and M_{IL-4} cells, and significantly lower than that of the $M_{IFN\gamma+LPS}$ cells. No changes were noted in TNFα and IRF3 (Figure 35B).

For the M_{IL-4} associated markers, TGM2 and KL4 protein expression were increased after IL-4 activation. No significant changes were found between the M_{ECM} groups and the M∅ and $M_{IFN\gamma+LPS}$ phenotypes. When macrophages were first activated IFNy+LPS, followed by exposure to SIS-ECM, a decrease in KLF4 protein expression was noted (Figure 35B).

BMDMs exposed to UBM-ECM or SIS-ECM degradation products show similar findings to THP-1 macrophages with some small differences. For example, BMDMs activated by 24h exposure to UBM-ECM showed increased expression of STAT1 to a level similar to that of the $M_{IFN\gamma+LPS}$ treatment group, which was not seen in the THP-1 groups. However, in both populations of macrophages, no changes were noted in TNFα expression levels (Figure 35D). Notably, an increase in iNOS expression was found only in the BMDM $M_{IFN\gamma+LPS}$ group. When macrophages were activated with IFNγ+LPS followed by UBM or SIS treatment, no changes were noted in iNOS and TNFα expression levels when compared to media controls. However,

SIS-ECM treatment inhibited STAT1 protein expression for the group first activated by IFNy+LPS. For the M_{IL-4} associated markers, M_{IL-4} significantly increased Arg1 protein expression, and SIS-ECM significantly increased Fizz-1 expression. No changes were noted in KLF4 (Figure 35D). β-actin was used as a loading control and the colorimetric intensity of the bands for each treatment group was standardized to its respective β-actin band intensity. Densitometry evaluation of each blot can be found in Figure 38.

A.4.4 ECM degradation products affect macrophage functional activity

THP1 macrophages showed low levels of phagocytosis across all tested conditions. Cytokine treatment did not significantly enhance the phagocytic function of THP1 macrophages. However, UBM-ECM activation alone caused an increase in THP1 phagocytosis (Figure 36A). BMDMs showed measurable basal phagocytic function. Phagocytosis by BMDMs increased with IFNγ+LPS and no notable changes were detected following IL-4 activation (Figure 36B). Similar to the THP-1 macrophages, UBM-ECM activation resulted in an increase in phagocytosis. In both BMDMs and THp1 macrophages, activation with IFNγ+LPS for 6h prior to 24h exposure to UBM-ECM or SIS-ECM did not affect the cells' phagocytic ability. THP1 macrophages did not produce nitric oxide (NO) in response to IFNγ+LPS or IL-4 stimulus. However, UBM treatment did show a slight increase in NO production. Interestingly, THP-1 macrophages challenged with IFNγ+LPS followed by UBM-ECM exposure did show a significant increase in NO production, but such changes were not observed with SIS-ECM exposure (Figure 36C). In BMDMs, NO production increased following IFNγ+LPS. BMDMs exposed to SIS or UBM alone had a slight increase in NO production. IFNγ+LPS activation followed by either UBM-ECM or SIS-ECM enhanced or prolonged cytokine effects compared to media controls (Figure 36D).

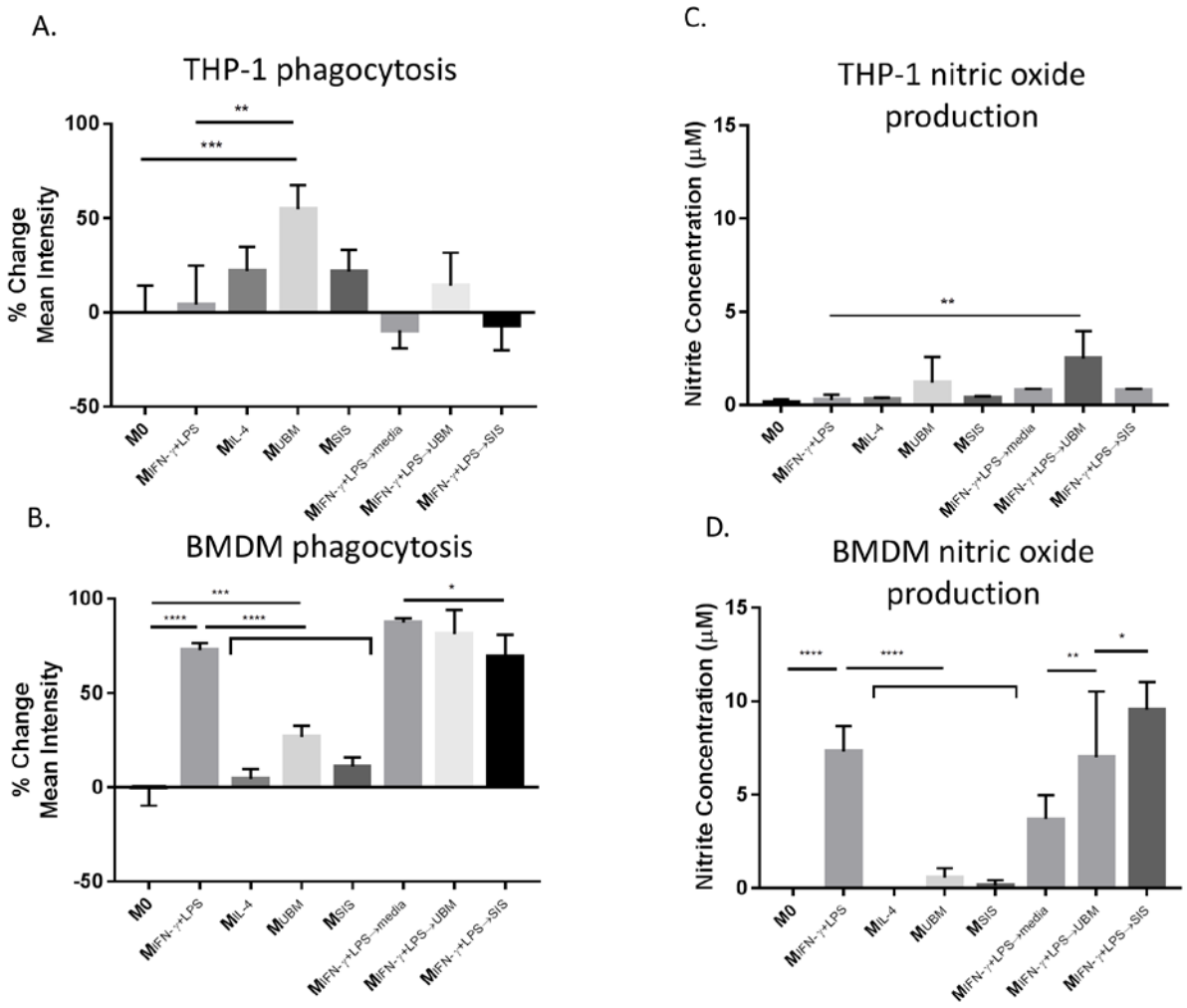

Figure 36. Functional assessment of ECM-treated macrophages. Phagocytosis activity in BMDM **(A)** and THP1 macrophages **(B)** was assessed using incubation with Vybrant FITC-labeled E.Coli particles then M.F.I analysis. Nitric oxide production from BMDM **(C)** and THP-1 macrophages **(D)** was assessed using the Greiss reagent system on macrophage supernatants following treatment

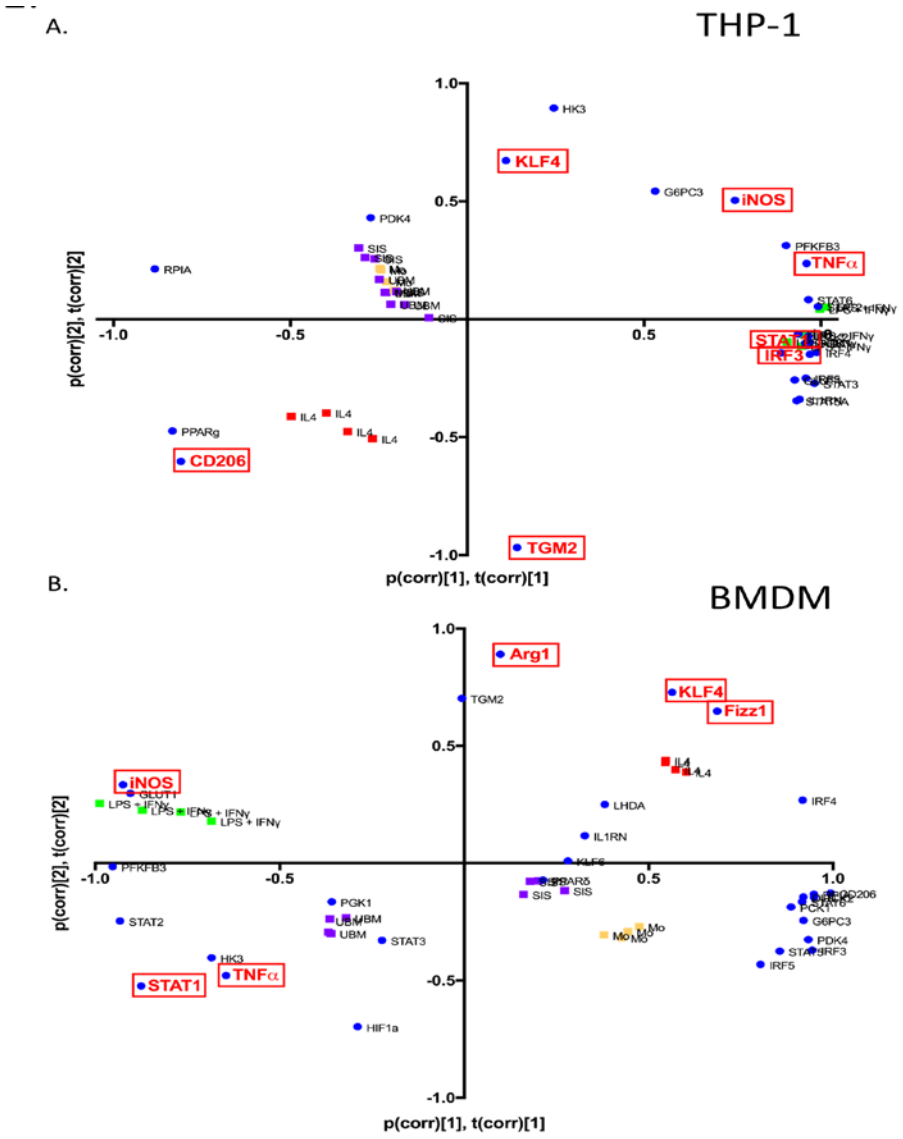

Figure 37. Principle component analysis (PCA) of delta Ct values scaled to unit variance. Biplot showign corrected principal component score values t(corr)[x] and loadings p(corr)[x] combined into one plot, where x is the component number. Genes that appear closer to the sample contributed to the distinction of that sample. The commonly cited genes associated with IFNγ+LPS and IL-4 activation that were chosen for further protein analyses for THP1 **(A)** and BMDM **(B)** derived macrophages and are highlighted.

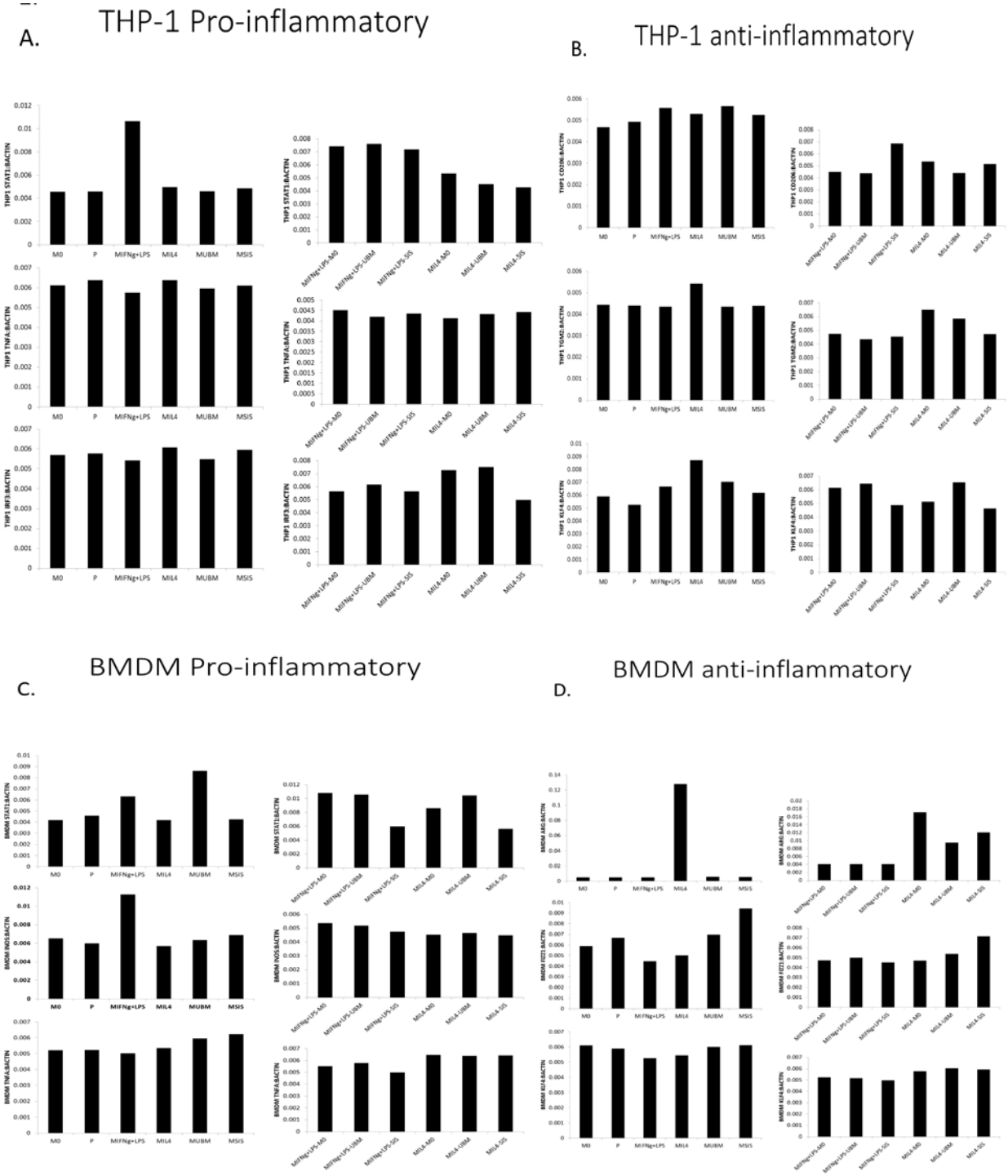

Figure 38. Densitometry was performed on western blots for all proteins that were probed. Color intensity of original blots was quantified using ImageJ for both the protein of interest and the respective loading control, β-actin. Intensity of the target protein band was normalized to its respective β-actin band

A.5 DISCUSSION

The results of the present study show clearly that BMDMs and THP-1 macrophages respond differently to the same stimulus. The phenotype of these two macrophage populations following activation by an ECM scaffold can appear very similar or vastly different depending upon whether gene expression, protein expression, or surface markers are evaluated. Furthermore, although SIS-ECM and UBM-ECM have both been associated with constructive, functional tissue remodeling outcomes in both pre-clinical animal models and in clinical applications in man, the macrophage phenotype resulting from activation with each ECM is distinct from those elicited by activation with either IFNγ+ LPS or IL-4. Finally, following activation by IFNγ + LPS, macrophages then exposed to degradation products of both ECM bioscaffolds show a marked downregulation of genes that are typically associated with an inflammatory profile.

ECM bioscaffolds typically promote a favorable tissue remodeling response when used to treat various types of soft tissue injury. This response includes the recruitment of endogenous stem cells, angiogenesis, and dampening of the inflammatory response. This pro-healing response has been attributed, in large part, to the effect of ECM on macrophage phenotype. The objective of the present study was to comprehensively characterize the M_{ECM} phenotype. The source of macrophages used in this study; specifically, primary cells isolated from murine bone marrow (i.e., BMDM) and a transformed human mononuclear cell line (i.e., THP-1) are commonly used, and therefore the results are of interest to the field of macrophage biology[349,350]. Since conclusions from such studies can have far-reaching implications, it is important to understand the effect of the source of macrophages upon study results.

There was a clear difference between the response of BMDMs and THP-1 macrophages to both canonical stimuli such as IFNγ + LPS or IL-4 as well as to SIS-ECM and UBM-ECM degradation products. Gene expression analyses showed that THP-1 macrophages were not significantly affected by activation with IL-4, SIS-ECM, or UBM-ECM exposure, but there was a notable increase in most of the evaluated genes following activation by IFNγ+ LPS. This response was in stark contrast to the BMDM gene expression signature that showed significant changes to all of the applied stimuli. We hypothesize that these changes are likely due to the endogenous differences between a cell line (i.e., THP-1) and primary cells (i.e., BMDM). Another difference between the two macrophage populations was the difference in macrophage function following activation. THP-1 macrophages were associated with very little nitric oxide (NO) production and phagocytosis regardless of their stimulus, whereas BMDMs showed an increase in NO production and phagocytic activity when stimulated with IFNγ + LPS similar to the response one would expect in vivo following exposure to a pro-inflammatory stimulus. Overall, the present findings suggest that the in vitro response of BMDMs respond more similarly than THP1 cells with respect to the behavior observed by macrophages in preclinical animal models and clinical studies that have examined ECM-mediated tissue remodeling[76,100].

Both SIS-ECM and UBM-ECM have been associated with an increased bioscaffold-localized M2:M1 ratio in preclinical animal studies, and a constructive, functional tissue remodeling response, but the macrophage phenotype has typically been characterized based upon a small number of cell markers[351,352]. In the present study, gene expression analysis of resting BMDMs showed that the macrophage response to SIS-ECM is similar to that of IL-4 activation. BMDMs exposed to UBM-ECM, in contrast, show a gene expression profile that is similar to that of the $M_{IFNy+LPS}$ phenotype. However, when macrophages are first activated with a pro-inflammatory

stimulus, both SIS-ECM and UBM-ECM down-regulate markers associated with a classic inflammatory response including iNOS, STAT1, STAT2, and KLF6 which is consistent with observed in vivo events. Both $M_{SIS\text{-}ECM}$ and $M_{UBM\text{-}ECM}$ augment nitric oxide production after IFNy+LPS stimulus in vitro, but the $M_{UBM\text{-}ECM}$ phenotype is associated with an increased phagocytic capability compared to the $M_{SIS\text{-}ECM}$ phenotype. The present work shows that the "M_{ECM}" phenotype differs depending upon the ECM source tissue and is perhaps more accurately defined as "$M_{'source\text{-}tissue'\text{-}ECM}$", for example "$M_{SIS\text{-}ECM}$" or "$M_{UBM\text{-}ECM}$". We postulate that the differences between UBM-ECM and SIS-ECM are due to different signature of cryptic peptides, matrix-bound vesicles (MBVs) miRNA cargo or other components within the ECM[75].

Following injury, ECM scaffolds are applied to a soft tissue site following injury. The macrophages that interact with the ECM scaffold are likely in an activated state rather than a resting state. In an attempt to mimic this scenario, the present study evaluated the phenotypic response of both resting macrophages and IFNγ+LPS activated macrophages. There were clear differences between the response of "resting" macrophages and "pre-activated" macrophages to ECM degradation products. As previously mentioned, the $M_{SIS\text{-}ECM}$ and the $M_{UBM\text{-}ECM}$ phenotypes are distinct from each other when naive macrophages are exposed to degradation products of ECM. However, $M_{IFNy+LPS}$ activated macrophages respond similarly to both ECM sources with a down-regulation of inflammatory markers. The results of the present study show that the activation state of macrophages can influence the phenotypic response to subsequent stimuli. These findings are consistent with those of *in vivo* studies that show ECM bioscaffolds promote an anti-inflammatory macrophage phenotype with associated constructive and functional outcomes when utilized in response to injury or disease [98,116]. The $M_{IFNy+LPS}$ may

better represent a physiologic macrophage's state in response to injury, when investigating the in vitro response to a given stimulus.

A.6 CONCLUSION

The present study provides a comprehensive analysis of the macrophage phenotype associated with ECM scaffolds derived from the small intestine and urinary bladder. The results of the study demonstrate that the phenotype associated with both SIS-ECM and UBM-ECM is distinct from the canonical $M_{IFNy+LPS}$ and M_{IL-4} phenotypes. Of note, there were also differences observed between SIS-ECM and UBM-ECM, suggesting that the microenvironment of the source tissue from which the ECM bioscaffolds are produced also plays a significant role in determining patterns of macrophage activation. Lastly, we note that there are challenges and risks associated with drawing conclusions about macrophage mediated events when results are based upon a particular macrophage population or a limited subset of macrophage markers. A greater understanding of the effect of macrophage phenotype upon the tissue remodeling process associated with ECM scaffolds will enhance both the design and associated production methods of such scaffolds materials, and would logically improve the clinical outcomes associated with their use.

A.7 ACKNOWLEDGEMENTS

This work was supported by the National Institutes of Health [R01DE022055]; and the Department of Defense [W81XWH-15-1-0026].

BIBLIOGRAPHY

1 Grogan, B. F., Hsu, J. R. & Skeletal Trauma Research, C. Volumetric muscle loss. *The Journal of the American Academy of Orthopaedic Surgeons* **19 Suppl 1**, S35-37 (2011).

2 Grasman, J. M., Zayas, M. J., Page, R. L. & Pins, G. D. Biomimetic scaffolds for regeneration of volumetric muscle loss in skeletal muscle injuries. *Acta Biomater* **25**, 2-15, doi:10.1016/j.actbio.2015.07.038 (2015).

3 Lin, C. H., Lin, Y. T., Yeh, J. T. & Chen, C. T. Free functioning muscle transfer for lower extremity posttraumatic composite structure and functional defect. *Plastic and reconstructive surgery* **119**, 2118-2126, doi:10.1097/01.prs.0000260595.85557.41 (2007).

4 Moneim, M. S. & Omer, G. E. Latissimus dorsi muscle transfer for restoration of elbow flexion after brachial plexus disruption. *The Journal of hand surgery* **11**, 135-139 (1986).

5 Tu, Y. K. *et al.* Soft-tissue injury management and flap reconstruction for mangled lower extremities. *Injury* **39 Suppl 4**, 75-95, doi:10.1016/j.injury.2008.08.034 (2008).

6 Floss, T., Arnold, H. H. & Braun, T. A role for FGF-6 in skeletal muscle regeneration. *Genes & development* **11**, 2040-2051 (1997).

7 Jarvinen, T. A., Jarvinen, T. L., Kaariainen, M., Kalimo, H. & Jarvinen, M. Muscle injuries: biology and treatment. *The American journal of sports medicine* **33**, 745-764, doi:10.1177/0363546505274714 (2005).

8 McCully, K. K. & Faulkner, J. A. Injury to skeletal muscle fibers of mice following lengthening contractions. *Journal of applied physiology* **59**, 119-126 (1985).

9 Charge, S. B. & Rudnicki, M. A. Cellular and molecular regulation of muscle regeneration. *Physiol Rev* **84**, 209-238, doi:10.1152/physrev.00019.2003 (2004).

10 Tidball, J. G. & Villalta, S. A. Regulatory interactions between muscle and the immune system during muscle regeneration. *Am J Physiol Regul Integr Comp Physiol* **298**, R1173-1187, doi:10.1152/ajpregu.00735.2009 (2010).

11 Turner, N. J. & Badylak, S. F. Regeneration of skeletal muscle. *Cell Tissue Res* **347**, 759-774, doi:10.1007/s00441-011-1185-7 (2012).

12 Lehto, M., Duance, V. C. & Restall, D. Collagen and fibronectin in a healing skeletal muscle injury. An immunohistological study of the effects of physical activity on the repair of injured gastrocnemius muscle in the rat. *The Journal of bone and joint surgery. British volume* **67**, 820-828 (1985).

13 Tidball, J. G., Dorshkind, K. & Wehling-Henricks, M. Shared signaling systems in myeloid cell-mediated muscle regeneration. *Development* **141**, 1184-1196, doi:10.1242/dev.098285 (2014).

14 Villalta, S. A., Deng, B., Rinaldi, C., Wehling-Henricks, M. & Tidball, J. G. IFN-gamma promotes muscle damage in the mdx mouse model of Duchenne muscular dystrophy by suppressing M2 macrophage activation and inhibiting muscle cell proliferation. *J Immunol* **187**, 5419-5428, doi:10.4049/jimmunol.1101267 (2011).

15 Deng, B., Wehling-Henricks, M., Villalta, S. A., Wang, Y. & Tidball, J. G. IL-10 triggers changes in macrophage phenotype that promote muscle growth and regeneration. *J Immunol* **189**, 3669-3680, doi:10.4049/jimmunol.1103180 (2012).

16 Murray, P. J. *et al.* Macrophage activation and polarization: nomenclature and experimental guidelines. *Immunity* **41**, 14-20, doi:10.1016/j.immuni.2014.06.008 (2014).

17 Kumar, A., Alvarez-Croda, D. M., Stoica, B. A., Faden, A. I. & Loane, D. J. Microglial/macrophage polarization dynamics following traumatic brain injury. *Journal of neurotrauma*, doi:10.1089/neu.2015.4268 (2015).

18 St Pierre, B. A. & Tidball, J. G. Macrophage activation and muscle remodeling at myotendinous junctions after modifications in muscle loading. *The American journal of pathology* **145**, 1463-1471 (1994).

19 St Pierre, B. A. & Tidball, J. G. Differential response of macrophage subpopulations to soleus muscle reloading after rat hindlimb suspension. *Journal of applied physiology* **77**, 290-297 (1994).

20 Tidball, J. G. & Wehling-Henricks, M. Shifts in macrophage cytokine production drive muscle fibrosis. *Nat Med* **21**, 665-666, doi:10.1038/nm.3896 (2015).

21 Tidball, J. G. & Welc, S. S. Macrophage-Derived IGF-1 Is a Potent Coordinator of Myogenesis and Inflammation in Regenerating Muscle. *Molecular therapy : the journal of the American Society of Gene Therapy* **23**, 1134-1135, doi:10.1038/mt.2015.97 (2015).

22 Verheijden, S., Schepper, S. D. & Boeckxstaens, G. E. Neuron-macrophage crosstalk in the intestine: a "microglia" perspective. *Frontiers in cellular neuroscience* **9**, 403, doi:10.3389/fncel.2015.00403 (2015).

23 Villalta, S. A., Nguyen, H. X., Deng, B., Gotoh, T. & Tidball, J. G. Shifts in macrophage phenotypes and macrophage competition for arginine metabolism affect the severity of muscle pathology in muscular dystrophy. *Hum Mol Genet* **18**, 482-496, doi:10.1093/hmg/ddn376 (2009).

24 Wei, J. & Besner, G. E. M1 to M2 macrophage polarization in heparin-binding epidermal growth factor-like growth factor therapy for necrotizing enterocolitis. *The Journal of surgical research* **197**, 126-138, doi:10.1016/j.jss.2015.03.023 (2015).

25 Wu, X. *et al.* Soluble CLEC2 Extracellular Domain Improves Glucose and Lipid Homeostasis by Regulating Liver Kupffer Cell Polarization. *EBioMedicine* **2**, 214-224, doi:10.1016/j.ebiom.2015.02.013 (2015).

26 Cho, D. I. *et al.* Mesenchymal stem cells reciprocally regulate the M1/M2 balance in mouse bone marrow-derived macrophages. *Experimental & molecular medicine* **46**, e70, doi:10.1038/emm.2013.135 (2014).

27 Kim, J. & Hematti, P. Mesenchymal stem cell-educated macrophages: a novel type of alternatively activated macrophages. *Experimental hematology* **37**, 1445-1453, doi:10.1016/j.exphem.2009.09.004 (2009).

28 Urish, K. L. *et al.* Antioxidant levels represent a major determinant in the regenerative capacity of muscle stem cells. *Molecular biology of the cell* **20**, 509-520, doi:10.1091/mbc.E08-03-0274 (2009).

29 Lavasani, M., Lu, A., Peng, H., Cummins, J. & Huard, J. Nerve growth factor improves the muscle regeneration capacity of muscle stem cells in dystrophic muscle. *Human gene therapy* **17**, 180-192, doi:10.1089/hum.2006.17.180 (2006).

30 Huard, J. *et al.* Human myoblast transplantation in immunodeficient and immunosuppressed mice: evidence of rejection. *Muscle Nerve* **17**, 224-234, doi:10.1002/mus.880170214 (1994).

31 Guerette, B., Asselin, I., Skuk, D., Entman, M. & Tremblay, J. P. Control of inflammatory damage by anti-LFA-1: increase success of myoblast transplantation. *Cell transplantation* **6**, 101-107 (1997).

32 Fan, Y., Maley, M., Beilharz, M. & Grounds, M. Rapid death of injected myoblasts in myoblast transfer therapy. *Muscle & nerve* **19**, 853-860, doi:10.1002/(SICI)1097-4598(199607)19:7<853::AID-MUS7>3.0.CO;2-8 (1996).

33 Glimm, H., Oh, I. H. & Eaves, C. J. Human hematopoietic stem cells stimulated to proliferate in vitro lose engraftment potential during their S/G(2)/M transit and do not reenter G(0). *Blood* **96**, 4185-4193 (2000).

34 Skuk, D. Myoblast transplantation for inherited myopathies: a clinical approach. *Expert opinion on biological therapy* **4**, 1871-1885, doi:10.1517/14712598.4.12.1871 (2004).

35 Skuk, D. *et al.* Dystrophin expression in myofibers of Duchenne muscular dystrophy patients following intramuscular injections of normal myogenic cells. *Molecular therapy : the journal of the American Society of Gene Therapy* **9**, 475-482 (2004).

36 Hardiman, O., Sklar, R. M. & Brown, R. H., Jr. Direct effects of cyclosporin A and cyclophosphamide on differentiation of normal human myoblasts in culture. *Neurology* **43**, 1432-1434 (1993).

37 Huard, J. *et al.* Human myoblast transplantation: preliminary results of 4 cases. *Muscle & nerve* **15**, 550-560, doi:10.1002/mus.880150504 (1992).

38 Collins, C. A. *et al.* Stem cell function, self-renewal, and behavioral heterogeneity of cells from the adult muscle satellite cell niche. *Cell* **122**, 289-301, doi:10.1016/j.cell.2005.05.010 (2005).

39 Montarras, D. *et al.* Direct isolation of satellite cells for skeletal muscle regeneration. *Science* **309**, 2064-2067, doi:10.1126/science.1114758 (2005).

40 Qu-Petersen, Z. *et al.* Identification of a novel population of muscle stem cells in mice: potential for muscle regeneration. *The Journal of cell biology* **157**, 851-864, doi:10.1083/jcb.200108150 (2002).

41 Mueller, G. M., O'Day, T., Watchko, J. F. & Ontell, M. Effect of injecting primary myoblasts versus putative muscle-derived stem cells on mass and force generation in mdx mice. *Hum Gene Ther* **13**, 1081-1090, doi:10.1089/104303402753812485 (2002).

42 Dellavalle, A. *et al.* Pericytes of human skeletal muscle are myogenic precursors distinct from satellite cells. *Nature cell biology* **9**, 255-267, doi:10.1038/ncb1542 (2007).

43 Dellavalle, A. *et al.* Pericytes resident in postnatal skeletal muscle differentiate into muscle fibres and generate satellite cells. *Nat Commun* **2**, 499, doi:10.1038/ncomms1508 (2011).

44 Evans, M. J. & Kaufman, M. H. Establishment in culture of pluripotential cells from mouse embryos. *Nature* **292**, 154-156 (1981).

45 Rohwedel, J. *et al.* Muscle cell differentiation of embryonic stem cells reflects myogenesis in vivo: developmentally regulated expression of myogenic determination genes and functional expression of ionic currents. *Dev Biol* **164**, 87-101, doi:10.1006/dbio.1994.1182 (1994).

46 Barberi, T. *et al.* Derivation of engraftable skeletal myoblasts from human embryonic stem cells. *Nat Med* **13**, 642-648, doi:10.1038/nm1533 (2007).

47 Mizuno, Y. *et al.* Generation of skeletal muscle stem/progenitor cells from murine induced pluripotent stem cells. *FASEB J* **24**, 2245-2253, doi:10.1096/fj.09-137174 (2010).

48 Riederer, I. *et al.* Slowing down differentiation of engrafted human myoblasts into immunodeficient mice correlates with increased proliferation and migration. *Molecular therapy : the journal of the American Society of Gene Therapy* **20**, 146-154, doi:10.1038/mt.2011.193 (2012).

49 Shwartz, Y., Blitz, E. & Zelzer, E. One load to rule them all: mechanical control of the musculoskeletal system in development and aging. *Differentiation* **86**, 104-111, doi:10.1016/j.diff.2013.07.003 (2013).

50 Ambrosio, F. *et al.* The effect of muscle loading on skeletal muscle regenerative potential: an update of current research findings relating to aging and neuromuscular pathology. *Am J Phys Med Rehabil* **88**, 145-155, doi:10.1097/PHM.0b013e3181951fc5 (2009).

51 Gnecchi, M. *et al.* Paracrine action accounts for marked protection of ischemic heart by Akt-modified mesenchymal stem cells. *Nat Med* **11**, 367-368, doi:10.1038/nm0405-367 (2005).

52 Murry, C. E., Reinecke, H. & Pabon, L. M. Regeneration gaps: observations on stem cells and cardiac repair. *J Am Coll Cardiol* **47**, 1777-1785, doi:10.1016/j.jacc.2006.02.002 (2006).

53 Gharaibeh, B., Lavasani, M., Cummins, J. H. & Huard, J. Terminal differentiation is not a major determinant for the success of stem cell therapy - cross-talk between muscle-derived stem cells and host cells. *Stem Cell Res Ther* **2**, 31, doi:10.1186/scrt72 (2011).

54 Perez-Ilzarbe, M. *et al.* Characterization of the paracrine effects of human skeletal myoblasts transplanted in infarcted myocardium. *Eur J Heart Fail* **10**, 1065-1072, doi:10.1016/j.ejheart.2008.08.002 (2008).

55 Gnecchi, M., Zhang, Z., Ni, A. & Dzau, V. J. Paracrine mechanisms in adult stem cell signaling and therapy. *Circ Res* **103**, 1204-1219, doi:10.1161/CIRCRESAHA.108.176826 (2008).

56 Arthur, A., Zannettino, A. & Gronthos, S. The therapeutic applications of multipotential mesenchymal/stromal stem cells in skeletal tissue repair. *J Cell Physiol* **218**, 237-245, doi:10.1002/jcp.21592 (2009).

57 Machingal, M. A. *et al.* A tissue-engineered muscle repair construct for functional restoration of an irrecoverable muscle injury in a murine model. *Tissue engineering. Part A* **17**, 2291-2303, doi:10.1089/ten.TEA.2010.0682 (2011).

58 Corona, B. T., Ward, C. L., Baker, H. B., Walters, T. J. & Christ, G. J. Implantation of in vitro tissue engineered muscle repair constructs and bladder acellular matrices partially restore in vivo skeletal muscle function in a rat model of volumetric muscle loss injury. *Tissue engineering. Part A* **20**, 705-715, doi:10.1089/ten.TEA.2012.0761 (2014).

59 Gregory, T. M., Heckmann, R. A. & Francis, R. S. The effect of exercise on the presence of leukocytes, erythrocytes and collagen fibers in skeletal muscle after contusion. *Journal of manipulative and physiological therapeutics* **18**, 72-78 (1995).

60 Gilbert, T. W. *et al.* Gene expression by fibroblasts seeded on small intestinal submucosa and subjected to cyclic stretching. *Tissue Eng* **13**, 1313-1323, doi:10.1089/ten.2006.0318 (2007).

61 Turner, N. J., Badylak, J. S., Weber, D. J. & Badylak, S. F. Biologic scaffold remodeling in a dog model of complex musculoskeletal injury. *The Journal of surgical research* **176**, 490-502, doi:10.1016/j.jss.2011.11.1029 (2012).

62 Londono, R. & Badylak, S. F. Biologic scaffolds for regenerative medicine: mechanisms of in vivo remodeling. *Ann Biomed Eng* **43**, 577-592, doi:10.1007/s10439-014-1103-8 (2015).

63 Vroman, L., Adams, A. L., Fischer, G. C. & Munoz, P. C. Interaction of high molecular weight kininogen, factor XII, and fibrinogen in plasma at interfaces. *Blood* **55**, 156-159 (1980).

64 Alon, R. & Ley, K. Cells on the run: shear-regulated integrin activation in leukocyte rolling and arrest on endothelial cells. *Curr Opin Cell Biol* **20**, 525-532, doi:10.1016/j.ceb.2008.04.003 (2008).

65 Lech, M. & Anders, H. J. Macrophages and fibrosis: How resident and infiltrating mononuclear phagocytes orchestrate all phases of tissue injury and repair. *Biochim Biophys Acta* **1832**, 989-997, doi:10.1016/j.bbadis.2012.12.001 (2013).

66 Sorokin, L. The impact of the extracellular matrix on inflammation. *Nat Rev Immunol* **10**, 712-723, doi:10.1038/nri2852 (2010).

67 Vestweber, D. Adhesion and signaling molecules controlling the transmigration of leukocytes through endothelium. *Immunol Rev* **218**, 178-196, doi:10.1111/j.1600-065X.2007.00533.x (2007).

68 Nieswandt, B. & Watson, S. P. Platelet-collagen interaction: is GPVI the central receptor? *Blood* **102**, 449-461, doi:10.1182/blood-2002-12-3882 (2003).

69 Watson, S. P. Platelet activation by extracellular matrix proteins in haemostasis and thrombosis. *Curr Pharm Des* **15**, 1358-1372 (2009).

70 Engler, A. J., Sen, S., Sweeney, H. L. & Discher, D. E. Matrix elasticity directs stem cell lineage specification. *Cell* **126**, 677-689, doi:10.1016/j.cell.2006.06.044 (2006).

71 Vogel, V. & Sheetz, M. Local force and geometry sensing regulate cell functions. *Nat Rev Mol Cell Biol* **7**, 265-275, doi:10.1038/nrm1890 (2006).

72 McWhorter, F. Y., Wang, T., Nguyen, P., Chung, T. & Liu, W. F. Modulation of macrophage phenotype by cell shape. *Proc Natl Acad Sci U S A* **110**, 17253-17258, doi:10.1073/pnas.1308887110 (2013).

73 Agrawal, V. *et al.* An isolated cryptic peptide influences osteogenesis and bone remodeling in an adult mammalian model of digit amputation. *Tissue Eng Part A* **17**, 3033-3044, doi:10.1089/ten.TEA.2011.0257 (2011).

74 Weathington, N. M. *et al.* A novel peptide CXCR ligand derived from extracellular matrix degradation during airway inflammation. *Nat Med* **12**, 317-323, doi:10.1038/nm1361 (2006).

75 Huleihel, L. *et al.* Matrix-bound nanovesicles within ECM bioscaffolds. *Science advances* **2**, e1600502, doi:10.1126/sciadv.1600502 (2016).

76 Brown, B. N. *et al.* Macrophage phenotype as a predictor of constructive remodeling following the implantation of biologically derived surgical mesh materials. *Acta biomaterialia* **8**, 978-987, doi:10.1016/j.actbio.2011.11.031 (2012).

77 Sicari, B., Turner, N. & Badylak, S. F. An in vivo model system for evaluation of the host response to biomaterials. *Methods Mol Biol* **1037**, 3-25, doi:10.1007/978-1-62703-505-7_1 (2013).

78 Sicari, B. M. *et al.* The promotion of a constructive macrophage phenotype by solubilized extracellular matrix. *Biomaterials* **35**, 8605-8612, doi:10.1016/j.biomaterials.2014.06.060 (2014).

79 Slivka, P. F. *et al.* Fractionation of an ECM hydrogel into structural and soluble components reveals distinctive roles in regulating macrophage behavior. *Biomaterials science* **2**, 1521-1534, doi:10.1039/c4bm00189c (2014).

80 Herman, A. R. The history of skin grafts. *J Drugs Dermatol* **1**, 298-301 (2002).

81 Gibson, T. & Medawar, P. B. The fate of skin homografts in man. *J Anat* **77**, 299-310 294 (1943).

82 Kahan, B. D. Individuality: the barrier to optimal immunosuppression. *Nat Rev Immunol* **3**, 831-838, doi:10.1038/nri1204 (2003).

83 Benditt, D. G. *et al.* Cellular electrophysiologic effects of dexamethasone sodium phosphate: implications for cardiac stimulation with steroid-eluting electrodes. *Int J Cardiol* **22**, 67-73 (1989).

84 Ratner, B. D. *Biomaterials science : an introduction to materials in medicine*. 3rd edn, (Elsevier/Academic Press, 2013).

85 Williams, D. F. On the mechanisms of biocompatibility. *Biomaterials* **29**, 2941-2953, doi:10.1016/j.biomaterials.2008.04.023 (2008).

86 Hoene, A. *et al.* In vivo evaluation of copper release and acute local tissue reactions after implantation of copper-coated titanium implants in rats. *Biomed Mater* **8**, 035009, doi:10.1088/1748-6041/8/3/035009 (2013).

87 Anderson, J. M., Rodriguez, A. & Chang, D. T. Foreign body reaction to biomaterials. *Semin Immunol* **20**, 86-100, doi:10.1016/j.smim.2007.11.004 (2008).

88 Alijotas-Reig, J., Garcia-Gimenez, V., Llurba, E. & Vilardell-Tarres, M. Autoimmune/inflammatory syndrome (ASIA) induced by biomaterials injection other than silicone medical grade. *Lupus* **21**, 1326-1334, doi:10.1177/0961203312458838 (2012).

89 Atala, A., Bauer, S. B., Soker, S., Yoo, J. J. & Retik, A. B. Tissue-engineered autologous bladders for patients needing cystoplasty. *Lancet* **367**, 1241-1246, doi:10.1016/S0140-6736(06)68438-9 (2006).

90 Dick, H. B. & Augustin, A. J. Solvent for removing silicone oil from intraocular lenses: experimental study comparing various biomaterials. *J Cataract Refract Surg* **26**, 1667-1672 (2000).

91 Pfleiderer, B., Xu, P., Ackerman, J. L. & Garrido, L. Study of aging of silicone rubber biomaterials with NMR. *J Biomed Mater Res* **29**, 1129-1140, doi:10.1002/jbm.820290913 (1995).

92 Stathi, K., Tarantili, P. A. & Polyzois, G. The effect of accelerated ageing on performance properties of addition type silicone biomaterials. *J Mater Sci Mater Med* **21**, 1403-1411, doi:10.1007/s10856-010-3991-y (2010).

93 Simon, A. K., Hollander, G. A. & McMichael, A. Evolution of the immune system in humans from infancy to old age. *Proc Biol Sci* **282**, 20143085, doi:10.1098/rspb.2014.3085 (2015).

94 Godwin, J. W., Pinto, A. R. & Rosenthal, N. A. Chasing the recipe for a pro-regenerative immune system. *Semin Cell Dev Biol*, doi:10.1016/j.semcdb.2016.08.008 (2016).

95 Okumura, R. & Takeda, K. Maintenance of gut homeostasis by the mucosal immune system. *Proc Jpn Acad Ser B Phys Biol Sci* **92**, 423-435, doi:10.2183/pjab.92.423 (2016).

96 Rogier, E. W. *et al.* Secretory antibodies in breast milk promote long-term intestinal homeostasis by regulating the gut microbiota and host gene expression. *Proc Natl Acad Sci U S A* **111**, 3074-3079, doi:10.1073/pnas.1315792111 (2014).

97 Zhan, Y. *et al.* Deficient neuron-microglia signaling results in impaired functional brain connectivity and social behavior. *Nat Neurosci* **17**, 400-406, doi:10.1038/nn.3641 (2014).

98 Badylak, S. F., Valentin, J. E., Ravindra, A. K., McCabe, G. P. & Stewart-Akers, A. M. Macrophage phenotype as a determinant of biologic scaffold remodeling. *Tissue engineering. Part A* **14**, 1835-1842, doi:10.1089/ten.tea.2007.0264 (2008).

99 Brown, B. N., Ratner, B. D., Goodman, S. B., Amar, S. & Badylak, S. F. Macrophage polarization: an opportunity for improved outcomes in biomaterials and regenerative medicine. *Biomaterials* **33**, 3792-3802, doi:10.1016/j.biomaterials.2012.02.034 (2012).

100 Valentin, J. E., Stewart-Akers, A. M., Gilbert, T. W. & Badylak, S. F. Macrophage participation in the degradation and remodeling of extracellular matrix scaffolds. *Tissue engineering. Part A* **15**, 1687-1694, doi:10.1089/ten.tea.2008.0419 (2009).

101 Agarwal, J. P. *et al.* The breast reconstruction evaluation of acellular dermal matrix as a sling trial (BREASTrial): design and methods of a prospective randomized trial. *Plast Reconstr Surg* **135**, 20e-28e, doi:10.1097/PRS.0000000000000809 (2015).

102 Badylak, S. F. *et al.* Esophageal preservation in five male patients after endoscopic inner-layer circumferential resection in the setting of superficial cancer: a regenerative medicine approach with a biologic scaffold. *Tissue engineering. Part A* **17**, 1643-1650, doi:10.1089/ten.TEA.2010.0739 (2011).

103 Gerdisch, M. W., Shea, R. J. & Barron, M. D. Clinical experience with CorMatrix extracellular matrix in the surgical treatment of mitral valve disease. *The Journal of thoracic and cardiovascular surgery* **148**, 1370-1378, doi:10.1016/j.jtcvs.2013.10.055 (2014).

104 Kissane, N. A. & Itani, K. M. A decade of ventral incisional hernia repairs with biologic acellular dermal matrix: what have we learned? *Plast Reconstr Surg* **130**, 194S-202S, doi:10.1097/PRS.0b013e318265a5ec (2012).

105 Ladowski, J. M. & Ladowski, J. S. Retrospective analysis of bovine pericardium (Vascu-Guard) for patch closure in carotid endarterectomies. *Ann Vasc Surg* **25**, 646-650, doi:10.1016/j.avsg.2010.11.008 (2011).

106 Lecheminant, J. & Field, C. Porcine urinary bladder matrix: a retrospective study and establishment of protocol. *J Wound Care* **21**, 476, 478-480, 482, doi:10.12968/jowc.2012.21.10.476 (2012).

107 Sicari, B. M. *et al.* An acellular biologic scaffold promotes skeletal muscle formation in mice and humans with volumetric muscle loss. *Science translational medicine* **6**, 234ra258, doi:10.1126/scitranslmed.3008085 (2014).

108 Agrawal, V. *et al.* Recruitment of progenitor cells by an extracellular matrix cryptic peptide in a mouse model of digit amputation. *Tissue engineering. Part A* **17**, 2435-2443, doi:10.1089/ten.TEA.2011.0036 (2011).

109 Reing, J. E. *et al.* Degradation products of extracellular matrix affect cell migration and proliferation. *Tissue Eng Part A* **15**, 605-614, doi:10.1089/ten.tea.2007.0425 (2009).

110 Vorotnikova, E. *et al.* Extracellular matrix-derived products modulate endothelial and progenitor cell migration and proliferation in vitro and stimulate regenerative healing in vivo. *Matrix Biol* **29**, 690-700, doi:10.1016/j.matbio.2010.08.007 (2010).

111 Sarikaya, A. *et al.* Antimicrobial activity associated with extracellular matrices. *Tissue Eng* **8**, 63-71, doi:10.1089/107632702753503063 (2002).

112 Allen, R. A. *et al.* Adrenal extracellular matrix scaffolds support adrenocortical cell proliferation and function in vitro. *Tissue Eng Part A* **16**, 3363-3374, doi:10.1089/ten.TEA.2010.0005 (2010).

113 Hammond, J. S. *et al.* Scaffolds containing growth factors and extracellular matrix induce hepatocyte proliferation and cell migration in normal and regenerating rat liver. *J Hepatol* **54**, 279-287, doi:10.1016/j.jhep.2010.06.040 (2011).

114 Voytik-Harbin, S. L., Brightman, A. O., Kraine, M. R., Waisner, B. & Badylak, S. F. Identification of extractable growth factors from small intestinal submucosa. *J Cell Biochem* **67**, 478-491 (1997).

115 Allman, A. J. *et al.* Xenogeneic extracellular matrix grafts elicit a TH2-restricted immune response. *Transplantation* **71**, 1631-1640 (2001).

116 Brown, B. N., Valentin, J. E., Stewart-Akers, A. M., McCabe, G. P. & Badylak, S. F. Macrophage phenotype and remodeling outcomes in response to biologic scaffolds with and without a cellular component. *Biomaterials* **30**, 1482-1491, doi:10.1016/j.biomaterials.2008.11.040 (2009).

117 Keane, T. J., Londono, R., Turner, N. J. & Badylak, S. F. Consequences of ineffective decellularization of biologic scaffolds on the host response. *Biomaterials* **33**, 1771-1781, doi:10.1016/j.biomaterials.2011.10.054 (2012).

118 Dziki, J. L. *et al.* Solubilized extracellular matrix bioscaffolds derived from diverse source tissues differentially influence macrophage phenotype. *J Biomed Mater Res A*, doi:10.1002/jbm.a.35894 (2016).

119 Sicari, B. M. *et al.* The effect of source animal age upon the in vivo remodeling characteristics of an extracellular matrix scaffold. *Biomaterials* **33**, 5524-5533, doi:10.1016/j.biomaterials.2012.04.017 (2012).

120 Dearth, C. L. *et al.* The effect of terminal sterilization on the material properties and in vivo remodeling of a porcine dermal biologic scaffold. *Acta biomaterialia* **33**, 78-87, doi:10.1016/j.actbio.2016.01.038 (2016).

121 Dearth, C. L. *et al.* Inhibition of COX1/2 alters the host response and reduces ECM scaffold mediated constructive tissue remodeling in a rodent model of skeletal muscle injury. *Acta biomaterialia* **31**, 50-60, doi:10.1016/j.actbio.2015.11.043 (2016).

122 Born, J. *et al.* Cytokine production and lymphocyte subpopulations in aged humans. An assessment during nocturnal sleep. *Mech Ageing Dev* **84**, 113-126 (1995).

123 Butcher, S. K. *et al.* Senescence in innate immune responses: reduced neutrophil phagocytic capacity and CD16 expression in elderly humans. *J Leukoc Biol* **70**, 881-886 (2001).

124 Carvalho Neves Forte, W., Martins Campos, J. V. & Carneiro Leao, R. Non specific immunological response in moderate malnutrition. *Allergol Immunopathol (Madr)* **12**, 489-496 (1984).

125 Gonzalez, C. *et al.* Hydrogen peroxide-induced DNA damage and DNA repair in lymphocytes from malnourished children. *Environ Mol Mutagen* **39**, 33-42 (2002).

126 Leigh, D. R. *et al.* Effect of implantation site and injury condition on host response to human-derived fascia lata ECM in a rat model. *J Orthop Res* **30**, 461-467, doi:10.1002/jor.21529 (2012).

127 Hotamisligil, G. S., Shargill, N. S. & Spiegelman, B. M. Adipose expression of tumor necrosis factor-alpha: direct role in obesity-linked insulin resistance. *Science* **259**, 87-91 (1993).

128 Xu, H. *et al.* Chronic inflammation in fat plays a crucial role in the development of obesity-related insulin resistance. *J Clin Invest* **112**, 1821-1830, doi:10.1172/JCI19451 (2003).

129 Godwin, J. W., Pinto, A. R. & Rosenthal, N. A. Macrophages are required for adult salamander limb regeneration. *Proceedings of the National Academy of Sciences of the United States of America* **110**, 9415-9420, doi:10.1073/pnas.1300290110 (2013).

130 Sadtler, K. *et al.* The Scaffold Immune Microenvironment: Biomaterial-Mediated Immune Polarization in Traumatic and Nontraumatic Applications. *Tissue Eng Part A*, doi:10.1089/ten.TEA.2016.0304 (2016).

131 Keane, T. J. *et al.* Restoring Mucosal Barrier Function and Modifying Macrophage Phenotype with an Extracellular Matrix Hydrogel: Potential Therapy for Ulcerative Colitis. *J Crohns Colitis*, doi:10.1093/ecco-jcc/jjw149 (2016).

132 Dziki, J. L., Sicari, B. M., Wolf, M. T., Cramer, M. C. & Badylak, S. F. Immunomodulation and Mobilization of Progenitor Cells by Extracellular Matrix Bioscaffolds for Volumetric Muscle Loss Treatment. *Tissue Eng Part A* **22**, 1129-1139, doi:10.1089/ten.TEA.2016.0340 (2016).

133 Sadtler, K. *et al.* Developing a pro-regenerative biomaterial scaffold microenvironment requires T helper 2 cells. *Science* **352**, 366-370, doi:10.1126/science.aad9272 (2016).

134 Kamran, N., Chandran, M., Lowenstein, P. R. & Castro, M. G. Immature myeloid cells in the tumor microenvironment: Implications for immunotherapy. *Clin Immunol*, doi:10.1016/j.clim.2016.10.008 (2016).

135 Villalta, S. A. *et al.* Regulatory T cells suppress muscle inflammation and injury in muscular dystrophy. *Science translational medicine* **6**, 258ra142, doi:10.1126/scitranslmed.3009925 (2014).

136 Faulk, D. M. *et al.* ECM hydrogel coating mitigates the chronic inflammatory response to polypropylene mesh. *Biomaterials* **35**, 8585-8595, doi:10.1016/j.biomaterials.2014.06.057 (2014).

137 Wolf, M. T. *et al.* Polypropylene surgical mesh coated with extracellular matrix mitigates the host foreign body response. *J Biomed Mater Res A* **102**, 234-246, doi:10.1002/jbm.a.34671 (2014).

138 Kajahn, J. *et al.* Artificial extracellular matrices composed of collagen I and high sulfated hyaluronan modulate monocyte to macrophage differentiation under conditions of sterile inflammation. *Biomatter* **2**, 226-236, doi:10.4161/biom.22855 (2012).

139 Hachim, D., LoPresti, S. T., Yates, C. C. & Brown, B. N. Shifts in macrophage phenotype at the biomaterial interface via IL-4 eluting coatings are associated with improved implant integration. *Biomaterials* **112**, 95-107, doi:10.1016/j.biomaterials.2016.10.019 (2016).

140 Lin, C. C., Metters, A. T. & Anseth, K. S. Functional PEG-peptide hydrogels to modulate local inflammation induced by the pro-inflammatory cytokine TNFalpha. *Biomaterials* **30**, 4907-4914, doi:10.1016/j.biomaterials.2009.05.083 (2009).

141 Su, J., Hu, B. H., Lowe, W. L., Jr., Kaufman, D. B. & Messersmith, P. B. Anti-inflammatory peptide-functionalized hydrogels for insulin-secreting cell encapsulation. *Biomaterials* **31**, 308-314, doi:10.1016/j.biomaterials.2009.09.045 (2010).

142 Jiang, K. *et al.* Local release of dexamethasone from macroporous scaffolds accelerates islet transplant engraftment by promotion of anti-inflammatory M2 macrophages. *Biomaterials* **114**, 71-81, doi:10.1016/j.biomaterials.2016.11.004 (2016).

143 Wang, M. *et al.* Improved osteogenesis and angiogenesis of magnesium-doped calcium phosphate cement via macrophage immunomodulation. *Biomater Sci* **4**, 1574-1583, doi:10.1039/c6bm00290k (2016).

144 English, K. Mechanisms of mesenchymal stromal cell immunomodulation. *Immunol Cell Biol* **91**, 19-26, doi:10.1038/icb.2012.56 (2013).

145 Swartzlander, M. D. *et al.* Immunomodulation by mesenchymal stem cells combats the foreign body response to cell-laden synthetic hydrogels. *Biomaterials* **41**, 79-88, doi:10.1016/j.biomaterials.2014.11.020 (2015).

146 Carlini, A. S., Adamiak, L. & Gianneschi, N. C. Biosynthetic Polymers as Functional Materials. *Macromolecules* **49**, 4379-4394, doi:10.1021/acs.macromol.6b00439 (2016).

147 Jones, M. K., Tomikawa, M., Mohajer, B. & Tarnawski, A. S. Gastrointestinal mucosal regeneration: role of growth factors. *Front Biosci* **4**, D303-309 (1999).

148 Odland, G. & Ross, R. Human wound repair. I. Epidermal regeneration. *J Cell Biol* **39**, 135-151 (1968).

149 Patt, H. M. & Maloney, M. A. Bone marrow regeneration after local injury: a review. *Exp Hematol* **3**, 135-148 (1975).

150 Taub, R. Liver regeneration: from myth to mechanism. *Nat Rev Mol Cell Biol* **5**, 836-847, doi:10.1038/nrm1489 (2004).

151 Sicari, B. M., Dearth, C. L. & Badylak, S. F. Tissue engineering and regenerative medicine approaches to enhance the functional response to skeletal muscle injury. *Anatomical record* **297**, 51-64, doi:10.1002/ar.22794 (2014).

152 Anastasi, S. *et al.* A natural hepatocyte growth factor/scatter factor autocrine loop in myoblast cells and the effect of the constitutive Met kinase activation on myogenic differentiation. *J Cell Biol* **137**, 1057-1068 (1997).

153 Cossu, G. & Sampaolesi, M. New therapies for Duchenne muscular dystrophy: challenges, prospects and clinical trials. *Trends Mol Med* **13**, 520-526, doi:10.1016/j.molmed.2007.10.003 (2007).

154 Dennis, R. G. & Kosnik, P. E., 2nd. Excitability and isometric contractile properties of mammalian skeletal muscle constructs engineered in vitro. *In Vitro Cell Dev Biol Anim* **36**, 327-335, doi:10.1290/1071-2690(2000)036<0327:EAICPO>2.0.CO;2 (2000).

155 Mertens, J. P., Sugg, K. B., Lee, J. D. & Larkin, L. M. Engineering muscle constructs for the creation of functional engineered musculoskeletal tissue. *Regen Med* **9**, 89-100, doi:10.2217/rme.13.81 (2014).

156 Qu, Z. *et al.* Development of approaches to improve cell survival in myoblast transfer therapy. *J Cell Biol* **142**, 1257-1267 (1998).

157 Corona, B. T. *et al.* Further development of a tissue engineered muscle repair construct in vitro for enhanced functional recovery following implantation in vivo in a murine model of volumetric muscle loss injury. *Tissue Eng Part A* **18**, 1213-1228, doi:10.1089/ten.TEA.2011.0614 (2012).

158 Levenberg, S. *et al.* Engineering vascularized skeletal muscle tissue. *Nat Biotechnol* **23**, 879-884, doi:10.1038/nbt1109 (2005).

159 Badylak, S. F. The extracellular matrix as a scaffold for tissue reconstruction. *Semin Cell Dev Biol* **13**, 377-383 (2002).

160 Musarò, A. in *Advances in Biology* Vol. 2014 1-16 (Hindawi Publishing Corporation, 2014).

161 Chen, X. K. & Walters, T. J. Muscle-derived decellularised extracellular matrix improves functional recovery in a rat latissimus dorsi muscle defect model. *J Plast Reconstr Aesthet Surg* **66**, 1750-1758, doi:10.1016/j.bjps.2013.07.037 (2013).

162 Merritt, E. K. *et al.* Functional assessment of skeletal muscle regeneration utilizing homologous extracellular matrix as scaffolding. *Tissue Eng Part A* **16**, 1395-1405, doi:10.1089/ten.TEA.2009.0226 (2010).

163 Sicari, B. M. *et al.* A murine model of volumetric muscle loss and a regenerative medicine approach for tissue replacement. *Tissue engineering. Part A* **18**, 1941-1948, doi:10.1089/ten.TEA.2012.0475 (2012).

164 Valentin, J. E., Turner, N. J., Gilbert, T. W. & Badylak, S. F. Functional skeletal muscle formation with a biologic scaffold. *Biomaterials* **31**, 7475-7484, doi:10.1016/j.biomaterials.2010.06.039 (2010).

165 Carlson, B. M. Regeneration fo the completely excised gastrocnemius muscle in the frog and rat from minced muscle fragments. *Journal of morphology* **125**, 447-472, doi:10.1002/jmor.1051250405 (1968).

166 Carlson, B. M. & Faulkner, J. A. The regeneration of skeletal muscle fibers following injury: a review. *Medicine and science in sports and exercise* **15**, 187-198 (1983).

167 Grefte, S., Kuijpers-Jagtman, A. M., Torensma, R. & Von den Hoff, J. W. Skeletal muscle development and regeneration. *Stem Cells Dev* **16**, 857-868, doi:10.1089/scd.2007.0058 (2007).

168 Huard, J., Li, Y. & Fu, F. H. Muscle injuries and repair: current trends in research. *J Bone Joint Surg Am* **84-A**, 822-832 (2002).

169 Wozniak, A. C., Kong, J., Bock, E., Pilipowicz, O. & Anderson, J. E. Signaling satellite-cell activation in skeletal muscle: markers, models, stretch, and potential alternate pathways. *Muscle Nerve* **31**, 283-300, doi:10.1002/mus.20263 (2005).

170 Zammit, P. S., Partridge, T. A. & Yablonka-Reuveni, Z. The skeletal muscle satellite cell: the stem cell that came in from the cold. *The journal of histochemistry and cytochemistry : official journal of the Histochemistry Society* **54**, 1177-1191, doi:10.1369/jhc.6R6995.2006 (2006).

171 Hawke, T. J. & Garry, D. J. Myogenic satellite cells: physiology to molecular biology. *J Appl Physiol* **91**, 534-551 (2001).

172 Mauro, A. Satellite cell of skeletal muscle fibers. *The Journal of biophysical and biochemical cytology* **9**, 493-495 (1961).

173 Muir, A. R., Kanji, A. H. & Allbrook, D. The structure of the satellite cells in skeletal muscle. *J Anat* **99**, 435-444 (1965).

174 Shi, X. & Garry, D. J. Muscle stem cells in development, regeneration, and disease. *Genes Dev* **20**, 1692-1708, doi:20/13/1692 [pii]10.1101/gad.1419406 (2006).

175 Crisan, M. *et al.* A perivascular origin for mesenchymal stem cells in multiple human organs. *Cell stem cell* **3**, 301-313, doi:10.1016/j.stem.2008.07.003 (2008).

176 Kharraz, Y., Guerra, J., Mann, C. J., Serrano, A. L. & Munoz-Canoves, P. Macrophage plasticity and the role of inflammation in skeletal muscle repair. *Mediators of inflammation* **2013**, 491497, doi:10.1155/2013/491497 (2013).

177 Saclier, M., Cuvellier, S., Magnan, M., Mounier, R. & Chazaud, B. Monocyte/macrophage interactions with myogenic precursor cells during skeletal muscle regeneration. *The FEBS journal* **280**, 4118-4130, doi:10.1111/febs.12166 (2013).

178 Ruffell, D. *et al.* A CREB-C/EBPbeta cascade induces M2 macrophage-specific gene expression and promotes muscle injury repair. *Proceedings of the National Academy of Sciences of the United States of America* **106**, 17475-17480, doi:10.1073/pnas.0908641106 (2009).

179 Agrawal, V., Brown, B. N., Beattie, A. J., Gilbert, T. W. & Badylak, S. F. Evidence of innervation following extracellular matrix scaffold-mediated remodelling of muscular tissues.

Journal of tissue engineering and regenerative medicine **3**, 590-600, doi:10.1002/term.200 (2009).

180 Agrawal, V. *et al.* Epimorphic regeneration approach to tissue replacement in adult mammals. *Proc Natl Acad Sci U S A* **107**, 3351-3355, doi:10.1073/pnas.0905851106 (2010).

181 Agrawal, V. *et al.* Partial characterization of the Sox2+ cell population in an adult murine model of digit amputation. *Tissue Eng Part A* **18**, 1454-1463, doi:10.1089/ten.TEA.2011.0550 (2012).

182 Badylak, S. F. Regenerative medicine and developmental biology: the role of the extracellular matrix. *Anat Rec B New Anat* **287**, 36-41, doi:10.1002/ar.b.20081 (2005).

183 Gilbert, T. W. *et al.* Liver-derived extracellular matrix as a biologic scaffold for acute vocal fold repair in a canine model. *Laryngoscope* **119**, 1856-1863, doi:10.1002/lary.20575 (2009).

184 Medberry, C. J. *et al.* Hydrogels derived from central nervous system extracellular matrix. *Biomaterials* **34**, 1033-1040, doi:10.1016/j.biomaterials.2012.10.062 (2013).

185 Karalaki, M., Fili, S., Philippou, A. & Koutsilieris, M. Muscle regeneration: cellular and molecular events. *In Vivo* **23**, 779-796 (2009).

186 Munoz-Canoves, P., Carvajal, J. J., Lopez de Munain, A. & Izeta, A. Editorial: Role of Stem Cells in Skeletal Muscle Development, Regeneration, Repair, Aging, and Disease. *Front Aging Neurosci* **8**, 95, doi:10.3389/fnagi.2016.00095 (2016).

187 Wada, M. R., Inagawa-Ogashiwa, M., Shimizu, S., Yasumoto, S. & Hashimoto, N. Generation of different fates from multipotent muscle stem cells. *Development* **129**, 2987-2995 (2002).

188 Liu, H. M. The role of extracellular matrix in peripheral nerve regeneration: a wound chamber study. *Acta Neuropathol* **83**, 469-474 (1992).

189 Mannello, F., Tonti, G. A., Bagnara, G. P. & Papa, S. Role and function of matrix metalloproteinases in the differentiation and biological characterization of mesenchymal stem cells. *Stem Cells* **24**, 475-481, doi:10.1634/stemcells.2005-0333 (2006).

190 Carruthers, C. A. *et al.* Histologic characterization of acellular dermal matrices in a porcine model of tissue expander breast reconstruction. *Tissue Eng Part A* **21**, 35-44, doi:10.1089/ten.TEA.2014.0095 (2015).

191 Reing, J. E. *et al.* The effects of processing methods upon mechanical and biologic properties of porcine dermal extracellular matrix scaffolds. *Biomaterials* **31**, 8626-8633, doi:10.1016/j.biomaterials.2010.07.083 (2010).

192 Wolf, M. T. *et al.* A hydrogel derived from decellularized dermal extracellular matrix. *Biomaterials* **33**, 7028-7038, doi:10.1016/j.biomaterials.2012.06.051 (2012).

193 Badylak, S. F., Kropp, B., McPherson, T., Liang, H. & Snyder, P. W. Small intestinal submucosa: a rapidly resorbed bioscaffold for augmentation cystoplasty in a dog model. *Tissue Eng* **4**, 379-387 (1998).

194 Freytes, D. O., Martin, J., Velankar, S. S., Lee, A. S. & Badylak, S. F. Preparation and rheological characterization of a gel form of the porcine urinary bladder matrix. *Biomaterials* **29**, 1630-1637, doi:10.1016/j.biomaterials.2007.12.014 (2008).

195 Freytes, D. O., Stoner, R. M. & Badylak, S. F. Uniaxial and biaxial properties of terminally sterilized porcine urinary bladder matrix scaffolds. *J Biomed Mater Res B Appl Biomater* **84**, 408-414, doi:10.1002/jbm.b.30885 (2008).

196 Wolf, M. T. *et al.* Macrophage polarization in response to ECM coated polypropylene mesh. *Biomaterials* **35**, 6838-6849, doi:10.1016/j.biomaterials.2014.04.115 (2014).

197 Brown, B., Lindberg, K., Reing, J., Stolz, D. B. & Badylak, S. F. The basement membrane component of biologic scaffolds derived from extracellular matrix. *Tissue Eng* **12**, 519-526, doi:10.1089/ten.2006.12.519 (2006).

198 van der Rest, M. & Garrone, R. Collagen family of proteins. *Faseb J* **5**, 2814-2823 (1991).

199 Beattie, A. J., Gilbert, T. W., Guyot, J. P., Yates, A. J. & Badylak, S. F. Chemoattraction of progenitor cells by remodeling extracellular matrix scaffolds. *Tissue engineering. Part A* **15**, 1119-1125, doi:10.1089/ten.tea.2008.0162 (2009).

200 Brennan, E. P. *et al.* Antibacterial activity within degradation products of biological scaffolds composed of extracellular matrix. *Tissue engineering* **12**, 2949-2955, doi:10.1089/ten.2006.12.2949 (2006).

201 Brennan, E. P., Tang, X. H., Stewart-Akers, A. M., Gudas, L. J. & Badylak, S. F. Chemoattractant activity of degradation products of fetal and adult skin extracellular matrix for keratinocyte progenitor cells. *J Tissue Eng Regen Med* **2**, 491-498, doi:10.1002/term.123 (2008).

202 Tharappel, J. C. *et al.* Doxycycline shows dose-dependent changes in hernia repair strength after mesh repair. *Surg Endosc* **30**, 2016-2021, doi:10.1007/s00464-015-4434-0 (2016).

203 Lehto, M., Sims, T. J. & Bailey, A. J. Skeletal muscle injury--molecular changes in the collagen during healing. *Res Exp Med (Berl)* **185**, 95-106 (1985).

204 Bonewald, L. F. Regulation and regulatory activities of transforming growth factor beta. *Crit Rev Eukaryot Gene Expr* **9**, 33-44 (1999).

205 Hodde, J. P., Record, R. D., Liang, H. A. & Badylak, S. F. Vascular endothelial growth factor in porcine-derived extracellular matrix. *Endothelium* **8**, 11-24 (2001).

206 Kagami, S. *et al.* Collagen type I modulates the platelet-derived growth factor (PDGF) regulation of the growth and expression of beta1 integrins by rat mesangial cells. *Biochem Biophys Res Commun* **252**, 728-732 (1998).

207 Roberts, R. *et al.* Heparan sulphate bound growth factors: a mechanism for stromal cell mediated haemopoiesis. *Nature* **332**, 376-378 (1988).

208 Wolf, M. T., Daly, K. A., Reing, J. E. & Badylak, S. F. Biologic scaffold composed of skeletal muscle extracellular matrix. *Biomaterials* **33**, 2916-2925, doi:10.1016/j.biomaterials.2011.12.055 (2012).

209 Faulk, D. M. *et al.* The effect of detergents on the basement membrane complex of a biologic scaffold material. *Acta biomaterialia* **10**, 183-193, doi:10.1016/j.actbio.2013.09.006 (2014).

210 Badylak, S. F. *et al.* Biologic scaffolds for constructive tissue remodeling. *Biomaterials* **32**, 316-319 (2011).

211 Boruch, A. V., Nieponice, A., Qureshi, I. R., Gilbert, T. W. & Badylak, S. F. Constructive remodeling of biologic scaffolds is dependent on early exposure to physiologic bladder filling in a canine partial cystectomy model. *J Surg Res* **161**, 217-225, doi:10.1016/j.jss.2009.02.014 (2010).

212 Badylak, S., Kokini, K., Tullius, B. & Whitson, B. Strength over time of a resorbable bioscaffold for body wall repair in a dog model. *J Surg Res* **99**, 282-287, doi:10.1006/jsre.2001.6176 (2001).

213 Gilbert, T. W., Stewart-Akers, A. M. & Badylak, S. F. A quantitative method for evaluating the degradation of biologic scaffold materials. *Biomaterials* **28**, 147-150, doi:10.1016/j.biomaterials.2006.08.022 (2007).

214 Carey, L. E. *et al.* In vivo degradation of 14C-labeled porcine dermis biologic scaffold. *Biomaterials* **35**, 8297-8304, doi:10.1016/j.biomaterials.2014.06.015 (2014).

215 Badylak, S. F., Park, K., Peppas, N., McCabe, G. & Yoder, M. Marrow-derived cells populate scaffolds composed of xenogeneic extracellular matrix. *Exp Hematol* **29**, 1310-1318 (2001).

216 Tottey, S. *et al.* Extracellular matrix degradation products and low-oxygen conditions enhance the regenerative potential of perivascular stem cells. *Tissue Eng Part A* **17**, 37-44, doi:10.1089/ten.TEA.2010.0188 (2011).

217 Tottey, S. *et al.* The effect of source animal age upon extracellular matrix scaffold properties. *Biomaterials* **32**, 128-136, doi:10.1016/j.biomaterials.2010.09.006 (2011).

218 Crisan, M., Corselli, M., Chen, W. C. & Peault, B. Perivascular cells for regenerative medicine. *J Cell Mol Med* **16**, 2851-2860, doi:10.1111/j.1582-4934.2012.01617.x (2012).

219 Khouw, I. M., van Wachem, P. B., de Leij, L. F. & van Luyn, M. J. Inhibition of the tissue reaction to a biodegradable biomaterial by monoclonal antibodies to IFN-gamma. *J Biomed Mater Res* **41**, 202-210, doi:10.1002/(SICI)1097-4636(199808)41:2<202::AID-JBM4>3.0.CO;2-M [pii] (1998).

220 Labow, R. S., Sa, D., Matheson, L. A. & Santerre, J. P. Polycarbonate-urethane hard segment type influences esterase substrate specificity for human-macrophage-mediated biodegradation. *J Biomater Sci Polym Ed* **16**, 1167-1177 (2005).

221 Lu, J. *et al.* The biodegradation mechanism of calcium phosphate biomaterials in bone. *J Biomed Mater Res* **63**, 408-412, doi:10.1002/jbm.10259 (2002).

222 Takebe, J., Champagne, C. M., Offenbacher, S., Ishibashi, K. & Cooper, L. F. Titanium surface topography alters cell shape and modulates bone morphogenetic protein 2 expression in the J774A.1 macrophage cell line. *J Biomed Mater Res A* **64**, 207-216, doi:10.1002/jbm.a.10275 (2003).

223 Dearth, C. L. *et al.* Inhibition of COX1/2 alters the host response and reduces ECM scaffold mediated constructive tissue remodeling in a rodent model of skeletal muscle injury. *Acta Biomater*, doi:10.1016/j.actbio.2015.11.043 (2015).

224 Turner, N. J. *et al.* Xenogeneic extracellular matrix as an inductive scaffold for regeneration of a functioning musculotendinous junction. *Tissue engineering. Part A* **16**, 3309-3317, doi:10.1089/ten.TEA.2010.0169 (2010).

225 Piccoli, M. *et al.* Improvement of diaphragmatic performance through orthotopic application of decellularized extracellular matrix patch. *Biomaterials* **74**, 245-255, doi:10.1016/j.biomaterials.2015.10.005 (2016).

226 Aurora, A., Roe, J. L., Corona, B. T. & Walters, T. J. An acellular biologic scaffold does not regenerate appreciable de novo muscle tissue in rat models of volumetric muscle loss injury. *Biomaterials* **67**, 393-407, doi:10.1016/j.biomaterials.2015.07.040 (2015).

227 Ambrosio, F. *et al.* The Synergistic Effect of Treadmill Running on Stem Cell Transplantation To Heal Injured Skeletal Muscle. *Tissue Eng Part A*, doi:10.1089/ten.TEA.2009.0113 (2009).

228 Cosgrove, B. D. *et al.* Rejuvenation of the muscle stem cell population restores strength to injured aged muscles. *Nature medicine* **20**, 255-264, doi:10.1038/nm.3464 (2014).

229 Engler, R. L., Schmid-Schonbein, G. W. & Pavelec, R. S. Leukocyte capillary plugging in myocardial ischemia and reperfusion in the dog. *American.Journal of Pathology.111.(1):98.-111.* (1983).

230 Payne, T. R. *et al.* A relationship between vascular endothelial growth factor, angiogenesis, and cardiac repair after muscle stem cell transplantation into ischemic hearts.[see comment]. *Journal of the.American.College.of Cardiology.50.(17):1677.-84.* (2007).

231 Ambrosio, F. *et al.* Functional overloading of dystrophic mice enhances muscle-derived stem cell contribution to muscle contractile capacity. *Arch Phys Med Rehabil* **90**, 66-73, doi:S0003-9993(08)01540-2 [pii]10.1016/j.apmr.2008.06.035 (2009).

232 Distefano, G. *et al.* Neuromuscular electrical stimulation as a method to maximize the beneficial effects of muscle stem cells transplanted into dystrophic skeletal muscle. *PLoS ONE* **8**, e54922, doi:10.1371/journal.pone.0054922PONE-D-11-25256 [pii].

233 Palermo, A. T., Labarge, M. A., Doyonnas, R., Pomerantz, J. & Blau, H. M. Bone marrow contribution to skeletal muscle: a physiological response to stress. *Developmental.Biology.279.(2):336.-44.* (2005).

234 Heher, P. *et al.* A novel bioreactor for the generation of highly aligned 3D skeletal muscle-like constructs through orientation of fibrin via application of static strain. *Acta Biomater* **24**, 251-265, doi:10.1016/j.actbio.2015.06.033 (2015).

235 Dziki, J. L. *et al.* An acellular biologic scaffold treatment for volumetric muscle loss: results of a thirteen patient cohort study. *Nature Regenerative Medicine* **(submitted Feb. 2016)** (2016).

236 Saxena, A. K., Marler, J., Benvenuto, M., Willital, G. H. & Vacanti, J. P. Skeletal muscle tissue engineering using isolated myoblasts on synthetic biodegradable polymers: preliminary studies. *Tissue Eng* **5**, 525-532 (1999).

237 Choi, J. S., Lee, S. J., Christ, G. J., Atala, A. & Yoo, J. J. The influence of electrospun aligned poly(epsilon-caprolactone)/collagen nanofiber meshes on the formation of self-aligned skeletal muscle myotubes. *Biomaterials* **29**, 2899-2906, doi:10.1016/j.biomaterials.2008.03.031 (2008).

238 Crisan, M., Corselli, M., Chen, C. W. & Peault, B. Multilineage stem cells in the adult: a perivascular legacy? *Organogenesis* **7**, 101-104, doi:10.4161/org.7.2.16150 (2011).

239 Hill, M., Wernig, A. & Goldspink, G. Muscle satellite (stem) cell activation during local tissue injury and repair. *Journal of anatomy* **203**, 89-99 (2003).

240 Tidball, J. G. Inflammatory cell response to acute muscle injury. *Medicine and science in sports and exercise* **27**, 1022-1032 (1995).

241 Tidball, J. G. Mechanisms of muscle injury, repair, and regeneration. *Comprehensive Physiology* **1**, 2029-2062, doi:10.1002/cphy.c100092 (2011).

242 Tidball, J. G. & Wehling-Henricks, M. Macrophages promote muscle membrane repair and muscle fibre growth and regeneration during modified muscle loading in mice in vivo. *The Journal of physiology* **578**, 327-336, doi:10.1113/jphysiol.2006.118265 (2007).

243 Li, Y. P. TNF-alpha is a mitogen in skeletal muscle. *American journal of physiology. Cell physiology* **285**, C370-376, doi:10.1152/ajpcell.00453.2002 (2003).

244 Wang, X. *et al.* Effects of interleukin-6, leukemia inhibitory factor, and ciliary neurotrophic factor on the proliferation and differentiation of adult human myoblasts. *Cellular and molecular neurobiology* **28**, 113-124, doi:10.1007/s10571-007-9247-9 (2008).

245 Camargo, F. D., Chambers, S. M., Drew, E., McNagny, K. M. & Goodell, M. A. Hematopoietic stem cells do not engraft with absolute efficiencies. *Blood* **107**, 501-507, doi:10.1182/blood-2005-02-0655 (2006).

246 Dziki, J. B., S.; Yabroudi, M.; Sicari, B.; Ambrosio, A.; Stearns, K.; Turner, N.; Wyse, A.; Boninger, M.; Brown, E.; Rubin, J. An Acellular Biologic Scaffold Treatment for Volumetric Muscle Loss: Results of a Thirteen Patient Cohort Study. *Nature Regenerative Medicine* **1** (2016).

247 Mase, V. J., Jr. *et al.* Clinical application of an acellular biologic scaffold for surgical repair of a large, traumatic quadriceps femoris muscle defect. *Orthopedics* **33**, 511, doi:10.3928/01477447-20100526-24 (2010).

248 Keane, T. J. & Badylak, S. F. The host response to allogeneic and xenogeneic biological scaffold materials. *Journal of tissue engineering and regenerative medicine*, doi:10.1002/term.1874 (2014).

249 Slivka, P. F. *et al.* Fractionation of an ECM hydrogel into structural and soluble components reveals distinctive roles in regulating macrophage behavior. *Biomater Sci-Uk* **2**, 1521-1534, doi:10.1039/c4bm00189c (2014).

250 Meng, F., Modo, M. & Badylak, S. F. Biologic scaffold for CNS repair. *Regen Med* **9**, 367-383, doi:10.2217/rme.14.9 (2014).

251 Mills, C. D., Thomas, A. C., Lenz, L. L. & Munder, M. Macrophage: SHIP of Immunity. *Front Immunol* **5**, 620, doi:10.3389/fimmu.2014.00620 (2014).

252 Roszer, T. Understanding the Mysterious M2 Macrophage through Activation Markers and Effector Mechanisms. *Mediators Inflamm* **2015**, 816460, doi:10.1155/2015/816460 (2015).

253 Badylak, S. F., Lantz, G. C., Coffey, A. & Geddes, L. A. Small intestinal submucosa as a large diameter vascular graft in the dog. *The Journal of surgical research* **47**, 74-80 (1989).

254 Badylak, S. F. *et al.* The use of xenogeneic small intestinal submucosa as a biomaterial for Achilles tendon repair in a dog model. *J Biomed Mater Res* **29**, 977-985, doi:10.1002/jbm.820290809 (1995).

255 Prevel, C. D. *et al.* Small intestinal submucosa: utilization for repair of rodent abdominal wall defects. *Ann Plast Surg* **35**, 374-380 (1995).

256 Crisan, M. *et al.* Perivascular multipotent progenitor cells in human organs. *Annals of the New York Academy of Sciences* **1176**, 118-123, doi:10.1111/j.1749-6632.2009.04967.x (2009).

257 Keane, T. J. *et al.* Preparation and characterization of a biologic scaffold from esophageal mucosa. *Biomaterials* **34**, 6729-6737, doi:10.1016/j.biomaterials.2013.05.052 (2013).

258 Gentile, N. E. *et al.* Targeted rehabilitation after extracellular matrix scaffold transplantation for the treatment of volumetric muscle loss. *American journal of physical medicine & rehabilitation / Association of Academic Physiatrists* **93**, S79-87, doi:10.1097/PHM.0000000000000145 (2014).

259 Reyes, O., Sosa, I. & Kuffler, D. P. Promoting neurological recovery following a traumatic peripheral nerve injury. *Puerto Rico health sciences journal* **24**, 215-223 (2005).

260 Viguie, C. A., Lu, D. X., Huang, S. K., Rengen, H. & Carlson, B. M. Quantitative study of the effects of long-term denervation on the extensor digitorum longus muscle of the rat. *The Anatomical record* **248**, 346-354 (1997).

261 Liu, F., Zhang, C. & Hoffman, R. M. Nestin-expressing stem cells from the hair follicle can differentiate into motor neurons and reduce muscle atrophy after transplantation to injured nerves. *Tissue engineering. Part A* **20**, 656-662, doi:10.1089/ten.TEA.2012.0657 (2014).

262 Klein, D. *et al.* Nestin(+) tissue-resident multipotent stem cells contribute to tumor progression by differentiating into pericytes and smooth muscle cells resulting in blood vessel remodeling. *Frontiers in oncology* **4**, 169, doi:10.3389/fonc.2014.00169 (2014).

263 Su, P. H., Wang, T. C., Wong, Z. R., Huang, B. M. & Yang, H. Y. The expression of nestin delineates skeletal muscle differentiation in the developing rat esophagus. *Journal of anatomy* **218**, 311-323, doi:10.1111/j.1469-7580.2010.01331.x (2011).

264 Han, N. *et al.* Electrodiagnostic Evaluation of Individuals Implanted With Extracellular Matrix for the Treatment of Volumetric Muscle Injury: Case Series. *Phys Ther*, doi:10.2522/ptj.20150133 (2015).

265 Biswas, S. K. & Mantovani, A. Macrophage plasticity and interaction with lymphocyte subsets: cancer as a paradigm. *Nature immunology* **11**, 889-896, doi:10.1038/ni.1937 (2010).

266 Mantovani, A., Sica, A. & Locati, M. Macrophage polarization comes of age. *Immunity* **23**, 344-346, doi:10.1016/j.immuni.2005.10.001 (2005).

267 Anderson, J. M. & Jones, J. A. Phenotypic dichotomies in the foreign body reaction. *Biomaterials* **28**, 5114-5120, doi:10.1016/j.biornaterials.2007.07.010 (2007).

268 Mills, C. D. Anatomy of a discovery: m1 and m2 macrophages. *Front Immunol* **6**, 212, doi:10.3389/fimmu.2015.00212 (2015).

269 Brigido, S. A., Boc, S. F. & Lopez, R. C. Effective management of major lower extremity wounds using an acellular regenerative tissue matrix: a pilot study. *Orthopedics* **27**, s145-149 (2004).

270 Hodde, J. & Hiles, M. Constructive soft tissue remodelling with a biologic extracellular matrix graft: overview and review of the clinical literature. *Acta chirurgica Belgica* **107**, 641-647 (2007).

271 Mostow, E. N. *et al.* Effectiveness of an extracellular matrix graft (OASIS Wound Matrix) in the treatment of chronic leg ulcers: a randomized clinical trial. *Journal of vascular surgery* **41**, 837-843, doi:10.1016/j.jvs.2005.01.042 (2005).

272 Badylak, S. F. *et al.* The use of extracellular matrix as an inductive scaffold for the partial replacement of functional myocardium. *Cell transplantation* **15 Suppl 1**, S29-40 (2006).

273 Dejardin, L. M., Arnoczky, S. P., Ewers, B. J., Haut, R. C. & Clarke, R. B. Tissue-engineered rotator cuff tendon using porcine small intestine submucosa. Histologic and mechanical evaluation in dogs. *The American journal of sports medicine* **29**, 175-184 (2001).

274 Derwin, K. *et al.* Porcine small intestine submucosa as a flexor tendon graft. *Clinical orthopaedics and related research*, 245-252 (2004).

275 Musahl, V. *et al.* The use of porcine small intestinal submucosa to enhance the healing of the medial collateral ligament--a functional tissue engineering study in rabbits. *Journal of orthopaedic research : official publication of the Orthopaedic Research Society* **22**, 214-220, doi:10.1016/S0736-0266(03)00163-3 (2004).

276 Ehashi, T. *et al.* Comprehensive genetic analysis of early host body reactions to the bioactive and bio-inert porous scaffolds. *PloS one* **9**, e85132, doi:10.1371/journal.pone.0085132 (2014).

277 Ma, Q. L. *et al.* Improved implant osseointegration of a nanostructured titanium surface via mediation of macrophage polarization. *Biomaterials* **35**, 9853-9867, doi:10.1016/j.biomaterials.2014.08.025 (2014).

278 Mokarram, N. & Bellamkonda, R. V. A perspective on immunomodulation and tissue repair. *Ann Biomed Eng* **42**, 338-351, doi:10.1007/s10439-013-0941-0 (2014).

279 Vasconcelos, D. P. *et al.* Development of an immunomodulatory biomaterial: using resolvin D1 to modulate inflammation. *Biomaterials* **53**, 566-573, doi:10.1016/j.biomaterials.2015.02.120 (2015).

280 Wang, Z. *et al.* The effect of thick fibers and large pores of electrospun poly(epsilon-caprolactone) vascular grafts on macrophage polarization and arterial regeneration. *Biomaterials* **35**, 5700-5710, doi:10.1016/j.biomaterials.2014.03.078 (2014).

281 Crapo, P. M. *et al.* Biologic scaffolds composed of central nervous system extracellular matrix. *Biomaterials* **33**, 3539-3547, doi:10.1016/j.biomaterials.2012.01.044 (2012).

282 Faulk, D. M., Wildemann, J. D. & Badylak, S. F. Decellularization and cell seeding of whole liver biologic scaffolds composed of extracellular matrix. *J Clin Exp Hepatol* **5**, 69-80, doi:10.1016/j.jceh.2014.03.043 (2015).

283 Crapo, P. M., Gilbert, T. W. & Badylak, S. F. An overview of tissue and whole organ decellularization processes. *Biomaterials* **32**, 3233-3243, doi:10.1016/j.biomaterials.2011.01.057 (2011).

284 Englen, M. D., Valdez, Y. E., Lehnert, N. M. & Lehnert, B. E. Granulocyte/macrophage colony-stimulating factor is expressed and secreted in cultures of murine L929 cells. *Journal of immunological methods* **184**, 281-283 (1995).

285 Zhang, X., Goncalves, R. & Mosser, D. M. The isolation and characterization of murine macrophages. *Current protocols in immunology / edited by John E. Coligan ... [et al.]* **Chapter 14**, Unit 14 11, doi:10.1002/0471142735.im1401s83 (2008).

286 Shearer, J. D., Richards, J. R., Mills, C. D. & Caldwell, M. D. Differential regulation of macrophage arginine metabolism: a proposed role in wound healing. *The American journal of physiology* **272**, E181-190 (1997).

287 Ho, V. W. & Sly, L. M. Derivation and characterization of murine alternatively activated (M2) macrophages. *Methods in molecular biology* **531**, 173-185, doi:10.1007/978-1-59745-396-7_12 (2009).

288 Nelson, S. M., Lei, X. & Prabhu, K. S. Selenium levels affect the IL-4-induced expression of alternative activation markers in murine macrophages. *The Journal of nutrition* **141**, 1754-1761, doi:10.3945/jn.111.141176 (2011).

289 Veremeyko, T., Siddiqui, S., Sotnikov, I., Yung, A. & Ponomarev, E. D. IL-4/IL-13-dependent and independent expression of miR-124 and its contribution to M2 phenotype of monocytic cells in normal conditions and during allergic inflammation. *PloS one* **8**, e81774, doi:10.1371/journal.pone.0081774 (2013).

290 Billack, B., Radkar, V. & Adiabouah, C. In vitro evaluation of the cytotoxic and anti-proliferative properties of resveratrol and several of its analogs. *Cellular & molecular biology letters* **13**, 553-569, doi:10.2478/s11658-008-0022-9 (2008).

291 Turner, N. J. & Badylak, S. F. The Use of Biologic Scaffolds in the Treatment of Chronic Nonhealing Wounds. *Adv Wound Care (New Rochelle)* **4**, 490-500, doi:10.1089/wound.2014.0604 (2015).

292 Suckow, M. A., Voytik-Harbin, S. L., Terril, L. A. & Badylak, S. F. Enhanced bone regeneration using porcine small intestinal submucosa. *Journal of investigative surgery : the official journal of the Academy of Surgical Research* **12**, 277-287 (1999).

293 Freytes, D. O., Tullius, R. S. & Badylak, S. F. Effect of storage upon material properties of lyophilized porcine extracellular matrix derived from the urinary bladder. *Journal of biomedical materials research. Part B, Applied biomaterials* **78**, 327-333, doi:10.1002/jbm.b.30491 (2006).

294 Keane, T. J. & Badylak, S. F. The host response to allogeneic and xenogeneic biological scaffold materials. *Journal of tissue engineering and regenerative medicine* **9**, 504-511, doi:10.1002/term.1874 (2015).

295 Keane, T. J. *et al.* Tissue-Specific Effects of Esophageal Extracellular Matrix. *Tissue engineering. Part A*, doi:10.1089/ten.TEA.2015.0322 (2015).

296 Sellaro, T. L., Ravindra, A. K., Stolz, D. B. & Badylak, S. F. Maintenance of hepatic sinusoidal endothelial cell phenotype in vitro using organ-specific extracellular matrix scaffolds. *Tissue engineering* **13**, 2301-2310, doi:10.1089/ten.2006.0437 (2007).

297 Cheng, N. C., Estes, B. T., Awad, H. A. & Guilak, F. Chondrogenic differentiation of adipose-derived adult stem cells by a porous scaffold derived from native articular cartilage extracellular matrix. *Tissue engineering. Part A* **15**, 231-241, doi:10.1089/ten.tea.2008.0253 (2009).

298 Cortiella, J. *et al.* Influence of acellular natural lung matrix on murine embryonic stem cell differentiation and tissue formation. *Tissue engineering. Part A* **16**, 2565-2580, doi:10.1089/ten.tea.2009.0730 (2010).

299 Sellaro, T. L. *et al.* Maintenance of human hepatocyte function in vitro by liver-derived extracellular matrix gels. *Tissue engineering. Part A* **16**, 1075-1082, doi:10.1089/ten.TEA.2008.0587 (2010).

300 Zhang, Y. *et al.* Tissue-specific extracellular matrix coatings for the promotion of cell proliferation and maintenance of cell phenotype. *Biomaterials* **30**, 4021-4028, doi:10.1016/j.biomaterials.2009.04.005 (2009).

301 Marcal, H., Ahmed, T., Badylak, S. F., Tottey, S. & Foster, L. J. A comprehensive protein expression profile of extracellular matrix biomaterial derived from porcine urinary bladder. *Regen Med* **7**, 159-166, doi:10.2217/rme.12.6 (2012).

302 Biswas, S. K. & Mantovani, A. Orchestration of metabolism by macrophages. *Cell metabolism* **15**, 432-437, doi:10.1016/j.cmet.2011.11.013 (2012).

303 Tan, Z. *et al.* Pyruvate dehydrogenase kinase 1 participates in macrophage polarization via regulating glucose metabolism. *Journal of immunology* **194**, 6082-6089, doi:10.4049/jimmunol.1402469 (2015).

304 Berridge, M. V. & Tan, A. S. Characterization of the cellular reduction of 3-(4,5-dimethylthiazol-2-yl)-2,5-diphenyltetrazolium bromide (MTT): subcellular localization, substrate dependence, and involvement of mitochondrial electron transport in MTT reduction. *Archives of biochemistry and biophysics* **303**, 474-482, doi:10.1006/abbi.1993.1311 (1993).

305 Haschemi, A. *et al.* The sedoheptulose kinase CARKL directs macrophage polarization through control of glucose metabolism. *Cell metabolism* **15**, 813-826, doi:10.1016/j.cmet.2012.04.023 (2012).

306 Owens, B. D., Kragh, J. F., Jr., Macaitis, J., Svoboda, S. J. & Wenke, J. C. Characterization of extremity wounds in Operation Iraqi Freedom and Operation Enduring Freedom. *J Orthop Trauma* **21**, 254-257, doi:10.1097/BOT.0b013e31802f78fb (2007).

307 Daly, K. A., Wolf, M., Johnson, S. A. & Badylak, S. F. A rabbit model of peripheral compartment syndrome with associated rhabdomyolysis and a regenerative medicine approach for treatment. *Tissue Eng Part C Methods* **17**, 631-640, doi:10.1089/ten.tec.2010.0699 (2011).

308 Wolf, M. T., Dearth, C. L., Sonnenberg, S. B., Loboa, E. G. & Badylak, S. F. Naturally derived and synthetic scaffolds for skeletal muscle reconstruction. *Adv Drug Deliv Rev* **84**, 208-221, doi:10.1016/j.addr.2014.08.011 (2015).

309 Ambrosio, F. *et al.* The synergistic effect of treadmill running on stem-cell transplantation to heal injured skeletal muscle. *Tissue Eng Part A* **16**, 839-849, doi:10.1089/ten.TEA.2009.0113 (2010).

310 Cezar, C. A. *et al.* Biologic-free mechanically induced muscle regeneration. *Proc Natl Acad Sci U S A* **113**, 1534-1539, doi:10.1073/pnas.1517517113 (2016).

311 Gieni, R. S. & Hendzel, M. J. Mechanotransduction from the ECM to the genome: are the pieces now in place? *J Cell Biochem* **104**, 1964-1987, doi:10.1002/jcb.21364 (2008).

312 Kohno, S. *et al.* Unloading stress disturbs muscle regeneration through perturbed recruitment and function of macrophages. *J Appl Physiol (1985)* **112**, 1773-1782, doi:10.1152/japplphysiol.00103.2012 (2012).

313 Tidball, J. G. *et al.* Mechanical loading regulates NOS expression and activity in developing and adult skeletal muscle. *Am J Physiol* **275**, C260-266 (1998).

314 Sicari, B. M., Zhang, L., Londono, R. & Badylak, S. F. An assay to quantify chemotactic properties of degradation products from extracellular matrix. *Methods Mol Biol* **1202**, 103-110, doi:10.1007/7651_2013_37 (2014).

315 Yaffe, D. & Saxel, O. Serial passaging and differentiation of myogenic cells isolated from dystrophic mouse muscle. *Nature* **270**, 725-727 (1977).

316 Distefano, G. *et al.* Neuromuscular electrical stimulation as a method to maximize the beneficial effects of muscle stem cells transplanted into dystrophic skeletal muscle. *PLoS One* **8**, e54922, doi:10.1371/journal.pone.0054922 (2013).

317 Chang, Y. J. *et al.* Cyclic Stretch Facilitates Myogenesis in C2C12 Myoblasts and Rescues Thiazolidinedione-Inhibited Myotube Formation. *Front Bioeng Biotechnol* **4**, 27, doi:10.3389/fbioe.2016.00027 (2016).

318 Ambrosio, F. *et al.* The emerging relationship between regenerative medicine and physical therapeutics. *Phys Ther* **90**, 1807-1814, doi:10.2522/ptj.20100030 (2010).

319 Badylak, S. F., Dziki, J. L., Sicari, B. M., Ambrosio, F. & Boninger, M. L. Mechanisms by which acellular biologic scaffolds promote functional skeletal muscle restoration. *Biomaterials* **103**, 128-136, doi:10.1016/j.biomaterials.2016.06.047 (2016).

320 Corona, B. T. & Greising, S. M. Challenges to acellular biological scaffold mediated skeletal muscle tissue regeneration. *Biomaterials* **104**, 238-246, doi:10.1016/j.biomaterials.2016.07.020 (2016).

321 Brown, B. N., Sicari, B. M. & Badylak, S. F. Rethinking regenerative medicine: a macrophage-centered approach. *Front Immunol* **5**, 510, doi:10.3389/fimmu.2014.00510 (2014).

322 Ballotta, V., Driessen-Mol, A., Bouten, C. V. & Baaijens, F. P. Strain-dependent modulation of macrophage polarization within scaffolds. *Biomaterials* **35**, 4919-4928, doi:10.1016/j.biomaterials.2014.03.002 (2014).

323 Patel, N. R. *et al.* Cell elasticity determines macrophage function. *PLoS One* **7**, e41024, doi:10.1371/journal.pone.0041024 (2012).

324 Throm Quinlan, A. M., Sierad, L. N., Capulli, A. K., Firstenberg, L. E. & Billiar, K. L. Combining dynamic stretch and tunable stiffness to probe cell mechanobiology in vitro. *PLoS One* **6**, e23272, doi:10.1371/journal.pone.0023272 (2011).

325 Bouten, C. V. *et al.* Substrates for cardiovascular tissue engineering. *Adv Drug Deliv Rev* **63**, 221-241, doi:10.1016/j.addr.2011.01.007 (2011).

326 Cortes, P., Riser, B. L., Yee, J. & Narins, R. G. Mechanical strain of glomerular mesangial cells in the pathogenesis of glomerulosclerosis: clinical implications. *Nephrol Dial Transplant* **14**, 1351-1354 (1999).

327 Mosser, D. M. & Edwards, J. P. Exploring the full spectrum of macrophage activation. *Nature reviews. Immunology* **8**, 958-969, doi:10.1038/nri2448 (2008).

328 Tidball, J. G. Interactions between muscle and the immune system during modified musculoskeletal loading. *Clin Orthop Relat Res*, S100-109 (2002).

329 Vassilakopoulos, T. *et al.* Nitric oxide production in the ventilatory muscles in response to acute resistive loading. *Am J Physiol Lung Cell Mol Physiol* **292**, L1013-1022, doi:10.1152/ajplung.00112.2006 (2007).

330 Motohashi, N. & Asakura, A. Muscle satellite cell heterogeneity and self-renewal. *Front Cell Dev Biol* **2**, 1, doi:10.3389/fcell.2014.00001 (2014).

331 Tedesco, F. S., Dellavalle, A., Diaz-Manera, J., Messina, G. & Cossu, G. Repairing skeletal muscle: regenerative potential of skeletal muscle stem cells. *J Clin Invest* **120**, 11-19, doi:10.1172/JCI40373 (2010).

332 Ciciliot, S. & Schiaffino, S. Regeneration of mammalian skeletal muscle. Basic mechanisms and clinical implications. *Curr Pharm Des* **16**, 906-914 (2010).

333 Wang, X. D. *et al.* Mechanical load-dependent regulation of satellite cell and fiber size in rat soleus muscle. *Am J Physiol Cell Physiol* **290**, C981-989, doi:10.1152/ajpcell.00298.2005 (2006).

334 Rana, D., Zreiqat, H., Benkirane-Jessel, N., Ramakrishna, S. & Ramalingam, M. Development of decellularized scaffolds for stem cell-driven tissue engineering. *Journal of tissue engineering and regenerative medicine*, doi:10.1002/term.2061 (2015).

335 Badylak, S. F., Freytes, D. O. & Gilbert, T. W. Reprint of: Extracellular matrix as a biological scaffold material: Structure and function. *Acta biomaterialia* **23 Suppl**, S17-26, doi:10.1016/j.actbio.2015.07.016 (2015).

336 Longo, U. G., Lamberti, A., Petrillo, S., Maffulli, N. & Denaro, V. Scaffolds in tendon tissue engineering. *Stem cells international* **2012**, 517165, doi:10.1155/2012/517165 (2012).

337 Salzberg, C. A. Nonexpansive immediate breast reconstruction using human acellular tissue matrix graft (AlloDerm). *Annals of plastic surgery* **57**, 1-5, doi:10.1097/01.sap.0000214873.13102.9f (2006).

338 Badylak, S. F. Decellularized allogeneic and xenogeneic tissue as a bioscaffold for regenerative medicine: factors that influence the host response. *Annals of biomedical engineering* **42**, 1517-1527, doi:10.1007/s10439-013-0963-7 (2014).

339 Badylak, S. F. *et al.* Esophageal reconstruction with ECM and muscle tissue in a dog model. *The Journal of surgical research* **128**, 87-97, doi:10.1016/j.jss.2005.03.002 (2005).

340 Daly, K. A. *et al.* The host response to endotoxin-contaminated dermal matrix. *Tissue engineering. Part A* **18**, 1293-1303, doi:10.1089/ten.TEA.2011.0597 (2012).

341 Roma-Lavisse, C. *et al.* M1 and M2 macrophage proteolytic and angiogenic profile analysis in atherosclerotic patients reveals a distinctive profile in type 2 diabetes. *Diabetes & vascular disease research* **12**, 279-289, doi:10.1177/1479164115582351 (2015).

342 Spiller, K. L. *et al.* The role of macrophage phenotype in vascularization of tissue engineering scaffolds. *Biomaterials* **35**, 4477-4488, doi:10.1016/j.biomaterials.2014.02.012 (2014).

343 Spiller, K. L. *et al.* Sequential delivery of immunomodulatory cytokines to facilitate the M1-to-M2 transition of macrophages and enhance vascularization of bone scaffolds. *Biomaterials* **37**, 194-207, doi:10.1016/j.biomaterials.2014.10.017 (2015).

344 Arnold, L. *et al.* Inflammatory monocytes recruited after skeletal muscle injury switch into antiinflammatory macrophages to support myogenesis. *The Journal of experimental medicine* **204**, 1057-1069, doi:10.1084/jem.20070075 (2007).

345 Gordon, S. & Taylor, P. R. Monocyte and macrophage heterogeneity. *Nature reviews. Immunology* **5**, 953-964, doi:10.1038/nri1733 (2005).

346 Ovchinnikov, D. A. Macrophages in the embryo and beyond: much more than just giant phagocytes. *Genesis* **46**, 447-462, doi:10.1002/dvg.20417 (2008).

347 Mantovani, A. *et al.* The chemokine system in diverse forms of macrophage activation and polarization. *Trends in immunology* **25**, 677-686, doi:10.1016/j.it.2004.09.015 (2004).

348 Wang, N., Liang, H. & Zen, K. Molecular mechanisms that influence the macrophage m1-m2 polarization balance. *Frontiers in immunology* **5**, 614, doi:10.3389/fimmu.2014.00614 (2014).

349 Chanput, W., Mes, J. J. & Wichers, H. J. THP-1 cell line: an in vitro cell model for immune modulation approach. *International immunopharmacology* **23**, 37-45, doi:10.1016/j.intimp.2014.08.002 (2014).

350 Francke, A., Herold, J., Weinert, S., Strasser, R. H. & Braun-Dullaeus, R. C. Generation of mature murine monocytes from heterogeneous bone marrow and description of their properties. *The journal of histochemistry and cytochemistry : official journal of the Histochemistry Society* **59**, 813-825, doi:10.1369/0022155411416007 (2011).

351 Jablonski, K. A. *et al.* Novel Markers to Delineate Murine M1 and M2 Macrophages. *PloS one* **10**, e0145342, doi:10.1371/journal.pone.0145342 (2015).

352 Sica, A. & Mantovani, A. Macrophage plasticity and polarization: in vivo veritas. *The Journal of clinical investigation* **122**, 787-795, doi:10.1172/JCI59643 (2012).